Selected reactions of ions and molecules in a flowing afterglow-selected ion flow/drift tube (FA-SIFDT)

A Thesis

Presented for the Degree

Of Doctor of Philosophy in Chemistry

In the

University of Canterbury

by

Daniel Bennett Milligan

University of Canterbury

2000

"One day when I was small
I saw the lights, turning on
In the town across the bay
I turned to my sister to say
There must be a story behind all that.

And soon there was...
Electrons, wire, and glass"

The falls - The Mutton Birds

Table of Contents

Acknowledgements.

As I suspect is the case for most pieces of work like this, to say that this represents the work of a single person is doing a great disservice to a very many people. It is only in the barest sense 'my' work and to adequately thank all the people to whom I owe a debt would take another volume. So to all those who appear in the next few paragraphs or who in my carelessness are omitted my gratitude far exceeds the few spare paragraphs that I can afford you.

First my thanks must go to Professor Murray McEwan, who has helped so much over the last 5 years. I feel privileged to have worked with, and come to know, Murray and I have benefited greatly from the association. Rarely has randomness served me better than when it landed me with Murray as an Honours supervisor. I sincerely wish him all the best for his future endeavours.

Thanks should also go to Dr. Colin Freeman who, though it is not in his official list of duties, has essentially become an assistant supervisor to me during this work. This has been especially true (and perhaps onerous) during the last months of this work.

I would like to thank my experimental co-workers in the SIFT lab over the years, Drs. David Fairley, Paul Wilson, Graham Scott and Ms Louise Wheadon for their invaluable help in obtaining and deconvoluting the data presented within these covers. Your efforts and input have always been invaluable to me. I must also thank other collaborators in this work; Drs. Vincent Anicich, David Smith, Patrik Spanel, Michael Mautner (let's hope I spelt it correctly this time), and Randall Allardyce, who have all provided me with many profitable lines of work. Also thanks to Dr Robert Maclagan for the theoretical calculations.

I must single out David and Patrik specifically for their gracious gifts of not only the superb software but also their invaluable experience in all fields of ion-molecule chemistry, especially the trace gas analysis. Without their visit early in the process of commissioning the FA/SIFDT the process would have been a much longer one.

As well as my academic colleagues I am also indebted to the technical staff who have helped me so much during the course of this work. I am sure they will be glad to see the door finally close on my work. As is always the case in a PhD. that

involves the building of a significant piece of equipment there are times when one is almost completely reliant on their expertise. They have also been unflagging providers of good spirit, even when I was almost camped on their doorstep. When I was little more than a glorified mechanic they reminded me that this was not such a bad fate. Thanks Russell, Geoff, Danny, Barry, Nick, Wayne, Rob, Dave, and Sandy.

I would also like to thank Dr. Veronica Bierbaum for allowing us to peruse the plans for her FA/SIFDT before embarking on building our own.

I thank the University of Canterbury for the provision of a Doctoral Scholarship for much of the course of this work. I am also indebted to the Marsden Fund for additional funding.

Now I would like to thank the people whose help was perhaps more indirect, but was still as important and appreciated. The biggest thanks to my Family, Mum Dad, Claire, Livingstone, Suleman, and the rest of the inhabitants of the ferny banks and my Grandparents on both sides. Also to those to whom I may not be related but are no less family (in alphabetical order as it was the only fair way I could think of): Aaron, Allan, Bianca, 21 Church Square, Clare, the climbers, Eden, Emma, Hooch, Jasper, Jill, Kath, Matt, Phil, Royce, Spud, Steph, Stephen, Suzie, Tim, Tina, Vanessa, and many other too innumerable to name. Thanks for your time.

To all the people named above and those I have foolishly forgotten, thanks, and this is yours.

List of Figures

List of Tables

Abstract.

The work presented herein revolves around the design, installation, testing, and use of a new flowing afterglow-selected ion flow drift tube (FA-SIFDT) at the University of Canterbury. This is the latest in the series of FA and SIFT apparatus that have been installed at Canterbury.

The second chapter contains a detailed description of the new instrument. Also present is a description of the characterisation of the of the new FA-SIFT in particular a comparison of two different types of venturi inlet, *viz.* an annulus and a hole type injector. The performance of both of these types of venturi inlet with respect to pumping efficiency, signal transmission, dissociation of weakly bound cluster ions, and the isomerisation of ions during injection. Despite the greater mechanical complexity of the annulus injector it is concluded that the annulus injector is slightly superior to the hole type injector, predominantly when the injection of ions needs to be at low energy.

Next a new application of the SIFT, namely its use in the real time detection, identification and quantification of trace components in gas samples, is presented. This technique has only recently been developed by overseas researchers and its use at Canterbury has been facilitated by the new FA-SIFDT. The technique has been applied to several systems: the analysis of the changes in the largest trace components of human breath (ammonia, acetone, isoprene) during exercise; the monitoring of breath concentrations of organic solvents following exposure; and the headspace analysis of the gases emitted by soil following fertilisation with an artificial urine solution.

The reactions of H_3^+, N_2H^+, and H_3O^+ with thirteen different hydrocarbons have been investigated. The rate coefficients and product distributions of these reactions were investigated in order to obtain a better understanding of exothermic proton transfer reactions. The H_3^+ was generated in two different manners in an effort to get accurate data about the products of proton transfer from ground state H_3^+. As expected, in most cases where the proton transfer was exothermic a rate coefficient just less than the collision rate was observed. The reactions became more dissociative as more energy was placed into the collision complex with the channels that predominated usually being between 100 and 200 kJ mol^{-1} exothermic.

The proton affinity of cyanogen (C_2N_2) has been investigated using the FA-SIFDT. The new value has been determined using the equilibrium method with reference to the C_2N_2/C_2H_2 and CH_3Cl/C_2N_2 cycles. The new value is 651±2 kJ mol^{-1}, some 24 kJ mol^{-1} less than the previously tabulated value. The reactions of methylated cyanogen were also investigated with the intention of determining the methyl cation affinity of cyanogen. Instead it has been determined that the $CH_3^+.C_2N_2$ adduct is strongly bonded, a characteristic that has previously been observed for alkyl ion-cyanide functionality type adducts.

Two classes of reaction relevant to the lower cosmic ray-induced ionosphere of Saturn's largest moon Titan have been investigated. The first class is the bimolecular reactions of the N_3^+ and N_4^+ ion species with a range of hydrocarbons likely to be present in Titan's atmosphere. These ionic species will be formed deep into Titan's atmosphere by the termolecular association of N^+ and N_2^+ (the primary ions formed in Titan's atmosphere) with nitrogen. The association reactions of some of the terminal ions in Titan's atmosphere, *viz.* H_3O^+, $HCNH^+$ and *c*-$C_3H_3^+$, with methane, ethylene and acetylene in the presence of both helium and nitrogen bath gases. The termolecular reaction rate coefficients are greatly enhanced in the presence of a nitrogen carrier gas. Preliminary results of an investigation into the structure of the $HCNH^+.C_2H_4$ and $HCNH^+.C_2H_2$ adducts is also presented.

The termolecular association of the CH_2CHCN^+ and CH_2CHCNH^+ ions derived from acrylonitrile with neutral acrylonitrile have been investigated over a wide range of pressure in both the SIFT and an ion cyclotron resonance (ICR) mass spectrometer. This has enabled the pressure dependence of these two reaction to be experimentally investigated and theoretically modelled. In the non-protonated case (CH_2CHCN^+) there is a competition between termolecular association and bimolecular reaction to give CH_2CHCNH^+. The reaction is observed to pressure saturate without a complete conversion to termolecular kinetics, an assumption made by the commonly used single-well model for association. A different, double-well, association mechanism is proposed for this reaction and modelled theoretically giving an acceptable fit. The CH_2CHCNH^+/CH_2CHCN system shows only termolecular kinetics and is well modelled by a single-well model.

Work begun by earlier researchers at Canterbury on the reactions of ionic species with neutral carbon atoms has been continued. However an effective method

for forming neutral carbon atoms has still not been found. The ultraviolet photolysis of carbon suboxide (C_3O_2) was hoped to solve this problem, however the wavelength of photolysis used was too long to get any significant C atom production. A vacuum UV flash system may be required.

Chapter 1
The motivating factors behind the study of ion-molecule chemistry.

Section 1.1: Ions in physical systems.

§1.1.1: Introduction

On first glance at the topics covered in this work, it may seem to the reader that these have been chosen in an almost random manner. What relationship could the analysis of trace gases in the human breath possibly have to the ionosphere of Titan? Yet in a very real sense there is a continuous chain of events, researchers and experimental apparatus that connects one to the other. The thread that links them is ion-molecule chemistry, but the spur that has driven research in ion-molecule chemistry along is the desire to understand the regions around us in which gas phase ions are observed.

Essentially any region of gas that interacts with radiation is a region in which gas phase ions can be observed. In the terrestrial atmosphere the ionosphere is generated by the interaction of radiation of UV and other wavelengths impinging on the Earth's atmospheric envelope. Indeed the same type of process generates ionospheres around other bodies in the solar system that possess a dense enough atmosphere. In interstellar space, in particular in the diffuse and dense interstellar clouds, stellar UV and cosmic rays ionise the simple chemical species that are abundant in these regions and thus initiate a complex web of ion-molecule chemistry.

It may seem that the results of studies in ion-molecule chemistry (and the results of experiments in other branches of physical chemistry) simply produce numbers that have no direct relevance to the physical world. When one looks at the final resting place of the output of much of this sort of work, e.g. compendia of rate coefficients and product distributions such as those complied by Anicich [1] and Ikezoe [2], it is easy to forget that most, if not all, of these chemical reactions were studied because of some physical observation of the presence of ions in a real system. In the following sections I will endeavour to present some of these observations and

to show a little of where ion-molecule chemistry has come from. The work presented in the following Chapters covers a wide range of the applications of ion chemistry and hopefully gives some hint as to where ion-molecule chemistry, at least at the University of Canterbury, is going.

In some of the gaseous regions referred to above, the ion chemistry involves both positive and negative ions. However, due to the focus of the remainder of the present work towards cations, the observation and reactions of anions will not be discussed in much detail. The bias towards positive ion chemistry exists not only in this thesis but across the whole of the ion-molecule literature, with several times more positive reactions having been studied than negative ion ones (see for example the compendium of Ikezoe [2]). A probable reason for this bias is that natural processes create positive ions more readily than negative ions leaving electrons as the negative charge carriers in many systems.

Section 1.2: Planetary ionospheres.

§1.2.1: Earth.

In 1901 Marconi succeeded in receiving a radio signal that had crossed the full width of the North Atlantic, from Newfoundland to Cornwall. Subsequently several other researchers repeated this unlikely observation [3]. It was soon realised that the radio signals were being reflected from a conducting layer in the Earth's upper atmosphere. The density of electrons and ions in this region of the atmosphere is sufficiently great that it affects the propagation of radio waves passing through it [4, 3, 5]. Indeed, due to the empirical nature of the early studies of the ionosphere, this ability to alter the progress of radio waves that pass through this region in space has essentially become the definition of an ionosphere, both on Earth and for other bodies in the Solar System.

During the course of the early study of the ionosphere (using a technique known as a radio ionosonde [6], which was essentially observing reflected radio waves) it was realised that there was not a single conducting atmospheric region, but several "layers". The first layer found was termed the E layer being situated approximately 80 km above the surface of the Earth. Above this another, weaker, layer was observed

and this was termed the F layer. A sketch of the altitude profile of the various "layers" observed in the Earth's ionosphere is shown in Figure 1.1.

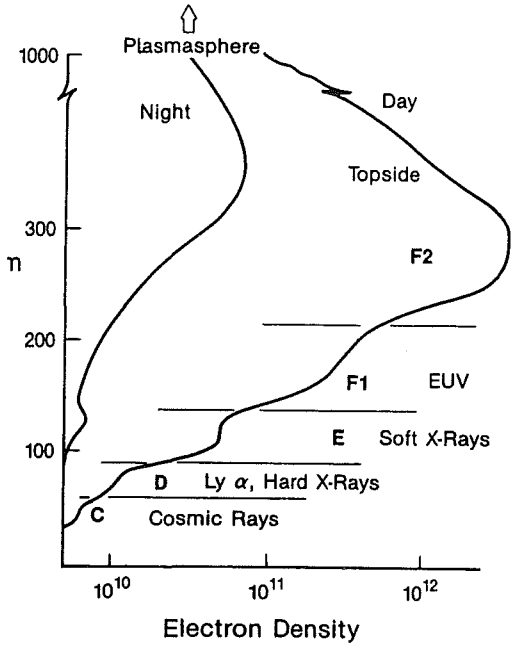

Figure 1.1: The altitude profile of the regions of the Earth's ionosphere. Adapted from Reference 4.

These "layers" are not really separated layers of ion and electron density. In the Earth's atmosphere there is only one definite peak of charge concentration which is around the F2 region. Instead the individual radio wave reflections observed arise from changes in the charge gradient, which affect the propagation of the radio waves differently. Thus these layers are more correctly thought of as broad regions of the atmosphere where the charge conditions are relatively similar. The regions are the result of the fact that different sources of ionisation are more, or less, effective at different altitudes.

The ionosphere is not a stable entity either, it changes with latitude, time of day, and in response to events in the sun. For example the charge maximum in the F2 region (which is also the charge maximum in the total ionosphere) can shift between 200 and 400 km above the Earth's surface, depending on the level of solar activity. The reason for this is that the ionisation is almost totally a result of radiation impinging on the atmosphere and the sun is obviously the major source of radiation in the Earth's region of space. In the upper atmosphere (above 90 km) solar X-rays and

vacuum UV photons ionise and dissociate H, He, O, N_2, and O_2 to produce the initial ions in this system. Because of the low atmospheric pressure, electrons are the only carriers of negative charge above approximately 80 km. Lower down in the mesosphere and stratosphere, the plasma is of the ion-ion type as electron attachment to electronegative neutral species becomes increasingly important and the ionosphere becomes characterised as an ion-ion plasma. An example of this type of reaction is shown in Reaction 101.

$$O_2 + \text{electron} + M \Rightarrow O_2^- + M \quad (101)$$

$$k = 1.4\times10^{-29}\ cm^6s^{-1}\ ^{7,4}$$

Here the ionisation is also caused predominantly by different means as the high energy UV radiation is absorbed higher in the atmosphere. In the D region most of the ionisation is caused by two specific selective photoionisation mechanisms in which solar UV penetrates below 90km through "windows" in the terrestrial absorption spectrum[11]. The most important mechanism is the almost resonant ionisation of neutral NO molecules by solar Lyman-α radiation at 121.6 nm.

$$NO + h\nu_{121.6} \Rightarrow NO^+ + \text{electron} \quad (102)$$

The other main source of photoionisation is the ionisation of excited metastable oxygen molecules ($O_2(^1\Delta_g)$) by Lyman-β radiation at 102.6 nm.

$$O_2(^1\Delta_g) + h\nu_{102.6} \Rightarrow O_2^+ + \text{electron} \quad (103)$$

Even lower in the atmosphere, in the C layer of the ionosphere, the majority of the ionisation is caused by the particle cascade initiated by the collision of cosmic rays with atmospheric gas molecules. Because of the magnetic field of Earth, ionisation caused by charged particle bombardment is much more effective at the higher latitudes where the shielding effect is less. The ion concentration 90 km above the surface is approximately 1 part per billion (ppb) and this decreases with decreasing altitude. The **absolute** ion concentration changes by about an order of magnitude from 90 km down to the surface, but the increasing density of the other species means the relative proportion of ions decreases much more rapidly. At the surface, ions are present at ~1 part in 10^{16}.

With this understanding of the atmospheric ionisation processes it was believed that the ions most likely to be present were simply those derived from the major atmospheric constituents N_2 and O_2. This suggested that the main ions would be

N_2^+, O_2^+, N^+, and O^+ and that at lower levels NO^+ would also be seen as a result of secondary chemistry of these ions with the abundant N_2 and O_2 molecules. However it was not until rocketry advanced enough that mass spectrometers could be carried directly into the upper atmosphere that these observations could be tested. In the years after the Russian launch of the Sputnik satellite, research into the properties of space and the upper atmosphere blossomed. The United States Air Force was particularly interested in the properties of the ionosphere because of the influence it had on their radio communications and in the early 1960's began a programme to measure atmospheric ions *in situ* using mass spectrometry [8]. A few years earlier (in 1958) Paul had described the construction of the R.F. field quadrupole mass spectrometer [9, 10] which, with its mechanical simplicity and fast time response, was ideal for rocket-borne experimental studies. On the 31st of October 1963 a Nike-Cajun rocket carried the first successful flight of a mass spectrometer up to 112 km, with data being collected from 61 to 112 km [8]. A diagram of the mass spectrometer housing and pump is shown below.

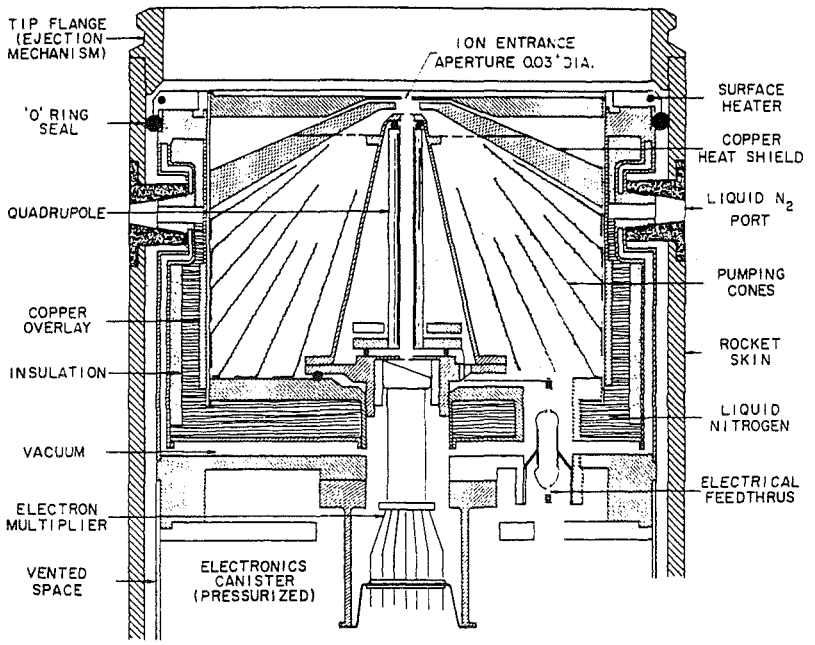

Figure 1.2: Schematic diagram of the first pumped rocket-borne mass spectrometer used to study ions in the Earth's ionosphere. Diagram from Reference 8.

The quadrupole is evacuated and sealed prior to launch and when the desired altitude is reached, the tip is blown off to open the mass spectrometer to the air. The ion

entrance orifice was biased slightly negative relative to the potential of the rocket skin in order to attract positive ions into the spectrometer. In order to keep the pressure in the quadrupole container low enough for the quadrupole mass spectrometer to operate, the pumping cones are coated with zeolite and cooled to liquid nitrogen temperature. This cryo-pumping is quite adequate to pump the small amount of air that enters the system at the heights involved. So confident were the team of Narcisi *et al.*[8] that they knew which ions they would see (and so limited was the time available for experiment) that the mass scan only ranged from 10-46 amu, followed by a step to masses 1, 2, and 4 and finally a measurement of **all** ions above m/z = 38. Because of the speed of the rocket, no time could be afforded to scan across regions of the mass scale where no ions were expected.

Above 82 km the expectations proved to be largely correct, NO^+ and O_2^+ being the major ions observed. Below this height however the major ions observed were *m/z* = 19, 37 together with other masses higher than the scan range of the mass spectrometer! This single result essentially "kick started" the whole field of ion-molecule chemistry. The ions observed were soon understood to be H_3O^+ and $H_3O^+.H_2O$ [8, 11, 3]. Later $H_3O^+.2H_2O$ and higher clusters were also identified. The problem with these observations was providing an explanation for the initial formation of H_3O^+. Although the direct formation reaction, Reaction 104, though it was known to be rapid at the time, it was considered unlikely to be the source for the observed H_3O^+. This is due to the fact that the water concentration in the mesosphere (and below) is not high enough to effect complete conversion of any H_2O^+ formed to H_3O^+ before the H_2O^+ undergoes charge transfer with the more abundant O_2 (Reaction 105).

$$H_2O^+ + H_2O \Rightarrow H_3O^+ + OH \quad (104)$$

$$k = 1.85\times10^{-9}\ cm^3s^{-1}.$$

$$H_2O^+ + O_2 \Rightarrow O_2^+ + H_2O \quad (105)$$

$$k = 3.30\times10^{-10}\ cm^3s^{-1}.$$

The possibility that the signals were the result of outgassing from the rocket was investigated and discounted, although outgassing was found to be the formation mechanism of the small amount of H_2O^+ observed.

At approximately the same time Eldon Fergusson, Art Schmeltekopf, and Fred Fehsenfeld of the Environmental Sciences Service Administration (ESSA) Aeronomy

Laboratory (now known as the National Oceanic and Atmospheric Administration, NOAA) in Boulder, Colorado began experimental work with a flowing afterglow (FA) apparatus [12, 13, 14]. This instrument (shown in Figure 1.3) allowed the study of the rate coefficients and product distributions of ion-molecule reactions to be efficiently studied.

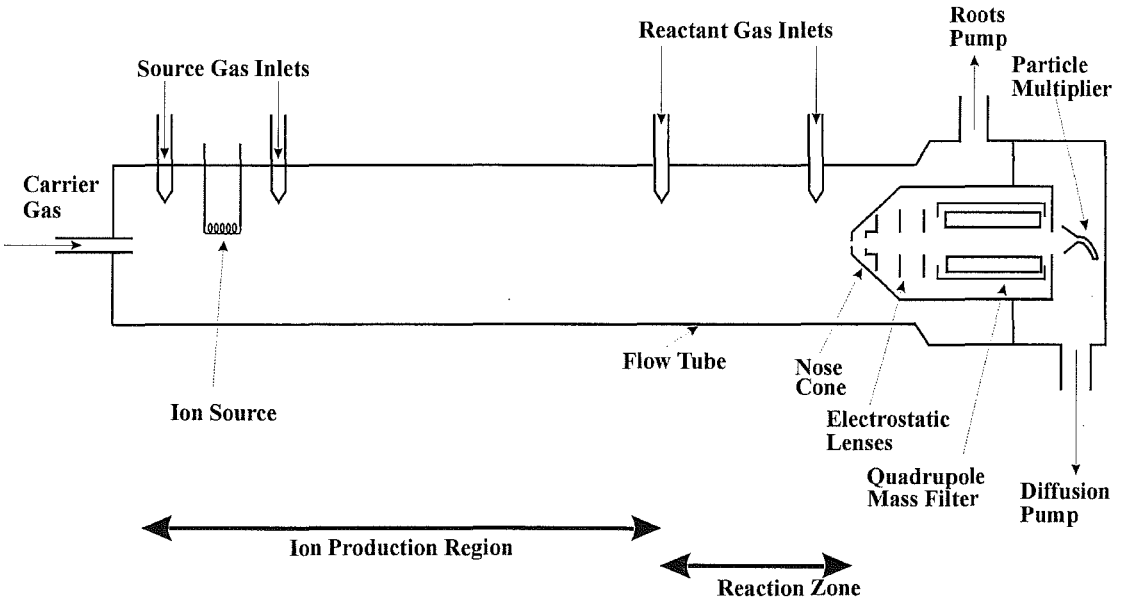

Figure 1.3: A schematic diagram of the layout of the original flowing afterglow instrument.

The active atmospheric ion program encouraged a massive growth in the laboratory study of ion-molecule chemistry [15, 16] and in the understanding of ionospheric processes. Soon after the first rocket flights the rate coefficients for the important processes in the upper atmosphere had been measured. By 1971 the mechanism and reactions responsible for the formation of the cluster reactions had been elucidated. Two main reaction schemes were found, one starting from O_2^+ and the other beginning with NO^+ [8, 11, 17, 18]. These schemes are shown below.

$$O_2^+ + O_2 + M \Rightarrow O_4^+ + M \quad (106)$$

$$O_4^+ + H_2O \Rightarrow O_2^+.H_2O + O_2 \quad (107)$$

$$O_2^+.H_2O + H_2O \Rightarrow H_3O^+ + OH + O_2 \quad (108a)$$

$$\Rightarrow H_3O^+.OH + O_2 \quad (108b)$$

$$H_3O^+.OH + H_2O \Rightarrow H_3O^+.H_2O + OH \quad (109)$$

$$H_3O^+.H_2O + H_2O + M \Rightarrow H_3O^+.2H_2O \quad (110)$$

$NO^+ + N_2 + M$ <=> $NO^+.N_2 + M$ (111)

$NO^+.N_2 + CO_2$ => $NO^+.CO_2 + N_2$ (112)

$NO^+.CO_2 + H_2O$ => $NO^+.H_2O + CO_2$ (113)

$NO^+.H_2O + H_2O + M$ => $NO^+.2H_2O + M$ (114)

$NO^+.2H_2O + H_2O + M$=> $NO^+.3H_2O + M$ (115)

$NO^+.3H_2O + H_2O$ => $H_3O^+.2H_2O + HNO_2$ (116)

The equilibrium reaction between NO^+ and nitrogen (Reaction 111) is essentially driven by the high concentrations of the N_2 molecule present in the atmosphere despite the fact that the bonding is very weak. Then successively more strongly bound molecules are added until the NO^+ series of hydrates is able to shift to the water series in Reaction 116.

The development of the selected ion flow tube (SIFT) in the mid 1970's by Adams and Smith [19, 20] gave another significant boost to the field of ion-molecule chemistry. One of the major problems with the FA was that the reactant ions had to be generated within the same flow tube as was used for investigating the reaction under study. Consequently contamination from other species (e.g. the neutral precursor for the ion, other fragment ions, photons and metastable neutrals) was commonly observed in the reaction region, complicating the analysis of the system under study. The SIFT technique utilises a remote ion source and thus overcomes many of these problems. Several good reviews of both the FA and the SIFT technique have been published over the years [21, 22, 23, 24] and more details on both techniques are given in Chapter 2, so little else will be said here.

§1.2.2: Extraterrestrial ionospheres.

Ionospheres have also been observed on other planets and on planetary satellites in the solar system. In most cases the ionospheres have not been directly sampled, but instead the structure has been observed by using the technique of radio occultation with an unmanned space probe [25, 26]. In this technique the radio signals from the probe are observed from Earth as the passage of the probe takes it behind the planet being observed. A diagram showing two different types of radio occultation experiments is shown in Figure 1.4.

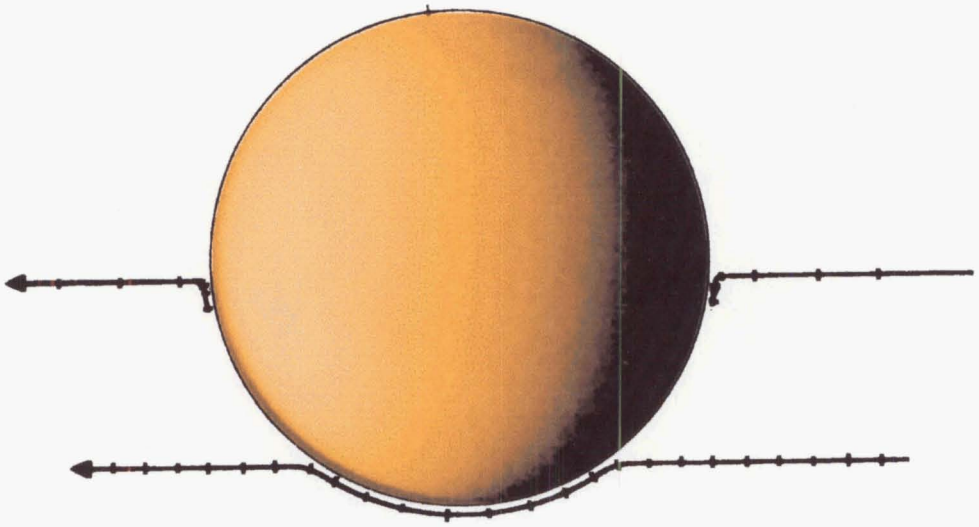

Figure 1.4: Two different types of radio occultation, one grazing, and one passing directly behind the planet. The solid lines represent the times that it is possible to receive radio signals from the probe. If the probe is viewed as travelling right to left, the right hand side is referred to as an ingress occultation and the left hand side is an egress occultation.

The radio waves thus pass through a section of the atmosphere and their path is altered (refracted) by the presence of neutral and charged particles in the atmosphere. A radio occultation is able to observe electron densities down to a level of 100 to 1000 electrons per cm^{-3}, depending on the wavelengths of the radio waves used [26]. Neutral constituents of the atmosphere can be detected in a conceptually similar manner by using visible or UV light. From these measurements of electron (and correspondingly ion) density, as well as a knowledge of the neutral composition of the ionosphere at the height observed, models of the ionospheric chemistry of these satellites can be generated.

The ionosphere of Venus [5, 27] is probably the best studied, after that of Earth, as the Pioneer-Venus Orbiter (PVO) [28, 29] spent approximately 14 years orbiting and studying the Venusian atmosphere and ionosphere. On board was a neutral and ion mass spectrometer (Pioneer-Venus Orbiter Ion Mass Spectrometer PVOIMS) which passed through the upper atmosphere many times [30]. The PVOIMS has provided *in situ* data on the ionosphere of Venus. However the ionosphere of Venus has been

found to be very dependent on solar activity, which changes the ionosphere's morphology radically. During one period of maximum solar activity, the path of the PVO took it right through the ionosphere down to an altitude of ~200 km. When solar activity is at a maximum the ionosphere can extend up to 800 km above the surface from a base at approximately 130 km. By contrast when solar activity is at its lowest the ionosphere of Venus shrinks down to a thin band around between 130 and 300 km. In the years of solar minimum, the PVO was operating in a much higher orbit and thus no *in situ* data is available on the solar minimum ionosphere of Venus.

Earth and Venus are of similar size and composition and Venus is only slightly closer to the Sun. Somewhat surprisingly then the Venusian atmosphere is very different to that of Earth. Venus suffers from a runaway greenhouse effect that has left it with an atmosphere which is 96.5% CO_2 and only 3.5% N_2 [31]. The main ions observed by the PVOIMS were O^+ and O_2^+, with the minor constituents C^+, CO_2^+, NO^+, N^+, He^+, and CO^+ (and the isobaric N_2^+), comprising less than 10% of the total ion density. The initial ionisation of the Venusian atmosphere (from both photoionisation and photoelectron impact ionisation) creates mainly CO_2^+ and O^+ as can be seen in Figure 1.5 (reproduced from the work of Nagy *et al.* [32]). These primary ions are what one expects from the neutral densities in the region in which the ionosphere is established. The neutral gas densities determined by the PVO neutral mass spectrometer are shown in Figure 1.6, which is adapted from the work of Niemann *et al.*[33].

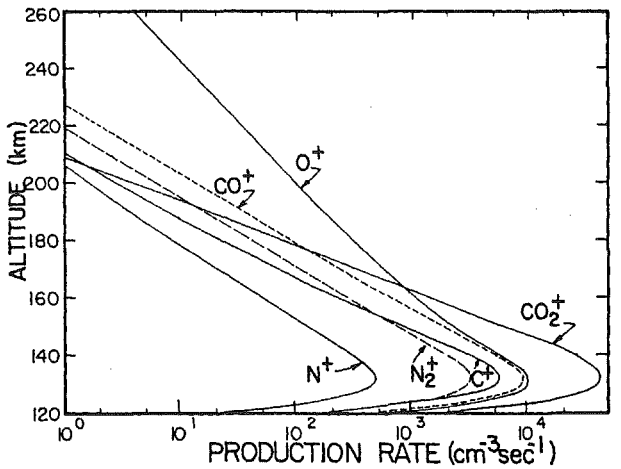

Figure 1.5: The initial ions produced by both photoionisation and photoelectron impact ionisation on the atmosphere of Venus.

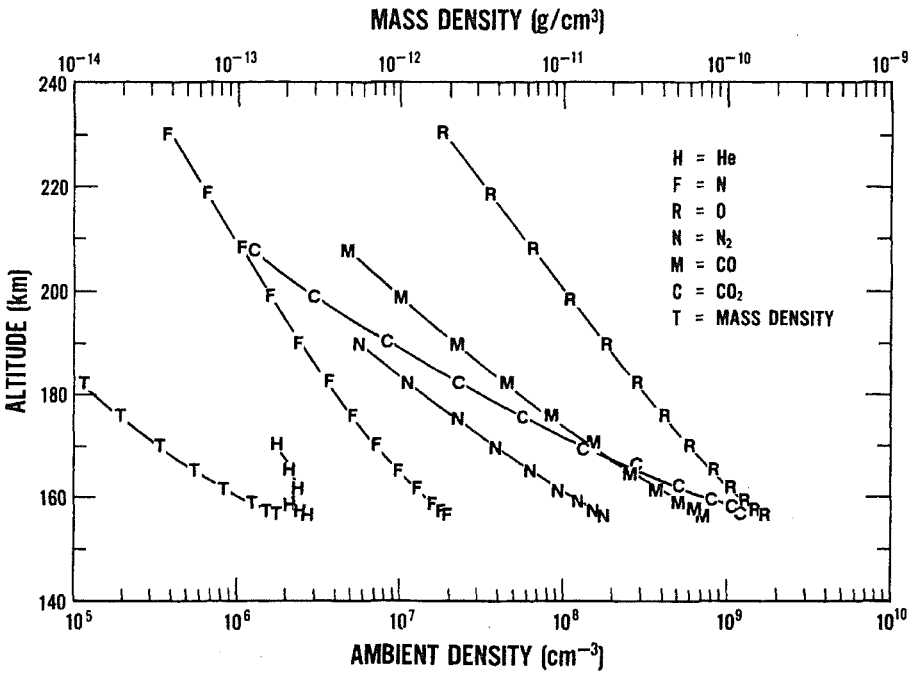

Figure 1.6: The neutral concentrations determined in the upper Venusian atmosphere determined by the neutral mass spectrometer aboard the PVO.

The major ion-molecule reactions are shown below.

$CO_2^+ + O$	=>	$O_2^+ + CO$	[0.60]	(117a)
	=>	$O^+ + CO_2$	[0.40]	(117b)
$O^+ + CO_2$	=>	$O_2^+ + CO$		(118)
$CO^+ + CO_2$	=>	$CO_2^+ + CO$		(119)
$C^+ + CO_2$	=>	$CO^+ + CO$		(120)

From the known reaction rate coefficients of these, and other more minor reactions, (and a basic model of the ion diffusion in the atmosphere of Venus) a model was constructed that gave very good agreement with the data returned by the PVOIMS instrument passes on the solar maximum ionosphere [32, 34]. The reactions shown above are also believed to be the most important reactions for the ionosphere of Mars, which has not yet been studied as extensively as that of Venus. The anticipated similarity of the Martian ionosphere is due to the fact that Mars has a similar neutral composition in its ionosphere to that of Venus.

The ionospheric structure of Saturn and Jupiter has been measured by radio occultation techniques. The Pioneer and Voyager spacecraft have visited these planets and have shown that both planets have a large amount of structure present in their

ionospheres [5, 35]. The most common ion formed in both ionospheres is H_2^+ as atomic and molecular hydrogen are the most common neutral species in these atmospheres. At high altitudes, where the relative amounts of atomic hydrogen are greater, Reaction 121 is important. At lower altitudes Reaction 122 forms H_3^+.

$$H_2^+ + H \Rightarrow H^+ + H_2 \quad (121)$$

$$H_2^+ + H_2 \Rightarrow H_3^+ + H \quad (122)$$

The rate of electron recombination is still under discussion [36, 37, 38] however it will play a large role in the lower altitude regions of the Jovian and Saturnian ionospheres where H_3^+ is an abundant ion. The ion-molecule chemistry of H_3^+ with the hydrocarbon molecules present in the lower ionospheres of these planets will also become important. Methane, acetylene, ethane, and benzene were all seen in the atmosphere of Jupiter prior to the Galileo entry probe. These neutrals provide the potential for extensive hydrocarbon chemistry, begun by the protonation of these neutral molecules by H_3^+ (for details of this class of reactions see Chapter 4).

The satellites Titan (Saturn) and Triton (Neptune) have also been shown to have ionospheres [35]. The Cassini-Huygens [39, 40] mission will encounter Titan and Saturn in 2004 and will make many observations of the ionosphere of Titan, including an entry probe. Chapter 6 of this thesis includes reactions that are relevant to the lower ionosphere of Titan.

Section 1.3: The interstellar medium

§1.3.1: Ions in the interstellar clouds.

Another major boost to the field of ion-molecule chemistry was the discovery of ions in the interstellar clouds (ISC). These vast regions of locally higher gas densities are spread throughout the galaxy and stretch between the stars. Obviously because they are so far from Earth there have never been any *in situ* (i.e. mass spectrometric) studies of these regions but they have been extensively studied using spectroscopic techniques. By observing the ISC, in both emission and absorption over a range of frequencies from radio to gamma waves, a large range of neutral and ionic species have been identified. The scientific discipline of observing these regions is

commonly refers to as *radio astronomy*. A selection of the molecules observed in both the diffuse and dense ISC is shown in Table 1.1.

Molecules				Ions
H_2	H_2O	*l* and *c* C_2H	CH_3CO_2H	CH^+
CH	C_2H	CH_2CN	C_2H_5OH	SO^+
OH	HCN	CH_2CO	CH_3OCH_3	HCO^+
CN	HNC	C_4H	C_2H_5CN	N_2H^+
CO	H_2S	HC_3N	HC_9N	H_3O^+
SO	NH_3	CH_3NH_2	$HC_{11}N$	H_2CN^+

Table 1.1: A selection of molecules and ions observed in the diffuse and dense interstellar clouds using spectroscopic techniques. Data taken from References 11, 41, and 42.

In order to understand why ion-molecule chemistry is important to the interstellar medium (ISM) and ISC in particular, it is first necessary to give an introduction to these regions of space, as the conditions are so different to those experienced anywhere within the terrestrial environment [11, 37, 41, 42]. There are two major classes of ISC, dense and diffuse, and they have quite different physical conditions and chemical make-up.

In the *diffuse clouds* there is not a large amount of dust present and therefore light can penetrate the clouds. This has two major consequences: first they are easier to observe as visible absorption spectroscopy can be performed by using background stars as light sources; and second, the chemical species are in more simple forms than those observed in the dense clouds as UV radiation dissociates molecules (and that of other wavelengths). Thus in the diffuse ISC the most common species are approximately equal amounts of molecular and atomic hydrogen. The gas densities are quite low (~10^2 molecules cm^{-3}) but the high radiation flux penetrating throughout heats them to temperatures of up to 100 to 200K. Ionisation in these regions comes mostly from the UV photons that are ubiquitous throughout them.

The *dense ISC* or "molecular clouds" contain much higher densities of gas (~10^4-10^6 molecule cm^{-3}) and are largely composed of molecular hydrogen, helium, and dust grains. These dust particles shield the centres of these clouds from the destructive UV radiation, and thus larger molecules can be formed in these regions.

Dust also shields the clouds from the heating effects of radiation and consequently the temperature is much lower, in the realm of 10 to 100K. Ion chemistry here is initiated by the ionisation of the main components by cosmic rays which can penetrate further through the shielding dust than do photons.

The question that remains is how molecules as large and complex as some of those seen in Table 1.1 are made in such a hostile environment. Most chemical reactions will stop almost completely at the temperatures encountered in the molecular ISC because, despite the fact that they are exothermic, they have activation barriers somewhere on their potential energy surfaces (PES). The reactions which form the molecules observed in the ISC also need to proceed with very high efficiencies as, due to the low gas densities, collision events are relatively rare. Ion-molecule reactions fit both of these requirements. The ion-induced dipole attraction between a cation and a neutral molecule means that the entrance to the PES is attractive even at low temperatures and many exothermic ion-molecule reactions occur with a rate coefficient that is limited only by the collision frequency. It is now generally accepted that ion-molecule chemistry provides one of the major mechanisms for building up molecules in the ISM. Other processes that are believed to be responsible for the formation of interstellar molecules are radical-neutral reactions and heterogeneous catalysis on the surface of the dust grains [41]. The neutral molecules observed in the ISC which are the result of ion-molecule chemistry come from the neutralisation of cations (through collisions with electrons), a process that is often dissociative. These cations have been built up in a step-wise fashion through a sequence of many steps from the simple neutral components that are seen in the young ISM [11, 37].

Exploring the reactions that are likely to occur in ISC has driven ion-molecule chemistry into new regions. The ion chemistry of hydrocarbons, previously only important in flames, has become very important as cloud modellers try to obtain pathways for forming the hydrocarbons observed in the ISC [43]. Chapter 8 of these thesis reports an attempt to measure one of the last remaining important reactions, Reaction 123, which is expected to begin the chain of reactions leading to larger hydrocarbons.

$$H_3^+ + C \Rightarrow CH^+ + H_2 \quad (123a)$$

$$\Rightarrow CH_2^+ + H \quad (123b)$$

$$CH^+ + H_2 \Rightarrow CH_2^+ + H \quad (124)$$

$$CH_2^+ + H_2 \Rightarrow CH_3^+ + H \quad (125)$$

The CH^+ ion has been directly observed in diffuse ISC [44]. The next logical step in the chain shown above, the reaction of CH_3^+ with hydrogen, is not a rapid bimolecular reaction. Instead in the pressure range used in several of the ion-molecule reactors a slow termolecular reaction, Reaction 126, is seen.

$$CH_3^+ + H_2 + M \Rightarrow CH_5^+ + M \quad (126)$$

Here the third reaction body (M) removes energy from the collision complex and stabilises it towards dissociation.

In the ISC the gas densities are so low that a process such as Reaction 126 is extremely unlikely which could leave the models with 'bottlenecks' in the chain of reactions that forms the larger molecules observed in the ISC. However in the ISC the initial collision complex will have much less energy content (and hence a longer lifetime) because the conditions are much colder than those experienced on Earth. It is proposed that in the ISM, certain of these collision complexes will live long enough that they will be able to radiate some of their excess energy away as photons and thus stabilise themselves. This process is referred to as *radiative association* [283, 284, 45]. Consequently reaction studies of termolecular associations, which measure how easily the collision complex can be stabilised by the removal of energy by a third body, are regularly used as an indicator of the effectiveness of radiative association in ISC. Both termolecular and radiative associations will be more efficient when the collision complex is less susceptible to unimolecular dissociation and therefore the experimentally-accessible termolecular associations are investigated in place of the radiative associations which are almost impossible to study experimentally. Both types of association reaction will also be temperature dependent and as a result, a number of variable temperature techniques have been developed over the years e.g. VT-SIFT [21, 22, 24], CRESU [46, 47]. A desire for a fuller understanding of the mechanism by which association reactions (and especially termolecular reactions) operate has fuelled studies of many association systems. One such system, that of non-protonated and protonated acrylonitrile ions (CH_2CHCN^+ and CH_2CHCNH^+) reacting with neutral acrylonitrile, is presented in Chapter 7.

Section 1.4: Trace Gas analysis.

§1.4.1: A novel application of ion-molecule chemistry.

During the last few years a new mission has been driving the accumulation of large databases of ion-molecule reaction rates. These rate coefficients are being used for the analysis of trace volatiles in environmental air or in breath samples using the new SIFT-MS [48, 49, 50, 51] or PTR-MS [52, 53, 54, 55] techniques. Both of these techniques are chemi-ionisation techniques that, unlike conventional MS-based chemi-ionisation techniques, make use of the ion-molecule kinetics to allow quantification of the amounts of volatile species present in the gas samples. Experiments with the SIFT-MS technique have been undertaken at the University of Canterbury and as these are more fully explained in Chapter 3 of this thesis they will not be repeated here. Instead, an example from results that have been presented previously in the literature will be shown in order to highlight the importance of understanding the underlying ion-molecule chemistry. It has been shown previously that there are large amounts of nitric oxide (NO) released from bacterially-infected urine that has been acidified [56]. The NO results from the large levels of nitrite formed from the bacterial reduction of the nitrates normally present in the urine. When these nitrites are acidified they produce nitrous acid which will subsequently decompose to give NO and water. The most likely decompostion reaction (in a sealed vessel) is shown in Reaction 127.

$$3HNO_2 \quad => \quad 2NO + HNO_3 + H_2O \qquad (127)$$

Using SIFT-MS Smith and Spanel [57] have shown that this nitric oxide can be reacted with O_2^+, to give NO^+ and a small amount of the first hydrate $NO^+.H_2O$.

$$O_2^+ + NO \quad => \quad NO^+ + O_2 \qquad (128)$$

$$NO^+ + H_2O + M \quad => \quad NO^+.H_2O + M \qquad (129)$$

As the analyses are performed on gases present in the headspace above urine (actually urine heated to 40°C to enhance volatilisation of the volatile compounds) there will be large amounts of water vapour in the sample. Levels of up to 25 parts per million (ppm) of NO were seen in the headspace above urine which had bacterial infection. These were several times greater than the normal levels which were less than 5ppm [57].

It was also possible to directly detect the nitrous acid (HNO_2) in the headspace gas over the infected urine samples.

$$H_3O^+ + HNO_2 \Rightarrow NO^+ + 2H_2O \quad (130a)$$

$$\Rightarrow NO^+.H_2O + H_2O \quad (130b)$$

No rate coefficient has yet been reported for Reaction 130, so this cannot be used currently to quantify the amount of nitrous acid present but it is still a good qualitative indicator. Note also that when analysis of NO concentrations is performed using an O_2^+ precursor (Reaction 128 shown above), gas phase nitrous acid is also included in the analysis as both neutral reactants give a NO^+ product.

$$O_2^+ + HNO_2 \Rightarrow NO^+ + (O_2 + OH) \quad (131)$$

In another experiment [58] Smith and Spanel have shown that patients with bladder or prostate cancer have formaldehyde present in the headspace of their urine. It has previously been shown that formaldehyde is emitted from certain type of tumor cells *in vitro*. Formaldehyde also has a higher proton affinity (PA) than water so the reaction of H_3O^+ with formaldehyde should proceed rapidly to give protonated formaldehyde, H_3CO^+.

$$H_3O^+ + H_2CO \Rightarrow H_3CO^+ + H_2O \quad (132)$$

The difference between the two PA values (PA of H_2CO – H_2O) is only ~22 kJ mol^{-1} and the reverse reaction could influence the measured values. This is an example of the way in which a good knowledge of the possible ion chemistry is essential when using SIFT-MS, and is a reason why the SIFT-MS technique will spawn many more investigations of ion-molecule reactions. The rate coefficient for Reaction 133 (the reverse of Reaction 132) has now been found to be very low, $k \approx 5x10^{-13}$ cm^3s^{-1} (near the limits of accurate determination for the SIFT technique), and as such will not affect the values measured for formaldehyde concentration greatly.

$$H_3CO^+ + H_2O \Rightarrow H_3O^+ + H_2CO \quad (133)$$

However another reaction that will affect the measured values was found. This reaction was the association of the H_3CO^+ ion with water as shown below.

$$H_3CO^+ + H_2O + M \Rightarrow H_3CO^+.H_2O + M \quad (134)$$

Reaction 134 is very similar to the association reactions that are known to occur with the H_3O^+ precursor ions (such as reaction 135).

$$H_3O^+ + H_2O + M \Rightarrow H_3O^+.H_2O + M \quad (135)$$

Reaction 135 is a reaction first investigated due to its possible relevance to the D region of the ionosphere and the two reactions in fact occur with similar rate coefficients. In a normal analysis, the upper hydrates of H_3O^+ would be included in

the primary ion count as well as they can also react with the neutral species under investigation. In this system however the most likely reaction of these upper water hydrates can proceed in **both** directions.

$$H_3O^+.H_2O + H_2CO \quad <=> \quad H_3CO^+.H_2O + H_2O \qquad (136)$$

The levels of water vapour will be higher than those of the formaldehyde so that even though the reverse reaction is slower it will still be important and will effectively convert "product" counts into "reactant" counts. This has lead to a simple correction for Reaction 134, *viz.* that only H_3O^+ and H_3CO^+ are counted as the loss processes for both of these ions with water are of similar magnitudes and should thus effectively cancel each other.

Many other medical topics have been investigated using SIFT-based trace gas analysis techniques. These topics range widely and include: the changes in breath composition with diet, and fasting [59]; the differences in breath between smokers, non-smokers, and people exposed to second-hand smoke [60, 61]; and the breath ammonia levels of patients with renal failure [62]. A wide range of non-medical applications have also been investigated including food odours and freshness [53, 63], and environmental air analyses where decaying or wounded plant material is present [53, 64]. These new studies have provided impetus for the investigation of many new ion-molecule reactions.

As remarked above, this Chapter is intended to give the reader some idea of the stories behind the collection of rate coefficient and product distribution data which will be presented later and to show why the chosen reactions have been studied. This is not to imply that research conducted purely for interest is not valid, but merely to show the linking thread between the individual Chapters of this work.

Chapter 2

Experimental: The design, commissioning and testing of the FA-SIFDT.

Section 2.1: Introduction.

§2.1.1: The lineage of the Canterbury FA-SIFDT.

The results reported herein were mainly obtained using the newly constructed Flowing Afterglow / Selected Ion Flow Drift Tube (FA-SIFDT) at the University of Canterbury [65]. This instrument, which traces it's lineage back to the selected ion flow tube constructed in this department in 1982-85 [66, 67], began construction in 1996 just prior to the commencement of this work. The design, relocation and commissioning of this apparatus comprised a large part of the work in the first year of my PhD, with additional modifications and testing continuing throughout my term of study.

The original selected ion flow tube (or SIFT) instrument at Canterbury is described in the work of Knight [66], Petrie [68], Wilson [69], Scott [70] and Fairley [71]. The current instrument is designed to address several limitations of the previous SIFT apparatus and to institute some new features that have been developed since the original SIFT was commissioned. The following chapter will outline the essential features of the new apparatus including the important differences from the earlier model SIFT and present some data that show the enhanced utility of the new instrument. Following the convention begun by Fairley [71] the current instrument will be designated by the terms FA-SIFDT or FA-SIFT and the previous one will be termed the SIFT or SIFDT.

2.2: Physical description of the FA-SIFDT apparatus.

§2.2.1: An introduction to the FA-SIFDT.

A schematic diagram of the FA-SIFT is presented in Figure 2.2. When Figure 2.2 is compared with the diagram of the earlier SIFT (Figure 2.3), the major

differences are obvious. A flowing afterglow ion source and the associated pumping lines, chamber, controls, and other accessories have been added. The quadrupole mass spectrometer chambers are pumped by an increased number of much higher speed diffusion pumps. The major motivating factor in the upgrade to a FA-SIFT was to increase the magnitude of the ion signals and the mass selectivity of the source and detection regions. We hoped to achieve this improvement both by increasing the gross number of ions available and by decreasing the losses of desired ions within the quadrupole mass spectrometer regions by such causes as unreactive scattering. The improvement was to be achieved through the incorporation of a flowing afterglow ion source and by decreasing the pressure in the vicinity of the quadrupole mass spectrometers.

A flowing afterglow (FA) source has previously been incorporated as the ion source of three other SIFT type apparatus; those of Smith and Adams at Birmingham [72], Bohme at York [73] and Bierbaum at Boulder [74, 75]. The first two instruments in this list were not entirely successful and we have not borrowed heavily from them, though they established the practicality of using a FA as an ion source for a SIFT. The Canterbury FA-SIFDT is most similar to the Boulder apparatus, which is the only apparatus of these three still in current use. During construction we had access to the schematics of the Boulder FA-SIFDT and consequently many sections of our FA source are based on very similar principles to theirs. We are indebted to Professor V. Bierbaum for the use of these schematics.

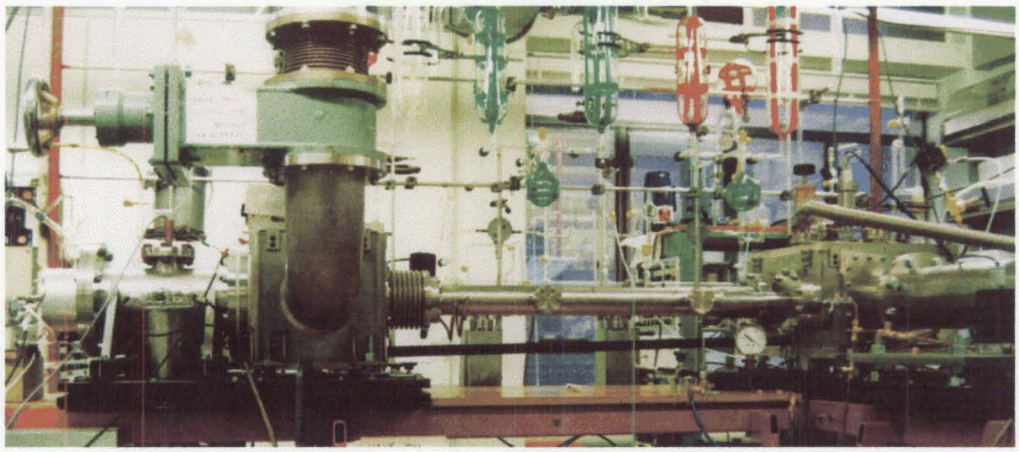

Figure 2.1: A picture of the current FA-SIFDT instrument installed at the University of Canterbury.

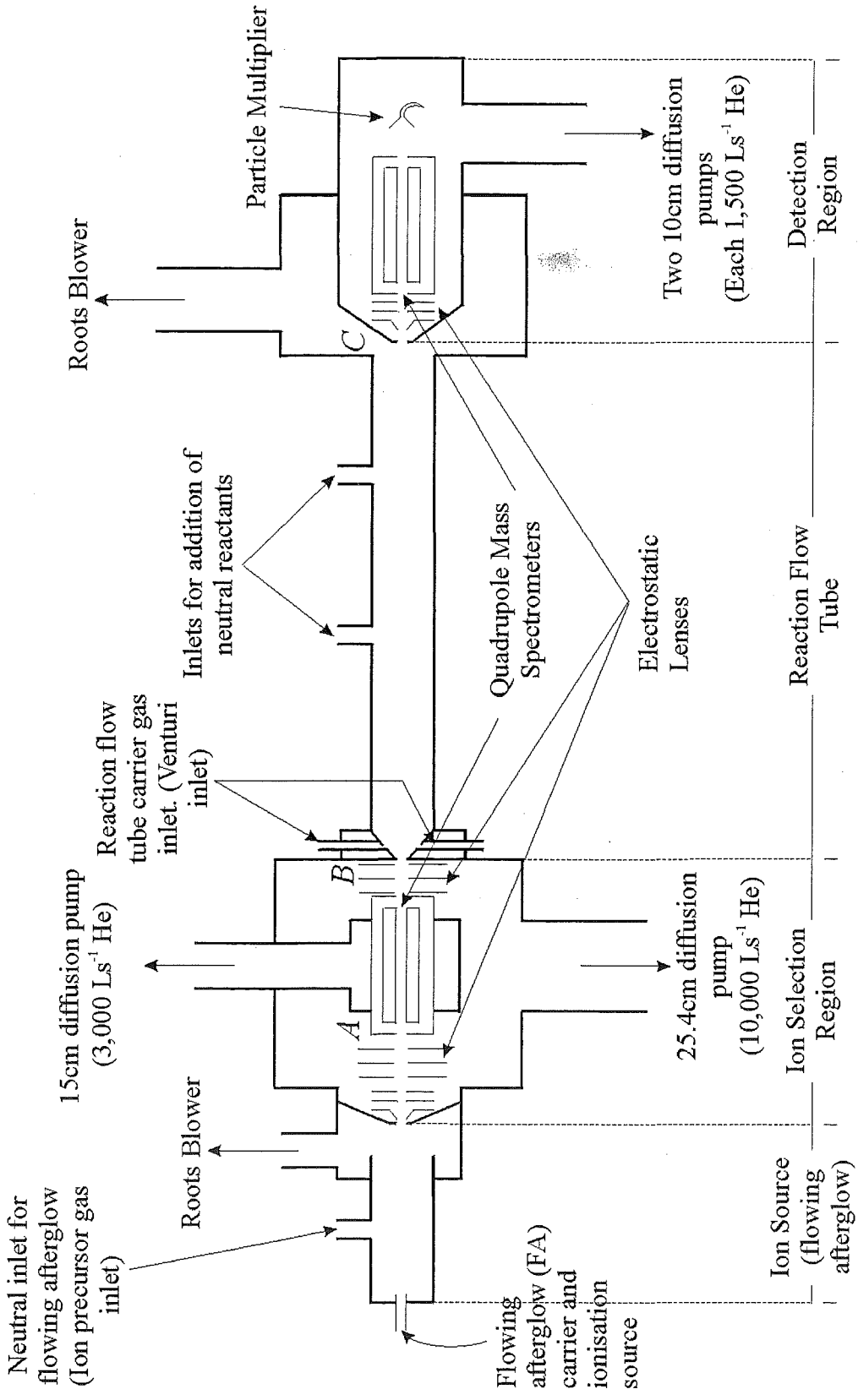

Figure 2.2: A schematic diagram of the FA-SIFDT at the University of Canterbury. The labels A, B, and C refer to the ion current collection points from §2.3.2.

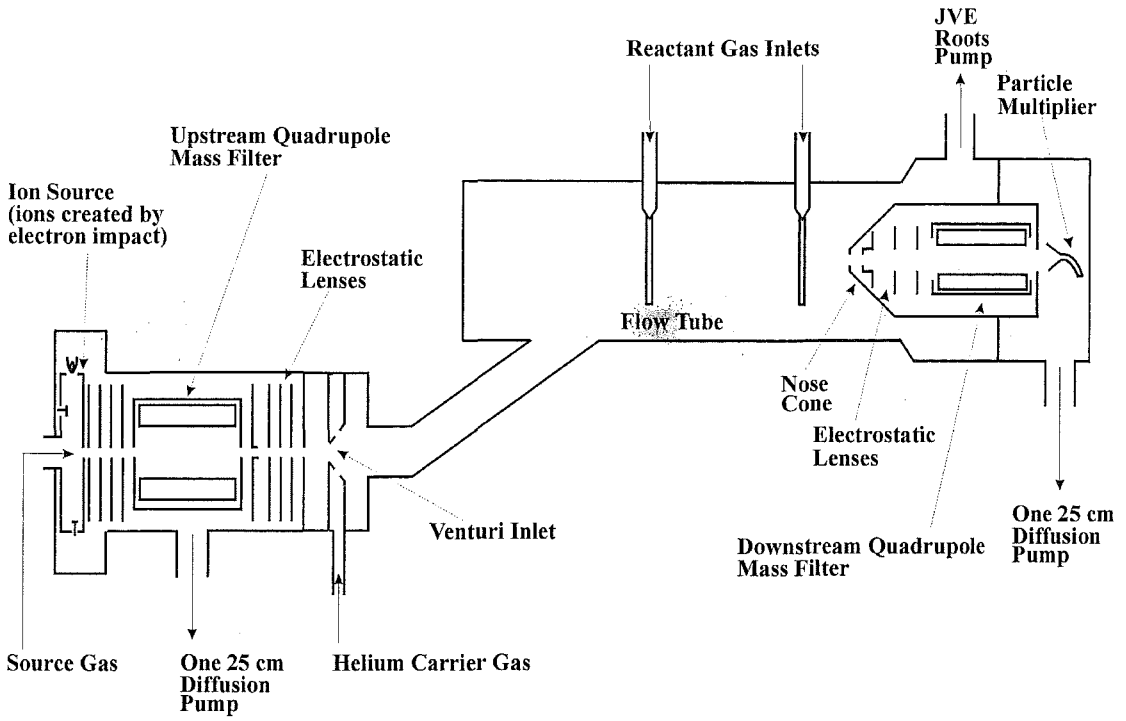

Figure 2.3: A schematic diagram of the previous SIFT installed at the University of Canterbury.

§2.2.2: The Flowing Afterglow (FA) Source

The genesis of the FA/SIFT can be traced to the original NOAA flowing afterglow constructed in Boulder Colorado in the late 1960's and prior to that to the flow tubes used in studying the optical emissions of afterglows [13, 14]. The development of the flowing afterglow was motivated by a desire to study the ion chemistry occurring in the Earth's upper atmosphere and greatly advanced our understanding of ion-molecule type chemical reactions. However, in many systems it becomes very difficult to extract good kinetic data or accurately determine products using the FA technique. This is essentially due to the fact that in the reaction tube there is always a mixture of ion species and neutrals. In a 'normal' experiment not only will the reactant and product ions and the reactant neutral be present but also He^+ ions, electrons, photons, and the neutral species from which the reactant ion was generated. These factors produce spurious ions in the reaction region which, when mass analysed and counted, may obfuscate the determination of the reaction rate coefficient and the product distribution.

The SIFT technique of Smith and Adams was developed to overcome this problem by having the ionisation source spatially separated from the reaction tube [19, 20]. In their technique the ions are mass selected after they leave the source but before they enter the reaction tube allowing only one ion mass to enter the reaction tube. This arrangement greatly simplifies the analysis of the reaction system as in the reaction region there are no ions other than the reactant, no photons or electrons, and no neutral gases other than the reagent and the unreactive carrier gas. However in this move towards a 'cleaner' reaction signal ion count was sacrificed. Traditionally SIFT instruments use a high or low pressure electron impact source and the Canterbury SIFDT had the option of both of these [70]. The high pressure/low pressure ion source results in one of the 'weaknesses' of the SIFT technique as they;

- are unable to produce large counts of some ions,
- can only produce ions that are derived directly from a neutral precursor; e.g. the molecular ion or the products formed from it by fragmentation,
- often produce many fragment peaks further reducing the amount of the desired ion available,
- are poor sources of cluster ions and other weakly bound species.
- produce non-thermal ions.
- require frequent cleaning. After a period of use the ion source has a tendency to accumulate an insulating film on the repeller and Einzel lens extraction assembly. This means higher voltages are required to transmit the ions and the propensity to dissociate or excite the ionic species is exacerbated.

It was with these limitations in mind that we decided to construct a FA ion source. The strengths of the FA lie in its ability to produce large thermalised ion signals and that the ion chemistry in the tube is well understood. The flow tube is therefore an ideal source for producing large signals of a wide range of different ion types. With appropriate design even ions that have no direct molecular precursor can be formed through multi-step syntheses in the FA tube. As mentioned earlier, three other groups have utilised a FA source with a SIFT, the Smith and Adams group [72], D.K. Bohme's group [73], and the Bierbaum group [74, 75]. The first two of these, though effective, had problems with generating large counts of certain types of ions. The

Bierbaum group redesigned their flowing afterglow to maximise the transmission of ions and to allow multi-stage ion syntheses to be performed, producing a widely applicable instrument. We have followed some of the principles they established.

The ion signal delivered to the SIFT reaction tube depends on a complex mix of factors, the ionisation source, the flowing afterglow geometry, the quadrupole transmission and the Venturi injector. The remainder of this chapter is set out in such a way as to follow the path of an imaginary ion, from formation to detection.

The major design considerations in the construction of Canterbury's FA source were maximising the ion signal for a wide range of ions. The design allows for differing sources of ionisation within the flowing afterglow tube and minimises diffusive losses while retaining the ability to perform multistage reactions to form more exotic ion species. The variable length flow tube, moveable ioniser, and a high speed roots blower pump similar to that utilised by Bierbaum *et al.* [74] enabled us to go some way towards achieving that goal. Ignoring for the moment the method of ionisation, which will be discussed later, the most important consideration in any FA is the ion loss processes. The main loss process for ions in any flow tube is diffusive loss to the walls. The fraction of ions lost to diffusion in the flowing after glow reaction tube at any point z downstream from the ionisation source is described by the following ratio;

$$\frac{[A^+]_z}{[A^+]_0} = \exp\left[\frac{-3.67Dz}{\bar{p}\bar{v}a^2}\right] \qquad (2.1)$$

Here $[A^+]_0$ is initial ion signal $[A^+]_z$ is the ion signal z cm downstream from creation, D is the diffusion coefficient, $\bar{p}$ is the average pressure in the tube, $\bar{v}$ is the average flow velocity, and a the radius of the tube. Thus to maximise ion current transmitted to the quadrupole region, and thence to the SIFT reaction tube, this fraction must be maximised. All the factors apart from D relate to the physical dimensions of the flowing afterglow, and so are design considerations. The diffusion coefficient is a property of the buffer gas and the plasma formed within it. Theoretically one could choose a buffer gas in the flowing afterglow that had a lower diffusion coefficient, but for reasons of purity and reactivity only a few may be utilised, namely nitrogen, hydrogen, argon and helium. The diffusion can theoretically be slowed by the addition of an electron attaching gas, eg SF_6 which converts the electrons to negative ions [72, 76].

In this work however, the addition of SF_6 did not produce a significant advantage in any of the systems studied.

In an afterglow of ions and electrons the positive ions undergo diffusion characterised by the ambipolar diffusion coefficient, D_a [12]. Ambipolar diffusion is governed by the mobility of the electrons that is high due to their small size and mass. The electrons diffuse towards the walls rapidly producing a charge imbalance near the axis of the tube. The plasma's desire for charge neutrality thus pulls the positive ions outward at an enhanced rate. Sulphur hexafluoride has a large electron capture cross section and thus becomes the predominant negative charge carrier in plasmas to which a trace is added. Thus the electrons no longer control the rate of diffusion. The addition of an electron attaching gas should also increase ion signals by reducing the rate of ion-electron recombination, which is about two orders of magnitude higher for electrons and ions than it is for polyatomic negative and positive ions.

From inspection of equation 2.1 it can be seen that a short, wide tube with a high pressure fast flowing buffer gas would produce the highest $[A^+]_z/[A^+]_0$ ratio, thus potentially delivering the greatest ion signals to the FA nose cone, but other considerations prevent the use of such a tube. If we also hope to use the tube for multi-step syntheses then there has to be enough spatial separation between successive inlets to allow for mixing and reaction to occur before the next step. This means that the buffer gas flow cannot be too fast and the tube cannot be too short. The flow velocity is essentially determined by the pumping speed generated by the roots blower providing that the pumping lines between the pump and the flow tube do not limit the flow. As the pumping speed is a measure of the amount of gas moved per unit time, then a higher buffer gas velocity can be achieved by reducing the tube diameter which reduces the "gas load" on the pump. Increasing the pressure in the FA may also create problems in the ion selection areas, as an increased flow tube pressure also results in an increase in the quadrupole chamber pressure thus reducing the transmission of the mass filter. To reduce the transmission of neutral gas from the source flow tube into the chamber the diameter of the exit orifice in the FA nose cone may be made smaller, but this results in a concurrent reduction in ion transmission.

Thus one can see that the physical dimensions are a compromise between several factors in an effort to obtain maximum ion signals for a wide range of ion types. The Canterbury FA source is depicted schematically in Figure 2.4. The flow

tube itself is constructed of 47.5 mm internal diameter (i.d.) stainless steel tubing and can be varied in length between 25 and 70 cm. This variation is achieved by having three modular tube sections, each 150mm long, attached to a single fixed section 250 mm long.

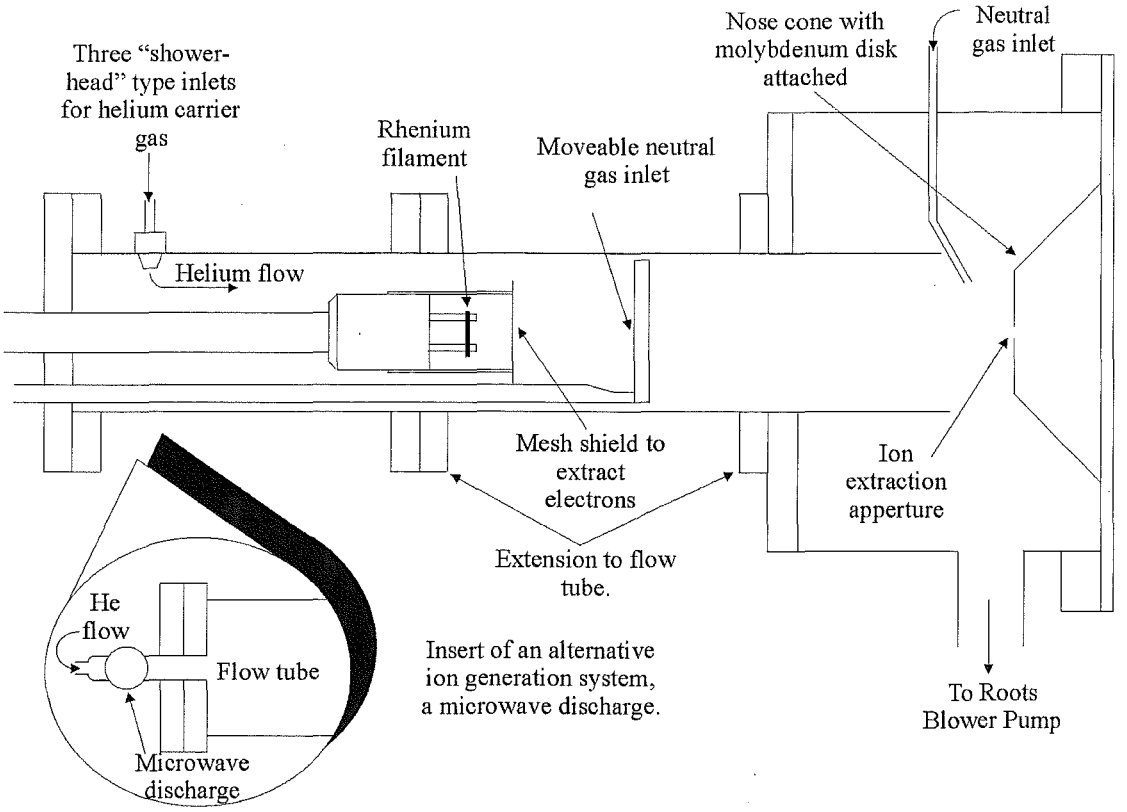

Figure 2.4: A schematic diagram of the Canterbury FA ion source. Also shown are the two most common ion generation methods and the changes in geometry necessary to use each.

All three of the modular sections can be removed, except when the moveable ioniser is in use. In this case at least one section must remain as the helium inlets for the moveable ioniser are mounted in one of the extension pieces. The fixed section of the FA source is made from two concentric pieces of tube; the inner one is the same internal diameter as the modular sections and is the flow tube proper, while the outer one is ~125 mm i.d. and allows for efficient pumping of the carrier gas away from the nose cone. The inner tube extends to within ~50 mm of the nose cone plane providing a region for the carrier gas to be pumped away from the selection region entrance orifice without inducing severe turbulence. This nose cone is also constructed from

stainless steel taking the form of a cone with a 135° internal angle. The end of the cone is blunted to mount a thin (0.285 mm) molybdenum disk that contains the 2 mm diameter hole to the ion selection chamber. The nose cone and molybdenum disk are electrically insulated from the rest of the FA source and the ion selection box and are usually biased to approximately +20-30V. They are not however insulated from each other, a measure which Smith and Adams [72] suggest could give greater transmission, though this modification may be made at a later date.

The FA source is pumped by an Edwards EH 1200 roots blower with an Edwards E2M 80 backing pump (3024 Ls^{-1} for air at 0.3 mbar) connected to the outer tube of the FA source via ~4.85 m of 125 mm i.d. aluminium tubing and ~45 cm of 100mm i.d. stainless tubing. This tubing has bellows sections connected to the gate valves on each end to prevent vibration transmission. Above the roots blower is a Consolidated Electronics 6" pneumatically operated valve. Isolating the FA source from the pumping line is an Airco Temescal FIG 5010-R 4" manual gate valve. The pressure in the FA can be altered within the range 0.1-1 Torr.

§2.2.3: Ionisation Sources

Microwave Discharges

Three sources of ionisation have been used in the FA source during the course of this work, a microwave discharge on a Pyrex tube, a movable electron impact type ioniser and a glow discharge. The microwave discharge is the most commonly used source due to its ease of use, versatility, and cleanliness. Several different microwave discharge tubes have been used in this work, but all consist of a microwave generator operating at ~2.5 MHz, a discharge head and a piece of 12 mm outside diameter (o.d.) Pyrex tube. The carrier gas is passed through the piece of tube which is surrounded by the discharge head just prior to its entry into the flow tube. In the following work two different microwave generators have been used to power the discharge head, an EMS Microtron 200 and an EMS Microtron 200 Mark 3. We have also used two different types of discharge head. Using the terminology of Fehsenfeld *et al.* [77] one is a type 5 cavity with tuneable frequency and coupling while the other is closer to a type 4 cavity with only tuneable coupling. The former cavity was preferred but was at times used to generate atoms at one of the downstream neutral inlets (see chapter 8)

necessitating the use of the other cavity of the FA. Though the microwave discharge is a simple, effective, source of ionisation it does have one major drawback; it generates photons along with the ionisation as a result of forming an afterglow type plasma. Because along the axis of the quadrupole there is line of sight from the FA to the SIFT reaction tube, these photons can pass right through to the SIFT reaction tube where they cause several problems. The Y-shaped entry to the SIFT flow tube prevents these photons from directly reaching the particle multiplier (a problem in early FA instruments). However some photons can generate ions (usually He^+) which react with the neutral reactant to produce spurious ion peaks. In most cases this is not a major problem as the photoionisation signals are much less than those resulting from the injected ions. Signals resulting from photoionisation are easily identified by electrically gating the ions off inside the ion selection box, which obviously has no effect on those ions generated in the reaction tube by photons. However these photon-induced ions can be a problem when the ion signal of a desired ion is low or when nitrogen was used as a carrier gas in the SIFT tube. These photons are also a problem at times during trace gas analysis as the level of neutral 'impurities' in the flow tube is higher due to the admission of environmental air into the tube. In the course of the soil nitrogen experiments (Chapter 3 §3.4.2) a constant background signal at $m/z = 30$ was observed. The signal was not due to direct photoionisation of nitric oxide but was instead a result of reactions involving nitrogen and oxygen atomic ions. In these cases the discharge was placed off axis with a Wood's horn [70] light trap between the discharge cavity and the FA to trap photons and prevent them from being reflected into the FA itself. This arrangement is shown in Figure 2.5.

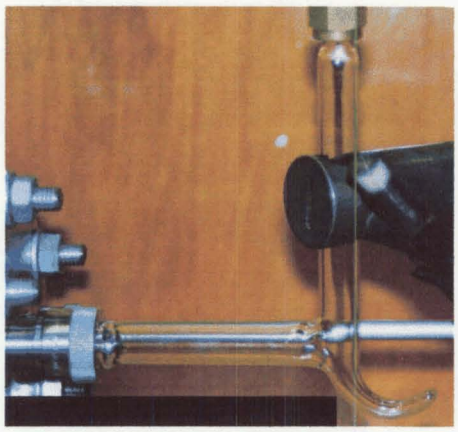

Figure 2.5: A picture of the microwave discharge head and a Wood's Horn light trap on the FA ion source.

Moveable Ioniser

Another available "dark" ionisation source is the moveable ioniser. This ioniser is essentially an electron impact type source mounted on a stainless steel tube, which is in turn sealed into the vacuum by a Cajon O-ring seal. This arrangement allows the ioniser to traverse the length of the flow tube though it cannot pass the moveable inlet without venting the system and disassembling parts of the FA. A schematic of this ioniser is shown in Figure 2.6.

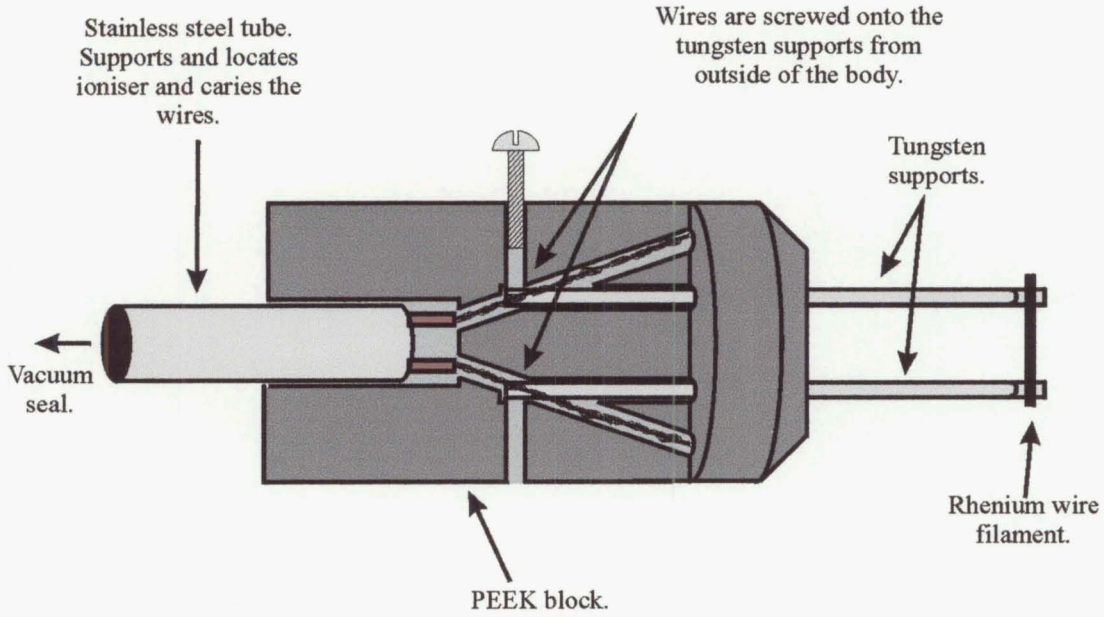

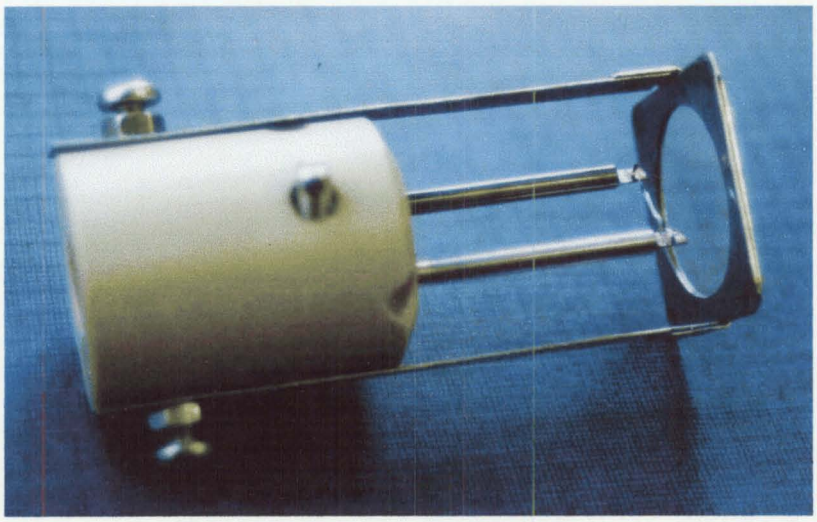

Figure 2.6 A cut away diagram (above) and picture (below) of the moveable ioniser used in the FA ion source.

The main body is made from polyetheretherketone (PEEK), an easy to machine temperature resistant polymer. The filament is a piece of 0.18 mm (0.007 ") thick rhenium ribbon spot welded onto 3.15mm tungsten rods. Current to the rhenium ribbon filament causes heating and it becomes sufficiently hot for the emission of electrons to occur. The current to the filament is supplied by a custom built regulated supply and is typically around 2mA. A fine stainless steel mesh is mounted downstream from the filament. This mesh is grounded and electrons are extracted from the filament by biasing it to approximately -80V which makes the grounded mesh positive with respect to the birth potential of the electrons.

Because the helium is not introduced through the ioniser as in the microwave discharge ionisers, one of the FA flow tube extensions has been modified to facilitate the introduction of helium. This particular extension has three 'shower-head' type inlets evenly spaced around the outside of the tube section 25mm downstream from the upstream end-plate, as shown in Figure 2.4. These inlets direct the helium in all directions and assist in a rapid transition to laminar flow. The modified tube section is of necessity the most upstream of all the sections comprising the FA tube when the moveable ioniser is in use.

Hollow Cathode

The last type of ioniser that has been employed in this work is, at the time of writing, still being refined. This ioniser is a glow type discharge much like a hollow cathode [24, 78, 79]. It is powered by a variable voltage (up to +400V), 50 mA custom built power supply to generate an electrical breakdown between the two cylindrical electrodes. The discharge itself consists of two cylindrical stainless steel electrodes approximately 10 mm apart in a 14mm outside diameter Pyrex tube. The electrodes are placed into the flow of the FA carrier gas in an arrangement much like the microwave discharge. The carrier gas is partially ionised this gas as it passes through the electrical breakdown between the electrodes.

Initial indications, from the measurement of the ion current that reached the molybdenum disk at the end of the SIFT reaction tube, were that the hollow cathode was a very effective source of ionisation. The ion current was about 3 times as much current as any other source (~70 pA to the SIFT nose cone Mo disk). However almost all this ionisation was in the form of He^+ ions and these ions could not be effectively

utilised in the FA. When neutral reactant gases were introduced to the FA, the ions remained mostly He^+ and did not react with the introduced neutrals to any great extent. The ions thus produced were also mostly unaffected by the upstream electrostatic lensing and quadrupole mass filter. This behaviour suggests that the ions formed are very energetic and retain excess kinetic energy through to the ion selection region, despite the large number of stabilising collisions that occur in the FA. The energy imparted to the ions produced by this source effectively negates one of the FA's main advantages, the ability to create thermal ions, and thus this source is impractical in its current form. Altering the distance between the electrodes (and thus the electric field in the breakdown region) may allow the source to produce more thermalised ions as presumably the ions are gaining energy in the region of the glow known as the cathode fall. Currently approximately 200 V are required to maintain the discharge in a helium carrier gas which gives a large field gradient around the electrodes. Further work on the geometry to attempt to minimise this voltage may be beneficial. Greater relaxation of the ions could also be achieved by having a longer, higher-pressure section of flow tube between the glow discharge and the ion selection region and the effects of this also need to be investigated. Despite the current problem, this form of discharge remains a promising source of ionisation.

Two inlets for the neutral ion precursor gas to the FA reaction tube are commonly used. The first is a point source type inlet made from syringe tubing that is ~1 mm downstream from the end of the flow tube i.e. ~ 50 mm from the molybdenum disk. The connection to the MKS 122A-00010AB 10 Torr absolute manometer is in the same plane as this inlet. The second inlet is a backwards facing ring-type inlet [80] which can traverse almost the whole length of the tube, (it is stopped ~30 mm from the upstream end plate) and is a similar design to that on Bohme *et al's* [73] FA-SIFT. This moveable inlet is sealed into the tube with a Cajon O-ring type fitting and its position is able to be adjusted without breaking vacuum to the FA tube. Another inlet (of the point-source rather than ring type) is available 35 mm from the downstream end of the tube section that mounts the helium inlets used with the moveable ioniser. This inlet has not seen much use in the current work due to the fact that the moveable ioniser has not been routinely used.

The newest modification to the flowing afterglow has been the provision of a vacuum lock for the insertion of a heated solids probe. A flange was added to the

outer skin of the FA tube approximately 60 mm (from the centre of the hole) upstream of the plane of the molybdenum disk and a hole drilled through the inner flow tube 20 mm (from the centre) from its end in line with the new flange. The Kratos heated solids probe passes through a vacuum lock mounted on the flange into the vacuum to introduce the vaporised solid directly into the carrier gas stream. This arrangement has allowed the introduction of acceptably large counts of relatively non-volatile molecules such as naphthalene ($C_{10}H_{10}$) (very high counts available), anthracene ($C_{14}H_{10}$), fluorene ($C_{13}H_{10}$), and phenanthrene ($C_{14}H_{10}$). A trace of phenanthrene introduced by this manner with the probe at 130°C is shown in Figure 2.7.

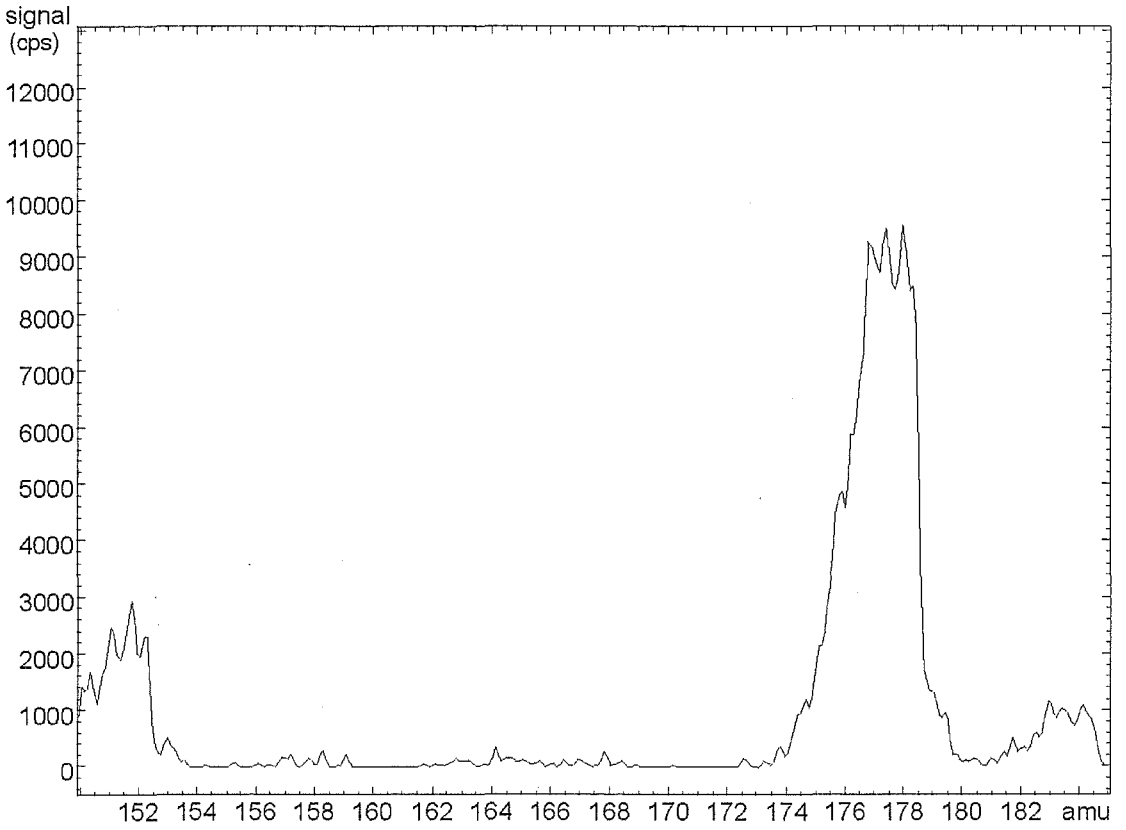

Figure 2.7: A mass spectrum of the ions observed in the SIFT reaction tube after ionisation of phenanthrene in the FA using the heated probe at 132 °C.

Problems with thermal loading of the probe by the helium carrier gas cause the heating controller to not operate quite as designed. As a result the upper temperature limit on the Kratos controller needs to be consistently over-set when temperatures above ~100° C are desired.

§2.2.4: The ion selection region.

The next section of the SIFT that the ions enter is the ion selection region. The ion selection region is a stainless steel box that houses the electrostatic lens arrays and the quadrupole mass filter. It also provides support for the Venturi and the flow tubes. The design considerations for this region are to maximise the transmission and control of the ions with electrostatic lenses while achieving the lowest possible pressures around the lenses and quadrupole mass filter so that the reduction in transmission caused by unreactive scattering of the ions is minimised. The general arrangement (shown in Figure 2.8) consists of three Einzel lens clusters, two upstream of the quadrupole mass filter assembly and one downstream of it.

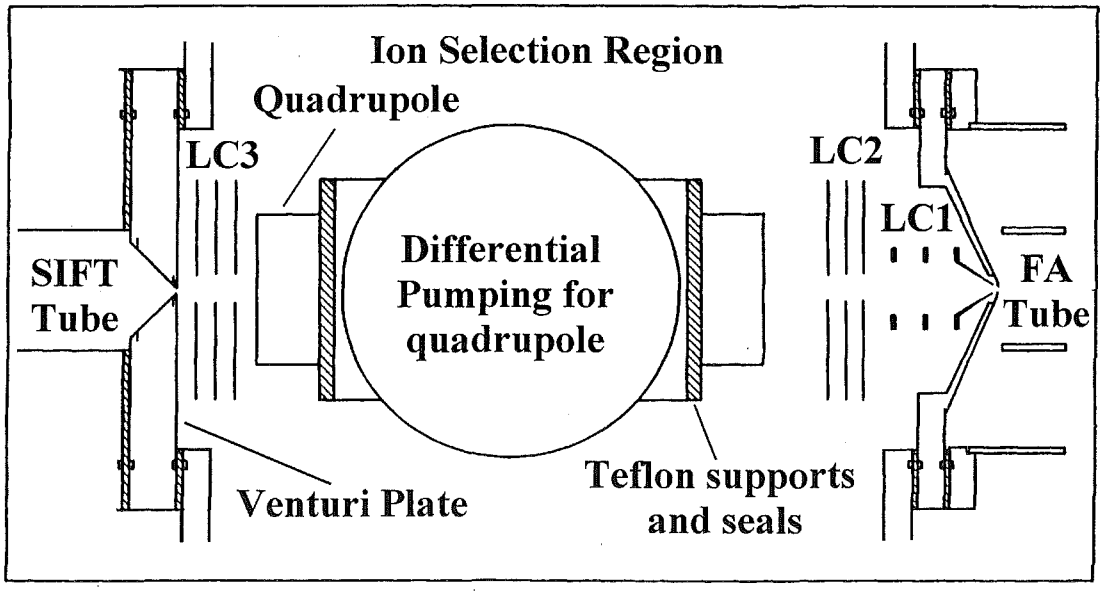

Figure 2.8: The schematic arrangement of the lenses and quadrupoles in the ion selection box.

The stainless steel vacuum chamber housing the ion selection region components is fabricated from 25mm thick steel plate. It is 400 mm long in the direction of flow, 420 mm across and 210 mm high. Because of the reasonably large orifices to both the FA and SIFT reaction tubes (each 2mm in diameter to regions of ~0.5 Torr) the gas load into this chamber is high. Therefore a large, high speed pump is required to maintain a low operating pressure for optimum quadrupole operation. The Canterbury SIFT uses a Varian VHS-400 10" diffusion pump (10,000 ls^{-1} He) backed by a Leybold-Hereaus

Trivac D65B rotary pump (18 ls^{-1}). All diffusion pumps utilise Dow Corning DC 705 silicone diffusion pump oil. The VHS-400 diffusion pump is topped with a custom made liquid nitrogen trap that is of a similar design to the Varian 361 series of cryotraps. The trap is fitted with a louvre-like baffle that means there is no optically direct path from the pump to the chamber. The baffle is thermally connected to the donut shaped liquid nitrogen reservoir to enhance trapping of diffusion pump oil and other condensables. The trap contains approximately eleven litres of liquid nitrogen and has a holding time of approximately six hours. The pump is able to be isolated from the box via a Temescal 10" pneumatic gate valve. This pneumatic valve is connected to the system protection circuit that is described later (§ 2.4.5).

To further improve the operation of the Extrel model 7-270-9 quadrupole, it is differentially pumped by a Varian VHS-6 150 mm (6") diffusion pump (2400 L s^{-1}, air) backed by a Leybold-Hereaus Trivac D30A rotary mechanical pump (12.7 L s^{-1}). This differential pumping is achieved by mounting the quadrupole in a side-arm (a piece of 150 mm (6") stainless steel tubing that projects into the ion source box) and allowing the 150 mm diffusion pump to evacuate the area around the quadrupole rods directly through several ~25 mm slots in the cylindical quadrupole case. Two Teflon supports (one on each end of the quadrupole case) locate it within the side-arm as well as electrically insulating it and proving a rough vacuum seal. These supports are sealed with O-rings to the quadrupole case and are simply push-fitted into the side-arm. Thus most of the pumping power from the 150 mm diffusion pump passes through the area around the quadrupole rods where a lower pressure will make the most difference to performance.

The VHS-6 pump is separated from the quadrupole via a Vacuum Research Company 6" pneumatic valve and a Varian model 316-6 liquid nitrogen trap to the VHS-6 diffusion pump. Problems have been encountered with the Varian trap in that its holding time for liquid nitrogen was only one hour. Most of the experiments reported in this work were made without lN_2 in this trap. Pumping to the quadrupole rods themselves is achieved through several ~25mm wide slots cut into the quadrupole case. These slots allow the full effect of this diffusion pump to reach the regions where lower pressures most improve quadrupole transmission, around the quadrupole rods and the entrance and exit apertures.

A typical operating pressure of ~$1x10^{-5}$ Torr is maintained in the ion selection chamber when ~0.5 Torr of helium is present in each of the reaction tubes. An ultimate pressure of ~$5x10^{-7}$ Torr is achievable with no gas load and after several hours pumping to thoroughly degas all the wall surfaces. The pressure in the box is routinely measured with an HPS cold cathode gauge connected to an HPS model 421 cold cathode gauge microcontroller and a Bayard-Alpert type ionisation gauge also. The differential pumping of the quadrupole assembly lowers the pressure within the quadrupole by about a factor of ten relative to the pressure in the ion selection chamber. The pressure in this side arm is measured using a Bayard-Alpert type ionisation gauge situated at the pump end of the 6" arm. The Vacuum Research Company 6" pneumatic valve is also connected to the protection circuit (see § 2.4.5.).

The Einzel lens system is designed to maximise both the transmission of ions and the pumping efficiency around each lens cluster. To this end the two lens assemblies closest to the quadrupole (labelled LC2 and LC3 in fig 2.8) are made with 36 - 4 mm holes drilled through the stainless steel to make them more transparent to pumping. A central ring of solid material is left around the central aperture to ensure that the electrostatic field is perturbed by the minimum amount. These two lens clusters are of very similar construction, each lens being constructed of 1.6 mm thick stainless steel with a 15.9 mm diameter central hole and an outside diameter of 71 mm. The insulating stand-offs are made of Teflon in both cases and are on a pitch circle of 30 mm radius, however the spacing between each lens is 10 mm in the case of LC2, the cluster upstream of the quadrupole and 22.5 mm in LC3, past the quadrupole. LC1, the Einzel lens system inside the FA nose cone is of quite different construction due its position relative to the FA. Because the aperture in the FA nose cone molybdenum disk is quite large (2mm diameter), the local pressure in this region will be much greater and the need to have fast efficient pumping is accentuated. Most of the ions that will eventually be transmitted by the quadrupole are those that already have trajectories near the central axis of the quadrupole. Therefore it is essential that this near axis path be cleared of gas particles quickly to minimise the losses to unreactive scattering. To this end, the first lens of LC1 is a skimmer type lens that is designed to split the outer component of the neutral flow off and hinder gases further from the axis from diffusing back in. The conical shape also helps get some electric field projection into the region of the molybdenum disk and aids in breaking down the

plasma sheath over the hole in the molybdenum disk. This skimmer lens is 14.7 mm long tapering from an internal diameter of approximately 25 mm at the back to 4 mm at the apex. The plane of the apex sits approximately 2 mm back from the molybdenum disk in the FA nose cone. The remaining two lenses are essentially stainless steel toroids, internal diameter 25.4 mm and external diameter 41.0 mm. These lenses are evenly spaced 19 mm apart from each other (and the front lens of LC2) on Macor™ ceramic stand-offs. The Extrel quadrupole is operated with electrostatic lenses in both the entrance and exit apertures (which are the mounting plates for the ELFS system supplied with the quadrupole, though the system itself is not used).

§2.2.5: The Venturi Injector.

The final electrostatic lens available is the Venturi plate itself. The Venturi plate is able to act as an electrostatic lens as it is electrically isolated from the surrounding plate. This insulation is achieved by placing a thin Teflon disk between the Venturi inlet plate and the mounting flange and Teflon washers under the eight mounting cap screws (for details of the arrangement of the Venturi inlet see section 2.5 later). The holes for these cap screws are also clearanced to prevent the plate and the screws from making electrical contact. Finally, the internal radius of the hole in the mounting plate 0.002" greater than that of the outside diameter of the Venturi inlet plate. Thus, when properly situated, the Venturi plate has 0.001" clearance all around it. One peculiarity of this system is that the Conflat™ seal on the tube side of the Venturi plate cannot be assembled using a copper gasket. The stress involved in tightening the stud bolts down onto a copper gasket causes the plate to deform sufficiently for an electrical short to develop between the inlet and mounting plates. Instead the seal is made using a teflon gasket of similar design to the usual copper one.

The Venturi injector is in some ways the core of any SIFT instrument. It is the component that marries the mass specificity of the quadrupole with the easily defined kinetics of the flow tube. Without the Venturi's ability to prevent backstreaming, the mass selection process could not work efficiently. Details of the performance and

specifics of the standard annulus (or NOAA) Venturi and an alternate hole-based Venturi are given later in this chapter. I will give a brief overview here. Traditionally the SIFT at Canterbury have operated with a type of Venturi that operates by injecting the helium bath gas through a narrow (about 0.001") circular annulus mounted in the wall of a cone that extends outwards from the inlet to the ion source region. This type of inlet is commonly referred to as a NOAA Venturi after the group that pioneered its use [81, 82]. In the upgrade described in this chapter this type of injector was retained but in a modified form. A second annulus was added further downstream in the cone with a radius similar to that of the flow tube. This annulus is much wider than the inner one, at 0.016", and as such is non-critical. This means it does not create a barrel shock like the narrow annulus and does not act as a Venturi injector. This outer annulus is designed to allow the introduction of a larger amount of carrier gas without the problems of turbulence that are sometimes associated with critical Venturi inlets. The flow of gas through the outer annulus should also help speed up the transition from turbulent to laminar flow by enclosing and smoothing the shock cells from the inner annulus [74, 72].

§2.2.6: The Reaction Flow Tube.

The flow tube is essentially the same as that described in Petrie's thesis [68] with the only modifications being those necessary to facilitate the interfacing between the tube and the newly constructed ion source and detection chambers. The upstream Y-piece is stud mounted off the ion source box with the Venturi injector plate mounted off one arm and a blank plate of identical thickness mounted off the other. The plates are sandwiched between the box and the flow tube with an O-ring on the box side and a Conflat™ seal on the tube side.

There are three neutral inlets available into the SIFT reaction tube. The middle inlet, at 71 cm from the plane of the SIFT nose cone orifice, has been modified to enable trace gas analysis to be carried out (see Chapter 3). This ring type inlet is connected via a length of heated ¼" stainless tubing to a bellows valve. The bellows valve is connected to a section of 25 gauge stainless steel hypodermic tubing. This tubing, which is 50 mm long and has a small internal diameter, provides a restriction

to the free flow of gas through it into the tube and is in essence a calibrated leak. The magnitude of this leak has been both theoretically and experimentally determined, details of which can be found in §3.3.2.

The other two neutral inlets are used to introduce neutral gases during reaction studies of ion-molecule systems. The inlet furthest downstream is 83 cm from the SIFT nose cone and the upstream inlet is 44 cm. Both are ring type inlets as described in the work of Upschulte *et al.* [80], with gas introduced in the opposite direction to the carrier gas flow. This design helps to enable rapid mixing of the neutral into the carrier and reduces the magnitude of the 'end correction' [80]. The most downstream inlet is the one usually used for kinetic investigations and the flow of gas through this inlet is controlled by a Duniway Stockroom variable leak valve (#7023, very similar to the Varian valve used further upstream). The inlet furthest upstream has a very similar valve attached, in this case manufactured by Varian and Associates (Model #951-5100). Each valve is set up identically, so as to minimise the dead volume past the leak valve [68]. Pressure measurement in the reaction tube is accomplished by a Baratron™ 10-Torr absolute capacitance manometer (Model #221AHS-A-10) that is attached to the flow tube via a curl of 0.25" copper tubing. This tubing connects to a port upstream from the SIFT nose cone which is placed approximately in the centre of the reaction region and as such reads the average pressure for this region. This Baratron™ can also read the pressure in the glass gas handling line.

The downstream end of the reaction tube has been modified to include a section of flexible bellows tubing to minimise the transmission of vibration from the mechanical pumps to the other components of the system. This bellows is approximately 80 mm long and 148 mm in diameter. A section of stainless steel tube concentric to the bellows but inside it is press fitted into the Conflat type flange that attaches the bellows to the reaction flow tube. This tube has the same internal diameter as the reaction tube and finishes approximately 40 mm from the molybdenum disk of the downstream nose cone. The bellows is bolted to the detection chamber and sealed with two concentric O-rings. The tube has been levelled and squared relative to the support frame using jacking bolts incorporated in the ion source chamber.

Previously the reaction tube was connected to the analyser region by a solid conical shaped piece of stainless steel. This essentially acted as an adapter between

the 77 mm diameter of the reaction tube and the ~150 mm diameter of the cylindrical tee housing the analyser region (i.e. the downstream QMS and the particle multiplier). Because the new FA-SIFT was designed to increase the pumping around the quadrupoles this arrangement has been abandoned and replaced instead with a new analyser chamber (see §2.2.7).

§2.2.7: The drift tube.

A major focus of Dr. David Fairley's PhD. thesis was the installation of a drift tube (DT) into the SIFT and FA-SIFT [71]. The DT allows the collision energy of the ion with the bath gas and the neutral reactant in the flow tube to be varied, a feature that was exploited in this work. The DT is unmodified since its installation by Dr. Fairley and as it is well described in sections 2.2 and 2.5 of his thesis [71] it will not be discussed further here.

§2.2.8: The Ion Analysis and Counting Region

The next section of the FA/SIFDT apparatus is the ion analyser region, containing the SIFT nose cone, the pumping port for the reaction tube blower pump, the analyser quadrupole mass spectrometer, the particle multiplier and the associated diffusion pumps. This is another section of the FA-SIFT that is significantly different from the earlier SIFT. The analyser chamber has been increased in size to allow the blower to more effectively pump away the carrier gas from the front of the nosecone. The size of the nose cone has been expanded and the angle at the front increased to reduce pumping restrictions around the quadrupole mass filter. The pumping in the chamber itself has also been increased by adding a second diffusion pump. The particle multiplier has been moved forward in an effort to increase the detection efficiency. These modifications are all intended to increase the transmission of ions and the sensitivity of their detection.

Physically the analyser chamber is of similar construction to the selection chamber at the upstream end. It is made of 20 mm thick stainless steel plate and is 303 mm in length and breadth and 345 mm high (all dimensions external). The lid is

usually a stainless steel plate and sealed with an O-ring however an interchangeable 25 mm thick perspex lid was used during some of the reaction studies. The perspex lid had no noticeable deleterious side effects. The steel analyser chamber has four ports around the side and one on the bottom (see Figure 2.2 for a schematic); the first of the side ports is the flow tube entry port connected via a bellows section described in §2.2.5. Opposite this is the nose cone entry port. The nose cone is mounted on an 11" ASA flange and enters at the rear of the chamber. The nose cone flange is sandwiched between two Acetal™ plates that electrically insulate it from the analysis chamber on one side and the downstream pumping tee on the other. Each flange is sealed with O-rings and clamped together with studding mounted in blind holes in the chamber. On the side of the analysis chamber closest to the gas handling line a 50-pin vacuum electrical feed-through is mounted which supplies all the electrical connections for the drift tube. Each of the 50 rings in the DT connects back trough this feed-through to the voltage divider. There is also a 2 ¾" Conflat type connector on this face that contains the vacuum feed-through for the molybdenum disk bias voltage. Finally, opposite these feed-throughs is the pumping port for the Japan Vacuum Equipment (JVE) model PMB-020 Roots blower and its model PKS-030 backing pump. This port is 152.4 mm in diameter and has a 6" stainless steel elbow welded onto it. Supported above this elbow is a JVE 6" manually operated gate valve (model VGH-06). The gate valve is connected to the JVE roots blower via approximately 6.6 metres of 6" aluminium tubing and a JVE model VLP-08 high vacuum pneumatic valve. The analysis chamber and flow tube are pumped by the JVE Roots blower pump when helium is flowing, but the manual gate valve is closed when helium is not flowing. The analyser chamber also connects directly to the SIFT flow tube via a 25 mm by pass line and a bellows valve. When helium is flowing in the SIFT reaction this bellows valve must be closed. At other times it is normally left open at all other times to allow the two VHS-4 diffusion pumps to evacuate the analyser chamber.

As stated earlier in this section the nose cone is mounted on studs at the back of the analysis chamber. The nose cone is designed to pare away the helium flow and sample the central section of the ion swarm without inducing turbulence in the sampling volume. The nose cone itself is a 211 mm long piece of 152.4 mm (6") diameter stainless steel tube with a conical section welded on the end. This cone has an internal angle of 126° and ends in an approximately 40 mm diameter circular plate.

A molybdenum disk (diameter 40 mm) is attached to the end plate. The molybdenum disk is screwed into an annular piece of PEEK plastic (38 mm diameter) which fits into a groove in the front of the nose cone and is screwed into the nose cone itself. The PEEK thus acts both as a mounting material and as an electrical insulator as the nose cone and the molybdenum are floated to different potentials. The molybdenum disk contains the entry orifice for the downstream quadrupole, which is 0.46 mm (0.018") in diameter. The back of the disk has been machined out in the vicinity of the orifice to reduce the thickness of the channel that the ions have to pass through. The back of the nose cone front plate has a 9.5 mm diameter hole bored through the centre, the downstream side of which opens out into a cone. This allows the front skimmer lens from the downstream quadrupole to project to within approximately 1 mm of the back of the Mo disk in the SIFT nose cones.

The SIFT nose cone contains the analyser quadrupole which is the reason why the nose cone was made of large diameter (6") tubing. Previously the i.d. of the nose cone was only just larger than the o.d. of the quadrupole case. As the diffusion pumps were (and still are) mounted behind the quadrupole it was thought that a pressure gradient existed between the apex of the nose cone and the rear of the quadrupole. The new lensing and nose cone angle have also increased considerably the area around the tip of the nose cone available for pumping. The area just behind the nose cone orifice is subjected to the greatest gas load and a special effort was made to increase the pumping speed in this region.

To further increase the pumping speed a second 10 cm Varian VHS-4 oil diffusion pump (pumping speed 1,500 L s^{-1} He) was added to the existing Varian VHS-4 diffusion pump. Having two pumps, each with it's own backing pump (Welch Scientific Company Duo-Seal model 1397 two stage mechanical pumps), effectively double the pumping speed of the FA/SIFDT in the analyser region. The two diffusion pumps are mounted together on a 6" Y-piece which is welded to the 150 mm (6") tee that contains the particle multiplier. This tee served the same purpose on the original SIFT.

The Welch backing pumps have been modified in the course of this work. These pumps were manufactured with single phase electrical motors but these didn't have enough torque to reliably turn the pumps over when oil had pooled into the vacuum chamber. This "vacuum-locking" occurred regularly after the pumps had

been sitting idle for a day or more. The single phase motors have been replaced with Jivh Dah Electrical and Industrial Company Ltd 1½ horsepower 3 phase motors which have performed without problem.

The quadrupole mass filter sits inside the nose cone supported on four legs screwed into the bottom of the quadrupole case. These legs are tipped with nylon screws that insulate the quadrupole case from the nose cone and allow the length of each leg to be adjusted independently. The quadrupole is secured into the nose cone via an insulated retaining strap that screws to the back of the nose cone flange. Proper alignment of the quadrupole relative to the hole in the molybdenum disk is essential. Because of the nature of quadrupole mass spectrometers, ions that have a starting position away from the axis of the quadrupole are less likely to be transmitted even if they are the correct mass to have an otherwise stable trajectory. The trajectory of an ion entering the analyser region should also be parallel to the axis of the quadrupole or it may strike one of the rods. To minimise both these undesirable effects it is important that the quadrupole be mounted centrally and square inside the nose cone. In early attempts the quadrupole was positioned so its axis was in line with the nose cone orifice by using a laser mounted off the front of the nose cone. However this procedure was cumbersome and the molybdenum disk was found to not always screw on centrally. We now find it easier to achieve a satisfactory alignment by eye. The legs of the quadrupole are set so as to make the top of the quadrupole case square to a flat surface. The quadrupole is then slid into the nose cone and the legs adjusted until the pinhole of light admitted by the hole in the molybdenum disk is central. To aid in this line up one should look at the ring of reflection that is observed to surround the hole when the assembled quadrupole and nose cone are viewed from the particle multiplier end of the nose cone. The ring is continuous when a satisfactory alignment has been achieved. The reflection has a crescent shape when the hole in not central.

A three-element Einzel type lens system is mounted on the front of the quadrupole to focus the ions into it. The first lens is a skimmer lens like the first lens behind the FA nose cone. This lens is 21.7 mm in length tapering from ~20 mm at the back to a 3 mm aperture at the apex. The tip of the skimmer sits < 0.5 mm behind the molybdenum disk. The next two lenses are the top-hat type lenses that were used in the previous SIFT. These lenses are all spaced approximately 7 mm apart. The

quadrupole has been described by Scott [71] and has one of the ELFS lens supports (the upstream or front one) still mounted as a focusing element.

After mass selection by the quadrupole the ions are detected by a particle multiplier (De-Tech Model 203 for most of the work). The mounting for this is the same as the original SIFT except that the stud length was lengthened during the course of the work to decrease the distance between the quadrupole and the particle multiplier. The spacing has been reduced by 10 mm to approximately 15 mm. The reason for this change was an attempt to detect more of the ions that exit the quadrupole with divergent trajectories. Count pulses from the particle multiplier are passed to an Advanced Research Instruments Company (badged by Modern Instrumentation Technologies Incorporated) model F-100T preamplifier/discriminator, which outputs ~30 ns wide TTL pulses. This in turn is connected to the PCL-812PG lab Card (via 50Ω termination to prevent ringing and the subsequent double counting of pulses) and the home-built pulse counter/ratemeter. The data acquisition and analysis is handled by this computer and has been previously described by Fairley [71] and Scott [70]. The new software for trace gas analysis is described in §3.3.4.

Section 2.3: Standard operating conditions and currents.

§2.3.1: Operating pressures.

Below are recorded a list of 'standard' operating conditions for the injection of a simple ion produced with helium in both FA and SIFT flow tubes. These pressures are for operation without any liquid nitrogen in the cold trap above the 6" diffusion pump and after sufficient pump down period.

Region	Without He flowing	With He Flowing
FA Flow Tube	*As Ion Source Box*	*0.35 Torr*
SIFT Flow Tube	*As SIFT Nose Cone*	*0.50 Torr*
Ion Source Box	*~5x10 $^{-7}$ Torr*	*1.4x10 $^{-5}$ Torr*
Source Quadrupole	*~7x10 $^{-7}$ Torr*	*1.8x10 $^{-6}$ Torr*
Inside SIFT Nose Cone	*~8x10 $^{-7}$ Torr*	*9.5x10 $^{-6}$ Torr*

Table 2.1: Standard operating pressures for the University of Canterbury FA-SIFDT.

§2.3.2: Ion Currents

The ion current at various lenses within the system is commonly used as a diagnostic during tune up to ascertain how well the system is set up. For an O_2^+ or H_3O^+ ion with a count rate of approximately 100,000 cps the appropriate values are:

(A) Quadrupole Lens 1 : 50-70 nA

(B) Venturi plate : 10-15 nA

(C) SIFT molybdenum disk : ~22pA

The labels A, B, and C refer to the points labelled on Figure 2.2.

Section 2.4: Ancillary Systems.

§2.4.1: The Glass Gas Handling line.

When the SIFT was moved from room 126 to room 148, it was decided to rebuild the glass gas handling line rather than attempt to move it. This glass line is

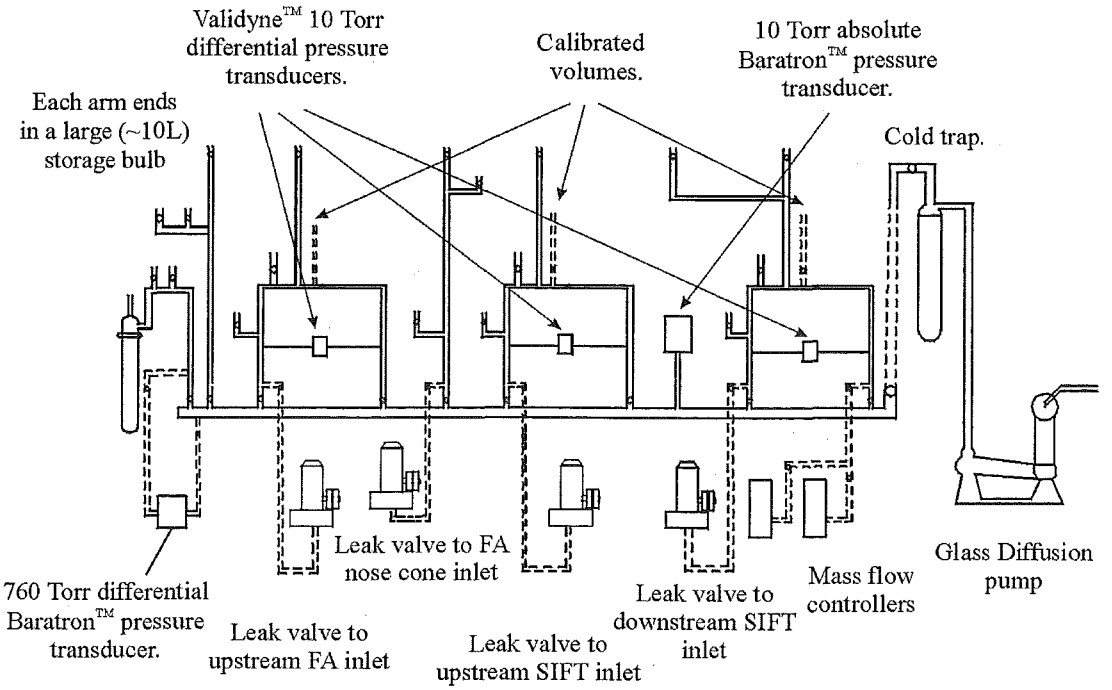

Figure 2.9: A schematic diagram of the glass gas handling line used on the Canterbury FA-SIFDT.

designed to allow gases and vapours to be introduced into the SIFT. The main difference between the current glass line and the previous one is the move from a two manifold system to a single manifold one. The gas line has always been designed in a modular way, with a separate section available for each neutral inlet position along the SIFT flow tube. Each section can be individually isolated from the diffusion pumping (a custom-built two-stage glass diffusion pump backed by a Alcatel model 2004A mechanical pump). The manifold connects the pumps to each section. Reducing the number of manifolds from two to one makes more space available on the gas handling line. A diagram of the basic layout is shown in Figure 2.9 below. The glass flow line and components are mounted on an aluminium tubing framework that is constrained within a steel frame.

Most of the gases used are stored in removable glass bulbs that are connected to the line with B14 ground glass joints. Other commonly used gases, e.g. oxygen, nitrogen, and argon are stored in 5L glass bulbs that are integral to the glass line.

The glass line has essentially been totally rebuilt a second time during my period of study as a result of problems with the original batch of vacuum taps. These G E taps were found to have intermittent leaks through the seal between the key and the barrel, they have subsequently been completely replaced with Kontes or Youngs brand taps.

§2.4.2: The Component Support Frame

The support frame was the only component of the FA/SIFDT that had been completed when I began my studies. Its design and construction where overseen by Dr. Paul Wilson. The frame is constructed of steel box tubing with the flow tube, quadrupoles and associated vacuum cans mounted on top and the diffusion pumps hanging below it. The major components are mounted on wheeled trolleys that sit atop the L-shaped frame. These trolleys are made in two parts with each part having an orthogonal set of wheels. This allows adjustment of the position of the components in the plane. Most of the components are also mounted on four pieces of threaded rod to allow adjustment of height, yaw and pitch.

§2.4.3: Pump Room layout and Backing Line Construction

The original SIFT was not a particularly comfortable instrument to operate. The major problem was the heat and noise generated by the mechanical pumps which were in close proximity to the operator. In the interests of operator comfort all the mechanical pumps for the FA-SIFDT were placed in a separate room. Previously only the JVE blower pump had been so isolated. The 'pump room' is adjacent to the room housing the SIFT and the vacuum lines between the mechanical and diffusion pumps pass through the wall. This arrangement has noticeably reduced the noise and heat around the FA-SIFDT.

All the mechanical pumps used to back the diffusion pumps are mounted on box steel frames via rubber anti-vibration mounts. These frames are bolted to the floor, so the anti-vibration mounts are necessary to prevent vibration transmission to the surroundings. The roots blower pumps are also mounted in this room, again via anti-vibration mounts to steel frames bolted to the concrete floor. The JVE blower and backing pump assemblies have oil drip trays built into the frame. Provision has also been made for oil drip trays on most of the other frames supporting mechanical pumps.

A side effect of this desire for physical separation between the operator and the mechanical pumps is that the vacuum lines between the mechanical and diffusion pumps are necessarily elongated. This extra length presents a problem by reducing the pumping speed of the mechanical pumps to the backing port of the diffusion pump. Long pipes can act as an impedance to flow. A reduction in the pumping speed delivered to the diffusion pump can compromise the performance of the diffusion pump. The impedance of a tube (U) is calculated by Equation 2.2, and the pumping speed (S) calculated using Equation 2.3 [83, 84].

$$U = \frac{\pi D^4}{128 \eta l} \bar{p} \tag{2.2}$$

$$\frac{1}{S'} = \frac{1}{S_0} + \sum \frac{1}{U_n} \tag{2.3}$$

Where D is the pipe diameter, η is the viscosity of the gas being pumped, l is the pipe length, and $\bar{p}$ the average pressure in the tube. S' is the pumping speed after the

restrictions, S_0 the initial pump speed, and U_n refers to the impedence of the individual tube sections. Thus the pumping lines could not contain long sections of restriction and the way to avoid this is to use large diameter tubing. In this work the vacuum lines were constructed from 100 mm o.d. stainless steel tubing with large conductance elbows of the same diameter where necessary. The diameter was only reduced down for the connections to the pumps at each end. These connections are the same line diameter as the earlier SIFT (1½" o.d.). The most restrictive pump line still transmits 70% of the pump speed to the diffusion pump backing port which is sufficient speed to exceed the inlet speed required for the VHS-400 pump to which it is connected. In addition each backing pump line has a glass volume of not less than two litres built into it to prevent oil from entering the pump line proper in the event of a "suck back". Finally all the pump exhausts connect via a manifold that is either connected to the departmental fume cupboard system to prevent the build-up of potentially harmful vapours in the laboratory.

§2.4.4: Carrier gas flow systems for the two flow tubes.

The carrier gas system is essentially the same as described by Fairley [71]. Two molecular sieve towers with cryogenic jackets are situated in the pump room. The two molecular sieve towers allow the independent cryo-scrubbing of the carrier gas supply to the FA and SIFT flow tubes when the need arises. Flow to the FA flow tube is metered via a MKS model 1179A14CS1BV-SPCAL mass flow controller (MFC), which is calibrated for helium and has a maximum flow of 10,000 sccm. The carrier gas for the SIFT flow tube is metered by a Tylan FC 261 flowmeter. Both of these metering devices are only calibrated for helium, though they can be used with other low mass gases, e.g. H_2. When gases other than helium are used the Tylan controller must be manually recalibrated with a bubble flowmeter. Other carrier gases like argon or nitrogen can be metered into either tube via an appropriately substituted MKS 1179A14CS1BV. This is identical to the MFC attached to the FA source (ie 10,000-sccm maximum flow) but it is calibrated for nitrogen.

§2.4.5: The SIFT System Protection Circuitry.

Because the operation of the quadrupoles, the particle multiplier, and the diffusion pumps at elevated pressure can seriously damage them, circuitry designed to prevent their operation when pressures are above the norm have been integrated into the start up control panel. This circuitry includes several 'interlocks' to prevent operator damage to the system. The water must be on and flowing before the backing pumps will operate and in turn the backing pumps must be on before the diffusion pumps or any of the electronic will switch on or the pneumatic valves open. The cold cathode gauge is the pressure-sensing element that triggers if an over pressure occurs. A flow meter in the cooling water lines senses the water flow and temperature sensors are mounted on each diffusion pump. Any elevation in pressure or temperature above a certain limit will shut the pneumatic valves and remove power from the electronics and the diffusion pumps. Note that the system only measures the pressure in the ion selection chamber, so it is possible to have an overpressure in the downstream analysis and detection region without an automatic shut-off.

Section 2.5 Venturi injector performance comparison.

§2.5.1: An introduction to Venturi injectors.

The relative performance of the two most common different types of Venturi injector, the annulus (NOAA) type and the hole (Birmingham) type, has been the subject of discussion in the literature for quite some time and several papers have been published comparing them [82, 85]. The Venturi nozzle is perhaps the most critical component in the development of the SIFT technique in that it allows a quadrupole mass filter to operate in a low pressure region between the higher pressure of the ion source and the reaction flow tube. This selection quadrupole essentially defines a SIFT as it allows ions of a single mass to be transmitted into the reaction tube. The role of the Venturi injector is to facilitate the transmission of ions against a pressure gradient, from the sub-millitorr ion selection region to the flow tube, which typically operates in the region 0.3-0.5 Torr.

The first SIFT constructed by Smith and Adams in Birmingham used 12 1 mm diameter holes spaced evenly around a 20 mm circle [86]. However when a SIFT was

constructed at the National Oceanographic and Atmospheric Administration laboratory (NOAA) in Boulder, a new type of injector was used. This consisted of a single narrow annulus concentric with the ion inlet aperture and set into the wall of an inverted cone that began at the ion inlet aperture. The walls of this cone typically make a 45° angle with the flow axis [81]. In both the hole and annulus injectors the inlet works by having a high flow of gas pass through a small cross sectional area which creates a barrel shaped shock wave. This shock wave is basically a region of much higher local pressure and prevents gas outside it from easily diffusing back into the ion source. The injected ions travel along the centre of the 'barrel' and thus traverse into the flow tube without having to pass a severe pressure gradient.

Without a Venturi injector, gas would flow back from the high pressure flow tube region to the ion selection chamber (known as backstreaming). These carrier gas molecules would have a high velocity in the reverse direction to the ion stream and would thus undergo energetic collisions with the individual ions in this stream. These collisions would not only deflect ions away from the ion inlet aperture but their energy could also dissociate and in some cases isomerise the ions. The increased pressure in the ion selection region would also compromise the performance of the quadrupole. Later Venturi injectors have incorporated a second non-critical inlet with a proportion of the carrier gas flow being diverted through this inlet. The second inlet is designed to minimise the appearance of shock cells, which are areas of pressure disturbance further down the flow tube than the primary barrel shock. These shock cell were identified by Duprerat *et al.* [82] and are likely to markedly increase the unfavourable interactions between carrier gas and ions. The process of injecting an ion against a pressure gradient is always going to be an energetic process and one can only hope to minimise this. It is the comparison of energy transfer during the injection process between the two types of inlet that this next section is concerned with.

The SIFT at the University of Canterbury have traditionally used a single annulus type injector and this has been carried through to the FA-SIFDT, though a second larger non-critical inlet has been added. In the following discussion; the term inlet will be used to refer to a single annulus or array of holes while injector will refer to the combination of two separate inlets, either of hole or annulus type. Two different inner inlets were constructed in the course of this work both of which are shown in Figure 2.10. The annulus inlet is the same as that used for all other work in this thesis

and is constructed of stainless steel, the hole inlet was only used for the comparison presented in this section and was thus made of brass which was easier to machine.

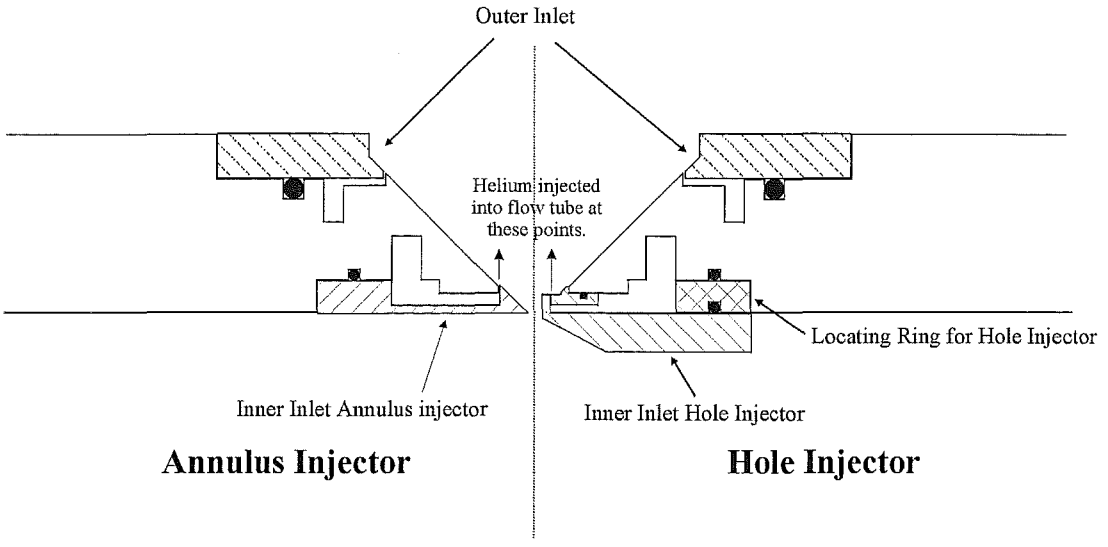

Figure 2.10: The two types of inlet used in this section. The annulus inlet on the left and the hole inlet on the right. The same outer non-critical inlet was used in both systems.

The dimensions of each injector are compared in Table 2.2.

Type	*'Orifice' dimensions (mm)*	*'Orifice' area (mm^2)*	*'Orifice' diameter (mm)*	*'Orifice' to Ion Entrance Aperture Separation (mm)*
Annulus Inner	Annulus width, 0.025	0.695	8.70	3.2
Hole Inner	12 hole, 0.25 diameter	0.695	4.25	3.0
Annulus Outer	Annulus width, 0.4	47	37.1	14.2

Table 2.2: Characteristics of the inlets used in this study.

The cross sectional area for gas injection is identical for both types of inner inlet so some sort of direct comparison should be possible. The performance as a pump or 'Venturi effect' (He), ion transmission efficiency (O_2^+), the transmission of weakly bound cluster ions ($H_3O^+.H_2O$), and the extent of isomeric conversion ($C_3H_5^+$) are

compared for the two different inner inlets, as the partitioning of carrier gas between inner and outer inlet is varied.

The experimental set-up was similar for all the experiments. The appropriate inner inlet was mounted in the injector, and then the helium was introduced at a pressure of approximately 0.35 Torr. The inner and outer inlets (which are interconnected in normal operation) were isolated from each other. In this test, the outer inlet was fed by the Tylan™ mass flow controller (MFC) and the inner inlet was fed by a MKS 10,000 standard cubic centimetres per minute (sccm) MFC. This MFC was the same one that is usually used to control the flow of helium to the FA which necessitated the use of a smaller MKS model 1159B-05000SV-SPCAL 5,000 sccm helium calibrated MFC in the gas line to the FA. As a result the highest pressure attainable in the FA was less than usual. For some of the tests the pressure was lower than ideal e.g. for the termolecular reaction forming the $H_3O^+.H_2O$ ion (Reaction 201) where the reaction rate increases with bath gas pressure.

$$H_3O^+ + H_2O + M \quad => \quad H_3O^+.H_2O + M \qquad (201)$$

In reaction 201, M represents a third collision partner and is most commonly the carrier gas, He. In these cases the FA pressure was raised by 'throttling' the FA blower by partially closing the gate valve between the FA and the blower to limit its pumping speed. The total pressure in the reaction flow tube was generated by adjusting the flow through the Tylan and MKS MFC, i.e. by altering the partitioning of the total flow of carrier gas between the inner and outer inlet.

§2.5.2: 'Venturi' Effect

The 'Venturi' effect or pumping performance of each of the two inlets was assessed. Ideally a Venturi inlet should act in a similar way to a pump pulling gas into the flow tube. At worst it should prevent gas from moving from the flow tube into the ion selection region. To ascertain how effectively each of the two inlets performed this task, all the pumping from the ion selection region (both the 6 and 10 inch diffusion pumps) were closed off using the gate valves. Next helium was run through the reaction flow tube at various partitioning ratios and the pressures in the source and flow tube regions were recorded. The reaction tube pressure was recorded as usual

with the 10 Torr Baratron™ pressure transducer that is attached to the glass line. Note that the ion selection region was never designed to run at the pressures that were achieved during parts of this experiment and we were out of the range of both the cold cathode and the ionisation gauge devices. To overcome this problem the FA was also isolated and the pumping by-pass to the ion selection box was opened, thus allowing the FA pressure transducer to be used to measure the pressure in the ion source box. It was necessary to run the helium for a minute or more when the flow was changed radically to establish stable pressures in both regions.

The results are shown below in Figure 2.11, following the convention of Dupeyrat *et al.* [82] P_1 refers to the reaction tube pressure and P_2 the ion selection region pressure. P_1 was maintained at approximately 0.35 Torr throughout all experiments this pressure corresponds to a flow of ~142 STP cm^3 s^{-1}.

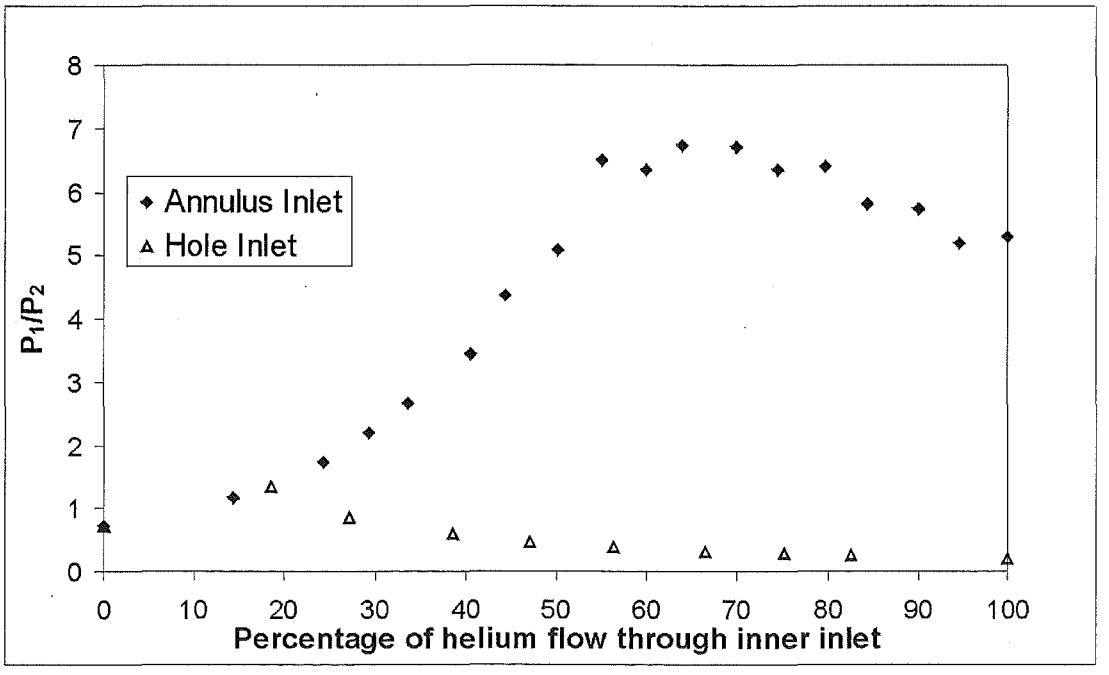

Figure 2.11: The pumping efficiencies of the two inlet types tested as the proportion of the helium passing through them is varied.

The higher the ratio P_1/P_2 then the more effective the inlet is as a pump. The value of the ratio is a measure of how much backstreaming occurs from the reaction tube into the ion selection region. Two things are immediately apparent from the Figure. Firstly the annulus is a more efficient pump and has less backstreaming than the hole injector. The annulus injector has a maximum P_1/P_2 of ~7 while that for the hole

injector is less than 1.5. Secondly, although both the inlets' Venturi effect are markedly altered by the partitioning ratio, the positions of maximum pumping efficiency are at different ends of the graph. The annulus inlet performs quite adequately with all the helium passing through the *inner* critical inlet while the hole inlet requires a significant proportion to be directed through the *outer* non-critical inlet. It is also worth noting the vales of P_1/P_2 achieved by Duprerat *et al.* with their injectors, their NOAA II annulus type injector had a P_1/P_2 ratio of ~5 at ~140 STP $cm^3\ s^{-1}$ (though it increases slightly after this) while their hole injector had a ratio of around 1.2. This is in reasonable agreement with the results seen in the current system.

§2.5.3: Transmission efficiency

In order to gauge the effectiveness at passing ions as the partitioning ratio was altered, a signal of O_2^+ was established and the effectiveness of transmission through each inlet was observed. The O_2^+ ion was chosen as it is easily formed in large number densities simply by allowing a small flow of air to enter a helium afterglow through the inlet directly in front of the FA nose cone. In all cases the helium afterglow was generated by the action of a microwave discharge on the helium carrier gas. The results of this experiment are presented in Figure 2.12. It should be noted that the magnitude of the change in ion signal is normalised to the ion signal achieved when all the helium was passed through the inner inlet. The numbers for the two different experiments thus cannot be directly compared against each other. Both inlets achieved similar magnitudes of ion signal when they were operated at their optimum partitioning ratio.

What can be compared however is the range of ratio that each inlet spans. It is evident that the performance of the hole injector is much more dependent on the outer inlet. The hole injector requires approximately 75% of the carrier gas to pass through the *outer* non-critical inlet to achieve its maximum performance, whereas the annulus injector is at almost peak performance with all the helium passing through the *inner* critical inlet. This result is entirely consistent with the smaller amount of backstreaming found with the annulus injector.

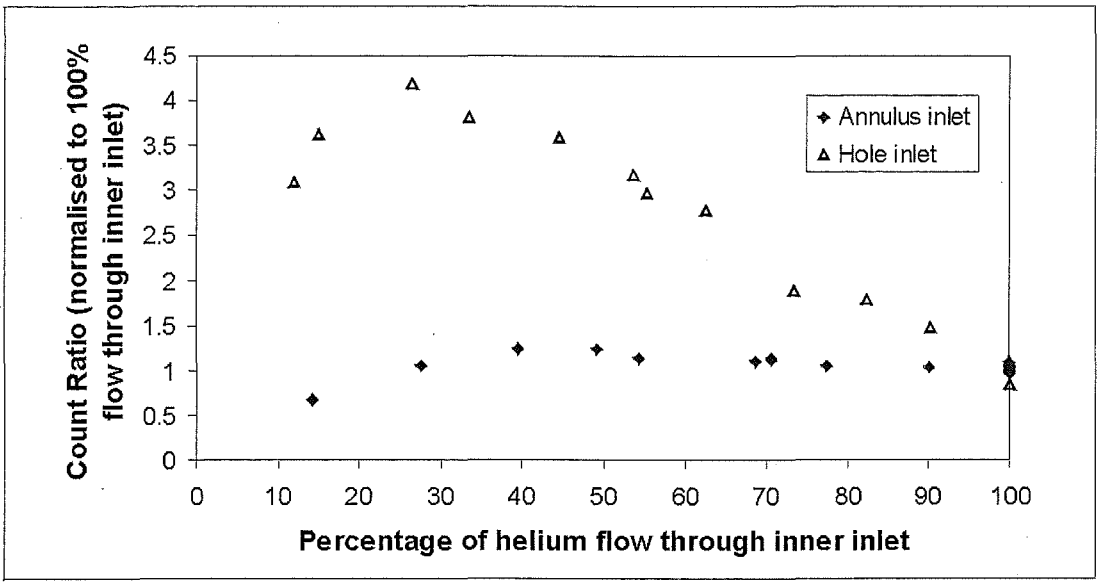

Figure 2.12: The variation in relative O_2^+ ion count with helium partitioning ratio. The count ratio is, in each case, normalised to the O_2^+ signal recorded when 100% of the helium was flowing through the inner inlet.

A comparison should be made at this point between our results and those of Fishman *et al.* [85] who performed a similar experiment with O^+ ions. For their hole type injectors designated Pitt-B, and Pitt-C, they found that their maximum signal intensity correlated with maximum backstreaming. For Pitt-D, which is most like our hole injector, they saw little correlation between transmission and backstreaming. The results of Fishman *et al.* at a glance appear somewhat counter-intuitive, as one would expect ions to be injected most easily when the amount of backstreaming and the associated turbulence in the flow tube was at a minimum. The enhancement in ion signals we observed were similar in magnitude to that reported by Fishman *et al.*, but there was no correspondence between the maximas in the ion signals (i.e. the transmission) and the pumping efficiency in their experiments as there was inthose performed at Canterbury. The reason for this lack of correspondence may lie in the type of ion and ion source used. Unlike our experiment the SIFT used by Fishman *et al.* SIFT used a Brinks type electron impact (EI) source [87] to generate an atomic ion when they performed this experiment. The rise in ion counts observed by Fishman *et al.* may bear little relation to the efficiency of the Venturi at transmitting ions as the performance of their ion source (which is contained within the ion selection chamber

in their system) may alter as the pressure in the ion selection region varies as a result of backstreaming.

§2.5.4: Cluster Ion Dissociation.

The $H_3O^+.H_2O$ ion was generated from a flow of water into a helium buffer gas in the FA. The most effective method of generating this ion was to 'throttle' the blower pump to the FA, raising the helium pressure and thereby increasing the rate of the termolecular reaction which forms $H_3O^+.H_2O$.

$$H_3O^+ + H_2O + He \quad => \quad H_3O^+.H_2O + He \qquad (201)$$

The FA was configured for use with a microwave discharge and at its minimum physical length. Water was admitted through the moveable inlet set at its most upstream position (see section 2.2.2) to maximise the time for Reaction 201 to occur.

The $H_3O^+.H_2O$ ion was extracted from the FA (using a FA nose cone voltage of 22.5V for both inlets), mass selected and injected. The ratio of H_3O^+ to the total counts of the hydronium ion and its first water cluster was evaluated at each flow using the analyser quadrupole.

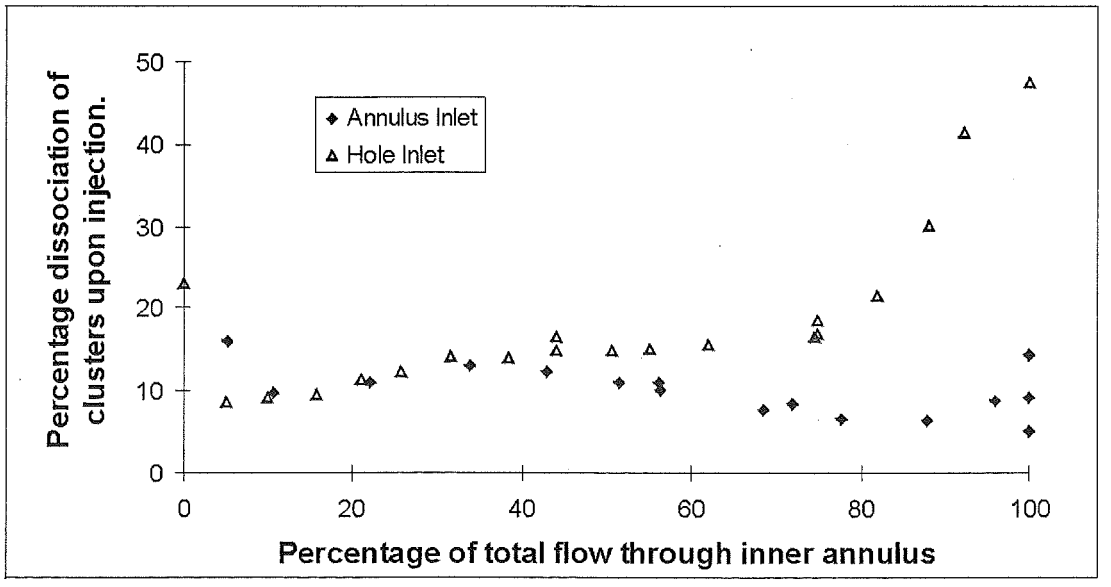

Figure 2.13: The variation in the extent of dissociation of the $H_3O^+.H_2O$ cluster ion with the fraction of the helium passing through the inner inlet.

Again one finds that although both injectors are quite capable of performing the task adequately i.e. injecting the cluster ion with minimal break up, however the variation with partitioning ratio is quite different (see Figure 2.13).

The performance of the annulus injector is relatively invariant in the regions where the pumping efficiency graph (Figure 2.11) indicates the inlet is acting effectively as a Venturi. In this region the maximum dissociation is approximately 12%. The extent of dissociation rises when less than 15% of the helium passes through the inner inlet. The injector is not operating as a Venturi in this region as Figure 2.10 shows that as the ratio P_2/P_1 is below 1 here. The minimum dissociation of around 7% occurs when approximately 85% of the helium flows through the critical inlet which is close to the position of the maximum in pumping efficiency. Above this flow the transmission of both the clustered and unclustered ions begins to drop, though not as much as observed for the hole injector.

For the hole injector however, there is a marked change in the extent of dissociation as the partitioning ratio is varied. Again this change approximately parallels the pumping efficiency, which indicates that the pumping efficiency is a good indicator of the amount of turbulence and shock cells in the flow tube itself. The minimum amount of cluster dissociation (approximately 7%) occurs with around 10-15% of the helium flow directed through the critical inlet. The maximum dissociation level however is now almost 50%, which means that the count rates for the H_3O^+ and $H_3O^+.H_2O$ are essentially equal. However when greater than 75% of the flow was directed through the inner annulus the counts dropped rapidly. In this region, the total signal ($H_3O^+.H_2O$ and H_3O^+)was less than 500 counts per second (cps) dropping further to only several tens of counts above 85%. At the lower percentage flows up to 5000 cps were observed. It is apparent that in the regions where the pumping action of the Venturi is in effect negative, (i.e. the ratio P_2/P_1 is less than 1) the injector transmits ions poorly. Further under these conditions the injection process is a very energetic process in that the cluster ions dissociate. Presumably the increased dissociation is due to the onset of non-laminar flow in the section of the tube immediately downstream of the injector and the formation of shock cells.

The dependence of the extent of dissociation upon the energy of extraction from the FA was also investigated by altering the voltage applied to the FA nose cone. This dependence was only investigated for the annulus injector. It was found that

dissociation could be essentially reduced to zero (<5%) when the FA nose cone voltage was 18 V. However at this lower voltage the ion signal was reduced as the number of ions with sufficient translation energy to traverse the plasma sheath was also reduced. The nose cone voltage of 22.5 V used in the previous experiments was therefore a compromise between sufficient ion counts to give reasonable statistics at most of the flow points measured and the extent of dissociation. In practice when weakly bound species are being injected there is always a trade off between ion signal and the extent of dissociation. This was always a problem in the original SIFT as the initial ion signals were usually lower than in the FA-SIFDT. In the new instrument we can afford to inject at lower energies that result in less dissociation as the initial ion signal from the FA is usually much higher than in the earlier SIFT.

§2.5.5: Isomerisation of $C_3H_5^+$ upon injection; the 2-propenyl and allyl cations.

In addition to the dissociation of ions , discussed in 2.5.3, another indicator for gain of internal energy during injection is the process of isomerisation. The energy barrier to isomerisation on a potential surface obviously varies for different ionic species but it can be quite low for some species. Sufficiently low for the isomer ratio to change as a result of the injection process. The $C_3H_5^+$ ion is such a species, it is known to have two low energy forms, the 2-propenyl and allyl cation. The global minimum on the $C_3H_5^+$ surface is the allyl structure, $CH_2CHCH_2^+$, with the 2-propenyl structure, $CH_3CCH_2^+$, 33 kJ mol^{-1} higher in energy [88]. The barrier between the two species is calculated to be 75 kJ mol^{-1}. Fairley and co-workers [88] showed that it was possible to generate only the 2-propenyl cation in the SIFT flow tube via proton transfer from H_3O^+ to propyne. The formation of a single isomeric structure is a consequence of there being only a small difference in proton affinity between allene or propyne and water. Consequently insufficient energy is deposited in the newly formed ion during proton transfer to surmount the barrier on the potential surface. However when $C_3H_5^+$ was formed in the FA source the ion, after injection into the SIFT reaction tube, was always found to have the allyl structure. Isomeric conversion

from the 2-propenyl to the allyl structure is presumably due to isomerisation using energy gained during the injection process.

The isomeric structures of $C_3H_5^+$ may be distinguished by the rate coefficient for their reactions with methanol. The 2-propenyl cation reacts with a rate coefficient of $1.7x10^{-9}$ cm^3s^{-1} while the allyl cation was found to have a rate coefficient of $7.3x10^{-10}$ cm^3s^{-1}. In the current experiment, the 2-propenyl cation was formed in the FA via the reaction of H_3O^+ with propyne and then injected through both the hole and annulus injector at a range of partitioning conditions and energies (FA nose cone voltages). In all cases the transmitted $C_3H_5^+$ ion was observed to react with methanol in a manner that suggested that it was primarily or exclusively the allyl cation.

The fact that isomerisation occurs during the injection process further emphasises the finding that the injection process is necessarily an energetic one. The isomerism observed here is however not necessarily solely a result of energy gained during the injection process ions may also gain energy as a result of the electrostatic lens in the injector cluster and from the passage from the FA source to the ion selection region. Unlike the $H_3O^+.H_2O$ case, ions that gain energy as a result of electrostatic sources will not be rejected by the upstream quadrupole, as they have the same *m/z* ratio regardless of whether they have been isomerised or not. The properties of this plasma sheath appear to be the most poorly characterised of any element in the FA-SIFT. Investigation suggests that the transition through the sheath will always be an energetic process. However the failure to transmit the 2-propenyl structure only into the SIFT reaction tube doesn't hamper operation of the FA-SIFDT greatly. Ions can usually be formed in the SIFT reaction flow tube by the reaction of a suitable precursor ion and a neutral introduced at the most upstream neutral inlet.

Section 2.6: Reagents and Physical conditions.

Reagents used are as described previously [71] with the following exceptions. Some of the acrylonitrile used was obtained by Reidel de Haan AG. Fluorene, anthracene, and Phenanthrene were supplied by Dr. M. Vala. N-butane and iso-butane (instrument grade) were supplied by BOC gases. Cyclopropane (99%+) was supplied

by Aldrich. Dimethylether (99%+) was obtained from Aldrich. Deuterated ethylene (min 99 atom %) was obtained from Isotec Inc. (Matheson). Sulphur dioxide was supplied by BDH. Allene was obtained from Alphagaz. Propyne was obtained from Scott Specialty gases. Krypton was sourced from Alphagaz.

Carbon suboxide was prepared using a method only slightly modified from that first presented by Miller and Fately [89]. This method is more fully described in Chapter 8 (§8.2.1).

All liquid reagents were purified by multiple freeze-pump-thaw cycles.

The carrier gas most commonly used was British Oxygen instrument grade helium (stated purity 99.99%) though a few reactions used zero grade helium (purity 99.995%). These gases were routinely further purified by passage through a molecular sieve trap immersed in liquid nitrogen. When nitrogen was used as a carrier in the SIFT flow tube, British Oxygen zero grade quality nitrogen was used (purity 99.998%). Further purification was achieved by passage through a dry ice/actone mixture. When hydrogen was used as the carrier gas in the SIFT flow tube, British Oxygen zero grade (purity 99.995%) was also the purity of choice. However due to its intermittent availability, at times technical grade hydrogen was used (no stated purity). For the FA, technical grade H_2 was the most common choice when hydrogen was used as a bath gas.

Collision rate coefficients were calculated using the parameterised method of Su and Chesnavich[114] for reactants with a dipole moment and Langevin theory for those with no dipole moment. Dipole moments and polarisabilities were obtained from the C.R.C. Handbook of Chemistry and Physics [90]. Ion and neutral energetics were obtained from the Posion program [91] and from the National Institute of Standard and Technology Chemistry Webbook [92].

Rate coefficients determined in this work are considered to have an experimental uncertainty of ± 20% for permanent gases and ± 30% for vapours, unless otherwise mentioned. Product distributions are considered accurate to within ± 20%.

Chapter 3

Trace Gas Analysis: A novel use for a Selected Ion Flow Tube.

Section 3.1: An overview of trace gas analysis with the SIFT.

§3.1.1: Introduction.

One of the 'problems' that has often had to be considered in the analysis of SIFT results is the presence of trace impurities in the carrier gas. Indeed it is common practice to pass the carrier gas through a cryo-trap in order to further purify it. In a typical commercially supplied cylinder as used at Canterbury University, these impurities are at the parts per billion by volume (ppb) level. Even at these low levels, in systems where the injected ions react with the most common impurities (nitrogen, oxygen, and argon primarily) they can cause significant interference if they are not filtered out.

It seems likely that the SIFT method for trace gas analysis was born from these observations. Trace gas analysis using a SIFT is, essentially, a new way of using chemical ionisation (CI) to determine the nature of the impurity species in a mixture. Conventional chemical ionisation has been used for at least 20 years now in mass spectrometry to identify the components of both gaseous and liquid mixtures taking advantage of the 'softer' ionisation conditions available as compared to EI. Usually the instrument used for this type of CI has been a standard mass spectrometer with a slightly modified electron impact (EI) source. In many cases these ion sources were capable of operating in both CI and EI modes. So then, why use the SIFT-MS or other SIFT based technique? The great advantage of SIFT-MS is the availability of a single, selectable, ion precursor or chemi-ionisation agent. The SIFT-MS user can tailor the ion chemistry to detect only certain components in a mixture e.g. the trace volatile organic compounds (VOC) in breath or the combustion products in vehicle exhaust.

§3.1.2: Chemical Ionisation vs. Electron Impact Ionisation.

Consider first the reasons why we should desire to ionise trace gaseous components with a CI system. **Both** EI and CI will effectively convert a trace neutral species into an ionic one. This is all that is required for the ions to be effectively characterised and detected by any of a range of mass spectrometric techniques. It is the nature of these ionic species, however, that differentiates the techniques. Conventional EI often suffers from the disadvantage that significant fragmentation of the trace species occurs, especially if that species is a complex organic molecule. The pattern of these break-up, or fragment, ions produced by EI is also often strongly dependent on the energy of the electrons used for ionisation, which can further complicate the spectrum. When the analyte is a mixture of organic compounds the overlap of these individual fragmentation patterns creates an extremely complex spectrum that makes the identification and quantification of the individual species difficult.

By contrast when CI techniques are used instead, the ionisation occurs via ion-molecule reactions, a reaction path that is usually of lower energy than EI (often referred to as 'softer' ionisation). The precursor ions react with the sample via either charge transfer (dissociative or non–dissociative) or proton transfer reaction to give ions which are indicative of the trace species. Even in the most energetic of these systems the amount of dissociation is generally less than that which would be observed should EI be used for the same system. Thus, ionic precursors can be chosen that give products with much less fragmentation, making the identification and quantification of VOC a much simpler task. An example of this is shown in Figure 3.1 where computed mass spectra are compared for EI and CI via charge transfer (O_2^+) and proton transfer (H_3O^+).

In traditional CI mass spectrometry [93] a reagent gas mixture is added to the source at pressures 10^3 to 10^4 times greater than that of the sample to be analysed. This reagent gas mixture will, under EI conditions, produce almost exclusively the ion desired to be used as a CI precursor. Common ionic precursors are sourced from such gas mixtures as pure methane (which produces approximately equal amounts of CH_5^+ and $C_2H_5^+$), 10% N_2O/H_2 mixtures (which produce NO^+) or 10% X/H_2 mixtures (X may be N_2, CO_2, N_2O, CO and predominantly produce XH^+).

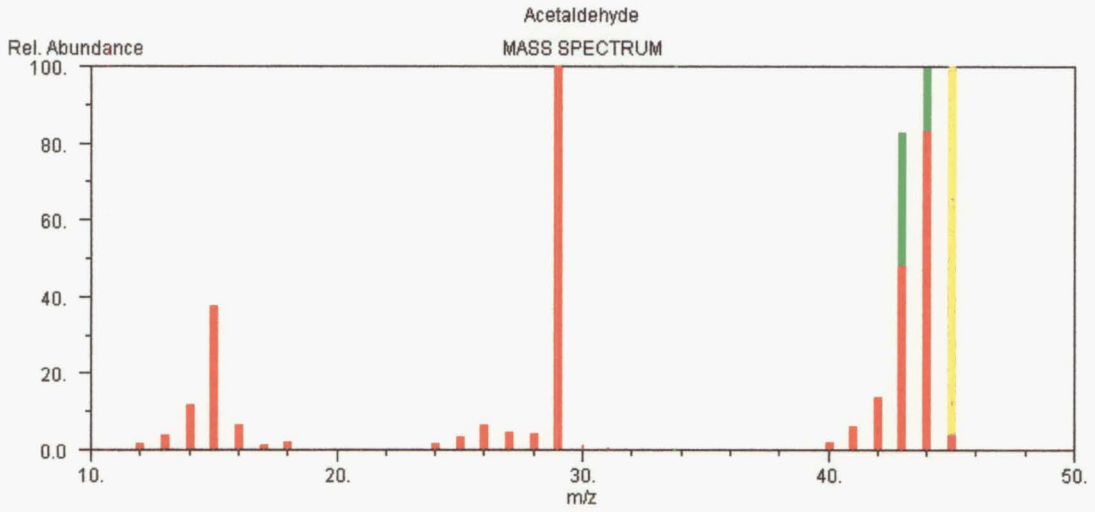

Figure 3.1: A comparison of the observed spectra from EI (red bars) and CI (O_2^+ (green bars) and H_3O^+ (yellow bar)) on acetaldehyde (C_2H_4O). The EI spectra is obtained from data on the NIST web-book [92] and uses 75 eV electrons.

Mass spectrometry, be it CI or EI, has three basic roles: molecular weight determination; structure elucidation; and quantification. In conventional CI the first role is usually achieved through non-dissociative proton transfer giving the MH^+ ion. This usually overlaps with the second role, as a rough determination of the proton affinity of the unknown species when combined with the molecular mass, will often give information about the nature of the unknown. The third role, quantification, is the hardest to perform by any technique. Ideally the unknown is ionised by a known reaction to produce an ion or ions that are not isobaric with any of the other ions produced in the ion source. This is often not achievable, so CI has been combined with gas chromatographic methods to allow separation of the mixture. An internal standard is often added to help correct for any handling losses caused by the separation procedures.

In breath analysis as well as other trace sample analyses, further complications can arise from interference from the sample matrix. For breath analysis this matrix is air and thus any ions that react with the major components of air (N_2, O_2, CO_2, Ar) will be unacceptable precursors, because the secondary reactions of the ions produced with the trace neutral species will have to be considered. Pressure effects further limit traditional CI techniques as MS instruments do not operate at pressures greater than approximately one millitorr. The partial pressure of the actual sample being analysed

is even less due to the excesses of reagent gas required to generate the chemi-ionisation precursor. The physical accuracy limits of MS-based CI techniques are thus quickly encountered. This has led towards a push to attempt to create higher pressure analysis techniques e.g. atmospheric pressure ionisation mass spectrometry [93], or ion mobility spectrometry [94, 95, 96, 97]. However both of these techniques directly ionise the atmospheric sample and consequently the ensuing ion chemistry is complex to model.

The application of SIFT techniques to the analysis of trace gaseous compounds eliminates several of these problems. Due to the preselection by a quadrupole mass filter, the precursor ions are easily varied and extremely pure. In the SIFT techniques the ion source and reaction regions are physically separated and reaction with the ion source gas is thus not possible. These factors simplify the analysis as all ionic products can be regarded as originating from the reaction of a single ion species with the VOC (or other trace components) from the air sample. Selecting a precursor ion which does not react with the major components of air can reduce matrix effects. One can also reduce the problems of interference from isobaric ions by changing the selected precursor ion. This can be carried out on a much shorter time scale in a SIFT apparatus than in a conventional chemi-ionisation system (for which ion source 'memory' effects often cause problems) making SIFT-based analysis a more practical method for structure determination of unknown VOC. The ion reaction region in the SIFT usually operates at approximately 0.5 Torr and is quite distinct from either of the quadrupole mass filters. Therefore higher sample flows can be used safely. This eliminates many of the problems associated with traditional MS-based gas analysis as no sample separation or preconcentration is required. Conditions in the spatially separated reaction region are well defined, which makes accurate modelling and deconvolution of the ion chemistry much simpler. The reaction time can be determined accurately from the known gas velocity, which when combined with the rate coefficient (easily measured for almost any gaseous neutral in the SIFT) gives an accurate measure of the amount of neutral present without the need for any calibration or internal standard.

§3.1.3: Brief Technical Descriptions of SIFT-based Trace Gas Analysis Techniques.

The SIFT is so ideally suited to trace gas analysis that two apparently similar but fundamentally different trace gas analysis and quantification techniques have grown from it. The first of these is the proton transfer mass spectrometry (PTR-MS) technique developed by Lindinger and his co-workers [52, 53, 54, 55]. This technique is most suited to quantification of trace species in environmental air and is not as well suited to the identification of unknown species as SIFT-MS. As the name implies, this technique relies on proton transfer from either H_3O^+ or NH_4^+ to detect the neutral species. The NH_4^+ precursor ion is most commonly used to aid in the separation of isobaric ions from different neutral compounds where the difference in proton affinity between H_3O^+ and NH_4^+ can introduce differences in reaction chemistry. These differences in reactivity can help elucidate the neutral structures. The reason for these choices of precursor ions will be given later (Section 3.2). PTR-MS is built around a flow/drift tube and is capable of quantifying concentrations of certain high-mass organic species down to the level of tens of parts per trillion (ppt) [53]. This high sensitivity is achieved by having a high precursor ion count and by using the gas to be analysed as the carrier gas. A high ion current, approximately a few million counts per second (cps), is achieved by a marriage between a hollow cathode ion source which produces large ion currents and a drift/flow tube which reduces diffusive losses. A schematic diagram of the PTR-MS apparatus is shown in Figure 3.2.

The relative kinetic energy in these PTR-MS experiments, i.e. the energy of interaction between the ionic reactants and the neutrals embedded in the carrier gas, is dependent on the drift velocity of the ions (v_d). This relative kinetic energy is derived from the steady-state velocity achieved when the acceleration provided to the ions by the electric field is matched by the retarding effects of collisions with the neutral [21, 97, 98]. The average kinetic energy acquired from the electric field is a function of the ratio E/N, where E is the electric field strength and N is the buffer gas density. The energy of interaction between ions and reactant neutrals can then be calculated from the well-known Wannier equations (Equations 3.1 and 3.2) [98].

$$KE_{ion} = (3/2)k_bT + \frac{M_B v_d^2}{2} + \frac{M_{ion} v_d^2}{2} \qquad (3.1)$$

$$KE_{cm} = \frac{M_r}{M_r + M_{ion}}(KE_{ion} - (3/2)\,k_bT) + (3/2)\,k_bT \qquad (3.2)$$

In these equations KE_{ion} is the ionic kinetic energy, KE_{cm} is the kinetic energy in the centre of mass frame between ionic and neutral reactants, M_r and M_{ion} are the respective masses of reactant neutral and ion, k_b is the Boltzman constant, and T is the temperature in degrees Kelvin.

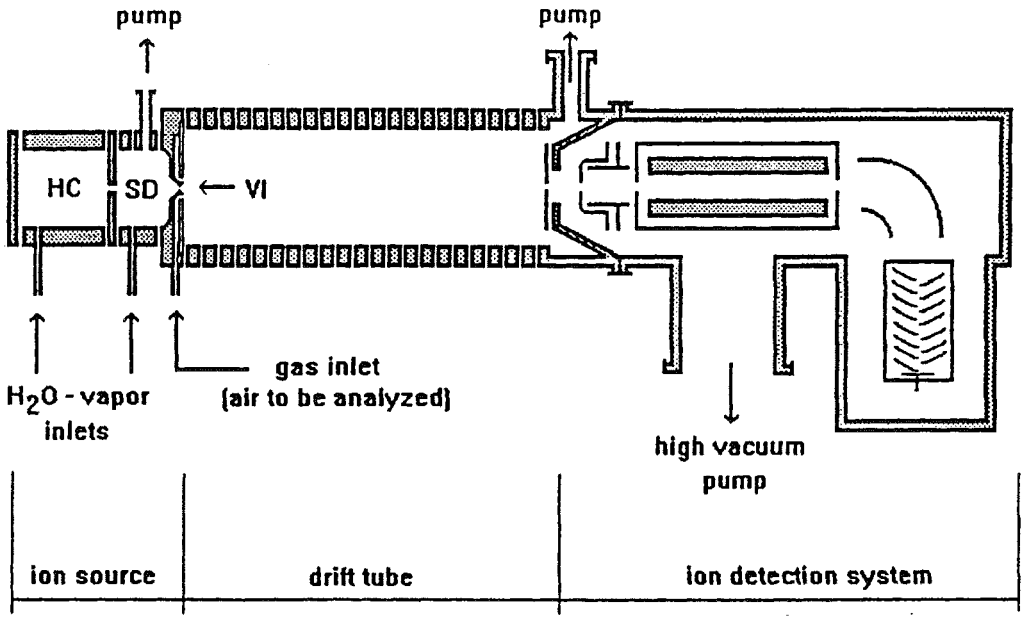

Figure 3.2: A schematic diagram of the proton transfer mass spectrometric method for analysis of trace gas components developed by Lindinger et al. Diagram from Reference 54.

In most cases the Lindinger group uses an E/N value of ~130 Td (1Td = 1 Townsend = 10^{-17} $cm^2V^{-1}s^{-1}$) which gives KE_{cm} values of about 0.25 eV. The Lindinger group maintains that this energy is a compromise between preventing the formation of cluster ions and not excessively promoting any dissociative reaction channels. Cluster ions pose a problem for both of the SIFT-based trace gas measurement systems as they react with the neutrals present but do not necessarily give the same products as the unclustered ions.

The second technique is essentially the method employed at the University of Canterbury. In this Section a broad introduction to the technique will be presented. Specific details pertaining to SIFT-MS at Canterbury can be found in the Experimental section of this chapter. This second method is much more similar to

standard SIFT techniques and has been named *selected ion flow tube mass spectrometry (SIFT-MS)* by its creators David Smith and Patrik Spanel [48, 49, 50, 51]. The mechanical modifications to a FA/SIFT instrument to allow it to perform trace gas analysis by this method are minimal, requiring only the slight modification of one neutral inlet. A small leak of ambient air or breath gas is admitted directly to the flow tube through this inlet allowing the trace components to react with the ions in the flow tube. The flow rate of this leak directly related to sensitivity of the method. The greater this flow the greater the sensitivity of the technique. However, unlike the Lindinger PTR-MS technique where the sample mixture is the flow tube carrier gas, the carrier gas in SIFT-MS is helium. Hence the flow of the sample gas can not be permitted to exceed a few percent of total flow rate in the reaction tube (essentially the helium flow) or it will introduce turbulence into the flow of carrier gas thus altering the ion mobilities and dynamics. The magnitude of this leak can either be variable, using a mass flow controller to measure and stabilise it, or fixed, by using a small length of capillary tube to conductively limit the amount of gas passing into the SIFT. This inlet is a standard upstream-facing ring inlet [80] and is usually placed significantly further upstream than the inlet used in SIFT kinetic studies (~90cm cf. ~45cm for the inlet usually used for kinetic studies at Canterbury). This allows additional time for the ions to react with the trace neutrals and this increases the sensitivity as the ratio $i\{R^+\}/[R]$ is increased. This ratio represents the sensitivity of the technique, the more ions ($i\{R^+\}$) produced per neutral molecule ([R]), the lower the limit of detection becomes for a certain initial ion current. A fast reaction between precursor ion and neutral will also increase this ratio.

Ions are created in a microwave discharge which in the Smith and Spanel instrument acts on a moist air/argon mixture. This allows simultaneous creation of the three ions most commonly used in the technique, *viz.* H_3O^+, NO^+, and O_2^+. Section 3.2 contains a detailed discussion on why these particular ions are used. The ion count is typically of the order of no more than several hundred thousand counts per second, so as not to age the particle multiplier too rapidly. If greater sensitivity is desired (and appropriate ion sources can be engineered) the signal may be increased up to the limiting count of the particle multiplier (~1,000,000 cps). Using the SIFT-MS ion source, precursor ions can be switched rapidly allowing the different chemistry of the

three available precursors to be exploited for rapid product identification e.g. between consecutive breaths.

The major modifications required in converting a standard SIFT to trace gas analysis are in the area of the computer interface. Rapid computer control of the quadrupoles and rapid count collection is vital to the success of the method. The only physical restriction on the time required for data analysis is the flow speed of the carrier gas, which takes about 10 ms to cover the 90 cm reaction length. Thus if the computer is capable of driving the quadrupole across the range of masses rapidly and the pulse counting system is effective, data analysis can proceed essentially in real time, allowing for example the time profile of a single breath to be observed. Figure 3.3 shows the computer control of the downstream quadrupole during the measurement of a single concentration point.

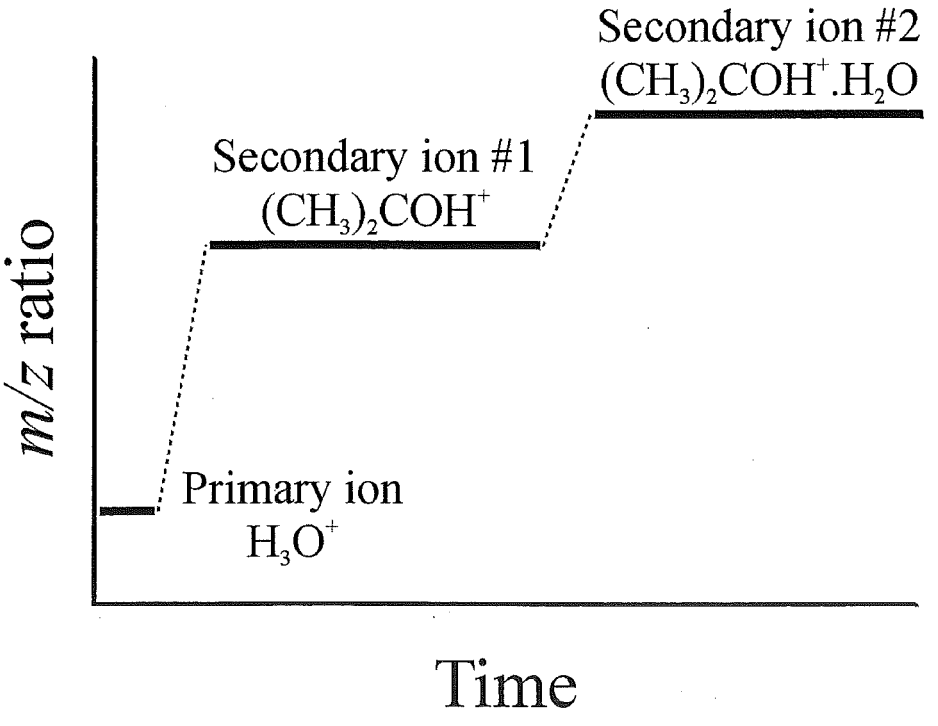

Figure 3.3: A time profile of the 'mass scanning' procedure used at the downstream quadrupole during a trace gas analysis. The example used relates to the measurement of acetone using an H_3O^+ precursor. The ions monitored are the primary (H_3O^+) and the two products ($(CH_3)_2COH^+$ and $(CH_3)_2COH^+.H_2O$).

At each mass in the 'scan' the ion counts are recorded. When the counts of the ionic precursor(s) and all the ionic products of the reaction between the precursor ion(s) and

a single neutral have been recorded, the concentration of that species in the air sample can be calculated.

§3.1.4: On the calculation of the amounts of trace species in air.

The application of the selected ion flow tube to trace gas analysis is essentially a reversal of the usual mode of operation. In normal operation one determines the flow of neutral gas necessary to remove a certain fraction of the initial ion count and by obtaining several such points it is possible to calculate the rate coefficient. In trace gas analysis, the ion counts of the primary (precursor) and secondary (product) ions are still measured but in this case the amount of neutral gas is not known. Instead, provided the rate coefficient is known, one can derive the trace gas concentration from the observed product ion signals. .

As in normal operation, in SIFT-MS the ions are convected along the flow tube in a flow of carrier gas, usually helium, which is moved by the action of a high speed Roots-blower type pump. The velocity of this gas (v_g) can be accurately determined from the carrier gas flow rate Φ_c, the pressure p_g, the tube diameter D_t, and the temperature T_g (K) using equation 3.3.

$$v_g = \frac{\Phi_c}{p_g} \frac{4}{\pi D_t^2} \frac{T_g}{273} \qquad (3.3)$$

The ion velocity however is greater than this carrier gas velocity, due mainly to the effects of diffusion. Under typical experimental conditions this ion velocity (v_i) is around 1.5 times the gas velocity (v_g) [21]. This value has been experimentally determined for the Canterbury SIFT to be 1.50 [71]. The reactant gas, i.e. the trace gas within an air or breath sample, enters the tube at some known finite distance, l, from the sampling nose cone through an inlet in the flow tube. The gas must then mix throughout the carrier gas in order to allow it to react with the precursor ion. This introduces a correction factor as mixing does not occur instantaneously and so the reaction length is usually represented as (l+ε) where ε is an 'end correction'. From this distance (l+ε) and the ion velocity (v_i), a reaction time t can be calculated.

$$t = \frac{l + \varepsilon}{v_i} \qquad (3.4)$$

In the SIFT technique the number density of the ions is always very much less than the number density of the neutrals so that the kinetics are pseudo first-order [21, 48] i.e.

$$\frac{dN_i}{dt} = -N_i k[A] - N_i \frac{D_i}{\Lambda^2} \tag{3.5}$$

Here N_i is the number density of the primary ions in the flow tube, k the rate coefficient for reaction of this primary ion with the trace gas and $[A]$ is the number density of this trace gas. The second term is a diffusion correction term. If one ignores the diffusion term from this equation it can be easily integrated.

$$I = I_0 \exp(-k[A]t) \tag{3.6}$$

Where I is the signal of the precursor ion with the trace species present in the tube and I_0 is the same signal **without** the trace species present. The error introduced by neglecting the diffusion losses is not as great as it would first appear, as both the primary and product ions have this loss. Thus only the differences in diffusion between the two species is important. This difference is usually small in SIFT-MS applications as the precursor and product ion masses, and hence their diffusion coefficients (D_i and D_p), are usually similar. If then the formation of product ion counts (P) is regarded as the only loss process then this value can easily be calculated:

$$P = I_0 - I \tag{3.7}$$

or

$$P = I_0 - (I_0 \exp(-k[A]t)) \tag{3.8}.$$

The ratio of these two values (both of which are measured in a standard trace gas experiment) is then,

$$\frac{P}{I} = \frac{I_o - I_o \exp(-k[A]t)}{I_o \exp(-k[A]t)} \tag{3.9}$$

and therefore

$$\frac{P}{I} = \frac{I_o(1 - \exp(-k[A]t)}{I_o \exp(-k[A]t)} \tag{3.10}.$$

This equation in turn simplifies to:

$$\frac{P}{I} = \frac{1 - \exp(-k[A]t)}{\exp(-k[A]t)} \tag{3.11}.$$

When $k[A]t << 1$ (note rate coefficients are always less than ~5 x 10^{-9} cm^3s^{-1}) Equation 3.11 above can be further simplified to

$$\frac{P}{I} = k[A]t \tag{3.12}.$$

Note that strictly I is the **initial** precursor ion count (prior to reaction with the trace species), however experimentally it is recorded after reaction. This places an experimental limit on the levels of trace gas that can be analysed using the SIFT-MS technique as the precursor ion should not be depleted by more than 10%. Equation 3.12 can be modified to account for differential diffusion to Equation 3.13,

$$\frac{P}{I} = k[A]td_p \tag{3.13}$$

where d_p is the differential diffusion correction term. Note that this differential diffusion term can also be determined theoretically [48] but is experimentally usually close to unity for the reasons that are noted above. Equation 3.13 can be rearranged to give the number density of the trace gas. When this new equation is expanded to allow for multiple ionic precursors and products it can be expressed as;

$$[A] = \frac{1}{t}\frac{\sum_{1}^{n} P_n}{\sum_{1}^{n} I_{in}k_n d_{pn}} \tag{3.14}.$$

Where P_n represents the ion counts of the nth product and I_n represents the ion counts of the nth precursor ion, and k_n is the rate coefficients for the reaction of nth precursor with the trace gas. For this analysis to be valid, one must make the assumption that the primary ion count is not significantly decreased by reaction with the trace gases, i.e. it is assumed that I_{in} approximates the initial precursor ion count. This assumption places an upper detection limit on the technique. Also note that the correction for any possible secondary reaction is simple, the ion products of the secondary reaction are simply included in the sum of the product ions. There is thus no need to know a rate coefficient for the secondary process as the secondary reaction cannot create or destroy ions. To calculate the partial pressure of the trace gas (p_a) we need to know the flow of the carrier, Φ_c, and the flow rate of the 'leak' to the atmosphere, Φ_s.

$$\frac{p_a}{p_{atmos}} = \frac{[A]k_bT}{p_{tube}\dfrac{(\Phi_c + \Phi_s)}{\Phi_s}} \tag{3.15}$$

Here the ratio p_a / p_{atmos} represents the partial pressure of the trace gas under study and k_b is the Boltzman constant. Taken together Equations 3.14 and 3.15 are the heart of calculating partial pressures from the SIFT-MS technique.

Section 3.2: The Chemi-ionisation precursors.

§3.2.1: The function of the chemi-ionisation precursors.

The choice of ionic precursors used for trace gas analysis is one of the most critical factors. In order to be useful as a precursor, an ion species must react rapidly with the trace species while not reacting at all, or at worst extremely slowly, with the major components of atmospheric air or breath i.e. N_2, O_2, CO_2, Ar and to a certain extent water. Ideally the reaction process should be a simple one, giving ionic products that will allow unambiguous identification of the VOC. One early system used Xe^+ ions [55] which have an ionisation potential (IP) of 12.13 eV, less than the IP's of all the major air constituents except oxygen (IP = 12.07 eV). Kr^+ and Hg^+ [49] have also been used as chemi-ionisation precursors and this technique has been applied to a commercial instrument. These precursors are not ideal however as they will react with some of the major atmospheric gases, Reactions 301 and 302 are the main examples.

$$Xe^+ + O_2 \Rightarrow O_2^+ + Xe \quad (301)$$
$$k = 1.1 \times 10^{-10}\ cm^3s^{-1}$$

$$Kr^+ + CO_2 \Rightarrow CO_2^+ + Kr \quad (302)$$
$$k = 6.0 \times 10^{-10}\ cm^3s^{-1}$$

The trace gas analysis system developed by Smith and Spanel uses three separate precursor ions. Having three possible chemi-ionisation agents allows not only accurate quantification of VOC but also aids in the identification of these trace species. In cases where interference from an isobaric ion prevents accurate quantification with one precursor, switching to a different chemi-ionisation precursor will often solve the problem.

An example of this is the analysis of isoprene (in the possible presence of methanol) with a H_3O^+ precursor [99]. Reaction 303 gives a product at $m/z = 69$ exclusively, making for apparently easy identification of isoprene. However when Reaction 304 occurs concurrently, the protonated methanol product can further cluster with two water molecules from the air to produce another $m/z = 69$ product also. The reactions of higher hydronium ion hydrates, $H_3O^+.H_2O$ and $H_3O^+.(H_2O)_2$, with methanol will also contribute to this interference. These higher hydrates are always present in H_3O^+ analyses due to the termolecular association of the hydronium ion with moisture in the air or in breath samples.

$$H_3O^+ + CH_2=C(CH_3)CH=CH_2 \Rightarrow C_5H_9^+ + H_2O \quad (303)$$
$$k = 1.5 \times 10^{-9}\ cm^3s^{-1}$$

$$H_3O^+ + CH_3OH \Rightarrow CH_3OH_2^+ + H_2O \quad (304)$$
$$k = 2.5 \times 10^{-9}\ cm^3s^{-1}$$

To avoid an overestimation of the quantity of isoprene present in a sample, O_2^+ is the precursor of choice for isoprene analysis rather than H_3O^+. Molecular oxygen ions charge transfer to isoprene, giving the molecular ion at $m/z = 68$ and dissociative products at $m/z = 67$ and 53, masses to which no other known VOC makes a significant contribution.

The following sections will discuss the reason for the choice of these particular ions and their common modes of reactivity. Smith and Spanel have begun to develop an extensive library of the reactions of these three ions necessary for trace gas analysis. So far the neutral species studied have included a range of alcohols [100], aldehydes [101], amines [102, 103], aromatic and aliphatic hydrocarbons[104], aromatic and aliphatic halocarbons [105, 106], carboxylic acids [107], ethers [108], esters [107], ketones [101], organosulphur molecules [109], sulfides [110], and thiols [110].

§3.2.2: H_3O^+ precursor ions.

The most common mode of reaction for protonated water ions is proton transfer. Water has a well defined proton affinity (PA) of 691 kJ mol^{-1}, which is greater than that of any of the major components in air [111] (see Table 3.1) so it will not transfer a proton to any of these species.

Major air components	Proton affinities (kJ mol^{-1})
H_2O	691.0
CO_2	540.5
N_2	493.8
O_2	421.0
Ar	369.2

Table 3.1: The relative proton affinities of the major species present in environmental air or breath. Values from Reference 111.

However, relative to most organic species (with the exception of a few small hydrocarbon species) water has a low PA, so that reaction with these species via proton transfer is possible. An interesting peculiarity of proton transfer reactions is that when they are exothermic they almost always proceed at or close to the collision rate [112, 113]. This fact has simplified the determination of the rate coefficients necessary for trace gas analysis considerably as in most cases Smith and Spanel have injected all three ions and assumed that, where energetically allowed, the H_3O^+ reaction proceeds at or close to the calculated [114] collision rate [102]. It is necessary to make the assumption of collision rate proton transfer as many of the VOC studied are derived from liquids with low vapour pressures and thus cannot be introduced into the SIFT easily at accurately measured flows. In most cases this proton transfer is non-dissociative, that is the product of the reactions has a *m/z* value of M+1 where M is the neutral VOC mass. Thus the use of H_3O^+ is a relatively simple method for accurately determining the molecular mass of a species as the $\{M+1\}^+$ ion is usually the highest mass ion observed. The H_3O^+ ion is often used as the first resort for mass determination of an unknown species. However, H_3O^+ is essentially unable to detect alkanes containing less than six or seven carbon atoms because of their low PA.

H_3O^+ however does react with water, albeit by slow sequential association reactions, to give $H_3O^+.(H_2O)_n$. SIFT-MS analysis of humid air or breath will give cluster ions of up to n=3. These association reactions can introduce some errors into concentration determinations as they represent an additional primary ion loss process. They also often react via a switching type mechanism [99] introducing additional ion products into the mix. These effects can be partially corrected for by including the primary and product hydrates into the respective ion count totals but this slows the data analysis and introduces uncertainty as to whether all relevant ions have been included. Smith and Spanel now perform the initial studies for each new neutral in the presence of varying levels of water [58, 99] to ensure that these effects are adequately accounted for.

Some functional groups are exceptions to this generally simple reaction mode of H_3O^+. Reactions with aliphatic alcohols are one example, where the loss of a water molecule is a common reaction course. Reaction 305, where C_3H_7OH is 1-propanol, is an example of this.

$H_3O^+ + C_3H_7OH \Rightarrow C_3H_7^+ + 2H_2O$ [0.90] (305a)

$\Rightarrow C_3H_9O^+ + H_2O$ [0.10] (305b)

Certain aldehydes and carboxylic acids also display a similar channel e.g. 1-pentanal, 1-hexanal, and butyric acid. Another exception to these generally simple proton transfer reactions is that some small amines give NH_4^+ as a minor product, which can complicate the simultaneous analysis of ammonia concentrations with H_3O^+. In practice however H_3O^+ is a poor choice for ammonia analysis as the presence of the large adjacent $m/z = 19$ peak from the primary H_3O^+ ions interferes significantly with an accurate determination of the number of counts in the $m/z = 18$ channel. Certain halogenated compounds have been shown to eliminate the corresponding halogen acid. Sulfides and thiols show a marked propensity to associate with water, although this is often in competition with proton transfer. Finally, ethers often show hydrocarbon 'elimination' where one of either R or R' is eliminated as a neutral from the R-O-R'H^+ intermediate. The unique reaction processes that occur when certain functional groups are present in a molecule are often useful in determining the nature of the VOC under study.

§3.2.3: O_2^+ Precursor ions.

The O_2^+ chemi-ionisation agent is used as often as H_3O^+. As mentioned earlier it is the reagent of choice when isoprene is to be detected in breath and is also the preferred ion for the quantification of ammonia. Thus the O_2^+ ions sees use in many of the routine breath analyses. The reactions of O_2^+ are characterised by charge transfer, often dissociative, as O_2^+ has an ionisation potential (IP) of 12.07 eV, significantly greater than most VOC. In smaller, less complex molecules a non-dissociative channel is often observed, as is the case for extremely stable molecules like aromatic compounds. The reaction rate coefficients of O_2^+ are in the most part, like those of H_3O^+, close to the Langevin collision rate, though the very low mass hydrocarbons provide notable exceptions.

The 'cracking-pattern' given by O_2^+ chemi-ionisation can, in combination with a molecular mass determination using H_3O^+, be used to determine which structural isomer of a compound is present. An example of this from the literature is

2-pentylamine and 2-methylbutylamine, both amines having the molecular formula $C_5H_{13}N$ [103]. Their respective structures are shown in figure 3.4.

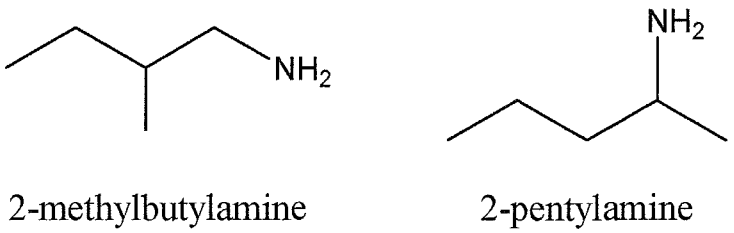

2-methylbutylamine 2-pentylamine

Figure 3.4: The structures of two $C_5H_{13}N$ isomers, 2-methylbutylamine and 2-pentylamine.

Both of the structures react with H_3O^+ to give mass 88 and 18 ions, $C_5H_{11}NH_3^+$ and NH_4^+ respectively with only slightly different branching ratios. Their reactions with O_2^+ however reflect the difference in the structures. 2-methylbutylamine predominantly produces $CH_2NH_2^+$, eliminating C_4H_9 via cleavage between C-1 and C-2 (the carbons α and β to the amine group). 2-pentylamine on the other hand produces $C_2H_4NH_2^+$, which again represents cleavage at the bond between the carbons α and β to the amine functionality.

§3.2.4: NO^+ Precursor ions.

The reactions of NO^+ are characterised by one or more of three possible channels, charge transfer, termolecular association, or hydrogen atom abstraction. Nitric oxide has an IP of 9.26 eV which is significantly lower than that of O_2^+. Accordingly when charge transfer is possible from NO^+ it is less energetic and therefore less dissociative than the corresponding charge transfer from O_2^+.

When charge transfer is not possible the other products are often seen, but not always. NO^+ is a less ideal precursor ion for many VOC as it does not react with all of them. This non-reaction is most marked for the smaller VOC. Analysis using NO^+ is further complicated by the fact that NO^+ can retain internal energy, The higher energy states are not effectively quenched by helium but are, however, quenched by air. NO^+ precursor ions produced from a microwave discharge acting directly on a dry air carrier are ideal for trace gas analysis. An example of the effect of internal energy on the products of NO^+ reactions can be found in the paper by Fairley *et al.* [115] who show

that internal energy can open up previously endothermic charge transfer and dissociative charge transfer channels.

H-atom abstraction is predominantly seen for alkanes, aldehydes, amines, ethers and alcohols and a similar process resulting in an HNO_2 product is observed for some carboxylic acids. A process similar to this latter one results in the formation of RNO_2 neutral products with some esters. Halogen atom abstraction is also seen in some halogenated aromatic and aliphatic species. The association products are most common when the neutral reactant is a ketone

Section 3.3: Experimental considerations.

§3.3.1: Modifications to the SIFT apparatus.

The only significant modification necessary to perform trace gas analysis with the University of Canterbury's flowing afterglow selected ion flow tube using the SIFT-MS technique was the modification of the middle neutral inlet. The minimal number of modifications required was partly due to the fact that the Canterbury SIFT already possessed an ion source capable of producing high ion counts in the form of the FA. The ion count requirements may present problems for other more conventionally designed SIFT apparatuses, requiring a re-design of the ion source section. The middle ring-type inlet was previously attached to the glass gas-handling line via a variable leak valve but this attachment has been completely removed. Instead a length of ¼" stainless steel tube now runs from the ring inlet back to a bellows-type on/off valve. This valve connects to a 50 mm length of 25 gauge (0.01" i.d.) stainless steel capillary tube that conductively limits the magnitude of the 'leak' from ambient air into the SIFT. The whole assembly is heated to approximately 130°C with resistive heating tape. This elevated temperature prevents deposition of water and trace species onto the tubing walls.

§3.3.2: Capillary flow rate calibration.

The flow (or leak) of the air sample into the flow tube is conductively limited by the small piece of capillary tubing open to the atmosphere. This provides a high

restriction to flow into the tube that is constant and reproducible as long as the pressure on both sides of it remains reasonably constant. The magnitude of this 'leak', though small, provides some restriction to the sampling time that is possible from vacuum tight closed containers.

The value used for the sample flow in the following work has been determined experimentally using the capacitance manometers usually used to measure flows for kinetic investigations. The largest available calibrated volume was used and the inlet connected to the glass line by way of a short length of plastic tubing. The flow was measured with and without helium flowing in the reaction tube, but the small difference in pressure between the two methods was found not to make a significant difference (as would be expected from the applicable equations, see below). The flow value thus determined was 3.4 ± 5% Torr L s^{-1}. The actual average of all the flows thus determined (3.351 Torr L s^{-1}) was entered as the flow through the capillary in all the following work.

Calculation of the sample flow rate using Equation 3.16, Poiseuille's law, and Equation 3.17 yields 4.28 Torr Ls^{-1} which is slightly higher than the experimentally determined value [83, 84]. This suggests that there is a small additional restriction in the capillary.

$$U = \frac{\pi R^4}{8\eta L}\bar{p} \qquad (3.16)$$

$$Q = U \times (p_1 - p_2) \qquad (3.17)$$

Here U is the conductance, Q the throughput, R the radius of the tube and L its length. The viscosity of the gas passing through the restriction (air in this case) is η and $\bar{p}$ is the average of pressure p_1 (atmospheric) and p_2 (tube pressure). The experimental result here is obviously the more accurate, as only small differences in the syringe tube from the ideal would affect the result greatly. As such the degree of agreement between theory and experiment is heartening.

§3.3.3: Reaction length determination.

The reaction length for the trace gas inlet also needs to be determined before trace gas analysis and quantification can be performed accurately. The physical

distance between the plane of the trace gas inlet and the molybdenum disk is approximately 73 cm but the effective reaction length is quite different from this. In this case the ε correction factor not only accounts for the physical mixing distance but is also used to correct for several other factors which arise because the drift tube is installed in the flow tube. The drift tube insert is approximately 67 cm long and has an internal diameter of 60.3 mm as opposed to the 73.2 mm i.d. of the main flow tube [71]. This means that the end correction (ε) must also account for a ~6 cm-long section of the tube which has a different internal diameter and the possible occurrence of turbulence at the point where the flow tube diameter changes.

To establish the correction factor several calibration reactions (whose rate coefficients are well known) were performed. The correction factor is obtained by comparing the physical length to the reaction length required to get the literature rates for the calibration reactions. The usual calibration reaction of $Ar^+ + O_2$ was used at a pressure of 0.470 Torr (close to the standard trace gas mode operating pressure) and a reaction length of 94.6 cm was determined. A separate determination at 0.370 Torr found a reaction length of 100.0 cm, an increase of 5.7% from the higher-pressure regime. This result confirms that the end correction is at least partly the result of turbulent flow in the reaction region, as the other factors included in ε should be pressure insensitive. Reactions 306 and 307 were also evaluated using both the upstream trace gas inlet and the downstream 'kinetics' inlet with similar rate coefficients being obtained at both inlets.

$$H_3O^+ + CH_3OH \Rightarrow CH_3OH_2^+ + H_2O \quad (306)$$

$$k = 2.5 \times 10^{-9}\ cm^3\ s^{-1}$$

$$N_2^+ + H_2 \Rightarrow N_2H^+ + H \quad (307)$$

$$k = 2.0 \times 10^{-9}\ cm^3\ s^{-1}$$

The reaction of $H_3O^+ + HCN$ was also investigated but problems with adsorption on to a new section of glass tubing prevented accurate rate coefficient determination in this case. Small effects from this problem were also seen in Reaction 306, although they did not affect the rate coefficient significantly in the latter case. The SIFT-MS technique as a whole has been validated by Spanel and co-wokers [51] using a motor driven syringe to provide a constant flow into a stream of gas.

§3.3.4: An introduction to the trace gas analysis program suite.

The programs used for trace gas analysis data collection and analysis at the University of Canterbury are, like those designed for kinetic investigations, written in Borland Pascal™ by Patrik Spanel. In the following section I will give a short introduction to the two programs that are used for trace gas analysis, the *Multitrace Recorder*, and the *Multiscaling Mass Scope*. For a similar introduction to the kinetics suite see the PhD. Thesis of Fairley [71].

The program that sees most use during trace gas analysis is the *Multitrace Recorder*. This program 'scans' the downstream quadrupole mass filter in the manner shown in Figure 3.3, thus counting both the precursor and product ions. The nature of this scan is determined by selecting the appropriate trace species and precursor from the "Select Molecules" dialog found in the "Options" pull down menu. This option accesses the H3OP.txt file that contains all of the data required for data collection and concentration determination of the desired species. An example, for the monitoring of acetone with an O_2^+ precursor is shown below.

```
acetone(O2+)
 1 precursors
  32 2.8e-9 1.0
 2 product
  43 1.0
  58 1.0
```

The first line contains the title that will appear in the list of molecules available. The third line has the mass of the precursor ion, followed by the rate coefficient for reaction between the precursor ion and the neutral. The last entry on this line is a multiplicative factor that allows correction for either differing diffusion rates for different ion masses or for mass discrimination by the analyser quadrupole. The products are then entered - 43 and 58 represent the mass of the two products formed

in this reaction. They are again followed by correction factors as in the third line. In most of the work presented in this chapter the correction factors were 1.0 as there was essentially no mass discrimination from $m/z = 19$ up to approximately $m/z = 100$. When the "acetone(O2+)" line is selected in the "Select Molecules" dialog it will place masses 32, 43, and 58 into the mass programmer function. This function can be called up by pressing the F6 key and allows the operator to fine-tune the position of the peak maximum. It contains all the masses to be counted.

Pressing the space bar starts a trace first bringing up a box which allows the parameters for the trace to be set. The "sample flow" box contains the flow through the capillary which is usually unchanging at 3.351 Torr L s^{-1}. The "ppm" box is an on/off flag and determines whether the program displays the concentrations (as ppm or ppb) or the raw number of counts. The "time primary' and "time products" are the amount of time for which the precursor and product ions are counted respectively. Normally these are set at 2e-2 seconds for precursor ions and 0.2 seconds for the products, though a time on the products of 0.15 s is often used during breath analysis to allow better time resolution during each breath. The "Points" box is the number of experimental points that are displayed at one time i.e. how many points will be taken and stored before the system begins to over-write earlier points. Files can be saved storing all currently viewed points, and later retrieved using the "File" pull down menu. In order to get ppm values from a retrieved file the ppm tag must be set to 1 in the "Analysis" dialog in the "Options" pull down menu and the correct molecule(s) must be selected. If this is not done only the raw number of counts will be displayed.

The *Multitrace Recorder* is designed for the quantification of known molecules and is the most accurate available method for doing this. However, when the gas sample contains unknown species, a mass scan is needed to ascertain at what mass(es) the products are. The *Mass Scope* program included in the kinetics suite could be used for this, but as the peaks from trace elements are invariably at low levels this program is not always ideal. With the original *Mass Scope* it is often hard to determine whether a particular peak is noise or real. In order to help the operator in making this decision a different program is usually used to make these mass scans.

The program of choice is *Muliscaling Mass Scope*. With this program several traces can be performed and the average of all these traces displayed and recorded. Signal averaging in this way should reduce the magnitude of all 'noise' counts as

noise counts should not be present at the same position in successive scans. The averaging procedure will therefore reduce the magnitude of each noise count. Products, even small ones, should be present on each scan and thus averaging will give an accurate indication of how many counts are present in a product channel. The number of traces to be averaged is set in the "Scan MS" window with the "Multitrace" setting. Other than this all the settings are identical to the kinetics suite *mass scope program*. Mass scans are usually viewed on a semi-logarithmic plot in trace gas analysis to enable small products to be seen easily. The *Mass Scope* will display a semi-logarithmic plot if the control and enter keys are pressed concurrently or if "Log Scale" is selected from the "View" drop down menu.

Section 3.4: Results.

The results presented in the following sections are preliminary with most of them being relatively recent pieces of work. This is not an indication that trace gas analysis has been undertaken at the University of Canterbury only in the last year or so, but instead it is an indicator of the learning curve that several researchers here have collectively traversed. The following results show that, at least for simple trace gas systems, analyses have become routine and that there exists a promising future for trace gas analysis using the University of Canterbury FA/SIFDT.

§3.4.1: Breath Analysis.

Among physicians there are many individuals who are known for being able to 'smell' a particular disease. In uncontrolled diabetes, where blood levels of acetone can soar, a fruity sweet smell is often observed on the patient's breath [116]. This is a telltale indicator to doctors able to smell acetone at low levels. Observations similar to these have been made since the time of the ancient Greeks, yet in order for breath testing to be an effective diagnostic tool, analytical techniques must be able to progress far enough to take the element of the "trained nose" from the equation.

At the alveolar interface only a thin layer separates the air in the lungs from the blood in the surrounding capillaries. VOC will diffuse from the higher

concentration region to the lower. This diffusion will occur from the blood to the breath in cases such as ingested alcohol, or vice versa in situations where atmospheric VOC concentrations are high e.g. where large amounts of volatile solvents are used. This two way interface is obviously necessary in order for the lungs to function and it means that the breath can be used as a simple, rapid, test for the presence of trace compounds in the blood.

Even those VOC originating in the blood may have different origins: some are directly ingested compounds e.g. ethanol from alcoholic drinks or sulfide compounds from garlic [53], some result from the degradation of ingested compounds in the digestive tract e.g. methanol from the digestion of fruit pectin [52]; while others are formed by metabolic pathways, e.g. pentane from lipid peroxidation [48, 117]. In many cases a VOC observed in breath will have multiple formation pathways contributing to the observed concentration. However when a disease process takes place it is possible for the breath concentration of certain VOC to alter markedly and provide a gaseous indicator to the disease. Medical science already uses several breath tests to monitor certain conditions, especially diseases of the stomach, intestine and colon.

One example is the bacteria *helicobacter pylori* which is strongly implicated in the formation of peptic ulcers and chronic gastritis [116]. One of the enzymes present in this bacteria is a urease, an enzyme which is not usually present in humans. Urea introduced to the body will be metabolised by the urease, producing carbon dioxide. If the urea is ^{13}C-labelled the ratio of $^{13}CO_2/^{12}CO_2$ in the dosed patient's breath will be radically changed and this can be detected. There are commercially available modified MS or GC-MS apparatus that are designed to carry out this task.

Why then is breath analysis not used more commonly in diagnosis? It would seem an ideal technique as it is non-invasive, painless, and in almost all cases breath is an abundant, easily available commodity. In the past the main problem has been the sampling of the breath. GC-MS usually requires preconcentration step(s) to remove the major air components, in many cases sampling the sum of several breaths. This trapping has some inherent problems, the greatest being that it discriminates against some compounds, however for most GC-MS processes it is a necessary evil. Two trapping methods are commonly used in breath sampling, cryogenic and adsorptive trapping. In cryogenic trapping the breath passes through a section of tube that is cooled, usually by immersion in liquid nitrogen, which captures the volatile

breath sample. All in all the SIFT is ideally suited for the analysis of breath, from either human or animal subjects.

A typical breath trace is shown in Figure 3.5, this trace shows the gases ammonia, isoprene, acetone, using an O_2^+ precursor and is an example of the output from the *Multitrace Recorder*.

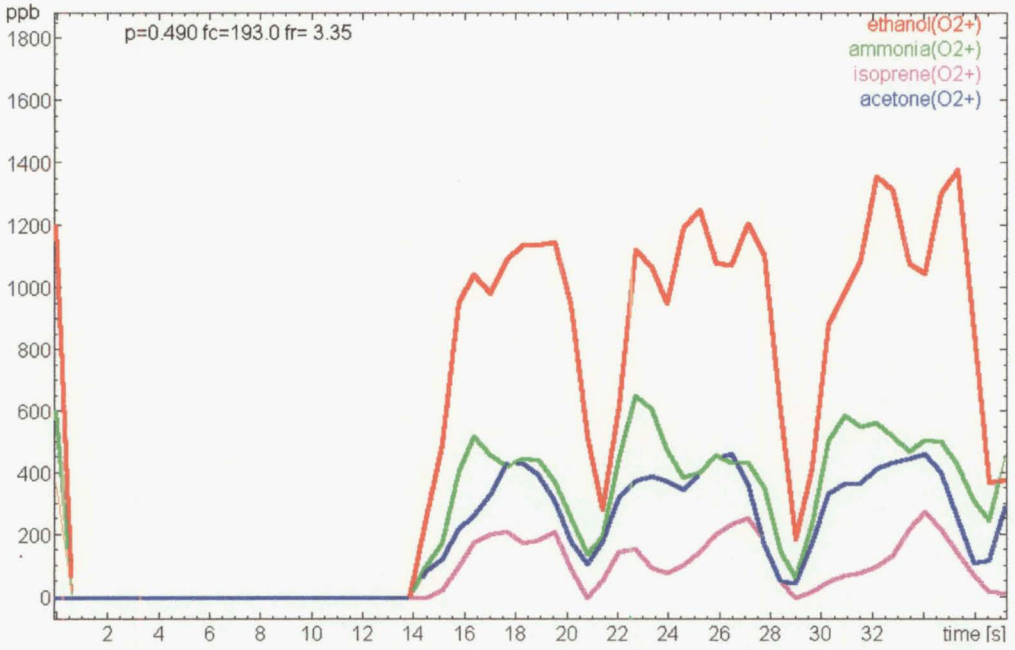

Figure 3.5: An example of a standard breath trace from a human subject. This trace shows the output of the Multitrace Recorder operating in ppm = 1 mode (see section 3.3.4 for an explanation), analysing breath for ethanol (red), isoprene (purple), ammonia (green), and acetone (blue) some time after a subject has had an alcoholic drink. The values are in parts per billion.

The rapid sampling time of the SIFT-MS technique means that time resolution within a single breath is possible and the rise and fall present on each breath in the ppb trace above represents a genuine physiological effect. Only the air in the base of the lungs, the so-called alveolar air, is in equilibrium with the blood and in each breath there is an amount of air that is sitting in the upper respiratory tract which is expelled first. This 'tidal' air receives trace gases by diffusion from, and mixing with, the alveolar air thus the concentration of trace species rapidly increases as the expired air is sourced from deeper in the respiratory tract. The concentration then reaches a steady state representing the alveolar concentration. Then as inhalation begins this level is diluted as external air is drawn into the mouth.

Two specific examples of applications for SIFT-MS to the analysis of trace gas components in breath will be shown. Both are still in the investigative stages at present but the results presented adequately show the potential of the technique.

§3.4.1.1: Changes in the major trace gases on breath during exercise.

This work was inspired by results presented in a 1998 paper by Lindinger, Hansel and Jordan [53]. Two traces were presented showing the levels of isoprene and acetone in the breath of a single human subject who cycled at a moderate rate for approximately four hours. In this time the breath acetone level was observed to rise sharply, continuing to rise until a sugar solution was fed to the subject. The breath isoprene level dropped soon after the start of the exercise and remained low throughout returning to a level similar to the initial one very soon after the termination of the exercise. An initial spike in the isoprene concentration was also observed over a short time scale, perhaps ten minutes.

It is of interest to know whether these effects show up in all humans and/or whether there are significant variations with factors like diet or fitness. With these questions in mind we proceeded to conduct the monitoring of several subjects undergoing physical exercise in two separate experiments. Although this work is not yet complete the results presented here demonstrate the applicability of the SIFT technique to sports physiology and give some tantalising hints that the whole story has not been told by the experiments of Lindinger *et al.* [53]

Acetone

The **first experiment** was performed with nine subjects, seven of whom ran around the campus (returning to the laboratory at approximately ten to fifteen minute intervals for sampling) and two of whom cycled on static resistance devices. Unfortunately, mainly due to pre-existing injuries, only five of the runners actually completed the targeted amount of exercise (approximately one hour) and this seriously limits the conclusions that can be drawn from this study. The trace species ammonia, acetone, and isoprene were observed before, during, and after exercise for these five subjects and an O_2^+ precursor was chosen. The results for ammonia show a degree of experimental scatter which is much greater than for either of the other two

trace species. This is probably due to the breath sampling method employed. As the sample inlet is routinely operated at ~130°C each athlete was provided with a piece of polyvinylchloride tubing that, once pushed onto one side of the trace gas inlet, provided a room temperature interface. Each athlete used their own single tube throughout the experiment and it appears that these tubes gained a background level of the more polar trace species (ammonia, and (to a lesser extent) acetone). Thus the values recorded represented not only the endogenous production of these species but also included an exogenous source as well. This effect manifests as experimental scatter. The more recent experiments have used disposable breath tubes (actually pieces of standard plastic (polyethylene) drinking straws) and the subjects are instructed to draw breath back through the straw as they inhale. These measures seem to minimise the build up of trace species on the walls of the sampling tube and provide more reliable levels for breath ammonia. A similar effect was seen to an even greater extent in another experiment where the sampling tube was left attached to the inlet throughout the experiment. The problem was extreme enough in this case that large droplets of water were observed in the PVC tube. As can be seen in Figure 3.6, a pattern is visible in the isoprene trace but the ammonia and acetone traces have so much "noise" superimposed on them that no clear pattern can be discerned.

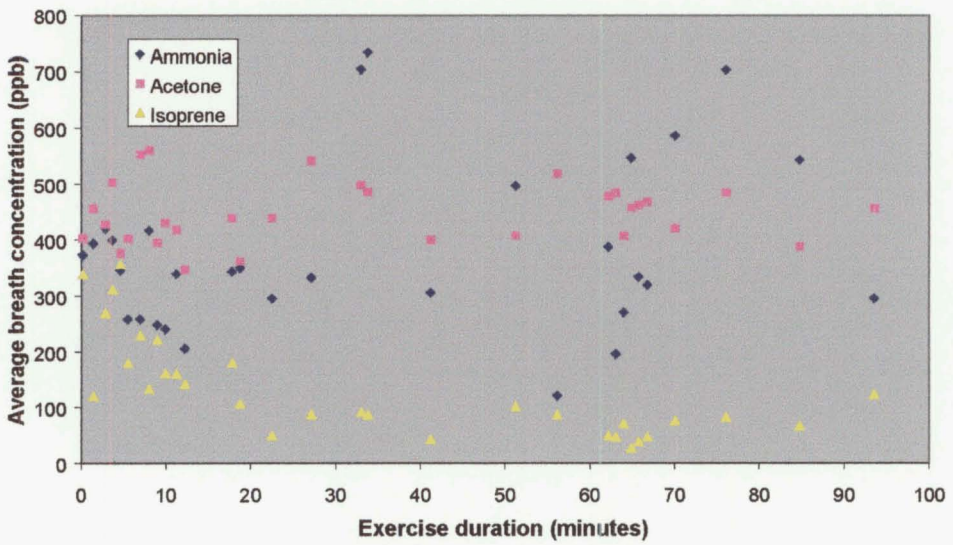

Figure 3.6: A plot of concentration versus time for ammonia, acetone and isoprene on the breath of a subject cycling on a stationary bicycle. Note the pattern visible in the variation of isoprene levels but the almost random scatter of the acetone and isoprene results, this is due to problems with adsorption onto the walls of the sampling tube.

The initial breath acetone levels in the subjects were between 100 and 600 ppb, a range that is quite normal for healthy subjects [59]. Acetone production in the body is a complex subject as it is strongly diet dependent. The overall feeding level of the body will affect acetone levels, which rise by factors of two to three as the body becomes starved [59]. The ingestion of garlic has also been shown to dramatically increase breath acetone levels [53]. Given the short time scale of the experiment, these dietary effects are unlikely to affect the acetone concentration during the experiment. In most cases, once exercise was started the acetone concentration in the subject's breath remained at the same level as measured prior to the commencement of the exercise for an induction period before it began to rise. Neither of the cyclists showed any rise, which is probably related to the insufficient amount of exercise that they performed during the test. The results from a selection of the subjects (who all exercised for approximately equal times) are shown in Figure 3.7. It can be seen that the patterns for acetone rise are different but that all subjects show a rise in acetone near the end of exercise.

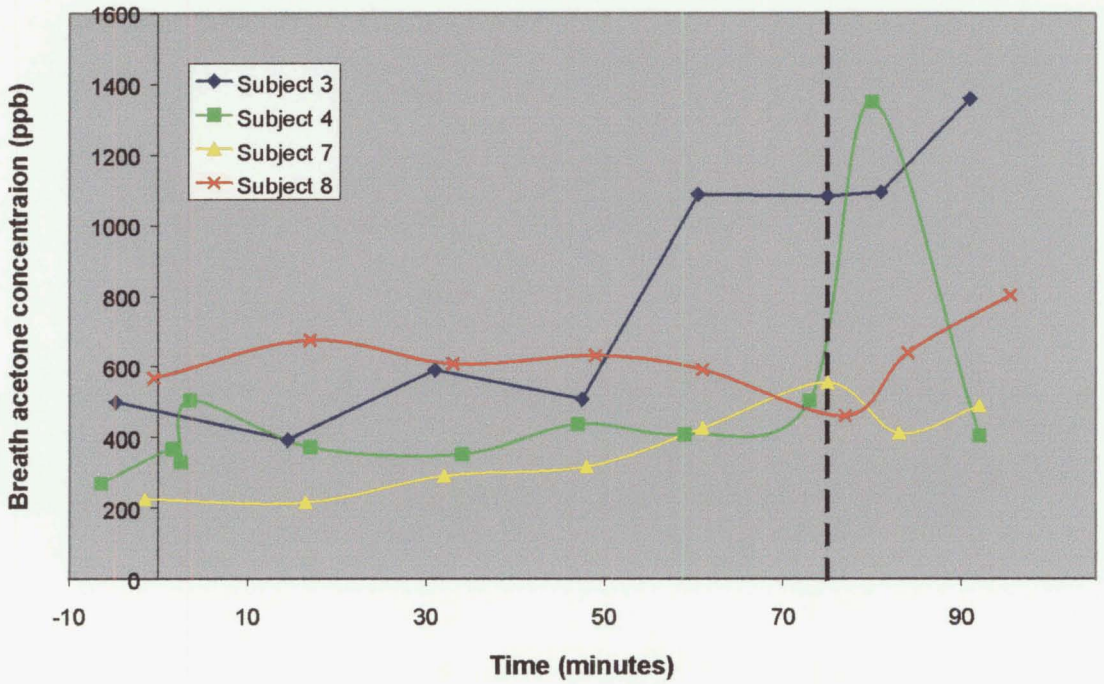

Figure 3.7: The profile of acetone concentration with exercise time for several subjects in the first study. Exercise (running in all cases) was begun at time = 0 and finished at approximately time = 75 min (dashed line).

The rise in acetone observed is consistent with physiology [118]. As the body exercises the energy is drawn more extensively from fatty acid catabolism. This may be because the short-term energy reserves (glucose, glycogen, and phosphocreatine) become locally depleted and the body has to shift its metabolism to other, more available, sources.

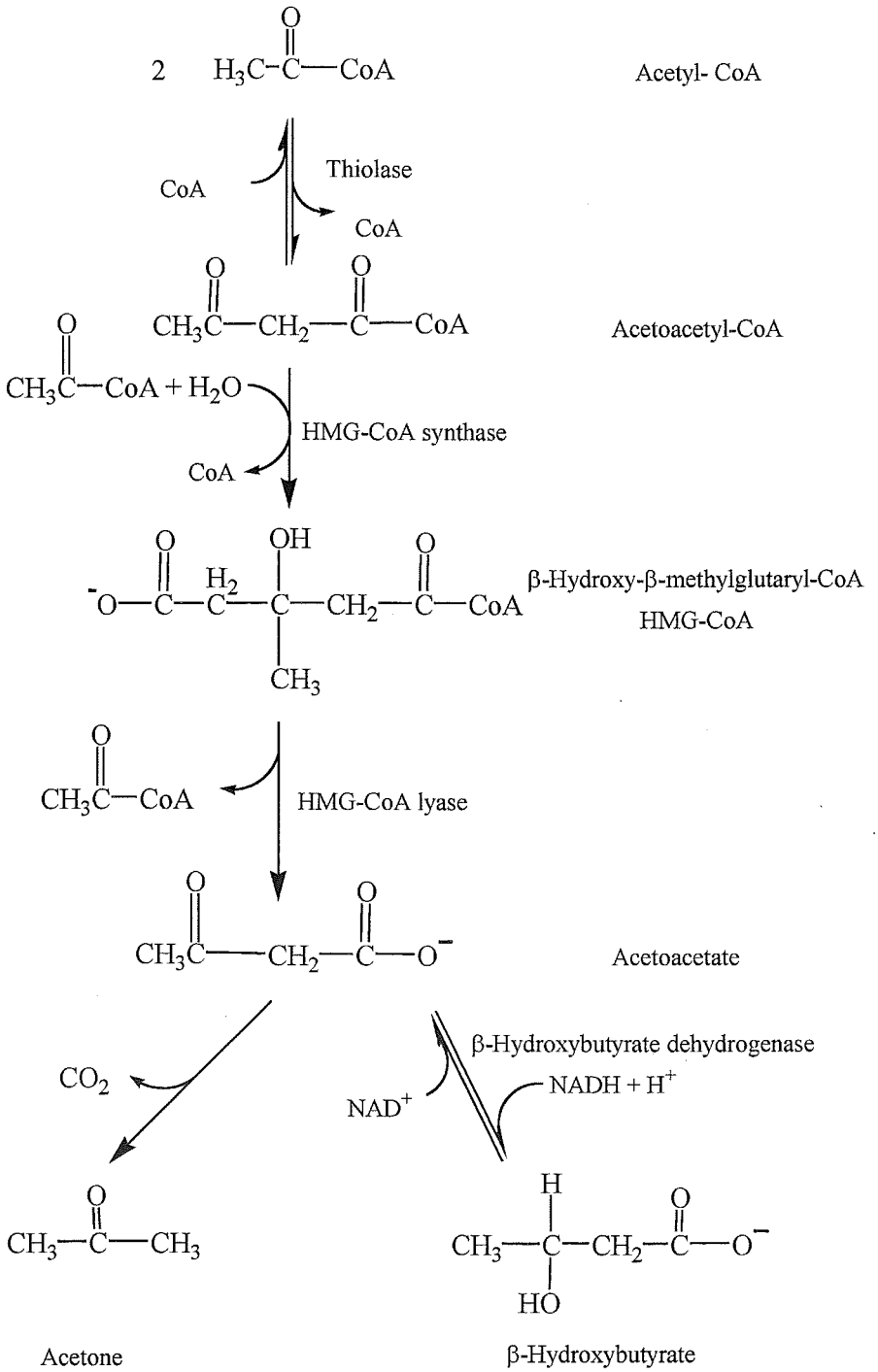

Figure 3.8: The formation route for ketone bodies.

The predominant energy reserve in the human body is in the form of fat, mostly triacylglycerols. When these triacyglycerol molecules are metabolised they can yield up to three fatty acids (long chain linear saturated carboxylic acids). These fatty acids are metabolised to produce acetyl-CoA. Coenzyme-A (CoA), a molecule built up of 3',5'-adenosine bisphosphate, pantothenic acid and β-mercatoethylamine, is prosthetic to many enzyme reactions and aids in certain enzymatic reactions by activating acyl groups. Most of the acetyl-CoA produced enters the tricarboxylic acid (TCA) cycle where it is oxidised to carbon dioxide. The energy evolved by this process is trapped into one of several molecules which are subsequently used to power the body. Some of the acetyl-CoA formed this way though gets diverted into another pathway, the formation of the so-called 'ketone bodies' (acetoacetate, acetone, and β-hydroxybutyrate) as is shown in Figure 3.8. The conversion of acetyl-CoA to 'ketone bodies' is especially apparent during periodds of fasting or starvation due to the build up of acetyl-CoA in the body [289].

The formation of ketone bodies occurs mainly in the liver mitochondria and from here acetoacetate and β-hydroxybutyrate are transported to other organs where the reverse process (i.e. converting acetoacetate and β-hydroxybutyrate to acetyl-CoA) provides significant metabolic energy. Acetone is essentially a by-product of this process being formed by non-enzymatic decarboxylation of acetoacetate. Ketone bodies are an easily transportable form of the energy derived from fatty acid metabolism as they can move through the circulatory system without the need for complexation with serum albumin or other fatty acid-binding proteins. Thus the blood concentrations of these ketone bodies will drastically increase as fatty acid catabolism becomes a more significant source of energy for the body. The rise in acetone will be especially marked as, unlike acetoacetate and β-hydroxybutyrate, acetone is not metabolised at other parts of the body for energy.

Smith and Spanel have previously observed this effect in human subjects who undergo long periods of fasting [59]. Without feeding, the body exhausts its short term energy supplies and has to convert to fatty acid catabolism. It is well known that during periods of extreme starvation ketone bodies are one of the major energy sources for the brain. Another interesting observation is the recovery of acetone levels in the work of Lindinger *et al.* [53]. approximately one hour after the subject ingested

60g of glucose the level of acetone peaked and began to drop. Presumably this is the result of the body switching away from fatty acid catabolism as its primary energy source, returning to the now available glucose. Subsequently the production rate of acetone will drop below the loss rate and the reservoir of acetone in the blood stream will begin to deplete. This is entirely parallel to the observation of acetone in the breath of patients with type I diabetes mellitus. In these patients, increased glucogenesis consumes oxaloacetate, rendering the TCA cycle less effectivethus forcing the body to switch to the formation of ketone bodies and results in high acetone levels.

In the **second exercise study** three subjects cycled at a constant pace for an hour. Many of the sampling problems had been resolved by this time and it was easier to sample the subjects at the appropriate time as they were no longer running in a remote location. Instead a stationary exercycle (Weider XR660) was set up adjacent to the SIFT to collect a breath sample and the subject needed only to slow down, step off, breathe two or three times and then return to exercise. This gave much more satisfactory results and the traces show a reduced scatter because of this. The three acetone traces for the different subjects (the precursor ion was again O_2^+) are each shown in Figure 3.9.

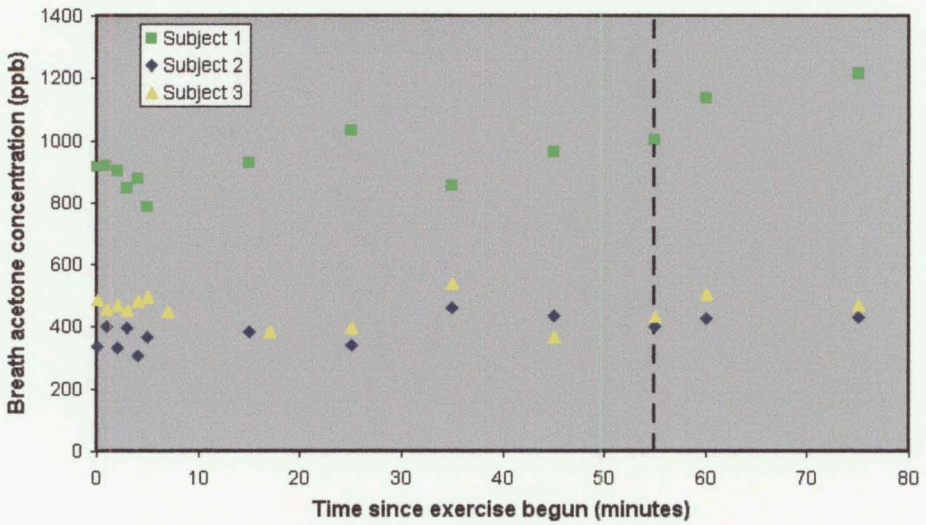

Figure 3.9: The acetone traces for the three subjects who participated in the second exercise study. The dashed line indicates the end of the exercise

One can easily see that the levels of acetone have not yet begun to rise significantly. Only one subject (subject 1) shows the beginnings of a rise which suggests that the

level of exercise was such that the body had no need to switch to fatty acid catabolism for energy so that the levels of acetyl-CoA and ketone body formation never rose significantly. It appears therefore that a similar experiment of a longer duration would be the ideal follow on to this work.

Isoprene

The isoprene traces appear to confirm some parts of the Lindinger experiments yet they do not completely agree. In the **first experiment** the scatter in experimental values is especially noticeable with some of the traces having a somewhat wave-like appearance. The initial values were between 50 and 150 ppb and again this seems to span the normal range, with the younger subjects generally having lower levels. Spanel *et al.*[99] report a mean value of 83 ppb with a standard deviation of 45 ppb. This trend for younger subjects to have lower isoprene levels has also been observed by Lindinger *et al.*[53] although they report values far higher than any value we have observed, with some levels greater than 600 ppb. The overall trends of the Lindinger experiment have been reproduced in that the levels of isoprene drop when the exercise is well established, in some cases there may be a later rise but the traces are not conclusive.

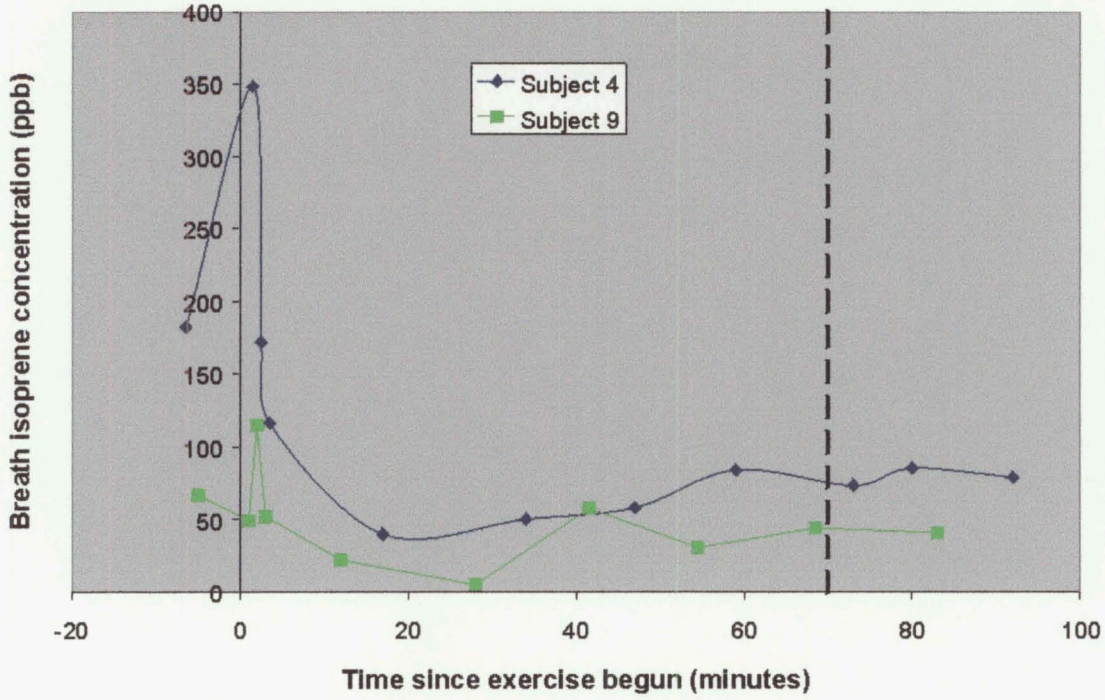

Figure 3.10: The isoprene traces for the two subjects in the first exercise experiment that were monitored more regularly at the start of their exercise.

Two subjects were monitored every minute for the first three minutes in an attempt to reproduce the initial spike in isoprene concentration observed by Lindinger and in these experiments the spike appears to be present. (These two athletes did "step-ups" and ran on the spot to cause an initial rise in heart rate.) Their plots are shown in Figure 3.10.

The **second exercise experiment** appears to confirm that the breath concentration of isoprene drops during exercise although the results are not so conclusive as before. Again no significant rapid recovery is observed. These traces are shown in Figure 3.11.

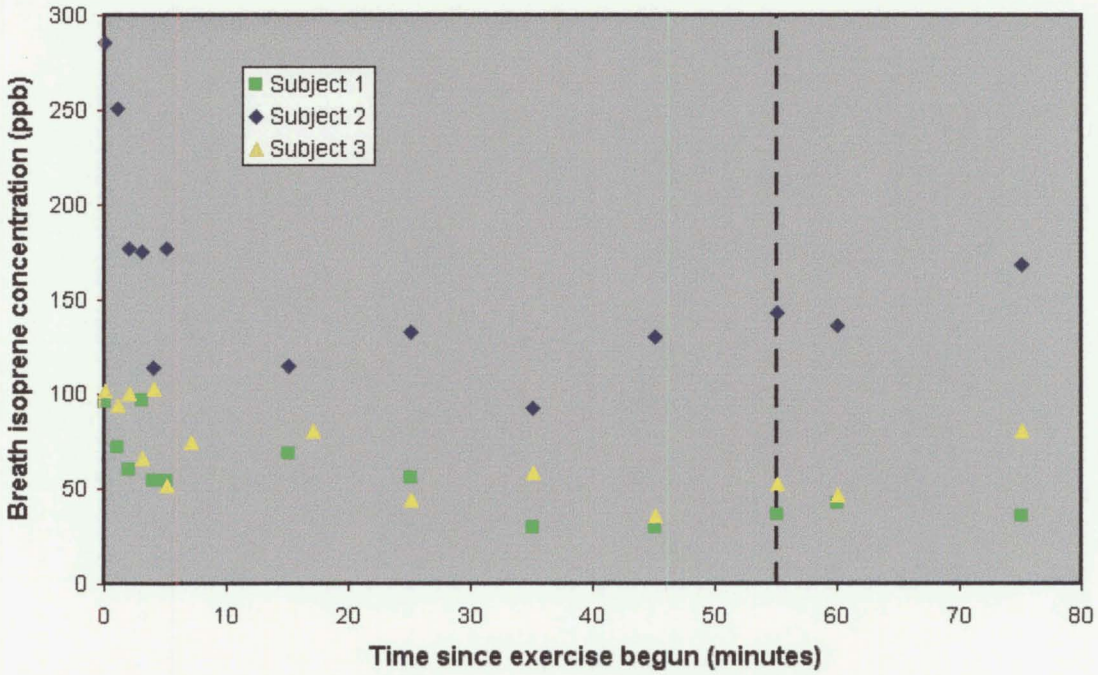

Figure 3.11: The isoprene traces for the three subjects who cycled for an hour in the second exercise study. The dashed line indicates the end of the exercise.

It should be noted however that there is no longer an initial rise visible, though this again may be related to the level of exercise performed in this experiment.

The origin of isoprene in the human body is not conclusively known, though it is probably related to the isoprenoid biosynthetic pathway. Its formation is definitely endogenous but whether the formation is enzymatic or non-enzymatic is unclear. Several studies have looked at breath isoprene and pentane in situations where the rate of lipid peroxidation is expected to be elevated. Pentane is known to be produced by this peroxidation, as are several other hydrocarbon species, however isoprene has not

been observed to follow the same trends as pentane. This suggests that enhanced peroxidation (most probably of isopreneoid compounds) is not a mechanism for the formation of isoprene which lends credence to an enzymatic process of formation. Lindinger *et al.* have also studied the formation process by PTR-MS [52], looking for the C5 allylic alcohols that would be a precursor in a non-enzymatic formation route for isoprene, but they found no evidence for these allylic alcohols.

It may be that the changes seen occurring in isoprene levels with exercise are more consistent with physical changes than biochemical ones. Isoprene is not very soluble in water or blood so the blood/breath ratio will strongly favour gas phase isoprene. As well as keeping the overall level of isoprene in the body low this will mean that isoprene will be more rapidly lost from the body when the breathing rate and heart rate are elevated. This happens during exercise and this will deplete the levels of isoprene in the body if the rate of loss exceeds the rate of production. The initial spike observed in isoprene may be a result of an initial heart rate rise without a concurrent rise in breathing rate. If this is the case more blood flows through the lungs during each inhalation period and therefore more isoprene crosses the blood/gas membrane. Thus each exhalation has a higher isoprene concentration. The absence of a spike in the cycling studies (as distinct from running) may be indicative of a more gradual start to the exercise allowing the body to adjust the heart and breathing rates concurrently.

Once the breathing and heart rate have settled into an exercise rhythm the breath concentration will level out, albeit at a lower level. When exercise is stopped one would expect the concentration of breath isoprene to rise again, but how rapidly it rises will depend on the relative values of production and loss. The Lindinger results suggest that re-equilibration occurs rapidly which indicates that the breath values essentially represent the entire endogenous production. If however the body is acting as a store for isoprene, even if only at a low level, the recovery time may be greater as the body will be depleted of isoprene after the exercise. The loss rate will be concentration-dependent, increasing as the blood concentration increases. If the production rate was only slightly greater than the loss rate at the blood isoprene concentration after exercise it may take some time for the equilibrium to be re-established.

Ammonia

Ammonia is formed in the body as a result of protein metabolism or as a result of the metabolism of skeletal muscle. It has been shown that during an incremental exercise program there is an increase in blood ammonia levels [119, 120] Ammonia is toxic to the body and is usually converted to urea and excreted. The results for ammonia in this study are far from conclusive, but one observation is immediately obvious, the levels of ammonia in the breath did not significantly increase in any of the subjects. The results from the second exercise study is shown below. The initial rise visible in two of the subject below was also seen in one of the two subjects who did step-ups in the first study.

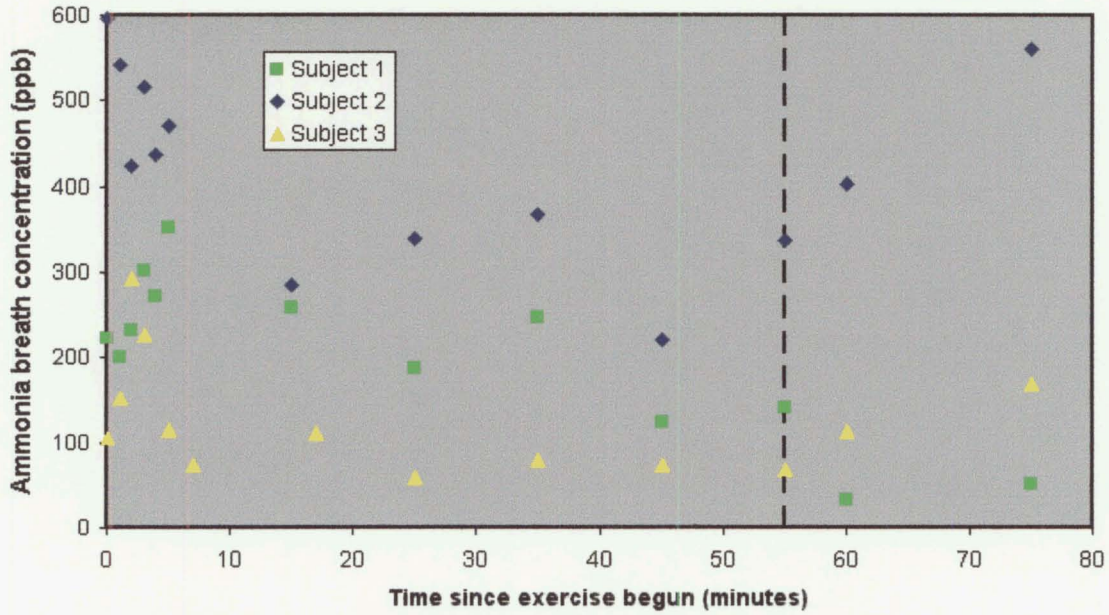

Figure 3.12: Breath ammonia concentrations for the subjects in the second exercise trial.

Two conclusions can be drawn from this observation. The first is that protein metabolism is not a significant source of energy during exercise. Smith and Spanel have shown that the breath ammonia concentrations of people who have consumed a protein meal rise markedly [59], which confirms that there is no problem in detecting this change in metabolism with the SIFT-MS technique.

The protein is hydrolysed in the body to its constituent amino acids which are converted in the liver to their corresponding α-keto acids by an aminotransferase. This liberates the ammonium ion, NH_4^+, which is then either lost via the breath as

ammonia or converted to urea and excreted. One can conclude from the absence of an increase in breath ammonia that in these experiments sugars and fatty acids were the main fuels for the subject's bodies.

The other pathway that produces blood and breath ammonia is the metabolism of skeletal muscle via the purine nucleoside cycle. The second conclusion which can be drawn from the ammonia profiles is that the exercise subjects are not burning muscle for energy. This is not unexpected due to the relatively moderate nature of the exercise. The purine nucleoside cycle has the net effect of converting aspartate to fumarate plus NH_4^+ thus when it is operating we should see a rise in breath ammonia. The aspartate formed is subsequently converted to citrate which is used to replenish the TCA cycle. Usually the TCA cycle operates without requiring this top-up mechanism. However during periods of strenuous exercise, side reactions can deplete the cycle thus impairing the ability of the body to provide energy for the necessary metabolic processes. The citrate provided by the destruction of skeletal muscle can help to replenish this deficit. The conversion of aspatate to fumarate occurs via the deamination of adenosine monophosphate (AMP) to inosine monophosphate (IMP) which in turn liberates NH_4^+ to the blood. The IMP then condenses with the aspartate to form an intermediate which liberates fumarate and regenerates the AMP. A new paper by Ament *et al.* [119] has studied the relationship between breath ammonia, blood ammonia, and blood lactate. The method used for determining breath ammonia was crude and involved simply trapping all of the expired base in a dilute sulphuric acid solution. Each subject underwent graded exercise, essentially stationary cycling where the workload gets steadily greater as time progresses, until exhaustion. It appears that the blood ammonia concentration correlates with blood lactate formation (see figure 2 in Reference 119). It is known that in graded exercise there is a sudden onset of blood lactate accumulation and thus there is also a sudden onset of breath ammonia rise. Ament *et al.* showed a rise in ammonia level of a factor of approximately 10 which was coincident with the beginnings of exhaustion and usually occurred when the heart rate had exceeded ~130 min^{-1}. This behaviour was not replicated in the present study and it thus seems likely that the subjects never reached a level of exhaustion where the purine nucleoside cycle was required to replenish the body's citrate stores. Testing using a more strenuous exercise regime seems the next logical step for this work.

It has been shown in these studies that SIFT-MS is a rapid and useful technique for monitoring the changes in expired breath gases in persons undergoing physical activity. The rough trends with time for acetone and isoprene levels have been repeatably shown, though there is significant scatter between subjects. The trends in breath ammonia are less certain due to the experimental difficulties encountered with the sampling tubes and the likelihood that there is little or no change under the current exercise regime. Further experiments of longer duration and/or at higher work rates would be the next logical steps in order to further elucidate the trends. It would also be prudent to try and confirm the relationship between blood lactate and expired ammonia as the body approaches exhaustion as this could provide a non-invasive method for determining the onset of blood lactate accumulation. The blood lactate concentration is commonly used by exercise physiologists to gauge fitness and exhaustion. A non-invasive indicator would almost certainly be of interest to them. At the same time it would also be interesting to monitor breath pentane and ethane, although these molecules may only be quantifiable as a sum of several different hydrocarbons due to the dissociative nature of the reactions of O_2^+, the only precursor that can detect these small saturated hydrocarbons. These marker molecules should enable one to track the levels of peroxidation in the body.

§3.4.1.2: Accumulation of Solvents into the human body from polluted environmental air.

The two-way membrane in the lungs which allows oxygen to pass from the air to blood also allows VOC to pass from the air into the bloodstream. This is a concern when the VOC are toxic, as many of the solvents and reactants used in industrial processes are. The cumulative exposure to these VOC is a serious concern to workers and their employers. The SIFT is an appropriate tool for the monitoring of VOC in the work place environment, as well as in the workers who are exposed to these substances. It is capable of easily, quickly and accurately measuring both the workers' breath solvent level and the solvent concentration in their environment.

The results presented in this section are an example of the above and they relate to the solvent exposure received by persons around a room in which a

polyurethane floor sealing compound has been used. The polyurethane studied used a solvent mixture that is relatively common for this type of application and contained a mixture of predominantly C9 aromatic hydrocarbons (mostly mesitylenes, or trimethyl benzene isomers), C8 aromatics (xylenes), and a small amount of butyl acetate. The mesitylenes and xylenes are also used as solvents in other industries and industrial processes. Both solvents are strong irritants and can be toxic with high continued doses.

There have been several previous studies of exposure to both of these solvents which have usually been performed by tracking the breakdown products in urine. Blood samples have also been used. There have been no previous attempts at quantifying the breath concentrations of these solvents.

The SIFT-MS mass spectrum collected for an air sample taken above a floor being sealed with the polyurethane is shown in Figure 3.13.

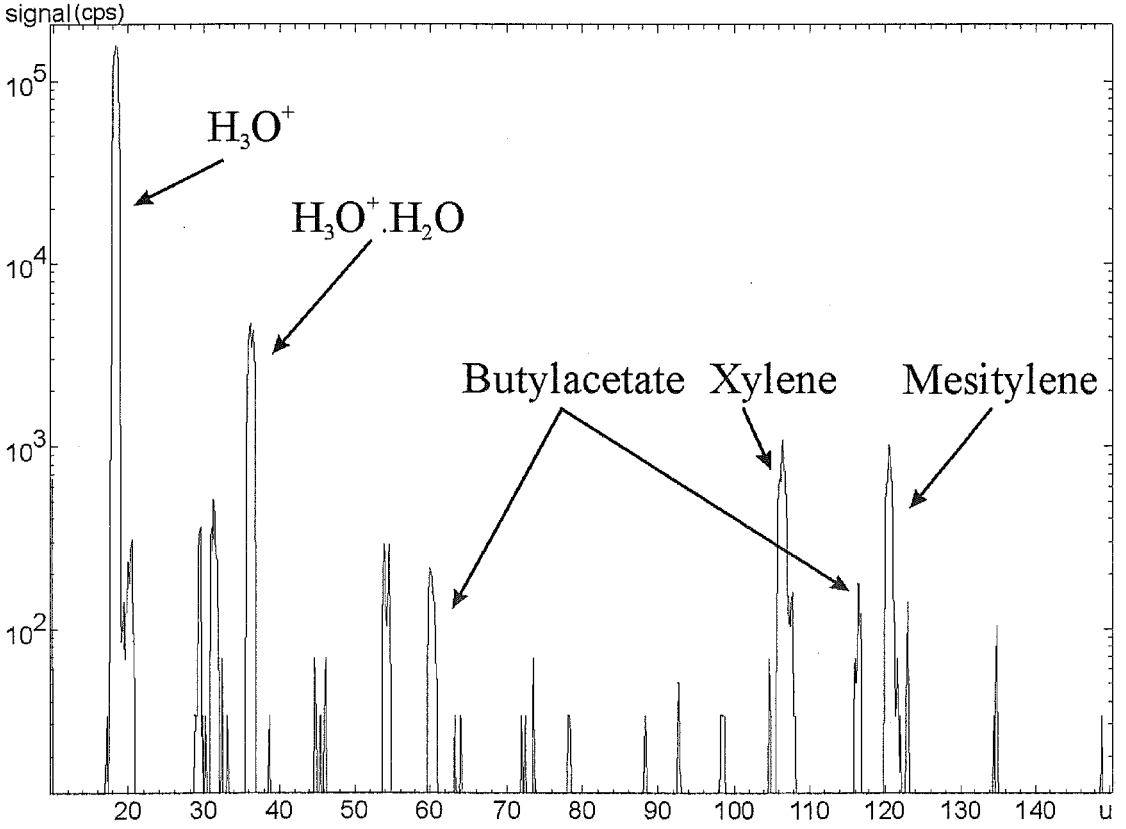

Figure 3.13: The mass spectrum produced by sampling air from an evacuated glass bulb that was opened above a floor that had been sealed with a commercially available polyurethane several hours prior to sampling.

This was obtained using an H_3O^+ precursor and the major trace peaks observed are at m/z = 107, 117, 121 and 135. Smith and Spanel [104] have shown that H_3O^+ transfers a proton to both xylene and mesitylene at the collision rate giving their respective protonated ions at *m/z* = 107 and 121. The reaction of H_3O^+ with butyl acetate has not been studied previously but the reaction of ethyl acetate has been reported [107]. The reaction of H_3O^+ and ethyl acetate gives only the protonated neutral with a rate coefficient that is similar to the Langevin rate. From this it seems likely that the m/z = 117 ion is due to protonated butyl acetate with the ion at 135 amu being the first cluster of this ion with water. The presence of a clustering reaction implies that this ion is unlikely to be a hydrocarbon species as these do not usually associate with water. An experimental measurement of the rate and products confirmed the presence of the 117 amu ion and also found a product at 61 amu ($C_5H_5O_2^+$) which was also seen in the spectrum of the air above the floor. This helps to confirm this assignment.

The *Multitrace Recorder* was then configured to monitor the C9 aromatics (mesitylene) and the C8 aromatics (xylene) and samples using other evacuated bulbs were made in collected locations. The building in which the vapour was collected has nine floors, many of which are connected by partially open ducting. The initial interest in the solvent vapour levels came as a result of complaints about contamination in a staff common room, one floor below the rooms that were being sealed. The levels in this room were found to be 1500 ppb (1.5 ppm) for both xylene and mesitylene. This is compared to the levels found in the room being sealed of 9100 ppb of xylene and 7500 ppb of mesitylene. This indicates that quite a significant amount of the organic vapour moved between rooms and floors and shows that persons other than the contractor applying the polyurethane sealant may receive doses of the solvent.

The contractor also consented to give us breath samples before and after the sealing of a room floor. These samples however could not be obtained on a single day, the 'before' was separated by a day from the 'after' sample. The results are further complicated by the fact that although the particular operator sampled apparently does not usually work with a filter mask, on the day that we obtained the 'after' sample he did. Models of breath trimethylbenzene suggest that the results taken at the end of a working day are most indicative of that day's exposure [121]. Thus if the mask is effective it will effectively invalidate the 'after' result as one may see a more

significant level as a result of previous exposure (i.e. the body background) than from that days exposure. The results obtained were xylene: 220 ppb both before and after and mesitylene: 45 ppb before and <15 ppb after. It appears that the mask has been effective in minimising exposure as the levels after exposure are similar or less than those ostensibly obtained before solvent exposure. The results also indicate that the xylenes have a longer lifetime within the body, as the breath solvent ratios are less than 1 : 0.2 (xylene:mesitylene) compared with exposure ratios (assuming the room concentrations are indicative) of approximately 1 : 0.82. The 'after' ratio may have been affected by the filter mask which may not filter out the two solvent components to an equal extent but this is only exacerbating an already apparent effect.

In a separate experiment two volunteer subjects were confined in a room in which the air had been in contact with large flat trays of mesitylene and xylene. Both subjects were male aged between 25 and 35 with no known previous exposure to either of the solvents. Unfortunately the temperature could not be well regulated in the exposure room so the solvent concentration varied significantly with time. To correct for this, samples of the room air (collected in an evacuated glass volume) were collected and analysed every half hour during the exposure. After exposure the breath concentrations of both xylene and mesitylene were monitored in the subjects until they reached background levels. The exposure profiles and the decay of the solvent concentration in each subject's breath are shown in Figure 3.14.

Subject	Parameter	C8 Aromatics (xylene)	C9 Aromatics (mesitylene)
1	Total dose [a]	13762	4776
1	Initial breath concentration [b]	527	92
2	Total dose [a]	7387	1957
2	Initial breath concentration [b]	243	29

Table 3.2: The dose received and uptake for two subjects exposed to a two part solvent mixture.

a) Values in ppb hours.

b) Values are alveolar concentrations in ppb.

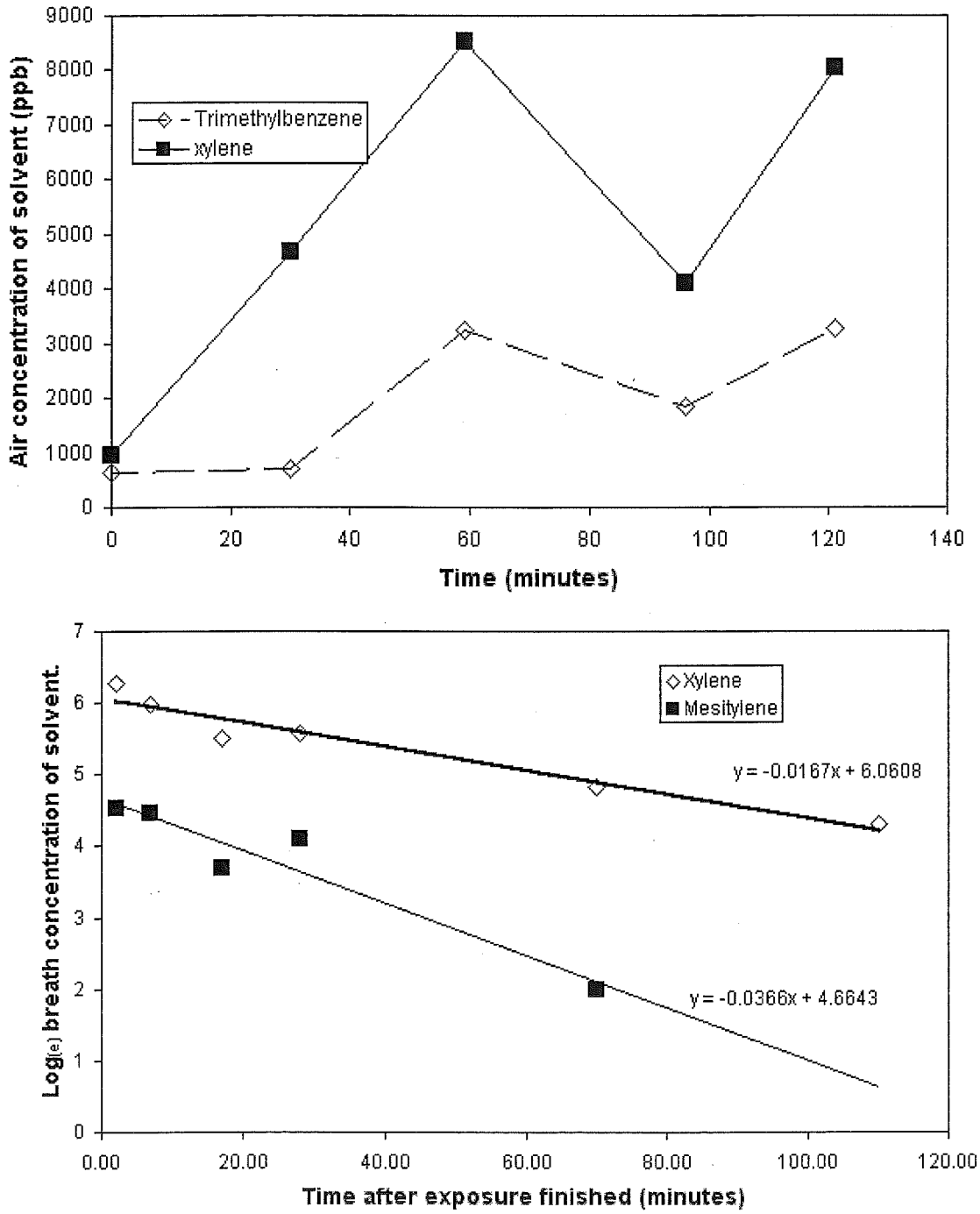

Figure 3.14: The top plot shows the concentration of xylene and mesitylene measured at half hour intervals during the period in the exposure chamber during the time subject 1 was inside the chamber. The lower plot shows the semi-logarithmic plots of the breath concentration of the two solvents for subject 1 of the subjects. Here t=0 corresponds to the removal of the subjects from the exposure chamber after two hours inside.

From the half-hourly measurements an estimate of the 'total dose' of each solvent has been determined by integrating the area beneath the curve obtained by connecting the points obtained for atmospheric solvent concentration. This dose is reported as a value in "ppb hours". Table 3.2 shows this dose and the initial breath concentrations for both solvents in each of the subjects.

The ratio (in units of hours^{-1}) of initial breath concentration to 'total dose' is remarkably similar. The mesitylene ratio is -0.037 for subject 1 and -0.047 for subject 2, similarly the ratios for xylene are -0.017 and -0.017. Note that the mesitylene ratio for subject 2 is only an approximate value as the total xylene exposure for this subject was not significant enough. However these results still suggests that the uptake of these species is approximately linear, i.e. the initial breath concentration is linearly dependent on the dose received. This is inconsistent with a report by Eide and Zahlsen [122] that the uptake of aromatics, specifically trimethylbenzene, is best described by a quadratic term. Of course there are not enough different concentrations present in this study to conclusively argue either case. Note also the apparently lower uptake ratio for mesitylene as opposed to xylene. Intuitively one would expect that these aromatics would behave similarly in the body as they only differ by one methyl group. The decay of breath solvent concentration after cessation of exposure has a roughly exponential decay with a semi-logarithmic plot yielding relatively straight lines. As can be seen from the semi-logaritmic decays presented in Figure 3.14 the slopes of these straight lines fall into two groups, both the xylene decays give exponential decay constants of approximately 25 min^{-1} whereas the mesitylene decays have a slope of approximately 55 or 60 min^{-1}. This suggests that the removal of mesitylene from the body is more rapid than that of xylene, even on a relatively short time scale. This may partly explain the lower uptake of mesitylene as the body may metabolise (and thus remove) it during the exposure time. An analysis of the metabolites of xylene and mesitylene excreted by the subjects would compliment this experiment. The extra oxidisable methyl group in mesitylene may account for the more rapid destruction.

The SIFT-MS technique has demonstrated its applicability for the study of solvent exposure. The levels of exposure that can be monitored are much lower than those usually reported in exposure studies. Due to the rapid and non-invasive nature of the sampling technique it is simple to obtain a time profile for the breath, and

consequently blood concentrations of the molecule itself. With SIFT-MS there is no need to rely on degradation products from sources such as urine, where the result is time averaged, or to use invasive sampling methods as in blood testing.

§3.4.2: Headspace Analysis: The gas phase emissions from fertilised soil.

This section of work was conducted in conjunction with Michael Mautner, Robert Sherlock, and Tim Clough from the Lincoln University Soil Science Department. The aim was to ascertain if SIFT-MS could be used to quantify and track certain of the gaseous emissions from a block of soil to which a nitrogenous fertiliser was added. The fertiliser chosen was an artificial urine solution comprised mainly of urea ($CO(NH_2)_2$). This was prepared by dissolving 51.39g potassium hydrogen carbonate ($KHCO_3$), 18.33 g potassium chloride (KCl), 15.54 g potassium sulphate (K_2SO_4), 55.10 g urea ($CO(NH_2)_2$), and 14.27 g glycine ($CH_2(NH_2)COOH$ in two litres of de-ionised water. The initial concentrations were designed to approximate the dose received by a section of pasture urinated upon by cattle during grazing. This level of 'fertilisation' is frequently enough to kill off most of the plants in the affected area.

When urea falls on to moist soil the chemical reaction between urea and water (Reaction 308) occurs [123, 124].

$$CO(NH_2)_2 + 2H_2O \quad => \quad NH_{3\,(aq)} + NH_4^+ + HCO_3^- \qquad (308)$$

This aqueous ammonia can then be liberated to the gas phase and is thus lost to the atmosphere where it no longer serves a useful purpose to the soil or those organisms that live in or on it. The soil is not usually capable of buffering the effect of this sudden influx of basic species and the pH of the soil rises rapidly to around 9. Loss of ammonia to the atmosphere also shifts the position of the NH_3/NH_4^+ equilibrium affecting the soil pH and other soil parameters and so an accurate quantification of ammonia loss is necessary.

The NH_4^+ is also, over a much longer time scale, converted via nitrite (NO_2^-) to nitrate (NO_3^-) ions by enzymatic means within some of the soil microbes. During this processing it is possible that, as the pH drops, some of these nitrite ions will be converted to nitrous acid which can in turn be converted to NO and be lost to the

atmosphere. Other gaseous compounds (e.g. N_2O) can be formed but were not monitored in this study.

Experimental

The experiment was designed to sample the gas evolved from a section of soil. To this end each sample consisted of approximately 200 cm^3 of dry soil placed into the bottom of a sealable glass container of approximately one litre internal volume. The vessels are approximately 160 mm tall with the soil occupying the bottom 40-45 mm. This leaves at least 0.75 litres of open head space above the soil. The soils were then watered with 100 ml of distilled water followed immediately after by 40 ml of the artificial urine containing 0.46 mol L^{-1} urea. The soils were then left, although the soil water level was maintained by watering approximately weekly, each time bringing the sample up to the same mass as it had been directly after the addition of the artificial urine solution. Sampling of the head space gas in the soil container occurred with a frequency that was intended to follow the total gas emission pattern, i.e. it occurred more regularly in the first few days and only sporadically after the first month.

At each time point in the study ammonia, nitric oxide, and nitrogen dioxide were monitored using the SIFT-MS technique. Each soil sample was capped for a period of time that was less than that required for the headspace to reach equilibrium with the soil. That is to say the partial volumes measured were predominantly due to the **emission rate** and were not strongly influenced by the adsorption rate of the soil sample or the enclosure. This time was usually five minutes (validation of this is shown in the results section following). The vessels containing soil samples were sealed with a screw down vacuum tight seal that had a rubber septum in it. This septum was pierced with an 85 mm long large bore needle, such that each head space gas sample came from the region of space approximately 30 mm above the centre of the soil block. The average total sample time was around 10 seconds and thus the pressure in the vessel was not significantly altered from atmospheric pressure during gas sampling. Multiple repetitions of each different sample type and blanks were measured at each time interval.

Results

The first experimental task was to determine that the collection time of five minutes was outside the equilibrium region for both gases. Because of the higher solubility of ammonia in water, one would expect that the ammonia would reach equilibrium more rapidly than nitric oxide, but both gases were checked. Initial samples prepared by the addition of solid urea rather than an aqueous solution showed that after five minutes the ammonia system was close to equilibrium. This is shown in Figure 3.15, but note that the extrapolation to zero time intercepts the axis at a finite concentration. Whether this non-zero intercept represents a degree of non-linearity in the collection method (i.e. that the container alters the equilibrium significantly such that the emission rate is altered) or an initial amount of ammonia present in the collection vessel with the seal off is unknown. The former effect is almost certainly present to some extent but is more likely to affect the times closer to equilibrium. A possible explanation is that the system approaches a value close to equilibrium in less than a minute but then takes several more minutes to finally reach it, with an attendant two fold rise in concentration of ammonia. This is unlikely. It seems more likely that it is the latter effect i.e. that the container is partially inhibiting air exchange with the surroundings even when uncapped. It is quite possible that equilibrium is established within the vessels before they are capped.

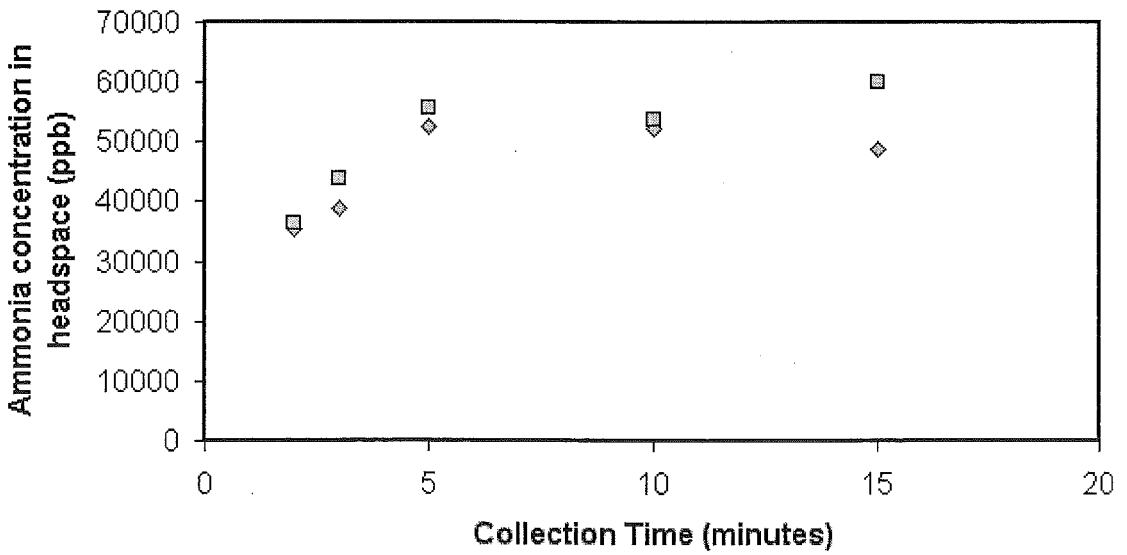

Figure 3.15: Two experiments showing the dependence of the observed ammonia concentration on the amount of time that the sample vessel was sealed for before sampling.

Experimental considerations mean that it is necessary to have a reasonably large sample volume and this means that gas exchange with the surrounding air is not entirely unhindered. Thus in the regions where emission is high the current results more correctly represent an upper limit.

Nitric oxide collection time experiments conducted at the same time as the ammonia ones discussed above suggest that five minutes was also outside the equilibrium region for this gas. However the samples were measured only a few days after fertilisation and the amounts of NO formed were quite small. Later experiments, shown in Figure 3.16 and 3.17, show that the time taken for nitric oxide to reach equilibrium is indeed longer than that for ammonia.

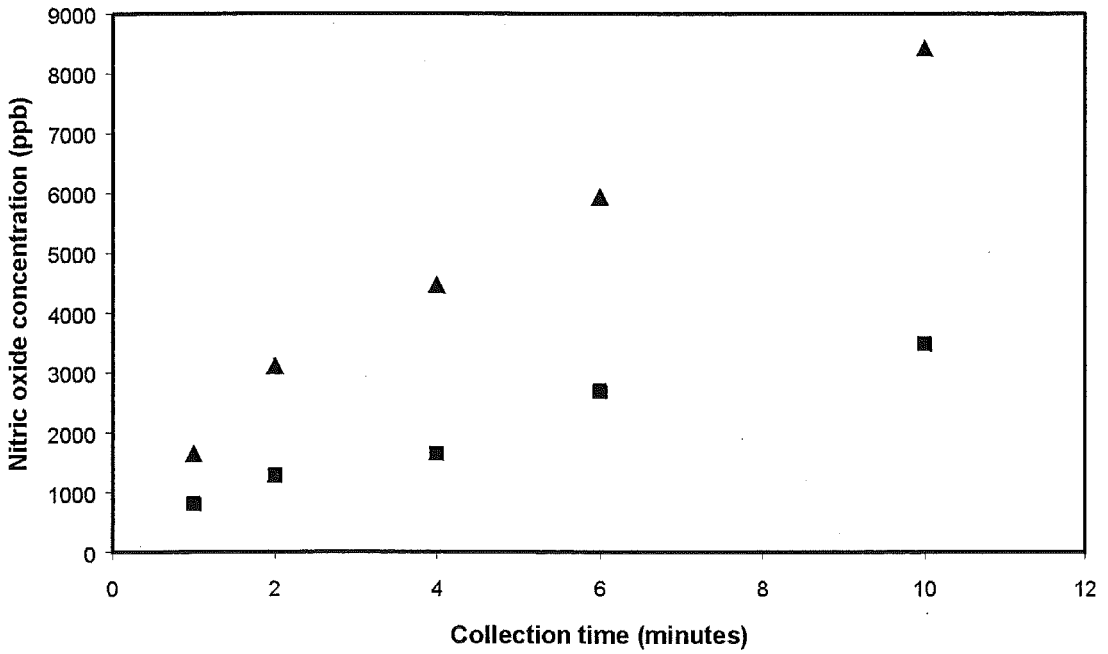

Figure 3.16: Plots of observed NO concentration versus the time each sample was sealed for two different emission rates. These different rates were prepared by adding different concentrations of "urine" to the samples at preparation time.

Together these graphs show that, at a five minute collection time, the headspace concentrations of NH_3 and NO are increasing linearly i.e. they represent **emission rates**. The corresponding graph for nitrogen dioxide was not able to be measured as the level of NO_2 was never observed to be above a trace amount. Nitrogen dioxide was measured as it can be formed by the reaction of NO with oxygen from air, however this process does not appear to be significant in the current work.

$$2NO + O_2 \Rightarrow 2NO_2 \quad (309)$$

The termolecular rate coefficient for this process is $4x10^{-38}$ cm^6s^{-1} [125], and even if the maximum level of nitric oxide (5 ppm) was left in the one litre volume for the full 5 minutes only 70 ppb of NO_2 would be observed. Thus the levels of NO_2 observed in the soil sample will be much less than 35 ppb, or lower than the accurate level of detection.

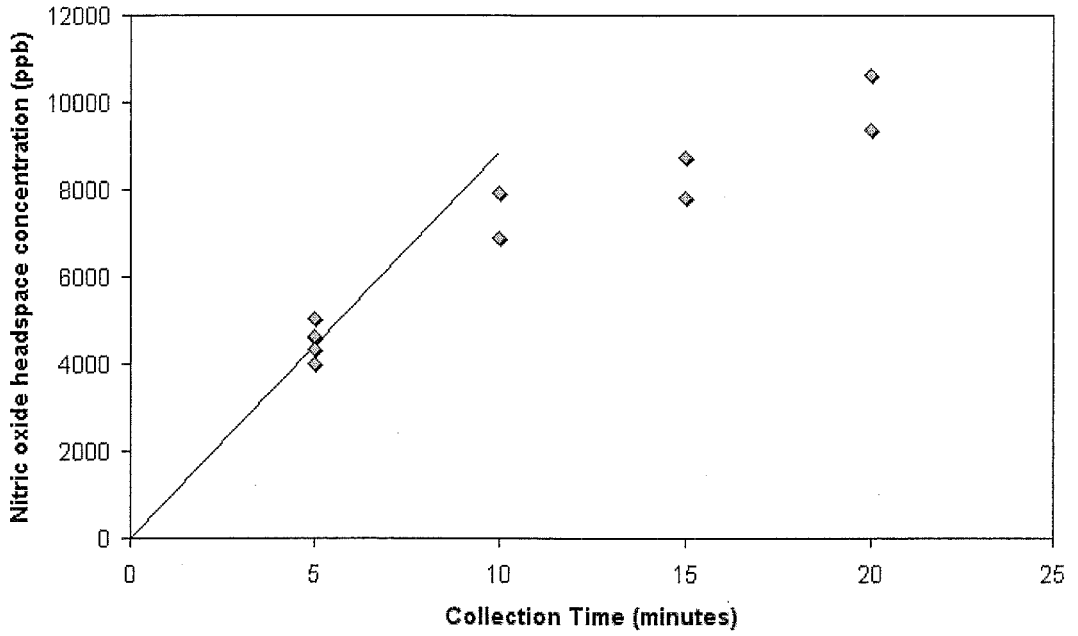

Figure 3.17: A range of longer collection times for a sample emitting nitric oxide.

It was also found that the method, or more correctly timing, of preparation of the soil samples had an effect on the emission rates. When samples were prepared by the concurrent addition of water and "urine" solution the levels were much different from those observed when the samples were watered, left to stand for several hours and then fertilised. Two different sets of samples were prepared using each method, one using the same concentration of urea as above and another using urea that was half the concentration (see Figure 3.18). The headspace gas concentrations in all the samples were monitored several times over the course of two days. The observed ammonia gas concentrations of the concurrently watered samples were reproducibly lower than the pre-watered samples. Agreement between the two replicates prepared at each concentration and method was good except for the two, high concentration, sequentially watered samples, which had a spread of almost 50% at the peak. In the dilute case the sequentially watered soil samples evolved approximately two and a

half times as much ammonia as those watered concurrently. A similar comparison for the undiluted samples is complex due to the spread observed for the sequentially watered samples at this concentration.

Presumably this difference in ammonia emission arises from differences in the local urea concentration and the urea disposition of the urea (i.e. the column density of soil the gas must pass through to be emitted) while the urea degradation takes place. The sequentially watered samples have a higher urea concentration at the surface of the soil as a result of less efficient mixing and thus give more gas directly to the atmosphere. Whether this means that the rate of gas emission is proportional to the local urea concentration or that passage through a soil layer results in the adsorption of the ammonia gas before it can be volatilised is unknown.

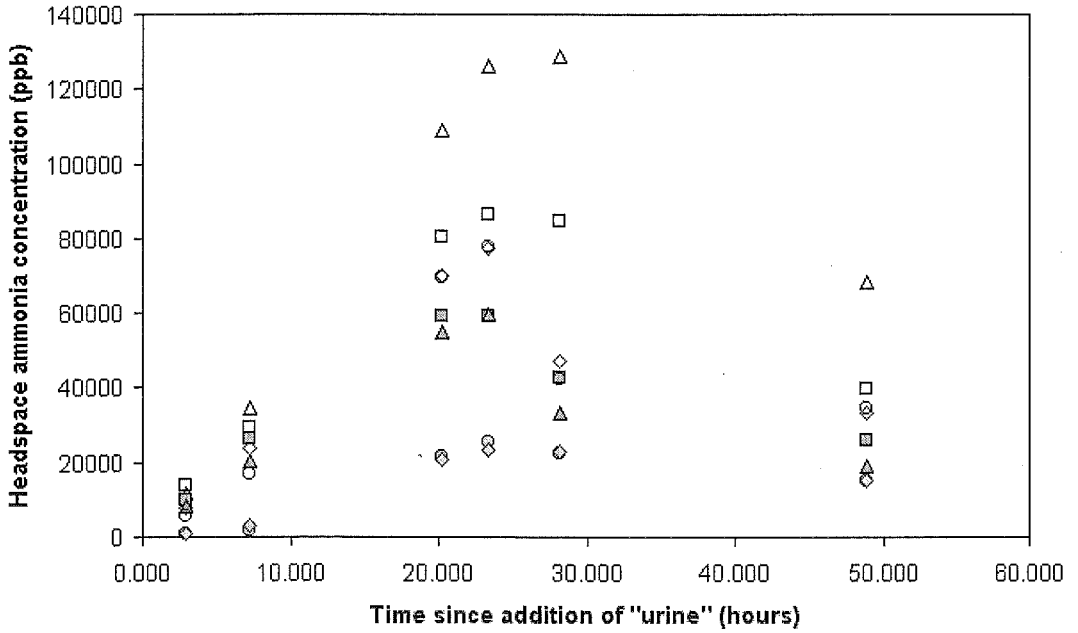

Figure 3.18: A comparison of sample preparation methods. The sample with black symbols were watered four hours before "urine" was added, the red samples were watered concurrent with "urine addition". In each case the hollow samples are at the standard concentration, while the others are half as concentrated.

The first iteration of these experiments involved four repeats of three sample types: blank, watered, soil, fertilised soil, and fertilised planted soil. Each was watered with 100 ml of water and 40 ml of the 0.46 mol L^{-1} "urine" solution at the same time. As mentioned earlier the urea concentration were great enough to cause 'burn-off' of plant material and this killed all the grass in the planted sample within the first week.

The planted samples were replanted with approximately 14g of new, clean grass 26 days later. This grass did not fare any better however and again died within a week or so. Whether the planted samples accurately reflect the influence of plant material in the soil is thus debatable. The initial rise in ammonia is shown in Figures 3.19.

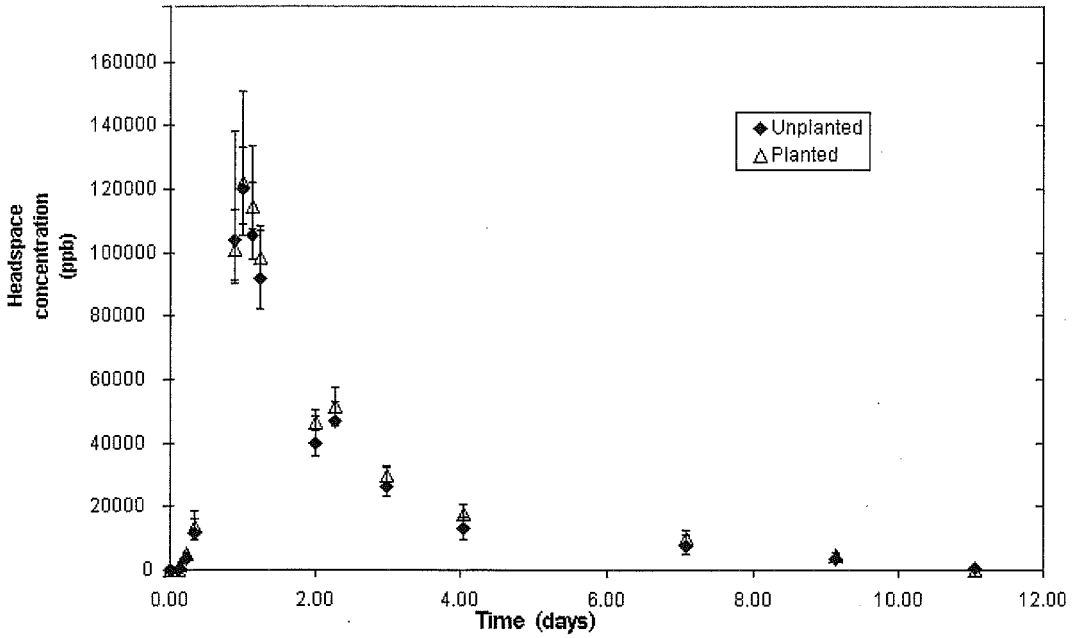

Figure 3.19: The initial rise in ammonia concentration. The solid points are the unplanted replicates and the hollow points the planted ones. The error bars represent the high and low values measured.

Several replicates of this system have been prepared and the above profile has been found to be reproducible in most cases. The ammonia concentration at the peak however has not been as reproducible, due to factors beyond the scope of the current experiments such as temperature variations, soil type, and the mixing of the "urine" solution with the soil.

Samples with varying concentrations of added "urine" were also prepared. In each case the total amount of liquid added was identical for each sample but the amount of the artificial urine solution added varied. The dependence of the ammonia emission on the initial amount of "urine" added is complex and is certainly not linear. The emission rate is believed to be strongly dependent on such factors as the soil packing and the temperature. However that the time profile of the emission is very similar within this set of samples. This profile was observed to be reproducible for other similarly prepared replicates.

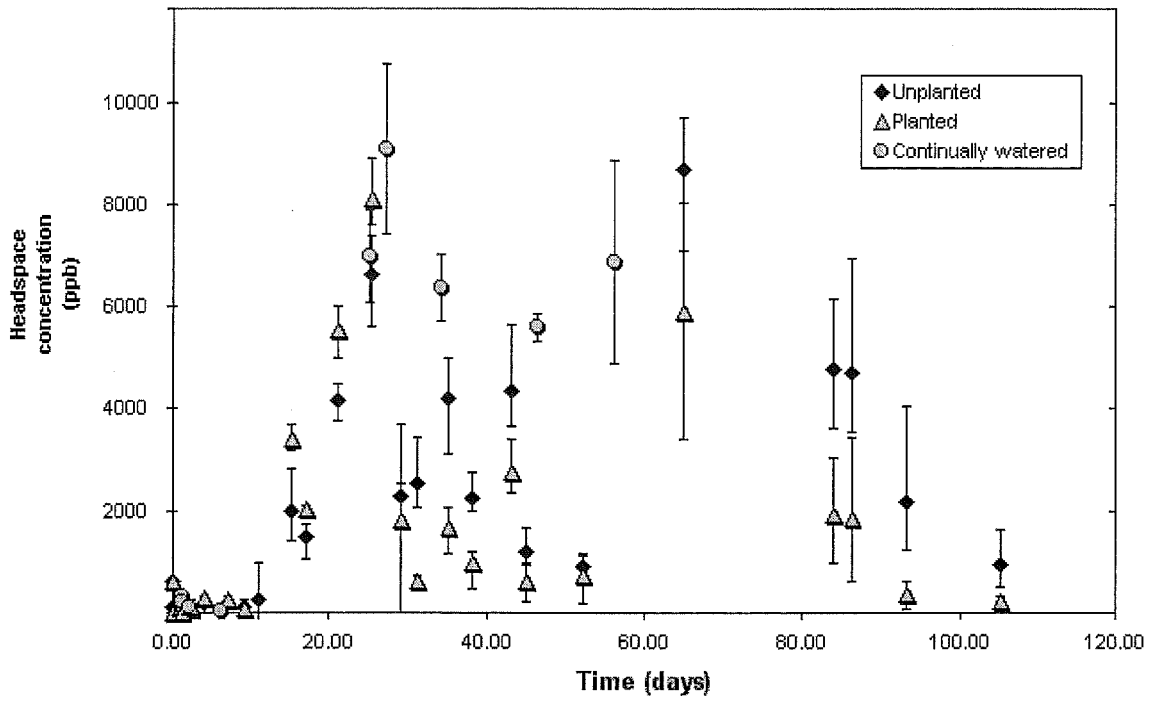

Figure 3.20: The headspace concentrations of nitric oxide throughout the experiment. The symbols (diamond, triangle, and circle) show the average value, with the errors bars showing the maximum and minimum values measured. The grey triangles are the original samples without plants, the black diamond the original samples with plants, and the grey circles a later replicate of the without plant samples. Note that in some cases the values became lower than zero when corrected for the back ground NO^+ levels, this is represented by error bars that continue to the X-axis.

The profile of the NO emission is less clear. This is partly a result of instrumental background noise and partly because of problems with the samples. The noise was caused by the formation of NO^+ as a result of reactions in the reaction flow tube initiated by the action of trace energetic particles or photons leaking from the FA ion source. These particles react with the major components of the air in the reaction flow tube and result in the formation of small amounts of NO^+. This NO^+ does not represent nitric oxide in the air and was found to be very variable. The most probable formation reactions are shown below. These ions (and atoms) are probably generated from photons or metastable helium atoms entering the primary (SIFT) flow tube.

$N^+ + O_2$ => $NO^+ + O$ [0.40] (310a)

=> $O_2^+ + N$ [0.52] (310b)

=> $O^+ + NO$ [0.08] (310c)

$k = 5.8 \times 10^{-10}$ cm^3s^{-1}

$O_2^+ + N$ => $NO^+ + O$ (311)

$k = 1.5 \times 10^{-10}$ cm^3s^{-1}

Nitric oxide is generated by microbial means from the nitrates in soil. It is known that the microbes that create the nitric oxide are unable to operate at elevated pH [123, 124], so one would not expect to see NO generation until after the bulk of the ammonia had been emitted. This is indeed the case with NO emission beginning approximately 350 hours after the samples were prepared. By way of comparison the ammonia emission was almost totally complete by 250 hours.

The dip in the emission rate from the planted samples at approximately 600 hours after preparation is a result of these samples being replanted. Presumably this drop in NO emission is a result of disturbing the soil while replanting. The concentration of artificial urine initially added was sufficient to kill all the grass present in the planted samples. At the 600 hour mark they were replanted, although this grass again did not live very long. It is not surprising that the grass died off initially as the levels of "urine" added simulate a bovine urine patch which will often cause browning in field situations. There is another drop in the emission rates between the 1000 and 1500 hour marks. This is believed to be the result of a physical process *viz* a drying out of the soil samples. The period roughly correlates with a period of extremely hot weather during which the samples were not watered more regularly, resulting in dryer samples. This may have prevented the microbes from producing NO during this period, when the temperature normalised and hydration was restored emission recommenced.

Confirmation of this explanation is provided by a later experiment (the black bars in Figure 3.20) which show an essentially flat concentration across this region.

Section 3.5: Conclusions.

The modifications carried out to the FA/SIFDT at the University of Canterbury to enable analysis and quantification of trace components in air samples via the SIFT-MS method have been shown to be practicable and effective. Breath analysis has been performed and reasonable agreement with the results reported by other researchers has been achieved. Two specific applications of breath analysis have been investigated in greater depth than others. These applications are: the monitoring of solvent contamination in the breath of subjects exposed to solvent vapours; and the monitoring of the major breath gases of subjects undergoing physical exercise in an attempt to monitor the physiological changes occurring during this exercise. Headspace analysis of the gases emitted by a fertilised soil sample has also been investigated, particularly the time profiles of ammonia and nitric oxide. SIFT-MS has shown to be an easy and rapid method for following the changes in the emissions of these gases.

The results presented in this Chapter are mostly of a preliminary nature and will require continued investigation to finalise them. However the SIFT-MS has been shown to be applicable to an amazing variety of applications and has an enormous potential to many industries. Therefore it should see increasing use at the University of Canterbury.

Chapter 4:

Reactions of H_3^+ ions with hydrocarbons: studies of the products of exothermic proton transfers.

Section 4.1 Introduction.

§4.1.1: H_3^+ in the galaxy.

An understanding of the chemistry occurring in the interstellar medium (ISM) has been the motivating factor for many of the ion-molecule reaction systems that have been studied using the SIFT. The unique physical conditions present in the ISM mean that ion-molecule chemistry has been proposed to be one of the main routes for the formation of more complicated species in this medium [42]. The ISM is a cold, disperse region where chemistry does not occur on a rapid time scale. Nevertheless in the centre of the cold dark interstellar clouds many polyatomic species have been observed.

Any buildup of these more complicated molecular species must be balanced against their dissociation back to more simple species. This is reason why the more complex species are clustered in the dark interstellar clouds. There they are shielded by the surrounding dust particles from dissociation by photons and to a lesser extent by cosmic rays, allowing these molecular species to live long enough to react further. These ion-molecule reactions can build molecules of higher complexity, or if the reaction is extremely exothermic, cause fragmentation. In an exoergic reaction, the exoergicity, if it is larger than the bond energy, may ultimately cause bond rupture. Hence many products of these reactions are fragments of the original larger neutral. A process that effectively reduces the complexity of the species in the ISM. The breaking of these bonds and the relative kinetic energy between the fragments formed provides a sink for the excess energy.

One of the prime chemical ion candidates for this role in the ISM is H_3^+. This ion is an extremely energetic species and is ubiquitous in the ISM. H_3^+ is one of the ions to have been directly observed in interstellar space [126] and has also been observed in the Jovian auroral electrojets [127]. Other likely candidates that might play a similar dissociative role are species such as He^+, HeH^+ and other high energy ions.

Section 4.2: Experimental

§4.2.1: Methods used for the generation of the H_3^+ reactant ion.

The H_3^+ ions used in this study were of necessity generated by two separate methods, as a single method could not be found that eliminated all possible sources of interference with the accurate measurement of the product ratios. The differences between the generation methods were quite radical; the first used a hydrogen carrier in the FA and a helium carrier in the SIFT reaction tube while the second reverses the order of these carrier gases. The former method represents the FA/SIFT operating in a 'standard' manner, with the reactant ion being generated in the remote ion source and subsequently being injected into the main reaction tube. In the latter method the ion of interest (H_3^+) is generated in the SIFT reaction tube via reaction of an injected ion with the hydrogen carrier gas. Hereafter the methods will usually be denoted by the type of carrier gas present in the **SIFT** reaction tube.

In the first (helium) method the initial process is the ionisation of hydrogen in the FA to give H_2^+ followed by the rapid reaction between H_2^+ and hydrogen as shown below [1]. Ionisation was usually provided by the linear geometry microwave discharge (see §2.2.3).

$$H_2^+ + H_2 \quad => \quad H_3^+ + H \qquad (401)$$
$$k = 2.0 \times 10^{-9} cm^3 s^{-1}.$$

Reaction 401 will be the primary formation method in the FA although there is also the possibility that the termolecular process, Reaction 402, generates some of the H_3^+ ions. This alternative reaction sequence is begun by the dissociative ionisation of hydrogen [2, 128, 129]. Note that in the current arrangement it is more likely that the third body will be helium rather than hydrogen but the kinetics for this process have not been measured with helium as the third body. The termolecular rate coefficient in helium will probably be slightly slower.

$$H^+ + 2H_2 \quad => \quad H_3^+ + H_2 \qquad (402)$$
$$k_3 = 3 \times 10^{-29} cm^6 s^{-1}.$$

There are several problems however with this first method which arise mainly as a result of vibrational excitation of the H_3^+. The H_3^+ formed by Reaction 401 is mostly vibrationally excited, retaining some of the exothermicity of its formation reaction as well as gaining energy from excitation of the H_2^+ reactants and translational energy

from the collision process. Furthermore the vibrational quenching reaction between $H_3^+(v)$ and hydrogen is known to be slow [36, 37, 38, 130, 131]. The estimated rate coefficients for this quenching process vary from 3 x10^{-10} to 10^{-12} cm^3s^{-1}, and are highly dependent on the initial vibrational state of the H_3^+. Blakley *et al.* [131] give rate coefficients for quenching of the order of 10^{-11} cm^3s^{-1} for H_3^+ with greater than ~3 vibrational quanta and give values an order of magnitude lower than this for those of H_3^+ with $v < 3$. Gougousi *et al.* [38] however conclude that it is only the v_1=1 state that is slowly quenched. With the FA source at 0.5-0.6 Torr (hydrogen) these rate coefficients should still result in most of the H_3^+ exiting the FA being in the vibrational ground state. This however does not ensure that the ions in the SIFT flow tube are not internally excited as energy **will** be gained during the injection process (see §2.5.4 and §2.5.5). The most graphic demonstration of this is the observed presence of HeH^+ ions in the flow tube. These ions can only be formed by Reaction 403, which is endoergic by 244 kJ mol^{-1} for the case when all the reactant H_3^+ ions are in their ground states.

$$H_3^+ (v\neq0) + He \quad => \quad HeH^+ + H_2 \qquad (403)$$

The amount of HeH^+ observed was highly dependent on the injection conditions. When higher voltages were used on the FA nose cone the ratio HeH^+/H_3^+ increased. As a result of this, the injection conditions for H_3^+ were quite different from those reported almost anywhere else in this thesis, with the FA nose cone voltage being in the range +12-17V and the venturi plate usually floated to +10V or more. Because the remainder of the electrostatic lenses in the ion selection region are arranged in Einzel type clusters which do not significantly affect the kinetic energy of the ions, the potential gradient that the ions experience across the quadrupole region (between the FA nose cone and the venturi plate) provides most of their kinetic energy. Reducing this gradient leads to lower kinetic energies and therefore lower energy injection but also reduces the transmission efficiency. The quenching rate for vibrationally excited $H_3^+$with helium as a collision partner will be less than that of hydrogen, especially for the higher vibrational states where symmetric proton transfer and vibrational–vibrational energy transfer between H_3^+ and H_2 [131, 132] may be important quenching mechanisms. Thus any energy gained will only be removed slowly. A good indicator of the vibrational state of the H_3^+ reactant is the reaction of H_3^+ with argon (Reaction 404).

$$H_3^+ + Ar \Rightarrow ArH^+ + H_2 - 52 \text{ kJ mol}^{-1} \quad (404)$$

This reaction is 52 kJ mol^{-1} endothermic and will only occur when the ion has some degree of internal excitation. Only three vibrational states of H_3^+ do not have enough energy to overcome this endothermicity and will not transfer a proton to argon. These states are the ground state, the $v_1 = 1$ breathing mode, and the $v_2 = 1$ bending mode. Accordingly if argon is added at the reaction inlet port, a good indication of the extent of vibrational excitation of the H_3^+ in the reaction region is found from the magnitude of the ArH^+ signal. This test was performed several times and when the HeH^+/H_3^+ ratio was at a minimum (i.e. well tuned injection conditions) excitation levels i.e. H_3^+ ions with $v>1$, are generally less than 10%.

A similar method to that presented above was used for generating the D_3^+ ions that were reacted with some of the smaller hydrocarbons. Due to the greater scarcity and expense of deuterium however, a helium carrier was used in the FA as well as the SIFT. A moderately large flow of D_2 was then introduced to the helium plasma at the FA nose cone and D_2^+ generated. Subsequently, by an equivalent reaction to Reaction 401, D_3^+ was generated and injected into the SIFT reaction tube. One complication for a D_3^+ reactant is that D_3^+ and HeD^+ (formed from energetic injection of D_3^+, see Reaction 403) are isobaric. Presuming that reaction of excited D_3^+ and any HeD^+ with argon is still exothermic then by comparing the D_3^+ and ArD^+ counts at high argon flows there is ~3% of these energetic ions present in the 6 amu signal.

The second method used for generating H_3^+ was to inject a signal of Kr^+ from the FA into a hydrogen carrier in the SIFT reaction tube [37, 70, 133]. This approach has several advantages. As the H_3^+ is not directly injected through the venturi, it cannot be excited by that process; the hydrogen carrier will in all probability be more effective at quenching any vibrationally excited H_3^+ ions; and finally, and most importantly, the formation reaction is slightly endothermic and should only produce ground state H_3^+. Excited H_3^+ can of course be formed from translational energy carried by the Kr^+, but this effect is probably small.

$$Kr^+ + H_2 \Rightarrow KrH^+ + H + 37 \text{ kJ mol}^{-1} \quad (405)$$

$$k = 2.1 \times 10^{-10} \text{ cm}^3\text{s}^{-1}.$$

$$KrH^+ + H_2 \Rightarrow H_3^+ + Kr - 1.25 \text{ kJ mol}^{-1}. \quad (406)$$

$$k = 3.8 \times 10^{-11} \text{ cm}^3\text{s}^{-1}.$$

This procedure effectively eliminates any concern over vibrational excitation, although experimental verification is not possible due to the rapid exothermic reaction between ArH^+ and the hydrogen carrier which regenerates H_3^+. The drawback of this method is that reactions of product ions, from H_3^+ and the neutral, with the carrier gas (H_2) can occur. Indeed due to the high number density of the carrier gas, even slow reactions (e.g. association reactions) can have a significant effect on the observed product distribution. The usual method used for determining the product branching ratio of a reaction (extrapolation to zero neutral flow) does not correct for the effect of the hydrogen carrier as the effect does not lessen with decreasing neutral reactant flow. Association reactions with the hydrogen carrier gas are especially problematical as they essentially reverse one of the major fates of excited hydrocarbon ions *viz.* H_2 loss. Thus the product distributions obtained in a hydrogen carrier are not always reliable. A combination of the two H_3^+ generation methods is necessary to accurately determine the product ratio for **ground state** H_3^+ ions in the SIFT.

Krypton ions are not simple to produce in the FA. Their IP of 14.0 eV is considerably less than both that of helium as well as the energy of the helium metastables (He 2 ^{3}S = 19.82 eV) and thus Kr^+ is not efficiently formed in the FA. In order to get reasonable counts of Kr^+ the krypton must actually be passed through the microwave discharge cavity. It was found that this method produced copious Kr^+ counts, enough that the signal of H_3^+ was usually greater than 100,000 cps with the hydrogen carrier method.

The isomeric structures of two of the product ions, $C_3H_3^+$ and $C_3H_5^+$, was also investigated during the course of the study. These investigations took place with a hydrogen carrier in the SIFT reaction tube. Although $C_3H_3^+$ associates with hydrogen the association rate coefficient is very small. It has only been observed in the hydrogen carrier used in the current investigation. Other researchers [134] have shown the rate coefficient for both isomers to be less than $5x10^{-12}$ cm^3s^{-1} (which corresponds to a termolecular rate coefficient of ~$5x10^{-28}$ cm^6s^{-1}). Both $C_3H_3^+$ and $C_3H_5^+$ can have two isomeric structures, the former has a linear and a cyclic structure, while the latter can take either the allyl or 2-propenyl form. For each ion it has been shown that the nature of the ion can be deduced from its reactivity with methanol [88, 134].

For the $C_3H_3^+$ ion, the linear $C_3H_3^+$ was reported by McEwan *et al.*[134] to give both proton transfer and association while the cyclic form was essentially unreactive.

The rate coefficient for the reaction of the linear isomer was $1.8x10^{-9}$ cm^3s^{-1}, but that may be slightly altered by the fact that investigation of the isomeric structures was performed in a hydrogen carrier as opposed to the helium one used by the original researchers.

The two $C_3H_5^+$ isomers also have different reaction rates. The allyl cation (which is at the energy minimum) reacts at $7.3x10^{-10}$ cm^3s^{-1} giving mainly proton transfer ($CH_3OH_2^+$) and hydrogen molecule abstraction ($C_3H_7^+$) while the 2-propenyl structure reacts at the slightly faster rate of $1.7x10^{-9}$ cm^3s^{-1} to give 70% proton transfer and 30% adduct formation (at ~0.5 Torr of helium) [88]. This latter result is likely to be significantly affected by the presence of a hydrogen carrier gas. Because of that possibility, the rate coefficient for the product ion of H_3O^+ and propyne (known to be entirely the 2-propenyl cation) with methanol in a hydrogen carrier was investigated. This rate coefficient was fond to be $2.2x10^{-9}$ cm^3s^{-1}, slightly higher than that measured in helium. These rate coefficients were used to identify the isomeric nature of several of the $C_3H_3^+$ and $C_3H_5^+$ products observed in this study.

Section 4.3:Results.

§4.3.1: Reactions investigated.

The reactions of H_3^+, N_2H^+, and H_3O^+ with a wide range of hydrocarbons have been studied in the current work. The hydrocarbons investigated were acetylene, ethylene, allene, propyne (methyl acetylene), cyclopropane, propene, propane, 2-butene, *n*-butane, *iso*-butane, benzene, toluene, and methyl cyclohexane. Due to the fact that two different methods were used for generating H_3^+ ions, the reactions with H_3^+ have also been studied in two different carriers. It was assumed that the N_2H^+ and H_3O^+ ions reacted identically in the different carrier gases. This should be a reasonable assumption as there should be no difference in vibrational energy present in these ions as they are formed by the same reactions in each of the carriers and any vibration as a result of reaction exothermicity should be as quenched effectively by either carrier. Previous experience suggests that ion excitation does not significantly feature in the reactions of N_2H^+ and H_3O^+. The reactions of the three ions (H_3^+, N_2H^+, and H_3O^+) are presented in Tables 4.1, 4.2, and 4.3 respectively.

Table 4.1: Reactions of the H_3^+ ion with the given neutral molecules.

Neutral	Rate Coefficient [a, b]		Carrier Gas	Products		Energetics [c]
Acetylene			helium	$C_2H_3^+$	1.0	-471
C_2H_2						
	2.6	2.81	hydrogen	$C_2H_3^+/C_2H_5^+$ [d]	1.0	-471
Ethylene			helium	$C_2H_3^+$	0.60	-54
C_2H_4				$C_2H_5^+$	0.40	-264
	2.7	2.91	hydrogen	$C_2H_3^+/C_2H_5^+$ [d]	1.0	-54
Allene			helium	$C_3H_3^+$	1.0	-111 or
$CH_2=C=CH_2$						-223
	2.9	3.42	hydrogen	$C_3H_3^+$ [e]	1.0	-111 or
						-223
Propyne			helium	$C_3H_3^+$	1.0	-218
CH_3-C≡CH						
	3.0	4.22	hydrogen	$C_3H_3^+$ [e]	1.0	-218
Cyclopropane			helium	$C_3H_5^+$	0.35	-290
c-C_3H_6				$C_2H_5^+$	0.60	-143
				$C_3H_3^+$	<0.05	-85
	2.6	3.32	hydrogen	$C_3H_5^+$	0.25	-290
				$C_2H_5^+$	0.75	-143
Propene			helium	$C_3H_5^+$	0.65	-181
CH_3-CH=CH_2				$C_3H_3^+$	0.10	-52
				$C_2H_3^+$	0.25	-89
	3.1	3.73	hydrogen	$C_3H_5^+$	0.70	-181
				$C_2H_3^+/C_2H_5^+$ [d]	0.30	-89
Propane			helium	$C_3H_7^+$	0.45	-203
C_3H_8				$C_2H_5^+$	0.55	-175
	3.0	3.51	hydrogen	$C_3H_7^+$	0.40	-203
				$C_2H_5^+$	0.60	-175
2-Butene			helium	$C_3H_7^+$	0.40	-252
$CH_3CH=CHCH_3$				$C_4H_9^+$	0.35	-226
				$C_2H_5^+$	0.25	-143
	2.8	4.18	hydrogen	$C_3H_7^+$	0.40	-252
				$C_4H_9^+$	0.35	-226
				$C_2H_5^+$	0.25	-143
n-Butane			helium	$C_3H_7^+$	0.45	-173
C_4H_{10}				$C_4H_9^+$	0.35	-132

				$C_2H_5^+$	0.15	-163
				$C_3H_5^+$	0.05	-110
	3.0	3.96	hydrogen	$C_3H_7^+$	0.45	-173
				$C_4H_9^+$	0.35	-132
				$C_2H_5^+$	0.20	-163
i-Butane			helium	$C_3H_7^+$	0.50	-249
C_4H_{10}				$C_4H_9^+$	0.30	-140
				$C_2H_5^+$	0.20	-155
	3.0	4.01	hydrogen	$C_3H_7^+$	0.60	-249
				$C_4H_9^+$	0.35	-140
				$C_2H_5^+$	<0.05	-155
Benzene			helium	$C_6H_7^+$	1.0	-347
C_6H_6						
	3.3	4.41	hydrogen	$C_6H_7^+$	1.0	-347
Toluene			helium	$C_7H_9^+$	0.75	-370
C_7H_8				$C_7H_7^+$	0.20	-257
				$C_6H_5^+$	0.05	-105
	3.9	5.90	hydrogen	$C_7H_9^+$	0.40	-370
				$C_7H_7^+$	0.50	-257
				$C_6H_5^+$	0.10	-105
Methylcyclohexane			helium	$C_7H_{13}^+$	0.35	-245
C_7H_{14}				$C_6H_{11}^+$	0.20	-295
				$C_4H_9^+$	0.23	-83 to -238
				$C_4H_7^+$	0.12	+35 to -87
				$C_3H_7^+$	0.10	-79 to-163
	4.2	5.18	hydrogen	$C_7H_{13}^+$	0.60	-245
				$C_6H_{11}^+$	0.25	-295
				$C_4H_9^+$	0.15	-83 to -238

Table 4.1: Reactions of the H_3^+ ion with the given neutral molecules.

a) Observed rate coefficient. Units 10^{-9} cm^3s^{-1}.

b) Calculated collision rate using the method of Su and Chesnavich [114] or Langevin theory.

c) The energetics for each observed product channel, in kJ mol^{-1}.

d) $C_2H_3^+$ was observed to associate with hydrogen to give $C_2H_5^+$. See text for fuller explanation.

e) A $C_3H_5^+$ product was also observed but this is believed to be the result of association with the hydrogen carrier.

Neutral	Rate Coefficient [a, b]		Products		Energetics [c]
Acetylene	1.4	1.20	$C_2H_3^+$	1.0	-157
C_2H_2					
Ethylene	? [d]	1.25	$C_2H_5^+$	1.0	-193
C_2H_4					
Allene	1.4	1.70	$C_3H_5^+$	1.0	-281
$CH_2=C=CH_2$					
Propyne	1.5	1.74	$C_3H_5^+$	1.0	-276
CH_3-C≡CH					
Propene	1.5	1.50	$C_3H_5^+$	0.45	-110
CH_3-CH=CH_2			$C_3H_7^+$	0.55	-173
Cyclopropane	1.4	1.34	$C_3H_7^+$	0.10	-290
c-C_3H_6			$C_3H_5^+$	0.90	-143
Propane	0.63	1.41	$C_3H_7^+$	1.0	-79 to -133
C_3H_8					
2-Butene	1.3	1.61	$C_4H_9^+$	0.10	-193
$CH_3CH=CHCH_3$			$C_4H_7^+$	0.40	-181
			$C_3H_5^+$	0.50	-155
i-Butane	1.3	1.54	$C_3H_7^+$	0.80	-94
C_4H_{10}			$C_4H_9^+$	0.20	-53
n-Butane	0.98	1.52	$C_3H_7^+$	0.75	-102
C_4H_{10}			$C_4H_9^+$	0.25	-61
Benzene	1.5	1.63	$C_6H_7^+$	1.0	-271
C_6H_6					
Toluene	1.3	1.83	$C_7H_9^+$	1.0	-306
C_7H_8					
Methylcyclohexane	1.7	1.87	$C_7H_{13}^+$	0.35	-174
C_7H_{14}			$C_6H_{11}^+$	0.25	-224
			$C_4H_9^+$	0.20	-12 to -167
			$C_3H_5^+$	0.20	-69

Table 4.2: The observed rate coefficients and products for the reactions of N_2H^+ with the range of hydrocarbons investigated.

a) Observed rate coefficient. Units 10^{-9} cm^3s^{-1}.

b) Theoretical collision rate. Calculated using the method of Su and Chesnavich [114] or Langevin theory.

c) The energetics for each observed product channel, in kJ mol^{-1}.

d) This rate coefficient could not be measured due to the mass overlap between product and primary

Neutral	Rate Coefficient [a, b]		Products	
Acetylene C_2H_2	NR [c]	1.34	-	
Ethylene C_2H_4	0.06 [d]	1.43	$C_2H_5^+$	1.0
Allene $CH_2=C=CH_2$	1.7	1.39	$CH_2CHCH_2^+$	1.0
Propyne $CH_3-C\equiv CH$	1.8	1.97	C_3H_5+	1.0
Cyclopropane c-C_3H_6	1.6	1.53	$C_3H_7^+$	1.0
Propene $CH_3-CH=CH_2$	1.7	1.73	$C_3H_7^+$	1.0
Propane C_3H_8	NR [c]	1.62	-	
2-Butene $CH_3CH=CHCH_3$	1.5	1.87	$C_4H_9^+$	1.0
n-Butane C_4H_{10}	<0.0033 [e]	1.77	$C_4H_9^+$	~70
			$C_4H_{10}.H_3O^+$	~30 [e]
i-Butane C_4H_{10}	<0.004 [e]	1.79	$C_4H_9^+$	f
			$C_4H_{10}.H_3O^+$ (?)	
Benzene C_6H_6	1.3	1.53	$C_6H_7^+$	1.0
Toluene C_7H_8	1.3	2.10	$C_7H_9^+$	1.0
Methylcyclohexane C_7H_{14}	0.71	2.22	$C_7H_{13}^+$	1.0

Table 4.3: The observed rate coefficients and products for the reactions of H_3O^+ with the range of hydrocarbons investigated.

a) Observed rate coefficient. Units 10^{-9} cm^3s^{-1}.

b) Theoretical collision rate. Calculated using the method of Su and Chesnavich [114] or Langevin theory.

c) NR indicates no observed reaction. The upper limit for these rate coefficients is $5x10^{-13}$ cm^3s^{-1}.

d) This value was only roughly determined as the reaction was not required to be accurately measured. The value obtained was in agreement with the literature value of $5.2x10^{-11}$ cm^3s^{-1}.

e) These reactions involve termolecular associations and thus the rate coefficient and product distributions will be pressure dependent. Rates and products are given for a helium carrier gas at 0.485 Torr.

f) See Text.

§4.3.2: Data Analysis.

The reactivity of the H_3^+ and N_2H^+ ions with the trace neutral contaminants in the carrier gases (particularly nitrogen and water) means that relatively extensive data analyses are required to extract accurate product distributions for the H_3^+ reactions from the raw data recorded. Indeed, this is one of the major reasons that the reactions of N_2H^+ and H_3O^+ were included in this study. In all cylinders of compressed gas that were used in this work, either helium or hydrogen, there were always trace amounts of neutral impurities present, mainly oxygen, nitrogen, and water. Even after the carrier gases are passed through a molecular sieve tower cooled to liquid nitrogen temperature, some of these impurities will pass through to the flow tube. Because of the rapid reactions which occur between H_3^+ and nitrogen (Reaction 407), H_3^+ and water (Reaction 408) and the similarly fast reaction between N_2H^+ and water (Reaction 409), [1] even trace levels of these neutral impurities cause significant impurity ion signals to be observed.

$$H_3^+ + N_2 \Rightarrow N_2H^+ + H_2 \quad (407)$$
$$k = 1.9\times10^{-9}\ cm^3s^{-1}.$$

$$H_3^+ + H_2O \Rightarrow H_3O^+ + H_2 \quad (408)$$
$$k = 5.3\times10^{-9}\ cm^3s^{-1}.$$

$$N_2H^+ + H_2O \Rightarrow H_3O^+ + N_2 \quad (409)$$
$$k = 2.6\times10^{-9}\ cm^3s^{-1}.$$

This is shown graphically in Figure 4.1 which shows a typical mass spectrum collected when H_3^+ ions are injected into a helium carrier gas. As a consequence of the above, when studying the reaction of H_3^+ with a neutral molecule, the reactions of N_2H^+ and H_3O^+ with the same neutral molecule are overlaid on the data obtained. This overlay must be removed before accurate product branching ratios for the H_3^+ reaction can be obtained. A similar complication is seen for the N_2H^+ data as some H_3O^+ will always form by Reaction 409. In order to obtain accurate product distributions, all the data obtained in the current sections were imported into a spreadsheet program (Microsoft Excel™) and a 'correction' for product counts generated by these other (impurity) ionic reactants was subtracted from each product channel. In most cases this correction was simply the branching ratio for the specific product channel multiplied by the number of counts lost from the relevant primary ion (i.e. H_3O^+ or

N_2H^+). That is the number of counts of H_3O^+ or N_2H^+ reacted away at a particular flow was used as a measure of the number of counts of its products that will be seen. Where appropriate a correction for mass discrimination was also used. Expressed symbolically this is:

Correction = (*Branching Ratio* (range 0.05-1.0)) x ($[A]_0$ - $[A]_x$) (4.1).

Here A is the primary ion (H_3O^+ or N_2H^+), $[A]_0$ represents the average number of counts due to species A with no neutral flowing and $[A]_x$ is the number of counts at a particular neutral flow, x.

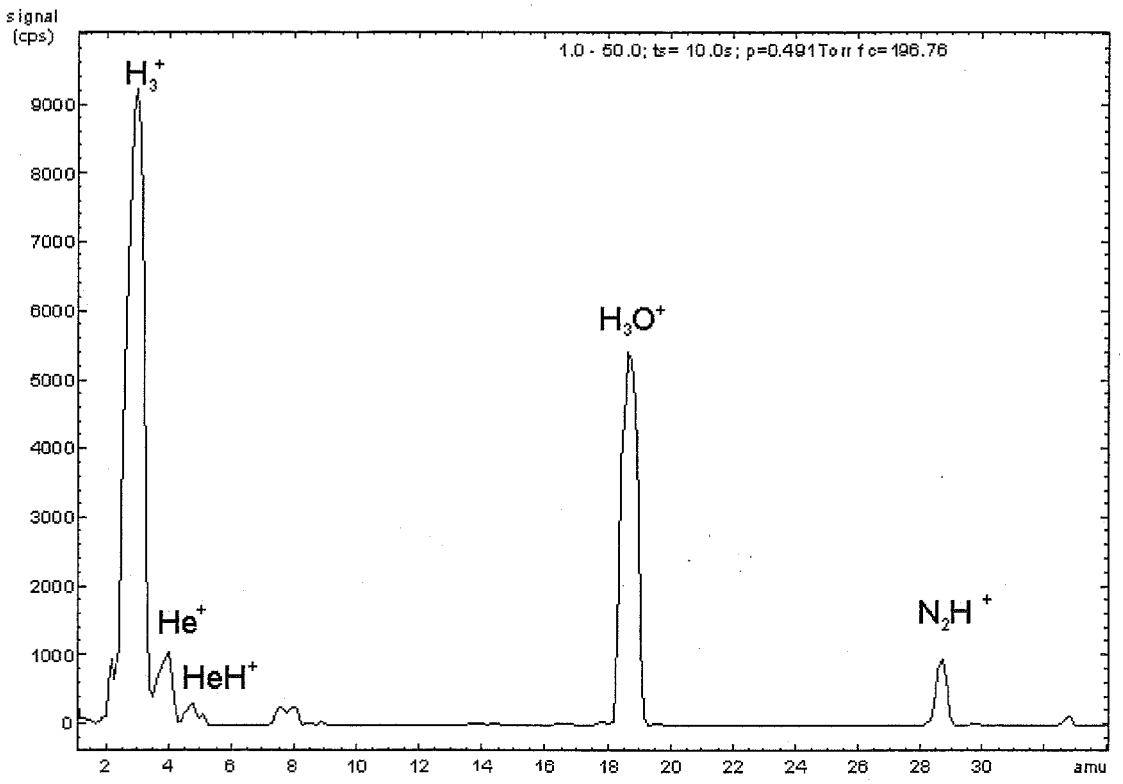

Figure 4.1: A mass spectrum of the ionic products that result from the injection of an H_3^+ ion signal into a helium carrier gas. The major secondary ions (H_3O^+, N_2H^+) are the result of exothermic reactions between the injected H_3^+ ion and trace contaminant species in the carrier gas (H_2O and N_2). The more minor contaminant ions (HeH^+ mainly) are the result of endothermic reactions, the rates of which are accelerated by energy gained by H_3^+ during the injection process.

The one exception to this general rule occurred when a $C_2H_5^+$ ion product featured in the reaction. In these cases there was a mass overlap between $C_2H_5^+$ and N_2H^+ at m/z = 29 and thus an expression for the number of counts of N_2H^+ removed

by reaction of the 29 signal could not easily be generated from the difference between the initial and current ion counts at $m/z = 29$. For these reactions an estimate of the number of counts of N_2H^+ was computed using the measured flow of neutral and the reaction rate coefficient for that neutral with N_2H^+ (measured separately). The expected number of counts of N_2H^+ remaining (unreacted) was then subtracted from the $m/z = 29$ channel to give an estimate of the count rate due to the $C_2H_5^+$ product channel. The difference between the computed "N_2H^+ counts remaining" value and the average "initial counts of N_2H^+" value was used to correct any channels to which the products of the N_2H^+ reaction contributed. When the reactions of D_3^+ were investigated, no data work-up was possible because of the nature of the reaction system and the desired information. The value of interest is the hydrogen to deuterium ratio in the product ions. As a branching ratio for the H:D transfer ratio for the DH_2O^+ ion with the neutral reactant was not available, one must assume the ratio is not seriously affected by the source (or energy of the transfer) of the deuteron. An apparent shift towards hydrogen retention may be observed as a result of proton rather than deuteron transfer from the DH_2O^+ ion. A relatively clean supply of helium was obtained for this experiment (mainly by baking clean the molecular sieves in the liquid nitrogen tower) so the levels of contaminant were low, as is shown in Figure 4.2.

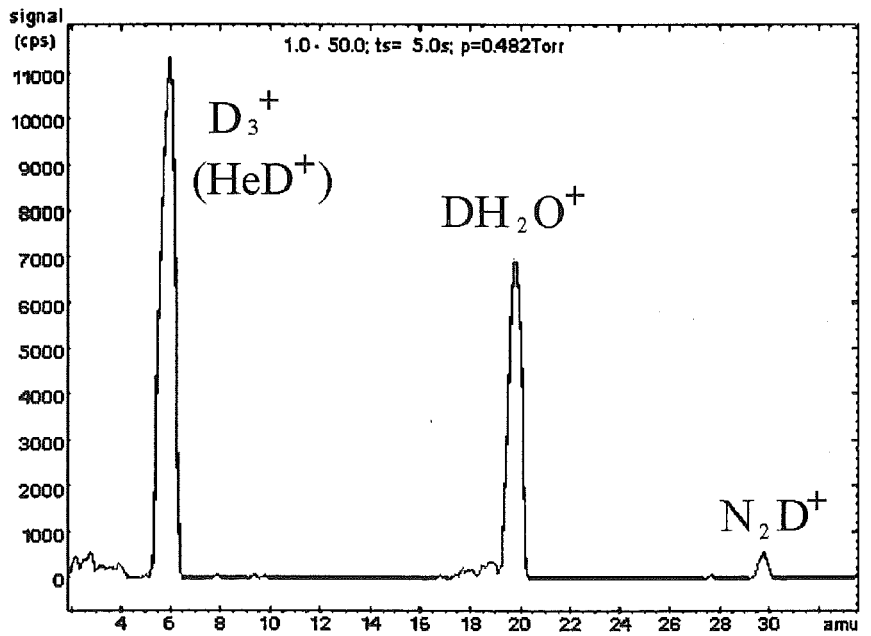

Figure 4.2: A mass spectrum obtained after the injection of D_3^+ into a helium carrier. Note that both D_3^+ and HeD^+ appear at 6 amu in this system.

§4.3.3: A note of the work of Aquilanti and Volpi.

A significant number of the reactions of H_3^+ presented in this section of work have been studied as long ago as 1966 by V. Aquilanti and G.G. Volpi [135, 136]. This represents some of the earliest kinetic work on H_3^+ and consequently there are a few comments that now may be made about the work with the benefit of hindsight. The method used to form the reactant ions in this study is also quite different to any of those used recently and bears description. The ions under study were formed in an ion source chamber by bombardment with beta rays which were emitted by tritium that had been absorbed on to the chamber walls prior to the reaction. This chamber was filled with a dilute mixture of the reactant hydrocarbon in hydrogen (or deuterium) and the ion signals were monitored as the partial pressure of the reactant gas was varied. Ions were accelerated by a positive 'repeller' electrode from the ion source towards the sampling slit which led into the analyser tube of a mass spectrometer. The amount of neutral reactant was altered in successive experimental runs and a constant reaction time was assumed in order to obtain the kinetic information.

The most striking difference between the results of Aquilanti and Volpi and current thinking is the model they used to interpret the observed ion signals. In their work, the formation of products from dissociative proton transfer is assumed to be influenced by a third body. That is, Aquilanti and Volpi believed that the collision complex lived long enough to undergo collisions with the third body. The less dissociative products in their view result from ions that have had a significant amount of energy removed by collision. A variation observed in the product distribution with pressure was taken by Aquilanti and Volpi to be proof of this model. In light of the current understanding of proton transfer from the H_3^+ ion, this variation would now seem to be the result of the presence of internally excited H_3^+ ions. The high pressure results of Aquilanti and Volpi (~0.3 Torr hydrogen) should be the most comparable to the results for ground state H_3^+ ions presented in the present work. Another factor that needs to be considered when comparing the current results to those of Aquilanti and Volpi, is that at no time is any mention of impurity ions made in either of their papers. It is possible that contributions to the product distribution from the reactions of H_3O^+ and N_2H^+ with the neutral reactant are included in their 'H_3^+' results but this is not stated explicitly. Finally, the rate coefficients obtained by these workers were

typically around a factor of three lower than results obtained using more contemporary techniques.

§4.3.4: Reactions investigated.

Acetylene

The reaction of H_3^+ with acetylene is one of the simplest of all the H_3^+ reactions reported here. The proton affinity of acetylene is 641 kJ mol^{-1}, much less than water so no reaction between H_3O^+ and acetylene was expected or observed.

N_2H^+ has previously been shown to produce only $C_2H_3^+$ [137] when reacting with acetylene with a rate coefficient of $1.4x10^{-9}$ cm^3s^{-1}. Further, the only product channel energetically available for the H_3^+ reaction is $C_2H_3^+$ and this is indeed the only product channel that was observed in the helium carrier gas (see Reaction 410 a, b, and c). This observation is in accordance with the other studies reported for this reaction [98, 135, 137, 138]. Using a D_3^+ reactant ion only $C_2H_2D^+$ was observed as was expected.

In a hydrogen carrier gas a $C_2H_5^+$ product ion was observed in addition to the $C_2H_3^+$ ion. This $C_2H_5^+$ ion is presumably the result of $C_2H_3^+$ associating with the hydrogen carrier gas. This reaction (Reaction 41) has been reported previously to proceed with a rate coefficient of $\sim 2x10^{-29}$ cm^6s^{-1} in hydrogen [2], which equates to an apparent bimolecular rate coefficient of $\sim 3x10^{-13}$ cm^3s^{-1} at the pressure of 0.350 Torr of hydrogen used in this study.

$$H_3^+ + C_2H_2 \Rightarrow C_2H_3^+ + H_2 + 222 \text{ kJ mol}^{-1} \quad (410a)$$

$$\Rightarrow C_2H_4^+ + H + H_2 - 211 \text{ kJ mol}^{-1} \quad (410b)$$

$$\Rightarrow C_2H^+ + 2H_2 - 360 \text{ kJ mol}^{-1} \quad (410c)$$

$$C_2H_3^+ + 2H_2 \Rightarrow C_2H_5^+ + H_2 \quad (411)$$

In the ICR work of Kim *et al.* [138] the endothermic channels 410b and 410c could be driven by internal excitation of the reactant ions and these were seen when excited ions H_3^+ were used as the reactant.

Aquilanti and Volpi also reported a small amount of $C_2H_5^+$ at the higher pressures used in their study. This ion probably results from the same association reaction of $C_2H_3^+$ with H_2 as seen in the hydrogen carrier gas SIFT experiment, although the magnitude of association was less in their case due to the lower pressure (0.3 Torr in the Aquilanti and Volpi study against 0.5 Torr here).

The average rate coefficient determined in this study was $2.6x10^{-9}$ cm^3s^{-1} which is significantly lower than the average value of $3.2x10^{-9}$ cm^3s^{-1} reported in the literature. It should be noted however that the collision rate for this process is only $2.8x10^{-9}$ cm^3s^{-1} which indicates that the rate coefficient has probably been previously over-estimated possibly due to the influence of vibrationally excited H_3^+

Ethylene

The proton affinity of ethylene is 681 kJ mol^{-1} (10 kJ mol^{-1} less than that of water) and thus the proton transfer from H_3O^+ to C_2H_4 is expected to be very slow. The rate coefficient for H_3O^+/C_2H_4 was not accurately measured in the current study as it was not fast enough to feature in the H_3^+ data analysis. However the rough rate coefficient obtained ($k = 6x10^{-11}$ cm^3s^{-1}) is in broad agreement with the literature value of $5.2x10^{-11}$ cm^3s^{-1} [1]. The product for this reaction, $C_2H_5^+$, is consistent with the endothermic nature of the proton transfer.

The reaction of N_2H^+ with ethylene also leads solely to $C_2H_5^+$. This concurrent reaction prevents an accurate measurement of the rate coefficient as both reactant and product occur at $m/z = 29$. However, as the PA of nitrogen is 494 kJ mol^{-1} (approximately 200 kJ mol^{-1} less than that of ethylene) the reaction is expected to proceed with a rate coefficient similar to the Langevin collision rate.

Several other researchers have studied the reaction of H_3^+ with ethylene using a wide range of instruments. Fiaux *et al.* [139] using a tandem ICR, Kim *et al.* using an ICR [138] and Rakshit using a selected-ion drift-chamber [140] all report a collision rate value for the rate coefficient and a product distribution of approximately 70% $C_2H_3^+$ and 30% $C_2H_5^+$. The current study finds a branching ratio of 60% $C_2H_3^+$ and 40% $C_2H_5^+$ in a helium bath gas.

Two other earlier studies also exist. The first of these by Aquilanti and Volpi [135] was performed in a modified mass spectrometer. In this paper the product distribution at the highest pressure was 30% $C_2H_3^+$ and 70% $C_2H_5^+$, a result that is very similar to the raw results (i.e. those not corrected for the effect of H_3O^+ and N_2H^+) obtained in the current study. The results obtained by these workers will also have association reactions with hydrogen overlaid. The other study, by Burt and co-workers [98], does not report a product branching ratio but their graphs show that $C_2H_5^+$ signal was higher than the $C_2H_3^+$signal, again probably as a result of its

formation via less exothermic reactions from impurity ions such as H_3O^+ and N_2H^+. In other work by Smith and Futrell [145] the product ratios for KrH^+ (PA Kr = 424.6 kJ mol^{-1} cf. H_2 = 422.3 kJ mol^{-1}) were 0.28/0.72 $C_2H_5^+/C_2H_3^+$ in good agreement with the H_3^+ results. The similar product distribution from two different proton donors with similar PA values suggests that the initial processes are similar i.e. the transfer of a proton without the formation of an intimate complex. This result also suggests that the final fate of the ions is dependant on the initial energy of the transferred proton i.e. the PA of the neutral initially bound to it. Finally, this result indicates that any energy carried away by the reactant neutral is likely to be in the form of translational rather than vibrational energy as the results are similar despite the inability of krypton to carry vibrational energy.

The product distribution observed here with the hydrogen bath gas showed no $C_2H_3^+$ at all, indicating that this ion has all undergone association reactions with hydrogen to form $C_2H_5^+$. This association reaction (Reaction 411) has been previously reported to proceed with a rate coefficient of ~$2x10^{-29}$ cm^6s^{-1} in hydrogen, which equates to an apparent bimolecular rate of ~$3x10^{-13}$ cm^3s^{-1} at the flow tube pressures used. With a rate coefficient of this magnitude total conversion of $C_2H_3^+$ to $C_2H_5^+$ would be expected in a reaction where the carrier gas was hydrogen.

As a result of reaction with D_3^+ three ions were observed, $C_2H_4D^+$, $C_2H_2D^+$ and $C_2H_3^+$ showing that the $C_2H_5^+$ and $C_2H_3^+$ ions are both direct products of proton (or deuteron) transfer. The statistical ratio of $C_2H_3^+$:$C_2H_2D^+$ should be 2:3 but was observed to be closer to 1:2 indicating that the reaction favours deuterium retention somewhat. This isotopic ratio is consistent with the studies of Fiaux *et al.* [139] if it assumed that their relaxed H_3^+ results (i.e. those H_3^+ ions that have undergone the most collisions in the ion source of their tandem ICR) are the most comparable to our own. By altering the number of stabilising collisions that the H_3^+ ions receive Fiaux *et al.* have been able to investigate the effect of reactant ion energy on the isotope ratio. They found that the ratio varied from ~0.66 (i.e. statistical elimination) for highly excited H_3^+ ions down to ~0.50 for the 'relaxed' ions that had undergone many collisions in the source. They rationalise these results in terms of the difference in zero-point energy between hydrogen and deuterium. Hydrogen has a larger zero-point energy than deuterium and this extra energy effectively lowers the activation energy barrier towards the elimination of hydrogen atoms from a $C_2H_4D^+$ complex. Similar

effects have been seen by Smith and Futrell (ref) in the decay of metastable $C_2H_4D^+$ in a tandem ICR. The magnitude of the effect observed in the H3+ case is less than that observed for metastable ions and suggests that the dissociation of the $C_2H_4D^+$ ions mostly occurs well above the threshold energy of the dissociation reaction.

The average rate coefficient of $2.7x10^{-9}$ cm^3s^{-1} for the reaction of H_3^+ with ethylene is consistent with the previous investigations of this reaction and is close to the Langevin collision rate of $2.9x10^{-9}$ cm^3s^{-1}.

Allene

The reactions of allene (or propadiene) have not been studied previously with either N_2H^+ or H_3^+, however Fairley has looked at the reaction with H_3O^+ [71]. In both this earlier study and the current one the sole product observed was $C_3H_5^+$ at $m/z = 41$. Fairley showed that these $C_3H_5^+$ ions exist entirely in the allyl structure, $CH_2CHCH_2^+$, which is the global minimum on the $C_3H_5^+$ potential energy surface. The average rate coefficient for this process was found to be $1.7x10^{-9}$ cm^3s^{-1}. The polarisability for allene can be estimated from the work of Miller [141] and thus a collision rate coefficient for the process H_3O^+ + allene can be found to be $1.39x10^{-9}$ cm^3s^{-1}. The observed rate coefficient is slightly higher than this but not significantly enough to be concerning.

The reaction of N_2H^+ with allene is very similar to the H_3O^+ reaction, giving only $C_3H_5^+$ as a product with a rate coefficient of $1.4x10^{-9}$ cm^3s^{-1}. This result is somewhat surprising as the dissociative channel leading to $C_3H_3^+$ is exothermic for both of the isomeric forms of $C_3H_3^+$.

$$N_2H^+ + CH_2{=}C{=}CH_2 \Rightarrow C_3H_5^+ + N_2 + 281 \text{ kJ mol}^{-1} \quad (412a)$$

$$\Rightarrow c\text{-}C_3H_3^+ + N_2 + H_2 + 152 \text{ kJ mol}^{-1} \quad (412b)$$

$$\Rightarrow CH_2C{\equiv}CH^+ + N_2 + H_2 + 47 \text{ kJ mol}^{-1} \quad (412c)$$

Note that channel 412a is assumed to produce the allyl structure as this is the global minimum. This product isomer has been seen to be produced in all cases where the energy available is greater than the ~75 kJ mol^{-1} barrier to interconversion which exists between the 2-propenyl and allyl cations [71, 88].

Reaction 413 was observed to proceed at $2.9x10^{-9}$ cm^3s^{-1}, which again is close to the collision rate of $3.42x10^{-9}$ cm^3s^{-1}.

$$H_3^+ + CH_2{=}C{=}CH_2 \Rightarrow C_3H_3^+ + 2H_2 + 111 \text{ or } 223 \text{ kJ mol}^{-1} \quad (413a)$$

$$\Rightarrow C_3H_5^+ + H_2 + 352 \text{ kJ mol}^{-1} \quad (413b)$$

$$\Rightarrow \quad C_3H^+ + 3H_2 \text{ -296 kJ mol}^{-1} \qquad (413c)$$

$$\Rightarrow \quad C_3H_4^+ + H + H_2 \text{ -45 kJ mol}^{-1} \qquad (413d)$$

The energetics for the formation of the $C_3H_3^+$ ion in channel 413a are not given above as it is not known which isomer is formed. For the linear isomer channel 413a is 111 kJ mol^{-1} exothermic and for the cyclic form it is 223 kJ mol^{-1} exothermic. The investigation of the reactivity of this $C_3H_3^+$ ion with methanol gave a curved semi-logarithmic decay indicating that two isomeric species were present. A model using the rate coefficients from the paper of McEwan *et al.* [134] (see §4.2.1, final paragraphs) found that approximately 70% of the ions were the linear isomer and 30% the cyclic. This distribution favours the less exothermic product and indicates that in most cases where $C_3H_3^+$ was formed from the reaction of H_3^+ and allene, the linear structure was retained. Presumably this is because there was no real driving force to form the energetically more favourable cyclic form, i.e. there was already enough energy to drive the reaction.

Only channel 413a is believed to be a true primary product. $C_3H_5^+$ was seen in the experiments using a hydrogen carrier and is probably the result of an association reaction. A small (<10%) amount of C_3H^+ (channel 413c) was seen in the helium carrier, but this is likely to come from the HeH^+ impurity ion. If channel 413c was the result of excited H_3^+ being present, the less endothermic channel 413d would a seem more probable product to observe first. This was not, however, observed in any significant amount.

Propyne

Propyne (or methylacetylene) is a structural isomer of allene and its reactivity with all three ionic reactants is very similar to that of allene. Both H_3O^+ and N_2H^+ give exclusively proton transfer as a product with rate coefficients of 1.8×10^{-9} and 1.5×10^{-9} cm^{3}s^{-1} respectively. The dipole moment and polarisability of propyne are known and the computed collision rate coefficients are: H_3O^+, 1.97×10^{-9} cm^{3}s^{-1} and, N_2H^+, 1.74×10^{-9} cm^{3}s^{-1}. Both reactions thus proceed at just less than the respective collision rate coefficients, as expected for exothermic proton transfers. Fairley has shown that the $C_3H_5^+$ isomer formed by the low energy protonation (i.e. from H_3O^+) of propyne is the 2-propenyl cation, which is not the global minimum on the potential energy surface [71, 88]. There is not enough energy available in the H_3O^+/propyne system

to overcome the barrier between the initially formed 2-propenyl cation to the more stable allyl cation. In the case of N_2H^+ the $C_3H_5^+$ ion formed is almost certainly the allyl cation for both the propyne and allene reactions.

The N_2H^+/propyne system was also investigated using the drift tube. As the voltage on the drift tube was increased, the $C_3H_3^+$ ion was observed to increase from ~3% at thermal energies up to 12% at –250V (i.e. 5 V cm^{-1}. at 0.34 Torr). This shows that despite the relatively small energy difference between N_2H^+ and H_3^+ (71 kJ mol^{-1}), kinetic energy is inefficient at boosting the energy of the N_2H^+ ion up to that of the H_3^+ ion. It does however show that when N_2H^+ is supplied more energy the next channel observed is the same channel as that observed in the H_3^+ case, confirming that the difference between the two cases is predominantly energy and not some other factor.

The reaction of H_3^+ with propyne gives, like that with allene, the $C_3H_3^+$ cation as the sole product in a helium carrier. A small amount of energetically impossible C_3H^+ was also observed and this is again assigned to interference from the small HeH^+ impurity. When a D_3^+ reactant ion was used, the ratio of deuteron loss to deuteron retention was approximately that expected from a statistical analysis of the system. The $C_3H_5^+$ cation was also seen in the hydrogen carrier from the H_3^+ reaction and this was probably formed from $C_3H_3^+$ which had associated with the hydrogen (see the allene discussion above). The $C_3H_3^+$ion was, as in the allene case above, formed in two ismomeric structures, approximately 70% of the products were *l*-$C_3H_3^+$ and 30% *c*-$C_3H_3^+$

Aquilanti and Volpi saw a mixture of $C_3H_3^+$ and $C_3H_5^+$, with more $C_3H_5^+$ forming as the pressure was increased. However, they also performed the same reactions with D_3^+ in a deuterium atmosphere and did not report a $C_3H_3D_2^+$ or $C_3H_2D_3^+$ ion which would be the result of dissociative deuteron transfer followed by an association reaction with deuterium. The fact that no $C_3H_5^+$ is observed in the helium carrier and that it apparently represents only ~30% of the products in the hydrogen carrier, is strongly suggestive that $C_3H_5^+$ is not a primary process in this reaction. The only other explanation would require that the H_3^+ in the helium carrier is extensively excited, a possibility that has been discounted by the previous non-reaction of the H_3^+ ions with an argon probe (see §4.2.1).

Propene

The reaction of H_3O^+ with propene proceeds at the collision rate (k_{expt} and k_{coll} = $1.7x10^{-9}$ cm^3s^{-1}) and gives only $C_3H_7^+$. This ionic product is the result of non-dissociative proton transfer and the reaction is 53 kJ mol^{-1} exothermic if the product is the *iso*-$C_3H_7^+$ ion.

Propene reacts with N_2H^+ with an observed rate coefficient of $1.5x10^{-9}$ cm^3s^{-1} (k_{coll} = $1.5x10^{-9}$ cm^3s^{-1}) and gives two products, $C_3H_5^+$ and $C_3H_7^+$.

$$N_2H^+ + C_3H_6 \Rightarrow C_3H_7^+ + N_2 + 173 \text{ kJ mol}^{-1} \quad [0.55] \quad (414a)$$

$$\Rightarrow C_3H_5^+ + H_2 + N_2 + 110 \text{ kJ mol}^{-1} \quad [0.45] \quad (414b)$$

The $C_3H_5^+$ ion above is assumed to be the allyl cation while the $C_3H_7^+$ ion is assumed to have the *iso*-$C_3H_7^+$ form, rather than the alternative cyclic or *n*-$C_3H_7^+$ forms, as this is the lowest energy linear isomer.

The behaviour of the N_2H^+/propene system was also probed using the drift tube feature of the FA-SIFDT. A plot of the product branching ratio against the drift tube voltage is shown below.

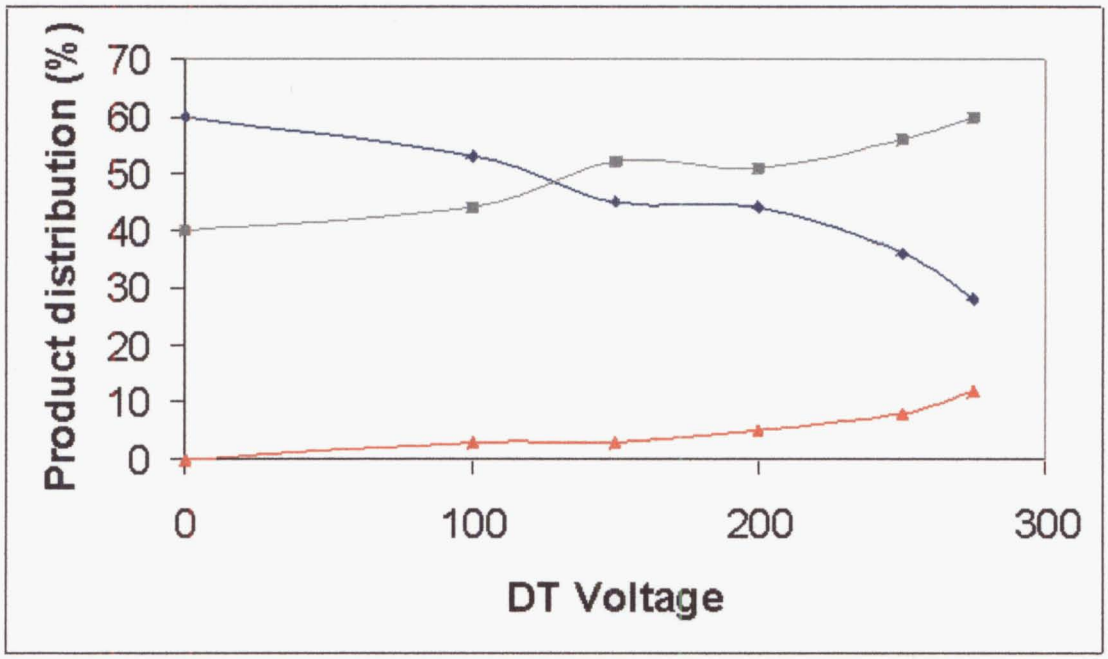

Figure 4.3: The variation of the branching ratio for the N_2H^+/propene reaction as the voltage of the drift tube is altered. The blue line is the $C_3H_7^+$ ion, the grey line the C_3H_5+ ion and the red line the $C_2H_3^+$ ion. The results were obtained in 0.34 Torr of helium.

When the results presented above are compared to the branching ratio for an H_3^+ reactant (see below) it is apparent that the voltage applied has narrowed the gap between the two observed distributions. Indeed the $C_2H_3^+$ product that is not seen in the N_2H^+ reaction at thermal energies has reached ~12% by 275V, around one half of the value finally seen for the H_3^+ system. The $C_3H_5^+$ product is, as expected, becoming less important, while the $C_3H_3^+$ one becomes conversely more significant. This appears to show that the difference between the N_2H^+ and H_3^+ reactions could be eliminated if enough energy could be placed in the N_2H^+ ion, indicating that the important factor in the dissociative fragments from exothermic proton transfer really is the energy of the reactant ion.

The reaction of propene with H_3^+ again gives different product distributions in the helium and hydrogen carrier gases.

$$H_3^+ + C_3H_6 \Rightarrow C_3H_5^+ + 2H_2 + 181 \text{ kJ mol}^{-1} \quad (415a)$$

$$\Rightarrow C_3H_3^+ + 3H_2 + 52 \text{ kJ mol}^{-1} \quad (415b)$$

$$\Rightarrow C_2H_3^+ + CH_4 + H_2 + 89 \text{ kJ mol}^{-1} \quad (415c)$$

The energetics shown above assume the allyl cation as the $C_3H_5^+$ product. This has been experimentally verified using its reactivity with methanol. The $C_3H_3^+$ ion formed here must be the cyclopropenyl radical as formation of linear $C_3H_3^+$ is 53 kJ mol^{-1} endothermic.

The product ratios for this reaction were 65% (a), 10% (b), and 25% (c) in helium and 70% (a) and 30% (c) in a hydrogen carrier. There are two possible reasons for the difference in the $C_3H_3^+$ branching ratio. Firstly it could be a is a result of the $C_3H_3^+$ ion formed associating with the hydrogen carrier gas and giving $C_3H_5^+$. Secondly, the least exothermic product (channel 415b) would be expected to be enhanced the most by internal excitation of the H_3^+ ion in a helium carrier. The reaction exothermicity (59 kJ mol^{-1}) is less than that observed for most authentic product channels observed elsewhere in this study. To answer this question one must examine the D_3^+ results.

With a D_3^+ reactant, the $C_3H_5^+$ and $C_2H_3^+$ products both give hydrogen to deuterium ratios (e.g. $C_2H_3^+$:$C_2H_2D^+$ ratio for the $C_2H_3^+$ product) that are close to the statistically expected ratio. The $C_3H_3^+$ ion however, is found to strongly favour deuteron loss. Statistically a $C_3H_3^+$:$C_3H_2D^+$ ratio of 4:3 is expected, instead the ratio observed is ~10:1. As $C_3H_3^+$ cannot be formed directly from the DH_2O^+ impurity this

ion should result from deuteron transfer from D_3^+ (and would be expected to show the statistical distribution) unless it is not a primary product of the D_3^+ (or H_3^+) reaction or the reaction mechanism is different from the others. Significant loss of the transferred deuteron will only occur if the collision complex has insufficient lifetime to make all the protons and deuterons equivalent. This is likely to result from highly energetic proton or deuteron transfer implying that $C_3H_3^+$ results from the more energetic impurity ions (mainly HeH^+).

Cyclopropane

Spanel, Smith and Henchman [142] have previously investigated the reactions of cyclopropane with all of the ionic reactants in this study. Both investigations find that H_3O^+ reacts at essentially the collision rate with cyclopropane to give $C_3H_7^+$. Spanel *et al.* obtained a rate coefficient of $1.5x10^{-9}$ while in the current study the rate coefficient was determined to be $1.6x10^{-9}$ cm^3s^{-1}. The collision rate coefficient for this process is $1.53x10^{-9}cm^3s^{-1}$. (It should be note that in Table 1 of Reference 83, the reactant labelled H_2O^+ is in fact H_3O^+).

The N_2H^+ rate and product distribution determined here are also in good agreement with that of Spanel, Smith and Henchman who found that Reaction 415 proceeded at $1.3x10^{-9}$ cm^3s^{-1} to give $C_3H_5^+$ [0.80] and $C_3H_7^+$ [0.20]. The results for the current study are shown below.

$$N_2H^+ + c\text{-}C_3H_6 \quad => \quad C_3H_7^+ + N_2 + 290 \text{ kJ mol}^{-1} \quad [0.10] \quad (415a)$$

$$=> \quad C_3H_5^+ + H_2 + N_2 + 143 \text{ kJ mol}^{-1} \quad [0.90] \quad (415b)$$

$$k = 1.4x10^{-9} \text{ cm}^3\text{s}^{-1}.$$

The exothermicity of channel 415a can be reduced to 258 kJ mol^{-1} if the cyclic structure is retained in the $C_3H_7^+$ product.

The agreement for the H_3^+ results between Spanel *et al.* [142] and the present work is satisfactory.. The rate coefficients are similar: $k_{obsd} = 2.6x10^{-9}$; $k_{Spanel} = 3.0x10^{-9}$; $k_{coll} = 3.32 \times 10^{-9}$ cm^3s^{-1} as are the product ratios in a helium carrier. The products seen in the Canterbury SIFT were $C_3H_5^+$ [0.60] and $C_2H_3^+$ [0.40] agreeing with Spanel *et al.* who also reported 40% $C_2H_3^+$ and 60% $C_3H_5^+$. A small amount of $C_3H_3^+$ [<0.05] was also seen in the helium carrier. This is probably the result of excited H_3^+ ions as it has a relatively low exothermicity (85 $kJmol^{-1}$ for the cyclopropenyl form) as compared to the other channels observed to occur throughout

this study and is also small. In a hydrogen carrier the ratio was observed to be $C_3H_5^+$ [0.25] and $C_2H_5^+$ [0.75]. This $C_2H_5^+$ product is presumably entirely the result of the association of $C_2H_3^+$ with hydrogen as direct formation of a $C_2H_5^+$ product is 131 kJ mol^{-1} endothermic. Thus the products can more correctly be written $C_3H_5^+$ [0.25] and $C_2H_3^+$ [0.75].

The reason for the difference in product distributions between carriers is not apparent as in the hydrogen carrier the **more** dissociative channel has been enhanced, a reversal of expectations. A difference in the stabilisation of the collision complex between helium and hydrogen may exist for this reaction but few real conclusions can be drawn without the benefit of a theoretical study.

$$H_3^+ + c\text{-}C_3H_6 \quad => \quad C_3H_5^+ + 2H_2 + 214 \text{ kJ mol}^{-1} \qquad (416a)$$

$$=> \quad C_2H_3^+ + CH_4 + H_2 + 122 \text{ kJ mol}^{-1} \qquad (416b)$$

$$=/=> \quad C_3H_3^+ + 3H_2 + 85 \text{ kJ mol}^{-1} \qquad (416c)$$

The $C_3H_5^+$ ion here has been shown (by its reactivity with methanol) to be essentially entirely the allyl cation.

Aquilanti and Volpi saw significant amounts of $C_3H_7^+$ in this reaction, further strengthening the case that they did not consider the effects of other less energetic proton transfer processes in their data analysis.

Propane

Propane has a low proton affinity, 625 kJ mol^{-1}, which makes proton transfer from water endothermic by 66 kJ mol^{-1}. A very slow reaction of H_3O^+ was observed to occur, $k_{expt} = 1.4x10^{-12}$ cm^3s^{-1}, giving $C_3H_7^+$. However only CP grade propane was available for these experiments so small impurities of propene or cyclopropane (which could both also give this product) in the reactant neutral cannot be ruled out. (In the analysis of the H_3^+ system H_3O^+ was assumed not to react.)

Despite being exothermic (from 79 to 133 kJ mol^{-1} depending on the $C_3H_7^+$ ion structure) the reaction of N_2H^+ with propane was also rather slow, the average rate coefficient being 6.3 $x10^{-10}$ cm^3s^{-1}. The collision rate for this process is $1.41x10^{-9}$ cm^3s^{-1} and thus the observed rate coefficient is less than half that expected. The product of this reaction is $C_3H_7^+$ as $C_3H_9^+$ is not a stable ion however this does not prevent the reaction from being exothermic. The slow reaction rate seen with N_2H^+

suggests that there is a barrier to formation of the $C_3H_7^+$ proton transfer product that is not represented by the ΔH_f values.

The H_3^+ reaction proceeds rather simply giving $C_2H_5^+$ and $C_3H_7^+$ in roughly equal proportions in both helium and hydrogen carrier gases.

$$H_3^+ + C_3H_8 \Rightarrow C_3H_7^+ + 2H_2 + 203 \text{ kJ mol}^{-1} \quad (417a)$$

$$\Rightarrow C_2H_5^+ + CH_4 + H_2 + 175 \text{ kJ mol}^{-1} \quad (417b)$$

The $C_3H_5^+$ ion above is assumed to be the allyl cation and the $C_3H_7^+$ ion has been assigned the *iso*-$C_3H_7^+$ form.

The results obtained from the reaction of D_3^+ and propane are extremely interesting. The levels of deuteron retention were very low, the expected ratio of $C_2H_5^+$:$C_2H_4D^+$ was 4:5 but the observed ratio was 3:1, $C_3H_7^+$:$C_3H_6D^+$ should be 2:7 and is greater than 4:1. These results will be a result of the fact that $C_3H_9^+$ is not a stable ions and thus the transferred deuteron does not have sufficient time to scramble before any elimination takes place. This would mean that the deuteron would be left still containing a significant amount of the energy that it entered the complex with. The presence of this energy means its departure is more probable as its bond to the complex is weaker.

The results of Aquilanti and Volpi [135, 136] are similar for this reaction as they reported $C_2H_5^+$ [0.65] and $C_3H_7^+$ [0.35]. In this case they were probably helped by the largely unreactive nature of the impurity ions that would have been likely to be present in their system.

2-Butene

2-Butene reacts rapidly with H_3O^+ to give an ion at $m/z = 57$, $C_4H_9^+$, which is simply the protonated neutral. The rate coefficient obtained was 1.5×10^{-9} cm^3s^{-1}, marginally less that the collision rate of 1.87×10^{-9} cm^3s^{-1}.

Reaction 418 also proceeds with a rate coefficient that is marginally less than the collision rate.

$$N_2H^+ + CH_3CH{=}CHCH_3 \Rightarrow C_4H_9^+ + N_2 + 193 \text{ kJ mol}^{-1}$$

[0.10] (418a)

$$\Rightarrow C_4H_7^+ + H_2 + N_2 + 181 \text{ kJ mol}^{-1}$$

[0.40] (418b)

$$\Rightarrow \quad C_3H_5^+ + CH_4 + N_2 + 155 \text{ kJ mol}^{-1}$$

[0.50] (418c)

The rate coefficient for the reaction of H_3^+ with 2-butene was found to be 2.8×10^{-9} cm^3s^{-1} (cf. collision rate = 4.18×10^{-9} cm^3s^{-1}) with three ionic products observed.

$$H_3^+ + CH_3CH{=}CHCH_3 \Rightarrow C_4H_7^+ + 2H_2 + 252 \text{ kJ mol}^{-1}$$

[0.40] (419a)

$$\Rightarrow \quad C_3H_5^+ + CH_4 + H_2 + 226 \text{ kJ mol}^{-1}$$

[0.35] (419b)

$$\Rightarrow \quad C_2H_5^+ + C_2H_4 + H_2 + 143 \text{ kJ mol}^{-1}$$

$$\text{or} \quad \Rightarrow \quad C_2H_5^+ + C_2H_6 + 279 \text{ kJ mol}^{-1}$$

[0.25] (419c)

The neutral products in channel 419c are probably C_2H_4 and H_2 rather than C_2H_6 as in most other cases in the current study at least one hydrogen molecule has been emitted in all channels.

The 2-butene system ideally shows the products shifting towards the more dissociative ones possible as can be seen from Figure 4.4 below.

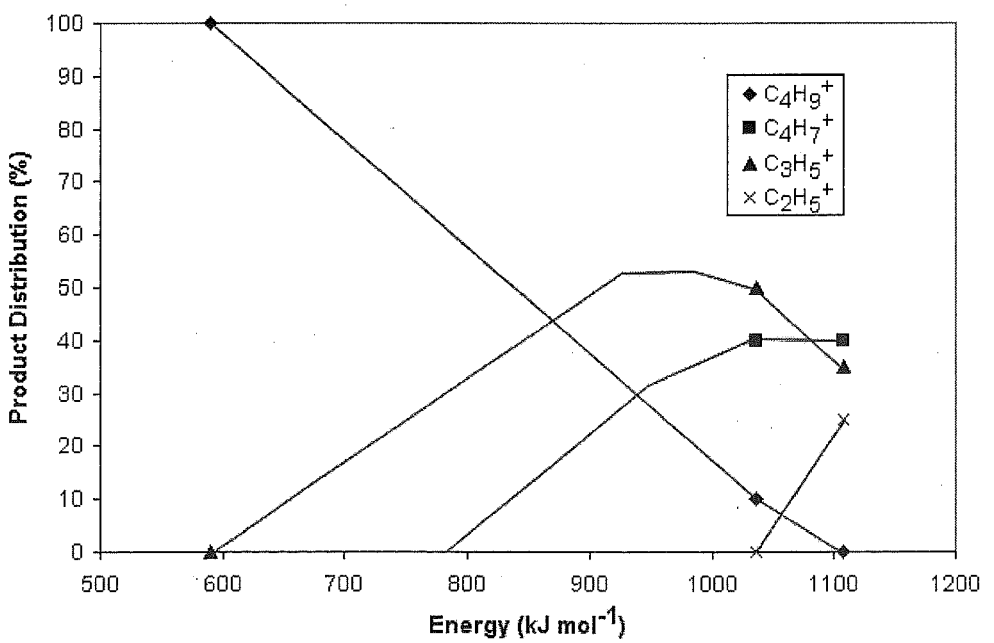

Figure 4.4: A graph of the observed product distributions plotted against the energy in the reactant ion (i.e. the neutral PA) for the reactions of H_3O^+, N_2H^+, and H_3^+ with 2-butene. The intervening energies have been interpolated from the data obtained.

iso-Butane

The proton affinity of isobutane is quite low (678 kJ mol^{-1}) and thus the reaction with H_3O^+ is slightly (13 kJ mol^{-1}) endothermic. The measured rate coefficient was 4.0 x 10^{-12} cm^3s^{-1} (k_{coll} = 1.79 x 10^{-9} cm^3s^{-1}) which, in accordance with the small endothermicity of the reaction, is slow. The products of this reaction have not been positively identified. Along with the expected 57 amu ion ($C_4H_9^+$) this reaction apparently gives a *m/z* = 37 ion as one of its products and, judging from the lack of ion count balance, other ionic products also. The reason for the contention that there are other ion products is that fewer total counts are seen in the *m/z* = 19, 37 and 57 ion peaks when the butane is flowing as compared to the "zero" flows where only H_3O^+ is present. A likely candidate for the other, unobserved, ion product is the adduct, $H_3O^+.C_4H_{10}$ (at *m/z* = 77), (see also the n-butane section below) which was unfortunately outside the scan range of the mass spectrum recorded when this reaction was investigated.

The ion at *m/z* = 37 could be C_3H^+ (although no exothermic reaction between $C_4H_9^+$ and butane that might give this product could be identified) or it may be $H_3O^+.H_2O$ as a result of water impurities present in the butane gas sample reacting with H_3O^+ via a termolecular process. The latter possibility is the more likely and means that the reaction rate reported here actually represents an upper bound. The ion counts in the 37 amu channel were generally less than 10% of those recorded for 57 amu (which apparently does not represent all the ion products of the reaction between H_3O^+ and *i*-C_4H_{10}) and thus the correction required is minor.

The N_2H^+ reaction is much faster than the H_3O^+ reaction and its rate coefficient was measured as 1.3x10^{-9} cm^3s^{-1}. The products of the reaction were found to be $C_3H_7^+$ [0.80], $C_4H_9^+$ [0.20]. A $C_3H_5^+$ [<0.05] channel was observed also but it is minor and so it is not considered to be a real product. Indeed as it is exothermic by only 31 kJ mol^{-1} it may represent contamination from some more energetic ion. Two other ion peaks were also seen (27 amu ($C_2H_3^+$) and 39 amu ($C_3H_3^+$)) both of which are endothermic, by 127 and 98 kJ mol^{-1} respectively. This suggests that there was indeed a problem with trace amounts of more energetic ions. In fact both of these product channels would also be endothermic for an H_3^+ reactant (the N_2H^+ was formed in a hydrogen carrier so that H_3^+ contamination could be possible) meaning that they must be the result of an extremely energetic impurity ion. He^+ or HeH^+ are

the most probable culprits and these may be formed by photoionisation or poorly-tuned injection conditions. Similar problems were observed for the N_2H^+ reaction with n-butane (see below).

For the H_3^+ reactant ion the observed rate coefficient was $3.0x10^{-9}$ cm^3s^{-1} which is close to the collision rate coefficient of $3.96x10^{-9}$ cm^3s^{-1}. This reaction is an exception to the general observation which may be made regarding the rest of this study as the H_3^+ reactant ion product distribution is only marginally more dissociative than that found with N_2H^+.

$$H_3^+ + \text{iso-}C_4H_{10} \Rightarrow C_3H_7^+ + CH_4 + H_2 + 249 \text{ kJ mol}^{-1} \quad (420a)$$

$$\Rightarrow C_4H_9^+ + 2H_2 + 140 \text{ kJ mol}^{-1} \quad (420b)$$

$$\Rightarrow C_2H_5^+ + C_2H_6 + H_2 + 155 \text{ kJ mol}^{-1} \quad (420c)$$

$$\Rightarrow C_3H_5^+ + CH_4 + 2H_2 + 102 \text{ kJ mol}^{-1} \quad (420d)$$

The energetics given above assume that the $C_4H_9^+$ ion has the iso-$C_4H_9^+$ structure rather than the more stable tertiary structure for which channel 420b would be 279 kJ mol^{-1} exothermic. The more stable tertiary ion structure was disregarded due to the amount of bond reorganisation required to form it. The $C_3H_7^+$ ion is in its most stable, iso-$C_3H_7^+$, form.

When the H_3^+ ions were generated from the reaction of Kr^+ ions with the hydrogen carrier the product distribution was 60% (a), 35% (b) and <5% (c). In a helium carrier the ratios were 50% (a), 30% (b), 20%(c). Channel 420d also began to be observed in the helium carrier. Because the relative importance of the $C_2H_5^+$ channel has also risen in the helium carrier it seems likely that there is a population of more energetic ions present for this reaction. It appears that the reactions involving butanes are very responsive to any extra energy in the reactant ions. The extra energy available in the H_3^+ can begin to give the $C_2H_5^+$ ion and also the next available product $C_3H_5^+$. $C_3H_5^+$ does not react with hydrogen and thus should be observed as a product in the hydrogen carrier if it was a true product of ground state H_3^+. For these larger hydrocarbons where there are so many more energetically available channels the identification of the products of ground state H_3^+ becomes much more complicated as small amounts of excess energy can open up a new channel.

n-Butane

The proton affinity of *n*-butane is not listed in the standard proton affinity tables (as compiled by Hunter and Lias [111]) but, judging from its reactivity with H_3O^+, it is apparently similar to iso-butane. The rate coefficient observed for Reaction 421 was slightly lower than that seen for the similar reaction of *iso*-butane having a value of 3.3×10^{-12} $cm^3 s^{-1}$.

$$H_3O^+ + CH_3CH_2CH_2CH_3 \Rightarrow C_4H_9^+ + H_2 + H_2O \quad (421a)$$

$$\Rightarrow C_4H_{10}.H_3O^+ \quad (421b)$$

Again ionic products other than the expected proton transfer were observed, at 37 and 77 amu. As in the *i*-butane case above, the $m/z = 37$ product is probably $H_3O^+.H_2O$ so the rate coefficient given above is an upper bound. The correction required for the increase in the apparent rate coefficient due to a slow reaction of H_3O^+ with water lowers the rate for Reaction 421 by approximately 10-15%. The ion observed at 77 amu is the adduct formed by the association of H_3O^+ and n-butane and represents approximately 30% of all the products at 0.485 Torr of helium. $C_4H_9^+$ is the least dissociative product possible from proton transfer to C_4H_{10} as $C_4H_{11}^+$ is not a stable ion and spontaneously loses a hydrogen molecule.

The reaction of N_2H^+ with *n*-butane proceeds slightly more slowly than does the similar reaction of *iso*-butane presented above (at 9.8×10^{-10} $cm^3 s^{-1}$, see Reaction 422 below). Two real products were seen, $C_3H_7^+$ [0.75] and $C_4H_9^+$ [0.25]. Two other minor ion signals were also seen but no exothermic reaction could be found to account for them. These signals were observed at 27 and 39 amu. They are presumably $C_2H_3^+$ and $C_3H_3^+$ respectively but the reactions to form them from N_2H^+ are 53 and 190 kJ mol^{-1} endothermic. Assignment of the $m/z = 27$ ion as HCN^+ requires an even more unfavourable reaction. The most likely explanation for these spurious ion signals is the presence of a highly energetic trace contaminant in the tube, perhaps He^+ or HeH^+. Ill-tuned injection conditions or photoionisation could conceivably create these ions, or other similar species. Similar ion signals were also seen in the reaction of N_2H^+ with iso-butane so it is unlikely that they are the result of a contaminant in the neutral reactant gas.

$$N_2H^+ + n\text{-}C_4H_{10} \Rightarrow C_3H_7^+ + CH_4 + N_2 + 102 \text{ kJ mol}^{-1} \quad [0.75] \quad (422a)$$

$$\Rightarrow C_4H_9^+ + H_2 + N_2 + 61 \text{ kJ mol}^{-1} \quad [0.25] \quad (422b)$$

$$k = 9.8x10^{-10}\ cm^3s^{-1}$$

The $C_3H_7^+$ ions above are assigned to the *n*-$C_3H_7^+$ isomer as the rearrangement required to reach the more energetically favourable iso-$C_3H_7^+$ form was considered too extensive to occur. A similar case may be made for the $C_4H_9^+$ retaining its *normal* form as well.

Slightly different results were observed for the reaction of H_3^+ with n-butane with the two different methods of ion generation. The general reaction is shown below.

$$H_3^+ + n\text{-}C_4H_{10} \Rightarrow C_3H_7^+ + CH_4 + H_2 + 173\ kJ\ mol^{-1} \quad (423a)$$

$$\Rightarrow C_4H_9^+ + 2H_2 + 132\ kJ\ mol^{-1} \quad (423b)$$

$$\Rightarrow C_2H_5^+ + C_2H_6 + H_2 + 163\ kJ\ mol^{-1} \quad (423c)$$

$$\Rightarrow C_3H_5^+ + CH_4 + 2H_2 + 110\ kJ\ mol^{-1} \quad (423d)$$

$$k = 3.0x10^{-9}\ cm^3s^{-1}.$$

When the H_3^+ ions were generated in the FA (i.e. when there was a helium carrier present in the SIFT reaction tube) the product ratio was approximately 45% (a), 35% (b), 15% (c), and 5% (d). In a hydrogen carrier the $C_3H_5^+$ (channel 423d) product was observed but was only ~1% while the $C_3H_7^+$ product had risen by the 5% that this channel previously represented. Whether this difference is the result of lower energy H_3^+ ions being present in the hydrogen carrier or of the association of $C_3H_5^+$ with the hydrogen carrier to form $C_3H_7^+$ is however unknown.

Benzene

The reactions of benzene with all the ionic species investigated here have all been studied previously by Spanel, Smith and Henchman [142]. The only ion product observed in all reactions by both this and the previous study was the protonated benzene ion ($C_6H_7^+$). The rate coefficients were all approximately equal to the collision rate. Spanel *et al.* began to see dissociative channels only when ArH^+ was used. This ions has an extra 52 kJ mol^{-1} of energy above that of H_3^+.

Toluene

Toluene, like benzene, has an enhanced stability due to the aromaticity of the ring and as such its proton transfer reactions are generally less dissociative. H_3O^+ reacts to yield only $C_7H_9^+$, which is simply the protonated neutral. The rate coefficient

for this process is $1.3x10^{-9}$ cm^3s^{-1}, which is surprising as this is somewhat lower than the collision rate of $2.16x10^{-9}$ cm^3s^{-1}.

The protonated nitrogen ion reacts at a similar rate ($k_{expt} = 1.3x10^{-9}$ *cf.* $k_{coll} = 1.83x10^{-9}$ cm^3s^{-1}) and also gives $C_7H_9^+$. A small (< 5%) $C_7H_7^+$ channel was also observed.

The reaction of H_3^+ with toluene becomes more dissociative, with a channel corresponding to methane loss also being observed.

$$H_3^+ + C_7H_8 \Rightarrow C_7H_9^+ + H_2 + 370 \text{ kJ mol}^{-1} \quad (424a)$$

$$\Rightarrow C_7H_7^+ + 2H_2 + 257 \text{ kJ mol}^{-1} \quad (424b)$$

$$\Rightarrow C_6H_5^+ + CH_4 + H_2 + 105 \text{ kJ mol}^{-1} \quad (424c)$$

In a hydrogen carrier the product distribution was found to be 75% (a) 20% (b) and 5% (c) but in a helium carrier the results were closer to 40% (a) 50% (b) and 10% (c). There are two possible explanations for this observation. Either there was a minor amount of excited H_3^+ (and perhaps also HeH^+) present in the helium carrier or that $C_7H_7^+$ can associate slowly with hydrogen. Which explanation is correct is however unknown.

The $C_6H_5^+$ ion product formed above (in 424c) was observed to associate with the hydrogen carrier to such an extent that there was no visible $C_6H_5^+$ signal in the hydrogen carrier, instead $C_6H_7^+$ was observed and counted. The energetics above assume that the ion is in the cyclic form as no energetics for the acyclic form were available. Other work suggests however that the $C_6H_5^+$ product of significantly exothermic ion-molecule reaction is likely to contain both the cyclic and acyclic isomers [71, 143] Giles, Adams, and Smith [144] show that one of the two $C_6H_5^+$ isomers associates with hydrogen much more rapidly than does the other isomer. In their experiments the fast reacting isomer was the predominant form and they tentatively ascribed the acyclic form to it. The case here appears to be similar as all the $C_6H_5^+$ had become $C_6H_7^+$ by the end of the flow tube, indicating that a relatively fast secondary reaction is occurring. However Fairley [71] has re-examined the system and determined that the cyclic (phenylium) isomer is the faster reacting one. Hence we tentatively ascribe a predominantly cyclic structure to the $C_6H_7^+$ ions formed in channel 424c.

For both the N_2H^+ and H_3^+ reactions ions at other masses were also observed, primarily at $m/z = 39$. This corresponds to $C_3H_3^+$ but the formation of this ion is not

energetically possible from either ion. It seems likely that there is an impurity in the toluene reactant used as the normally clear liquid had begun to yellow significantly. The nature of this impurity is however unknown.

Methylcyclohexane

The analysis of these H_3^+ reaction systems becomes more complex as the molecules get larger and the number of possible exothermic channels increases. It would appear that molecules of the size and complexity of methyl cyclohexane are approaching the limits of the product analysis method used in the current study.

The reaction of H_3O^+ with methyl cyclohexane is quite slow, the rate coefficient was found to be 7.1×10^{-10} cm^3s^{-1}. A comparison with the collison rate cannot be made, as the dipole moment has not been reported for methyl cyclohexane. A lower bound of $\sim 2 \times 10^{-9}$ cm^3s^{-1} can be obtained for the collision rate by assuming that this dipole moment is zero. If the dipole moment of toluene is substitued for that of methyl cyclohexane the collision rate is found to be 2.22×10^{-9} cm^3s^{-1}. The observed rate coefficient is thus less than one third of this lower estimate of the collision rate which suggests that this proton transfer is slightly endothermic. The proton affinity of C_7H_{14} has not been reported due to the fact that $C_7H_{15}^+$ is not a stable ion. Thus the major product observed in this reaction is $C_7H_{13}^+$. This product ion corresponds to proton transfer with accompanied loss of a neutral hydrogen molecule.

N_2H^+ reacts with methyl cyclohexane more rapidly than does H_3O^+, with the rate coefficient presumably being much closer to the collision rate. The experimentally determined rate coefficient was 1.7×10^{-9} cm^3s^{-1} ($k_{coll}=1.87 \times 10^{-9}$ $cm^3s\text{-}^1$). The observed product channels are shown below.

$$N_2H^+ + C_7H_{14} \Rightarrow C_7H_{13}^+ + H_2 + N_2 + 174 \text{ kJ mol}^{-1} \quad [0.35] \quad (425a)$$

$$\Rightarrow C_6H_{11}^+ + CH_4 + N_2 + 224 \text{ kJ mol}^{-1} \quad [0.25] \quad (425b)$$

$$\Rightarrow C_4H_9^+ + C_3H_6 + N_2 + 12 \text{ to } 167 \text{ kJ mol}^{-1} \quad [0.20] \quad (425c)$$

$$\Rightarrow C_3H_5^+ + C_4H_{10} + N_2 + 69 \text{ kJ mol}^{-1} \quad [0.20] \quad (425d)$$

The ΔH_f value for $C_4H_9^+$ could range from 694 to 849 kJ mol^{-1} depending on the isomeric form assigned for this ion and accordingly a range is given. In channel 425d the $C_3H_5^+$ ion is assumed to have the allyl structure and the C_4H_{10} is the *iso*-form as these are in both cases the more stable structures. A very small amount of $C_4H_7^+$ (<5%) was also seen. This channel is presumably a more dissociative form of channel 425c) and is at most 16 kJ mol^{-1} exothermic (for the most stable $CH_3CHCH{=}CH_2^+$ structure, other structures are endothermic). It was discounted as not being an authentic product due to the very low level at which it was observed.

The problems with the interpretation of this neutral reactant system really begin when the H_3^+ reaction is investigated. The difference between the product distributions observed when the H_3^+ ions are generated via the two available methods is more marked than that observed elsewhere in this study. The two distributions still broadly agree but the possible energy effects and hydrogen associations makes the accurate determination of the products of ground vibrational state H_3+ complex.

$$H_3^+ + C_7H_{14} \Rightarrow C_7H_{13}^+ + 2H_2 + 245 \text{ kJ mol}^{-1} \quad (426a)$$

$$\Rightarrow C_6H_{11}^+ + CH_4 + H_2 + 295 \text{ kJ mol}^{-1} \quad (426b)$$

$$\Rightarrow C_4H_9^+ + C_3H_6 + H_2 + 83 \text{ to } 238 \text{ kJ mol}^{-1} \quad (426c)$$

$$\Rightarrow C_4H_7^+ + C_3H_6 + 2H_2 + -35 \text{ to } 87 \text{ kJ mol}^{-1} \quad (426d)$$

$$\Rightarrow C_3H_7^+ + C_4H_8 + H_2 + 79 \text{ to } 163 \text{ kJ mol}^{-1} \quad (426e)$$

In a helium carrier the product distribution is 35% (a), 20% (b), 23% (c), 12% (d), and 10% (e). The ratio in a hydrogen carrier however is 60% (a) and 25% (b) and 15% (c), a small (<5%) $C_3H_7^+$ channel was also observed. The difference between the two distributions suggests that there is some energy effect present here. The amount of non-dissociative reaction (Channel 426a) is significantly greater in the hydrogen carrier than in the helium one and the other channels are correspondingly reduced. Channel 426d is perhaps energetically questionable and may not be seen in the hydrogen carrier due to association of $C_4H_7^+$ with hydrogen to give $C_4H_9^+$. However

the channel 426c (in hydrogen) is significantly less than the sum of 426c and 426d (in helium) with suggest that the H_3^+ has a small amount of internal excitation.

It could also be possible (though it seems unlikely) that the hydrogen carrier gas alters the stabilisation of the initial collision complex. Another possibility is that an unobserved, energetic, contaminant ion was present. This seems unlikely as the mass scans went down to ~2amu, covering most of the other likely candidates. Thus the effects observed are probably due to differences in energy between the H_3^+ species generated via the two different methods. It is interesting to note that $C_3H_7^+$ is seen in the H_3^+ case but that $C_3H_5^+$ is seen in the N_2H^+ reaction. With most other neutral reactants the H_3^+ reaction has produced most of the species seen in the N_2H^+ reaction, especially those that are energetically marginal in the N_2H^+ case.

A possible comparison from the literature comes from the work of Spanel *et al.* [142] who have studied proton transfer from a range of ionic reactants to, among other things, cyclohexane. With H_3^+ they observed two channels, both dissociative. The branching ratio was 60% $C_6H_{11}^+$ (H_2 loss, 252 kJ mol^{-1} exothermic) and 40 % $C_3H_7^+$ (C_3H_6 loss, 81 to 165 kJ mol^{-1} exothermic depending on which $C_3H_7^+$ structure is assigned).

$$H_3^+ + \text{c-}C_6H_{12} \Rightarrow C_6H_{11}^+ + 2H_2 \quad [0.60] \quad (427a)$$

$$\Rightarrow C_3H_7^+ + C_3H_6 + H_2 \quad [0.40] \quad (427b)$$

The reaction between methyl cyclohexane and H_3^+ (in helium) is not drastically different to this, with channels of similar exothermicity receiving similar amounts of the total products. That is, the exothermicities of channels 426a and 426b are of similar magnitude to that seen for channel 427a and between them they produce a similar amount of the total products.

Reaction Mechanisms.

In the reactions and discussions presented prior to this point little consideration has been given to the manner in which the observed ionic products have been formed. There has been an underlying assumption that the first step has been the transfer of a proton from either hydrogen, water, or nitrogen, but is this assumption warranted? In many cases the reaction products could be formed by another process. An example of this is the (M-1) amu products observed in many cases (where M is the atomic mass of the neutral reactant). These ions have been presumed to form via a

two-step process; proton transfer followed by the loss of a neutral hydrogen fragment. Direct hydrogen ion abstraction would give an identical product however. These reaction types are shown below.

Proton transfer:

$$XH^+ + C_xH_y \Rightarrow C_xH_{y+1}^{+*} + X \quad (428)$$

$$C_xH_{y+1}^{+*} \Rightarrow C_xH_{y-1}^{+} + H_2 \quad (429)$$

Hydride ion abstraction:

$$XH^+ + C_xH_y \Rightarrow C_xH_{y-1}^{+} + H_2 + X \quad (430)$$

One can also question whether the reactions take place in an intimately bound complex or whether the particles involved are transferred at longer distances.

The isotopically labelled results obtained in this and other studies give the first clue. In the current work D_3^+ was reacted with several of the small hydrocarbons. The simplest piece of evidence garnered from these experiments was the almost complete lack of any products with two deuterium atoms present in the same ion. This finding is consistent with practically all other investigations that have attempted isotopic labelling [139, 290, 291], independent of whether the labelling was present in the reactant ion or neutral. That is to say that if H_3^+/D_3^+ was reacted with C_xD_y/C_xH_y at most one of the hydrogen isotopes from the reactant ion was seen in the ionic products. Only the very early work of Aquilanti and Volpi [135, 136] showed any evidence of ionic products with more than one label. However in their work these reactions that yielded multiply labelled ions were at extremely low levels and were likely the result of secondary reactions. This observation effectively rules out the formation of an intimate complex in the reactions of H_3^+ with hydrocarbons and thus the reaction must proceed by a different mechanism.

The two prime candidates for this mechanism are a polarisation-stripping type proton transfer, where a loosely-bound moiety in which the hydrogen and the hydrocarbon retain their chemical identities is formed, and hydride atom abstraction. Also possible is an apparent hydride ion abstraction (as distinct from hydride ion abstraction). In this case the proton is transferred without randomisation of the energy involved is not randomised and the transferred proton is lost almost immediately. Apparent hydride abstraction is indistinguishable from hydride ion abstraction. Further decomposition of the ion formed from the unimolecular decay (Reaction 429) is also possible and certain reactions may also decay via the loss of methane

molecules. It is likely that when the difference in proton affinities between the proton donor and the hydrocarbon reactant is lower (i.e. the H_3O^+ and some N_2H^+ reactions) it is not energetically possible to form dissociative products. In these cases the reaction will proceed by simple proton transfer. However that is not the case for H_3^+ ions.

The most basic difference between the two mechanisms is that with deuterated ions, proton transfer (even dissociative proton transfer) gives a possibility of D being present in the product ions while there is no chance of this happening with a hydride ion (or apparent hydride ion) abstraction mechanism. In no case however, was some isotopic labelling of the product ions not observed; that is none of the reactions proceed solely via hydride ion abstraction. In reactions of ArD^+ (PA argon = 369.2 kJ mol^{-1}) Smith and Futrell [145] found that CH_3^+ products in the ArD^+/CH_4 reaction and $C_2H_5^+$ products in the ArD^+/C_2H_6 system showed higher H/D ratios when excited ions were used than when the ArD^+ had been relaxed by collision. This was interpreted as an increase in hydride ion abstractions (or apparent hydride ion abstraction) for the more excited ions. Similar behaviour was observed for the D_3^+/C_2H_6 system also. These workers [291] also concluded that hydride ion abstraction (or apparent hydride ion abstraction) comprised 23% of the reaction for the D_3^+/C_2H_6 reaction even when the ions had been significantly relaxed. This hydride ion abstraction would be expected to raise the H/D ratio for the (M-1) products as no deuteron is transferred to those ions that undergo hydride abstraction. Smith and Futrell also found that hydride ion abstraction reduces further decay of the product ions as it does not deposit as much energy in them.

An examination of the labelled results obtained in this study shows that all but the D_3^+/C_3H_8 system yield statistical loss of deuteration if the loss of a hydrogen molecule (be it H_2 or HD) is assumed to come from an ion equivalent to the D+-neutral complex. Several conclusions can be drawn from this observation. The first is that the initial complex has a finite lifetime when a stable protonated ion exists. This lifetime must be longer than that required for isotope scrambling to take place. More will be said about the ion lifetime later in this section. Secondly, it can be concluded that a major part of the reaction proceeds via proton transfer. The statistical ratio of deuterium retention to loss for those ions with a stable neutral does not however necessarily mean that there is only proton transfer occurring. Smith and

Futrell [139, 291] have shown that the isotope ratio of the product ion usually drops with the excitation of the D_3^+ ions. This effect is probably due to the increased isotope effect as the larger zero-point energy of H (and thus the increased ease of losing H_2 as opposed to HD) becomes more important. Hydride ion abstraction raises the isotope ratio and thus a statistical isotope ratio could represent a balance between these two effects. Alternatively, though unlikely in the light of the differences in isotope ratio with ion energy shown by Smith and Futrell, the dissociation may be happening at high enough energies that zero-point effects are negligible. A special case is that of propane for which the ion formed upon initial protonation, $C_3H_9^+$, is not a stable species. In this reaction there is essentially no isotope scrambling with almost no deuterium retained in the products. The reaction mechanism in this case is probably much similar to the apparent hydride ion abstraction mechanism presented earlier.

It is interesting to note that in many cases, a substantial amount of the product ions do not decompose despite having sufficient energy to do so. For example 25-35% of the products of the reaction of H_3^+ with cyclopropane remains as $C_3H_5^+$ despite dissociation to $C_3H_3^+$ being 143 kJ mol^{-1} exothermic. Similarly in the H_3^+/2-butene reaction 35% of the ion products do not dissociate despite extremely exothermic competition channels (252 and 143 kJ mol^{-1} exothermic). In the case of the cyclopropane, the absence of extensive fragmentation could be the result of participation by the hydride ion abstraction channel as Smith and Futrell [291] have shown that hydride ion abstraction apparently deposits less energy into the product ion than does proton transfer. This is however not the case for 2-butene. Therfore the bulk of the energy available from proton transfer must thus not be deposited in the protonated ion and thus must be carried away by the neutral species that transferred the proton, i.e. H_2, N_2, or H_2O. There are two major ways that the neutral species could carry this excess energy away; either through translational or vibrational excitation. One can compare the reactions of O_2H^+, KrH^+ and H_3^+ (all of which have very similar proton affinities; 421.0, 424.6, and 422.3 kJ mol^{-1} respectively) with the hydrocarbons (CH_4, C_2H_4, C_2H_6) that have been studied by Smith and Futrell [292]. In the most relaxed states the product ratios for all these ions are very similar. Vibrational excitation is thus not acting as an efficient method for removal of this excess energy as krypton is an atomic species and can not have vibrational excitation. It is thus likely that some of the energy difference between H_3^+ and the protonated

hydrocarbon is removed as relative translation between the hydrogen molecule and the protonated hydrocarbon ion.

As mentioned earlier, the ion lifetime must be longer than that required for scrambling as relatively statistical isotope ratios are observed. Further information can be obtained from a comparison of the results of Smith and Futrell [139, 291]. The product ratios in these experiments, obtained at low pressures ($<10^{-5}$ Torr), are very similar to the results obtained in the SIFT. Thus one can conclude that the lifetime of the excited ions, i.e. the time required for unimolecular dissociation, is less than the collision time for the SIFT at 0.5 Torr ($\sim 3 \times 10^{-8}$ s). One must note however that there is increasing evidence that ion-neutral collisions are often 'weak' and thus many may be required to adequately remove the energy from the excited hydrocarbon ions.

The reactions observed in this Chapter can thus be best characterised by a long-range proton transfer to form an excited ion that will subsequently decay in a time window of between the time required for proton shuffling and the collision time in the SIFT. In the more energetic reactions hydride ion abstraction is also possible. When no stable protonated ion exists, unimolecular decay will happen almost immediately.

§4.3.5: HeH^+ and He_2H^+ reactions.

In an effort to explore an even wider range of proton transfer energetics the reactions of HeH^+ with some of the neutrals discussed above were also investigated. The reactions of the He_2H^+ ion were also investigated. As this ion forms via an extremely slow association between HeH^+ and the helium carrier it is necessary to know the products of the reactions of HeH^+ in order to correct the data. The PA of H_2 is 422.3 kJ mol^{-1} while that of helium is some 245 kJ mol^{-1} lower at 177.8 kJ mol^{-1}. The reactions of HeH^+ could therefore reasonably be expected to be even more dissociative than those of H_3^+. The reactions of HeH^+ with the hydrocarbons methane, acetylene, ethylene, propane and benzene were chosen for study along with several other non-hydrocarbon neutrals, *viz* hydrogen, argon, krypton, neon, ammonia and water. Previous investigations of the HeH^+ ionic reactant have investigated its

reactivity with ethylene [145], hydrogen [146, 147], krypton [147] and neon [148]. A problem was encountered in the current study in that when the product distributions of the various reactions were analysed, significant amounts of apparently endothermic product channels were observed.

As an example, in the reaction between HeH^+ and water, both H_2O^+ and H_3O^+ were apparently observed to be products in approximately equal amounts. If these were both products of the reaction of HeH^+ (believed to be the most energetic ion present) and water the reactions that would have to be occurring are shown below.

$$HeH^+ + H_2O \Rightarrow H_3O^+ + He + 519 \text{ kJ mol}^{-1} \quad (431a)$$

$$\Rightarrow H_2O^+ + He + H - 84 \text{ kJ mol}^{-1} \quad (431b)$$

That is the process that gives channel 428b is 84 kJ mol^{-1} **endothermic**. As 431b was apparently a significant product channel this suggests that there is a serious problem here. Initially it was thought that there was internal excitation present in the HeH^+ ion i.e. a similar problem to that possibly present with H_3^+.

In this first investigation, the HeH^+ ions were generated by admitting a very small flow of hydrogen into the FA close to the upstream end of the FA. This low flow generated H_2^+ which, in the absence of further hydrogen to react with (which would form H_3^+ rapidly), undergoes a slow reaction with the helium carrier [148].

$$H_2^+ + He \Rightarrow HeH^+ + H \quad (432)$$

$$k = 1.35 \times 10^{-10} \text{ cm}^3\text{s}^{-1}.$$

As the ions then passed through the venturi injector into the SIFT, the internal energy gained during injection could have been retained through to the reaction region if helium is ineffective at quenching vibrational excitation of the HeH^+ ions. Smith and Futrell [145] have previously studied the reaction of HeH^+ with ethylene in a tandem ICR. This instrument has a spatially separate ion source (in this case the ion source and selection region of a 180° magnetic sector instrument) which, much like a SIFT, allows mass selection of the ion prior to its injection into the reaction region i.e. the ICR cell. As the ions were generated in a separate ion source the investigators had control of the ion source conditions without affecting the conditions in the ICR cell. They used this feature to monitor variation of the product distribution with respect to the average number of collisions in the ion source (the number of collision in the ion source was shown to correlate with the internal energy of the reactant ions). Thus they

essentially monitored the product distribution as the amount of internal energy in the reactant ions was reduced. The ratios they found are shown below in Table 4.4.

However when this same reaction was observed in the present SIFT, using HeH^+ ions generated in the FA, a significant $C_2H_2^+$ channel was observed in spite of this being 143 kJ mol^{-1} endothermic.

$$HeH^+ + C_2H_4 \Rightarrow C_2H_3^+ + He + H_2 + 290 \text{ kJ mol}^{-1} \quad (433a)$$

$$\Rightarrow C_2H_4^+ + He + H + 119 \text{ kJ mol}^{-1} \quad (433b)$$

$$\Rightarrow C_2H_2^+ + He + H + H_2 - 143 \text{ kJ mol}^{-1} \quad (433c)$$

Product Ion	Excited HeH^+	Relaxed HeH^+
$C_2H_5^+$	0.00	0.00
$C_2H_4^+$	0.55	0.25
$C_2H_3^+$	0.45	0.75

Table 4.4: The product distributions for the reaction of HeH^+ with ethylene obtained by Smith and Futrell [145]. The ions were either in an excited state (no collisions in the ion source region) or a relaxed state (many collisions in the ion source region) before reaction occurred.

The experiments of Smith and Futrell showed that helium (they actually used a 5:1 mixture of $He:H_2$ in their ion source) could quench excited HeH^+ and that their excited HeH^+ did not produce $C_2H_2^+$. Thus it is unlikely that the problem in our experiments is the presence of an excited HeH^+ fraction.

In order to further check this suggested explanation the HeH^+ ions were created in an alternative manner. In these experiments the FA used a hydrogen carrier and the H_3^+ ion was selected with the upstream quadrupole mass spectrometer. This ion was then injected into the helium carrier of the SIFT reaction tube at high energies (i.e. high voltages on the FA nose cone). A signal of HeH^+ (as well as H_3^+, H_2O^+, H_3O^+, and N_2H^+) was then observed. This method of forming HeH^+ is essentially driving the endothermic reaction:

$$H_3^+ + He \Rightarrow HeH^+ \quad (434)$$

with the energy from the injection process. When ethylene was added to this system significant amounts of $C_2H_2^+$ were still observed.

Under these conditions another, poorly resolved, peak at mass 1.5 was observed on the injection scans. This mass is probably H^+ at $m/z = 1$ as the low mass section of the scan appears to be slightly non-linear (for example H_3^+ occurs at approximately 3.4 amu). In the earlier experiments (when the HeH^+ was generated from the FA), this non-linearity in the downstream quadrupole was not in evidence. In fact m/z = 5 apeared at approximately 4.7 amu, and so the scan of injected peaks (which was terminated at "1 amu" in each case) would only show part of the peak shoulder as the lowest mass accessed on this scan was 1 amu. A "peak" consistent with this expectation was apparent. The reaction of H^+ with ethylene has not been measured previously but other H^+ reactions predominantly give charge transfer and dissociative charge transfer. The reaction of H^+ and ethylene to give $C_2H_2^+$ is 36 kJ mol^{-1} exothermic and so is apparently possible. Thus it seems likely that the product distributions are being seriously affected by the presence of the H^+ ion, which is probably being formed by "break-up" of the HeH^+ ion during injection through the venturi orifice. As the amount of H^+ present was not recorded during the determination of the product distributions they cannot be corrected for this interference.

In the course of the reaction studies with the HeH^+ ion another interesting species was observed in the SIFT flow tube. This was He_2H^+ at $m/z = 9$, a species that has only ever been observed once previously in flow tube experiments [146, 149] in an FA at 200K. There are however several theoretical investigations of this, and higher, helium clusters. The weakly bound He_2H^+ species is formed from HeH^+ by a termolecular reaction with the helium carrier gas.

$$HeH^+ + 2He \Rightarrow He_2H^+ + He \quad (435)$$

This process is believed to be termolecular as the ratio of He_2H^+:HeH^+ increases with increasing pressure. Adams, Bohme, and Fergusson [146], who have previously observed the ion, assigned a different formation process to it, namely the bimolecular Reaction 433.

$$He_2^+ + H_2 \Rightarrow He_2H^+ + H \quad (436)$$

As this previous observation occurred in a FA reactor it was impossible to separate Reactions 435 and 436. However in the current system there is no hydrogen present in

the SIFT reaction tube which eliminates Reaction 436 as a possibility in our system. Reaction 433 may also produce the He_2H^+ ion in the FA apparatus used by Adams *et al.*, however it would be in concert with Reaction 435. A number of theoretical investigations of He_2H^+ and higher helium clusters have also been made [150, 151, 152, 153].

If the reactions of HeH^+ with various species are to be studied further in the Canterbury FA-SIFDT in the future, a better method for generating the ion would be to inject H_2^+ into the SIFT flow tube and to generate HeH^+ from Reaction 432 with the (helium) SIFT carrier gas. It would be necessary to use a very small hydrogen flow into the FA to generate the H_2^+ ion current or H_3^+ would result. This is probably best done using a helium/hydrogen mixture.

Section 4.4: Conclusions

The rates and products of the reactions of H_3O^+, N_2H^+ and H_3^+ with a range of hydrocarbon reactants have been studied. In agreement with expectations the rate coefficients for almost all of the exothermic proton transfers were close to the limiting collision rate coefficients. The rate coefficients observed for many of the H_3^+ reactions were further from the collision rates than the others. It is not clear whether this is a real trend or the result of the fact that reaction rate coefficients as fast as these provide considerable experimental challenges to accurate measurement - especially when the reactants are condensable. The differences between the H_3^+ reactions performed using ions generated from a hydrogen carrier with krypton ions and those performed using injected H_3^+ ions were mostly minimal when the H_3^+ ions were injected at low energies. When low mass fragments were formed in the hydrogen carrier gas association reactions with hydrogen often obscured the branching ratios somewhat.

In most cases it appears that dissociative channels only begin to become significant when the reaction exothermicities exceed 100 to 150 kJ mol^{-1}. Consequently channels that occur by the elimination of stable molecules, mainly H_2, CH_4, C_3H_6 and C_4H_8, are favoured and quite commonly seen. The relative importance of these dissociative channels increases as the energy in the reactant ion increases, as would be expected.

The second most simple polyatomic ion, He_2H^+, has also been observed in the Canterbury SIFT at thermal energies. This ion apparently is formed via the slow association of the HeH^+ ion with the helium carrier gas. The HeH^+ ion was a minor contaminant in many of the H_3^+ reactions. The investigation of the reactions of He_2H^+ was hindered by the inability to inject the HeH^+ ion without interference from another, highly energetic, ion which interfered with the determination of the product distributions for both HeH^+ and He_2H^+. This contaminant ion has tentatively been assigned as H^+.

Chapter 5

The Proton Affinity and Methyl Cation Transfer Reactions of Cyanogen.

Section 5.1: Introduction.

§5.1.1:Cyanogen.

Cyanogen (NCCN, denoted hereafter as C_2N_2) has long been considered a prime candidate for being present in interstellar clouds since molecules containing CN functionalities comprise a sizeable minority of all the molecules detected in the interstellar medium (ISM) [42]. However, C_2N_2 itself has not been detected and will not be trivial to detect due to its symmetry and lack of a permanent dipole moment. This lack of a dipole moment makes it essentially invisible to the conventional radio frequency methods of detection [154, 155, 156]. Cyanogen has however been detected in the stratosphere of Titan by the Voyager 1 space craft from the infrared spectrum of Titan's atmosphere [157]. A likely precursor for cyanogen in the interstellar medium is the protonated form, $HC_2N_2^+$ and thus a knowledge of the proton affinity (PA) of cyanogen becomes important for interstellar modelling. The proton affinity is also relevant in modelling the ionosphere of Titan due to the abundance of ions that can potentially transfer a proton to it: e.g. $HCNH^+$, $C_2H_5^+$, H_3O^+ (see Chapter 6 for further details on Titan's atmosphere and ionosphere).

§5.1.2: Proton affinities.

The proton affinity of a neutral species is a measure of its propensity to give up a proton (H^+) upon reaction with another species [68,111, 158]. For a species, **X**, the proton affinity of X is defined as shown in equation 5.1.

$$(PA)\ X = \Delta H°_f(X) + \Delta H°_f(H^+) - \Delta H°_f(XH^+) \qquad (5.1)$$

That is to say the PA is a measure of the enthalpy change in the reaction

$$XH^+ \quad => \quad X + H^+ \qquad (5.2)$$

Thus the higher the proton affinity the more stable the protonated species is. Reaction 5.1, or it's reverse, however, is very rarely directly measurable and $\Delta H°_f (XH^+)$ is only known for a selected few molecules [111]. Experimentally proton affinities are usually determined by one of two methods, the bracketing or the equilibrium method.

The *equilibrium method* relies on separately studying the rate of a reaction system like that shown in Equation 5.3 in **both** directions. The equilibrium method is usually the more accurate of the two methods.

$$XH^+ + B \quad <=> \quad BH^+ + X \qquad (5.3)$$

From these reactions the equilibrium constant and subsequently the enthalpy change can be determined.

$$K = k_f/k_b \qquad (5.4)$$

and $$\Delta G° = -RT \, ln \, K \qquad (5.5)$$

also $$\Delta G° = \Delta H° - T\Delta S° \qquad (5.6)$$

$\therefore$ $$\Delta H° = -RT \, ln \, (k_f/k_b) + T\Delta S° \qquad (5.7)$$

$$\Delta H° = PA(X) - PA(B) \qquad (5.8)$$

This $\Delta H°$ is equal to the difference between the PA of species X and species B (equation 5.8), which allows one to define the PA of X from the known PA(B), the measured reaction rates, and an estimate of the change in entropy for the reaction. This entropy can be calculated from equation 5.6 and the gas phase basicity (GB) and proton affinity of the reference compound (B) as;

$$GB(B) = -\Delta G°((B + H^+) => BH^+) \qquad (5.9)$$

and $$PA(B) = -\Delta H°((B + H^+) => BH^+) \qquad (5.10).$$

A comparison of the relative proton affinities of two compounds whose proton affinities differ by less than 20kJ mol^{-1} is then easily made by establishing what species proton transfers to the other. By comparing a large range of different compounds, 'ladders' of proton affinities can be and anchored to a few reference compounds for which absolute proton affinities are known.

The *bracketing method* [159] is most commonly used when one cannot find a convenient equilibrium system where the reaction coefficients are measurable in both the forward and backward direction. In the bracketing method one studies the reaction between the neutral and a selection of protonated ionic species with known PA values. From the presence or absence of reaction one can bracket the unknown PA between

the reactive species with the highest PA and the unreactive species with the lowest PA. In essence the bracketing method relies on the fact that exothermic proton transfer reactions are usually fast i.e. proceed at or near the calculated collision rate [112, 113]. Bracketing, however, can be prone to error as slightly endothermic channels may give an observable product and exothermic products may be masked by the presence of other, significantly more exothermic, channels.

Section 5.2: The proton affinity of cyanogen.

§5.2.1:Previous measurements.

The proton affinity of cyanogen has previously been measured by Petrie [160] on the first SIFT constructed at Canterbury University [66] using the equilibrium method. It has also been measured by others [159, 161] using bracketing methods. These results led to a tabulated value of 674.7 kJ mol^{-1} [111]. The spread in these experimental values is small (< 5 kJ mol^{-1}) and this would appear to indicate their accuracy. However high-level ab initio studies of C_2N_2 by Petrie [179] and Botschwina *et al.* [162] have produced results that while mutually consistent (655 and 657 ± 5 kJ mol^{-1} respectively) are irreconcilable with the experimental values. This has raised doubts about the PA of cyanogen. Several factors suggest that it may be the experimental value that is in error, but before mentioning these reasons it is necessary to give a short description of each of the experiments.

The first, by Raksit and Bohme [159], was a SIFT bracketing study, which derived a PA for C_2N_2 of 678±8 kJ mol^{-1}. This conclusion was based on the occurrence of fast proton transfer between SO_2H^+ and C_2N_2 (Reaction 501) and the observation of a proton transfer channel in the reaction of protonated cyanogen with ethylene (Reaction 502).

$$SO_2H^+ + C_2N_2 \Rightarrow C_2N_2H^+ + SO_2 \quad (501)$$
$$k = 8.2 \times 10^{-10}\ cm^3s^{-1}$$

$$C_2N_2H^+ + C_2H_4 \Rightarrow C_2H_5^+ + C_2N_2\ (0.70) \quad (502)$$
$$\Rightarrow C_2N_2H^+.C_2H_4\ (0.30)$$
$$k = 5.6 \times 10^{-10}\ cm^3s^{-1}\ @\ 0.20\ Torr\ H_2$$

These reactions bracketed the proton affinity between PA (SO_2) = 674.5 kJ mol^{-1} and PA (C_2H_4) = 680 kJ mol^{-1}. These proton affinity values are those listed in the original paper and have since been revised, though current tabulated [111] values would not significantly affect the conclusions of this experiment. However there is growing evidence [163] that the tabulated PA(SO_2) is seriously in error (see Section 5.2.2.4 and 5.2.2.5 for further discussion)

The second investigation was undertaken by Deakyne et al.[161] on an Ion Cyclotron Resonance (ICR) Spectrometer. This bracketing experiment yielded a PA of 674±8 kJ mol^{-1} in excellent agreement with that of Raksit and Bohme. A bracketing experiment was performed, as the reagent they believed most appropriate for an equilibrium study, ethylene, presented problems in the ICR. Protonated ethylene undergoes a rapid bimolecular reaction with neutral ethylene (Reaction 503) and makes the determination of the reaction rate with cyanogen especially difficult.

$$C_2H_5^+ + C_2H_4 \quad => \quad C_3H_5^+ + CH_4 \qquad (503)$$

$$k = 3.55 \times 10^{-10} \text{ cm}^3\text{s}^{-1}$$ [6C]

The reactions of $COSH^+$ (PA (COS) = 632 kJ mol^{-1}), $C_2H_3^+$ (PA (C_2H_2) = 641 kJ mol^{-1}), and CF_3CFOH^+ (PA (CF_3CFOH) = 670 kJ mol^{-1}) with cyanogen were all found to transfer a proton. Also Reaction 502 was re-examined and the proton transfer confirmed. Double resonance [164] techniques confirmed the link between reactant and product ion in all reactions except that of protonated acetylene with cyanogen. These results bracketed the PA between 670 and 680 kJ mol^{-1}. Though the authors claim to have obtained rough equilibrium values they do not report them. A theoretical value (MP3/6-31G**//HF/6-31G**) of 668 kJ mol^{-1} was also reported, suggesting the experimental value was perhaps a little high, but not grossly inaccurate.

The third investigation was performed at the University of Canterbury by Petrie *et al.*[160] using the older version SIFT. This investigation was an equilibrium measurement with the equilbria involving C_2N_2, C_2H_4, and CH_3Cl being investigated by measurement of the rates of proton transfer in both the forward and reverse directions. On the basis of these reactions C_2N_2 was assigned a PA of 674±4 kJ mol^{-1}.

Why then are the experimental results so different from those obtained from ab initio techniques? One point to note is the results of a recent experimental and theoretical study into the proton affinity of CH_3Cl by Glukhovtsev *et al.* [165]. Using G2 theory and high-pressure mass spectrometry techniques these workers showed errors

in the proton affinities of several of the halogenmethanes. The authors of this study now recommend a value for the proton affinity of *methyl chloride* of 649.8 kJ mol^{-1} over 30 kJ mol^{-1} lower than the longstanding tabulated value. This leaves the equilibrium study of Petrie *et al.*[160] with a serious inconsistency. Two proton equilibria were established in that study. The two proton transfer partners (CH_3Cl and C_2H_4) should therefore have proton affinities of similar magnitudes (< ~10 kJ mol^{-1}). However, with the recent lowering of the PA of methyl chloride this is no longer the case. Also two species with proton affinities slightly higher than ethylene have just had their PA significantly lowered as a result of new high-pressure mass spectrometric measurements of proton transfer equilibria [165]. These new results and inconsistencies have motivated this new study into the proton affinity of cyanogen.

§5.2.2: Experimental details

The results presented below were obtained on the University of Canterbury FA/SIFDT at room temperature (295±10 K). For the protonated ions the moveable ioniser was the preferred source of ionisation. A hydrogen carrier was present in the FA source, and the H_3^+ ion formed then transferred a proton to the neutral species producing the protonated species of interest. The neutral precursor was invariably the non-protonated neutral and was introduced through the inlet closest to the FA nose cone. Helium was used as the bath gas in the SIFT flow tube at a pressure of 0.480 Torr.

§5.2.3: Results and Discussion.

The rate coefficients and product distributions determined in the current study are shown in Table 5.1.

Table 5.2 contains the gas phase basicities and proton affinities of the species involved in the determination.

Reactants			Branching	Rate Coefficients (x 10^{-9} cm^3s^{-1})		
Ion	Neutral	Products	Ratio [a]	k_{col} [b]	k_{obs}	k_{PT}
		$C_2N_2H^+ + C_2H_2$	0.75			
$C_2H_3^+$	C_2N_2	Adduct	0.25	1.6	1.1	0.83
		$C_2H_3^+ + C_2N_2$	0.15			
$C_2N_2H^+$	C_2H_2	Adduct	0.85	1.1	0.48	0.072
CH_3ClH^+	C_2N_2	$C_2N_2H^+ + CH_3Cl$	1.00	1.0	0.20	0.20
$C_2N_2H^+$	CH_3Cl	$CH_3ClH^+ + C_2N_2$	1.0	2.1	0.16	0.16
SO_2H^+	C_2N_2	$C_2N_2H^+ + SO_2$	1.00	1.0	1.2	1.2
$C_2N_2H^+$	SO_2	Adduct	1.00	1.7	0.030	-
$C_2H_5^+$	C_2N_2	Adduct	1.00	1.5	0.31	-
$C_2N_2H^+$	C_2H_4	$C_2H_5^+ + C_2N_2$	1.00	1.1	0.88	0.88

Table 5.1: The rate constants and product ratios for the reactions relevant to the determination of the proton affinity of cyanogen.

a) The product branching ratios were determined in 0.48 Torr of helium.

b) Calculated using the parameterised method of Su and Chesnavich [114] for reactants with a dipole moment and Langevin theory for reactants with no dipole moment.

Species	Proton Affinity (Tabulated) [a]	Proton Affinity (Corrections)	Gas Basicity [a]
C_2N_2	674.7	651.2 [b]	645.8
CH_3Cl	647.3	-	621.1
C_2H_2	641.4	-	616.7
C_2H_4	680.5	-	651.5
SO_2	672.3	627 [c]	643.3

Table 5.2: Proton affinities and gas basicities of species relevant to the determination of the proton affinity of cyanogen.

a) PA and GB in kJ mol^{-1} from Reference 111 (Lias et al).

b) This work.

c) Theoretical value from Reference 163.

Based on these results we calculate a value of the proton affinity of cyanogen at 651.2 ± 2 kJ mol^{-1}. This value is calculated using the current SIFT determination of the C_2H_2/C_2N_2 proton transfer equilibrium and a previous unpublished determination of the CH_3Cl/C_2N_2 equilibrium by McEwan. The calculated thermochemical values for the proton affinity determination are shown in Table 5.3.

Reaction	$\Delta G°$ [a]	$\Delta S°_{300}$	$\Delta H°$ [a]	PA (C_2N_2) [a]
$C_2H_2 + H^+ => C_2H_3^+$		-82 [b]		
$CH_3Cl + H^+ => CH_3ClH^+$		-87 [b]		
$C_2N_2 + H^+ => C_2N_2H^+$		-96 [b]		
$C_2H_3^+ + C_2N_2 <=> C_2N_2H^+ + C_2H_2$	-6.1	-14 [c]	-10.3	651.7
$CH_3ClH^+ + C_2N_2 <=> C_2N_2H^+ +$ CH_3Cl	-0.6	-9 [c]	-3.3	650.6

Table 5.3: The thermochemical values used in the determination of the proton affinity of cyanogen.

a) $\Delta H°$, $\Delta G°$, and the proton affinity are all measured in kJ mol^{-1}. The ΔH values are calculated using $\Delta H = \Delta G + T\Delta S$

b) Calculated as stated in text below. Units are J mol^{-1} K^{-1}.

c) The sum of the $\Delta S°$ half reactions. The units are J mol^{-1} K^{-1}.

The $\Delta S°$ values shown in Table 5.3 for the 'half-reactions" are calculated from the difference between the listed proton affinity and gas basicity [111] which in essence is how Lias *et al.*'s estimate of the change in entropy is found. These entropy changes have been calculated in order to reconcile the scales of proton affinity and gas basicity. The agreement between the two new estimates for PA(C_2N_2) is excellent.

The acetylene/cyanogen proton transfer equilibrium.

$C_2H_3^+$ ions were formed by protonating acetylene in the FA source using hydrogen as a carrier gas. Proton transfer and adduct formation were observed in both directions. This is another example of the propensity of cyanogen to easily add alkyl group ions to itself.

The methylchloride/cyanogen proton transfer equilibrium.

The results presented for this reaction are essentially the same as those presented in Reference 198, but using a more current value for the proton affinity of methylchloride [165]. These results are from an ICR experiment performed by McEwan some time ago that was not independently published. The system was partially investigated in the FA/SIFDT but the same problems with break up of the CH_3ClH^+ ion to $CHClH^+$ (Reaction 504) that caused problems for Petrie and co-workers [159] prevented it from being fully explored. The close agreement between the ICR

determination of the PA of cyanogen and our SIFT determination suggests that there is no need to replicate the ICR results.

$$CH_3ClH^+ \Rightarrow CH_2Cl^+ + H_2 \quad (504)$$

$$CH_3ClH^+ + C_2N_2 \Leftrightarrow C_2N_2H^+ + CH_3Cl \quad (505)$$

The reverse of Reaction 505 was however observed to give slow proton transfer and also a small amount (10%) of adduct. The total observed rate coefficient was 2.2×10^{-10} cm^3s^{-1}.

The ethylene/cyanogen proton transfer system.

This proton transfer reaction (Reaction 506) was reported by Petrie *et al.* to apparently proceed measurably in both directions.

$$C_2H_5^+ + C_2N_2 \Leftrightarrow C_2N_2H^+ + C_2H_4 \quad (506)$$

This observation appeared at the time to be in agreement with the methylchloride result, but with the subsequent devaluing of the PA of CH_3Cl is now in contradiction with it. Our new investigation finds that the sole product of the reaction between $C_2H_5^+$ and cyanogen (Reaction 506 forward) is an adduct with a rate coefficient of 3.1×10^{-10} cm^3s^{-1} at 0.48 Torr of helium.

$$C_2H_5^+ + C_2N_2 \Rightarrow C_4H_5N_2^+ \text{ (structure indeterminate)} \quad (507)$$

Petrie *et al.* report a rate of 1.6×10^{-10} cm^3s^{-1}, primarily forming the adduct with a $C_2N_2H^+$ product and up to 5% proton transfer. It seems now that the proton transfer was most likely from $C_2H_3^+$ formed as a result of break up of the $C_2H_5^+$ ion during injection into the SIFT tube or from $C_2H_3^+$ formed in the source region and inadequately screened from the reaction flow tube by the injection quadrupole. These sources of interference have been eliminated in the new FA/SIFDT and no proton transfer was observed. For the reverse reaction of 506, proton transfer from $C_2N_2H^+$ was the only observed product with a rate coefficient close to the Langevin collision rate.

The sulphur dioxide/cyanogen proton transfer system.

With a tabulated proton affinity of 672.3 kJ mol^{-1} (cf. $PA_{lit}(C_2N_2)$=674.7 kJ mol^{-1}), SO_2 was an excellent candidate for establishing a proton transfer equilibrium if the tabulated value for cyanogen was correct. However as expected no equilibrium was observed, instead rapid proton transfer was only observed from SO_2H^+ to

cyanogen (Reaction 508). This is not as the tabulated PA of SO_2 would predict and suggests that PA(SO_2) is in fact *lower* than that of cyanogen.

$$SO_2H^+ + C_2N_2 \quad => \quad C_2N_2H^+ + SO_2 \qquad (508)$$

Support for this lower sulphur dioxide PA (lower even than cyanogen) comes from recent theoretical work from Fairley and associates [163] who assign a PA of 627 kJ mol^{-1} to the trans $OSOH^+$ structure at 0K. This value is 24 kJ mol^{-1} lower than the PA of C_2N_2 determined here and suggests that proton transfer from SO_2H^+ to C_2N_2 should proceed at close to the Langevin rate, as indeed it does.

Supplementary proton transfer reactions.

The reactions of several of the reference bases with each other were also studied. The results for this are presented in Table 5.4. These reactions provide further support for the lower theoretical PA(SO_2) proposed by Fairley *et al* [163]. Reaction 509a efficiently transfers a proton from SO_2H^+ to C_2H_2 while the reverse (Reaction 510) only produces CH_2SOH^+.

$$SO_2H^+ + C_2H_2 \quad => \quad C_2H_3^+ + SO_2 \qquad (509a)$$

$$=> \quad CH_2SOH^+ + CO \qquad (509b)$$

$$C_2H_3^+ + SO_2 \quad => \quad CH_2SOH^+ + CO \qquad (510)$$

Reactants		Products	Branching	Rates (x 10^{-9} cm^3s^{-1})	
Ion	Neutral		Ratio [a]	k_{col} [b]	k_{obs}
$C_2H_3^+$	CH_3Cl	$CH_3ClH^+ + C_2H_2$	0.75	2.5	1.1
		Adduct	0.15		
		$C_3H_5^+ + HCl$	0.10		
$C_2H_3^+$	SO_2	$CH_2SOH^+ + CO$	1.00	2.0	1.2
SO_2H^+	C_2H_2	$C_2H_3^+ + SO_2$	0.40	1.2	1.1
		$CH_2SOH^+ + CO$	0.60		
SO_2H^+	C_2H_4	$C_2H_5^+ + SO_2$	1.0	1.2	1.0
$C_2H_5^+$	CH_3Cl	Adduct	1.00	2.4	0.16
$C_2H_5^+$	SO_2	Adduct	1.00	2.0	0.0088

Table 5.4: The rate coefficients and products of the supplementary proton transfer reactions performed during this study.

a) The product branching ratios were determined in 0.48 Torr of helium.

b) Calculated using the parameterised method of Su and Chesnavich [114] for reactants with a dipole moment and Langevin theory for reactants with no dipole moment.

The products for Reactions 509 and 510, specifically the presence of a protonated product in Reaction 509 and the lack of one in Reaction 510, indicate that the proton affinity of SO_2 is less than that of C_2H_2 (PA= 641.1 kJ mol^{-1}). This result is consistent with the observations from the cyanogen reactions (see Reaction 507 and Table 5.1).

Also of note is the formation of the CH_2SOH^+ product from both directions in the C_2H_2/SO_2 system. This suggests that it is a very stable ionic product. The structure of this ion could be either of the isomers CH_2SOH^+ or CH_3SO^+ but theoretical results [166, 167] suggest it is likely to be the protonated sulfine $CH_2{=}S{=}OH^+$. The ab initio calculations give ΔH_f values of 739 kJ mol^{-1} for CH_2SOH^+ and 838 kJ mol^{-1} for CH_3SO^+. An ion of *m/z*=63 (the same mass as the CH_2SOH^+ ion observed in these reactions) has previously been observed to be formed from ionised dimethylsulphoxide (DMSO CH_3-(S=O)-CH_3). It was originally assumed that this ion was formed by the cleavage of one CH_3 unit to give CH_3SO^+ and this is indeed the case for ions formed from high energy DMSO e.g. in the ion source of a conventional sector mass spectrometer [168, 169]. However when the ion is formed from DMSO ions dissociating in the field-free region, i.e. lower energy DMSO ions, the product has been shown by collisional activation spectroscopy in a mass spectrometer to be CH_2SOH^+ [167]. As the SIFT operates at thermal temperatures and the ions involved in reactions are thermalised by collisions with the buffer gas particles in both FA and SIFT reaction tubes, it seems likely that the product formed in the $C_2H_3^+/SO_2$ and SO_2H^+/C_2H_2 systems is CH_2SOH^+, perhaps by a cycloaddition mechanism like that shown in Figure 5.1. The second complex is similar to the electrostatic collision complex that will be formed initially in both Reactions 509 and 510. The presence of channel 509b suggests that the proton transfer observed (Reaction 509a) probably occurs in an intra-complex manner i.e. after the formation of a collision complex and not one where the proton is transferred via a harpoon-like mechanism.

Figure 5.1: A possible reaction scheme for the formation of the protonated sulfine product in Reaction 509. This scheme may also apply to Reaction 508b.

The observation of proton transfer from $C_2H_3^+$ to CH_3Cl shows that the proton affinities of these two species are similar in accordance with the new PA of CH_3Cl.

Investigations of the structure of the association ions formed.

Like the methylated ions discussed below the association products formed from the reaction of protonated cyanogen with a hydrocarbon (see Table 5.1) can be of two distinct forms, either a cluster type ion (where the individual moieties retain their own separate chemical identities), or as a covalently bound ion. The association products $HC_2N_2^+.C_2H_2$ and $CH_3C_2N_2^+.HCN$ were also investigated using the drift tube (DT). No fragmentation of these ions was observed with 250V on the DT at 0.48 Torr (i.e. 5 V cm^{-1}) which would indicate that they are relatively strongly bound.

The reactivity of these adducts is partly consistent with a covalent structure. The adduct of protonated cyanogen and acetylene (denoted hereafter as $C_4N_2H_3^+$) was formed in the FA, mass selected and then reacted with water vapour, propane, and methanol. No reaction was observed between the $C_4H_3N_2^+$ ion and either propene or water.

$$C_4N_2H_3^+ + H_2O \quad => \quad NR \quad \{k \leq 5x10^{-13} \text{ cm } s^{-1}\} \qquad (513)$$

Water has a higher PA than cyanogen and thus one would expect that if the $C_4N_2H_3^+$ ion was a weakly bound cluster ion, a reaction would be observed (either proton transfer from the $C_2N_2H^+$ moiety to water or a ligand switching reaction). This sort of reactivity was not found. Propane has a slightly lower PA than cyanogen so proton transfer would not be expected. However $C_4N_2H_4$ has several stable neutral structures (both linear, $NCCH_2CH_2CN$, and cyclic) which could mean that the $C_4N_2H_3^+$ ion would extract a hydride ion from C_3H_8 in order to stabilise its carbocation and rearrange to one of these structures. As no $C_3H_7^+$ ion is observed, and indeed no reaction at all takes place, it is likely that the carbocation is already stabilised. A possible form for this stabilised ion is $N{\equiv}C\text{-}CH{=}N\text{-}C^+{=}CH_2$ where the adjacent heteroatom and double bond will spread the charge density.

When methanol was the neutral reactant however, the reactivity appears to be consistent with at least a fraction of the product $C_4N_2H_3^+$ ions having an electrostatic structure (Reaction 514).

$$C_4N_2H_3^+ + CH_3OH \quad => \quad CH_3OH_2^+ + C_2N_2 + C_2H_2 \qquad (514)$$

Methanol has a PA of 754 kJ mol^{-1} [111], so proton transfer from C_2N_2 could be expected. The semi-logarithmic decays of the *m/z* = 79 primary ion had a curved appearance indicating that two isomers were present in the reactant ion. The initial rate is approximately $5x10^{-10}$ cm^3s^{-1} and the rest of the curve is indicitive of an unreactive fraction (a little under half of the ions with a rate of $3x10^{-12}$ cm^3s^{-1}). This is shown in Figure 5.2. The products observed were predominantly the result of proton transfer to methanol but a small amount of adduct was also observed. This suggests that both a covalent and electrostatic fraction is present in the $C_4N_2H_3^+$.

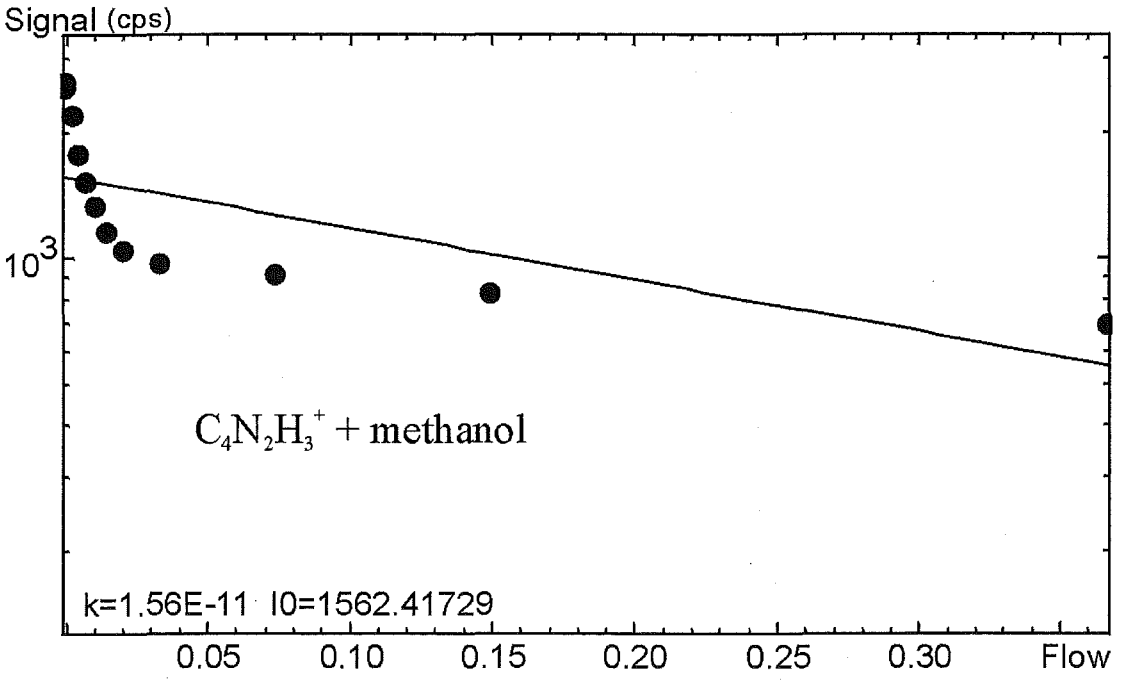

Figure 5.2: The semi-logarithmic decay observed when methanol was reacted with the $C_4H_3N_2^+$ ions generated from the association of $C_2H_3^+$ and C_2N_2.

Protonated methanol and the proton bound dimer of methanol were both observed indicating a proton transfer had taken place. These observations suggest that both electrostatic (i.e. capable of proton transfer to methanol) and covalent structures (unreactive) of $C_4N_2H_3^+$ are formed in the reaction between $C_2H_3^+$ and C_2N_2.

Section 5.3: Methyl Cation Transfer Reactions.

§5.3.1 Methyl cation transfer reactions involving cyanogen.

Another property of molecules which is conceptually similar to proton affinity is that of methyl cation affinity (MCA). This property is a measure of the relative ease with which a molecule will transfer a CH_3^+ cation to another molecule. The methyl cation affinity is defined as the enthalpy change for reaction 5.11.

$$BCH_3^+ \quad => \quad CH_3^+ + B \qquad MCA(B) = \Delta H_{298} \qquad (5.11)$$

Here B represents the entity (often referred to as a "base") for which the MCA is being determined. The MCA of a molecule usually correlates with its proton affinity and the intrinsic nucleophilicity of the atom to which the methyl cation is attached [170, 171].

Alkylated cyanogen ions have previously been observed to form effectively [172] but the subsequent reactions of these species have not been investigated. McEwan *et al.* believe, however, that the adduct formed is strongly bound. The reactivity of these alkylated ions will be heavily influenced by the nature of the bonding between the alkyl cation and the cyanogen molecule. These alkylated ions may be able to transfer alkyl cations to other species and act as alkylating agents in the interstellar medium. Indeed the low PA of cyanogen suggests that alkylated cyanogen ions may be highly effective alkylating agents. Should this be the case it would suggest that the bonding is primarily electrostatic in character. Alternatively if, the alkylated cyanogen ions are strongly bound they would not readily transfer these cations. In this latter case the alkylated cyanogen ions would provide an effective starting point for rapidly building more complex species.

Several of the reactions presented previously in Table 5.1 show association products. Reaction 507 is a good example of the formation of this type of adduct ion. Here the product of the reaction of $C_2H_5^+$ and C_2N_2 is quite possibly the alkylated ion CH_3CH_2NCCN. Similar behaviour was observed in the reaction of $C_2H_3^+$ with cyanogen in this study and has also been previously observed for CH_3^+ ions reacting with cyanogen [159, 172].

As previously stated, there is a general correlation between PAs and MCAs. Such correlations are especially useful when series of related bases (e.g. a series of molecules containing an oxygen donor atom or a series of nitriles) are

compared [170, 171] . In their 1990 paper, Deakyne and Mautner [171] show that the relationship between MCA and PA is reasonably linear for a series of CN type donors (see Figure 3 of that paper). From such observations it may reasonably be inferred that cyanogen, with its low PA, would be an effective alkyl donor. To explore this possibility the reactions of methylated cyanogen with a range of neutral molecules were investigated in the present study using the FA-SIFT.

§5.3.2: Experimental conditions.

The Canterbury FA/SIFDT is ideally suited to the study of this class of reactions as the alkylated ions can be easily formed in the FA and then mass selected by the upstream quadrupole. The products of these alkylated ions with neutral reactants added downstream in the SIFT flow tube can then be studied without interference from other species. The method of ionisation used in the flowing afterglow for these studies was, in most cases, the linear geometry microwave discharge. Methylated CH_3NCCN^+ ions were formed from the reaction of CH_3^+ with cyanogen (Reaction 510). The methyl cations were formed from the action of helium ions and metastables on a flow of methylbromide vapour that was added upstream of the point where the cyanogen was added to the FA. This two-step process allowed the methylated ions to be mass selected and directly injected into the reaction flow tube.

§5.3.3: Results and Discussions.

The products and rate coefficients of the reactions studied in this section are presented in Table 5.5. As may be seen in Table 5.5, no methyl cation transfers were observed from CH_3NCCN^+ to any of the neutral bases investigated. One possible exception to this general observation comes from the reaction between $CH_3C_2N_2^+$ and dimethyl ether. In this case a small $(CH_3)_3O^+$ ion signal was observed in the flow tube. However, as no methyl cation transfer was observed to species having higher MCAs (e.g. trimethylamine $(CH_3)_3N$ for which MCA = 528 kJ mol^{-1} (cf. MCA $(CH_3)_2O$ = 390 $kJmol^{-1}$) it seems likely that the small $(CH_3)_3O^+$ ion signal is not a result of the primary reaction process. It is likely the $(CH_3)_3O^+$ ions are formed from ions present

as a result of ionisation by stray photons entering in the flow tube. A possibility is Reaction 512, instigated by the ionisation of dimethyl ether in the SIFT reaction tube.

$$(CH_3)_2OH^+ + (CH_3)_2O \quad => \quad (CH_3)_3O^+ + CH_3OH \qquad (512)$$

The results in Table 5.7 are comparable as the methylated ion of $(CH_3)_2O$ which has a known low methyl cation affinity [158, 171] of 390 kJ mol^{-1}. $(CH_3)_3O^+$ shows no reaction with neutrals of similar MCA (CH_3CN and CH_3COCH_3) but it has previously been shown to rapidly transfer a methyl cation to trimethylamine [171].

Reactants		Products	k_{obs}[a]	k_{col}[a]	PA(Neutral)
Ionic	Neutral				
CH_3NCCN^+	C_2H_2	-	NR[B]	0.99	641.1
CH_3NCCN^+	HCN	$CH_3NCCN^+.HCN$	0.0062	3.2	712.9
CH_3NCCN^+	$(CH_3)_2O$	$CH_3NCCN^+.O(CH_3)_2$	0.025	1.6	792.0
CH_3NCCN^+	CH_3CN	$CH_3NCCN^+.NCCH_3$	0.27	3.6	779.2
CH_3NCCN^+	$(CH_3)_2CO$	$CH_3NCCN^+.OC(CH_3)_2$	0.40	2.6	812.0
CH_3NCCN^+	$(CH_3)_3N$	$CH_3NCCN^+.N(CH_3)_3$	1.2	1.3	948.9
$CH_3OH_2^+$	C_2N_2	$CH_3OH_2^+.C_2N_2$	0.08	1.5	-
$CH_3BrCH_3^+$	C_2N_2	-	NR[B]	1.1	-

Table 5.5: The rate coefficients and products for the reactions studied during the investigation of the methyl cation affinity of cyanogen.

a) Rate coefficients expressed in units of 10^{-9} cm^3 s^{-1}.

b) NR indicates that no observable reaction occurred. The rate coefficient thus has an upper limit of ~$5x10^{-13}$ cm^3s^{-1}.

The lack of methyl cation transfer from these methylated cyanogen ions can be interpreted in two ways; either NCCN has a very high methyl cation affinity, or the ion formed from methylation of cyanogen is strongly (i.e. covalently) bound. In order to test the former of these possibilities the reactions of $CH_3BrCH_3^+$ and $CH_3OH_2^+$ with cyanogen were investigated. $CH_3OH_2^+$ was formed by protonating methanol in the FA source and $CH_3BrCH_3^+$ was conveniently formed from the association of CH_3^+ ions and CH_3Br vapour used as a source for these CH_3+ ions. If cyanogen has a high MCA then these alkylated cations should transfer their alkyl cations to it effectively. $CH_3OH_2^+$ has previously been shown by Karpas and Mautner [173] to effectively transfer CH_3^+ to species with relatively low MCAs (e.g. methanol, formaldehyde) and therefore should easily transfer CH_3^+ to cyanogen if it has a high MCA. No such

transfer was observed. Nor was any transfer observed from $CH_3BrCH_3^+$. The only product seen in both of these cases was an adduct. The lack of methyl cation transfer either to or from cyanogen suggests that there is a barrier to this type of reaction on the potential energy surfaces. This barrier will promote association-type reactions, consequently all the alkylated cyanogen ions observed in this study (and others [159, 160, 172]) have been formed via an association mechanism rather than an alkyl transfer one. In a prior investigation of the CH_3^+/C_2N_2 system McEwan *et al.* concluded that the $C_3H_3N_2^+$ ion formed via the association was strongly (i.e. <~150 kJ mol^{-1}) bound [172]. They base this conclusion on the fact that association was observed even at pressures of ~$1x10^{-4}$ Torr. This suggests that the formation of the $C_3H_3N_2^+$ ion is highly facile, and indicates strong bonding. Similar behaviour has been observed for the CH_3^+/CH_3CN [174, 175, 176], and CH_3^+/HCN [177, 178] systems, implying that the methyl cation forms a strong bond to the R-CN moiety in these molecules.

Although the CH_3NCCN^+ ion shows no reactivity through methyl cation transfer channels, it associates with lone pair donor "bases" to form much larger ionic species (see Table 5.5). In most cases however, these associations are not particularly efficient. An interesting trend is that the rate coefficients for these reactions increase as the PA of the base increases presumably because the PA of the neutral reactant also correlates with the strength of the CH_3NCCN^+-B bond. The collision complex between the methylated cyanogen ion and the neutral species is thus in a deeper well and consequently more energy is required to cause the complex to dissociate back to reactants. This increases the lifetime of the collision complex and thus increases the probability that the complex will be collisionally stabilised before it dissociates to reactants. In kinetic terms this is represented by an increase in the relative importance of the $\beta k_s[M]$ term in equation 5.12.

$$A^+ + B \underset{k_{-1}}{\overset{k_f}{\rightleftharpoons}} [AB^+]^* \xrightarrow{\beta k_s[M]} AB^+ \qquad (5.12)$$

§5.3.4: Supplementary methyl cation transfer reactions.

The following reactions are included as they were begun under the auspices of this work. Subsequently they have become the core of a planned investigation of the

energetics of methyl cation transfer that will be continued by Drs. Mautner and Wilson. They also show that the inability to observe methyl cation transfer in the previous section from CH_3NCCN^+ was a result of the energetics of the system. The results are presented below in Table 5.6.

Reactants		Products		k_{obs}[a]	k_{col}[b]
Ionic	Neutral				
$(CH_3)_3O^+$	$(CH_3)_2CO$	$(CH_3)_3O^+.(CH_3)_2CO$		0.012	2.7
$(CH_3)_3O^+$	CH_3CN	$(CH_3)_3O^+.CH_3CN$		0.020	3.7
$CH_3OCH_2^+$	$(CH_3)_2CO$	$CH_3OCH_2^+.(CH_3)_2CO$	[0.15]	0.69	
		$(CH)_3CO^+ + CH_2O$	[0.85]		
$CH_3OCH_2^+$	$(CH_3)_2O$	$CH_3OCH_2^+.(CH_3)_2O$	[0.90]	0.14	
		$(CH_3)_3O^+ + CH_2O$	[0.10]		
$CH_3OCH_2^+$	CH_3CHO	$CH_3OCH_2^+.CH_3CHO$	[0.90]	0.35	
		$(CH_3)_2COH^+ + CH_2O$	[0.10]		

Table 5.6: The results for those methyl cation transfer reactions not involving cyanogen that were investigated during this study.

a) The experimentally determined rate coefficient. The unit are 10^{-9} cm^3s^{-1}.

b) The collision rates for each reaction, calculated using the method of Su and Chesnavich [114]. The units are 10^{-9} cm^3s^{-1}.

$(CH_3)_3O^+$ reactions

The $(CH_3)_3O^+$ ion was generated from moderately high pressures of dimethylether added to a helium afterglow in the FA flow tube at the nose cone neutral inlet.

Reaction with acetone

The reaction between $(CH_3)_3O^+$ and acetone was found to give only an association product (Reaction 515a) despite the fact that the proton affinities of the various reactants would suggest that the methyl cation transfer reaction should proceed (PA ($(CH_3)_2O$) = 792 $kJmol^{-1}$ and PA ($(CH_3)_2CO$) = 812 $kJmol^{-1}$).

$$(CH_3)_3O^+ + (CH_3)_2CO \Rightarrow \text{adduct} \quad (515a)$$

$$\Rightarrow (CH_3)_3CO^+ + (CH_3)_2O \quad (515b)$$

At thermal energies the only product observed was the adduct (515a). This channel was found to proceed with an apparent bimolecular rate coefficient of 1.2×10^{-11} cm^3s^{-1}

at 0.49 Torr. The initial determinations of this rate coefficient gave a curved semi-logarithmic decay but later investigations showed a straight decay. The curvature in the first attempts probably resulted from overlap between $(CH_3)_3O^+$ (61 amu) and photoionised acetone (59 amu as protonated form) as the resolution in the initial studies was very low. A low resolution was used in an attempt to minimise mass discrimination effects above 100 amu. Later the problem of mass discrimination was addressed by altering the lens and ΔM setting neither of which compromise the resolution seriously. The proton bound dimer of acetone was observed and shown to be the result of photoionisation. This provides further evidence for the contention that protonated acetone was causing problems in the early rate determinations.

A small ion signal was observed at the correct mass to charge ratio to be the methyl cation transfer product (73 amu). This ion however, was found to be present at essentially identical levels with the primary ion gated off (this was achieved by reversing the polarity of the last electrostatic lens in the ion selection region). One of the reason for investigating these reactions is that it is surmised that there is a barrier on the potential surface, preventing an otherwise exothermic methyl cation transfer from occurring. Thus the reactant ions were taken to an elevated "temperature" by placing a voltage on the drift tube. At these elevated energies (~50V, 0.49 Torr) the 73 amu ion was visibly different with or without the primary ion signal, thus indicating that Reaction 515b was now occurring.

Reaction with acetonitrile

The rate coefficient for the reaction between $(CH_3)_3O^+$ and CH_3CN is also very small , at ~2.0×10^{-11} cm^3s^{-1}. The main product observed was the adduct at 102 amu, however there may have been an extremely minor MCT channel. Like the dimethylether case this methyl cation transfer channel is most likely the result of some break-up or impurity ion rather than representing a genuine product channel. Due to the slow rate, the proton bound dimer (and logically the non-clustered, protonated form) of acetonitrile was observed to be a major contaminant ion. These ions were presumably formed by stray photons entering the reaction tube.

$CH_3OCH_2^+$ Reactions.

The $CH_3OCH_2^+$ ion (essentially methylated formaldehyde) was exceedingly easy to generate high counts. Dimethoxymethane was added to the FA at the nose cone inlet using a helium carrier and a microwave discharge as the source of ionisation. (The parent ion was even easier to generate with up to 250,000 cps observed at one time).

Reaction with acetone

In order to study the $CH_3OCH_2^+$/acetone reaction, a mixture of acetone in helium was needed as the neutral flows of acetone required were too difficult to measure from pure acetone accurately. Two primary products were observed, *m/z* = 73, corresponding to methyl cation transfer and the adduct at 103 amu. The product branching ratio favours methyl cation transfer but the traces recorded indicate that the adduct is actually the major product, further investigation of this system is warranted. The rate coefficient was found to be 6.9×10^{-10} cm^3s^{-1}. The mixture composition was determined by comparing the rate coefficient for the H_3O^+/acetone reaction (using the mixture) with the literature rate coefficient for a pure acetone neutral reactant (k_{lit} = 3.8×10^{-9} cm^3s^{-1}). Note that this is only an *apparent* bimolcular rate coefficient due to the presence of an association channel.

Reaction with dimethylether

Adduct formation is the major product channel of the reaction between $CH_3OCH_2^+$ and $(CH_3)_2O$. The rate coefficient was found to be 1.4×10^{-10} cm^3s^{-1} at 0.49 Torr (this rate coefficient is also an apparent bimolecular rate coefficient) with a product branching ratio of approximately 90% adduct and 10% methyl cation transfer.

$$CH_3OCH_2^+ + (CH_3)_2O \Rightarrow CH_3OCH_2^+.(CH_3)_2O \quad [0.90] \quad (516a)$$

$$\Rightarrow (CH_3)_3O^+ + CH_2O \quad [0.10] \quad (516b)$$

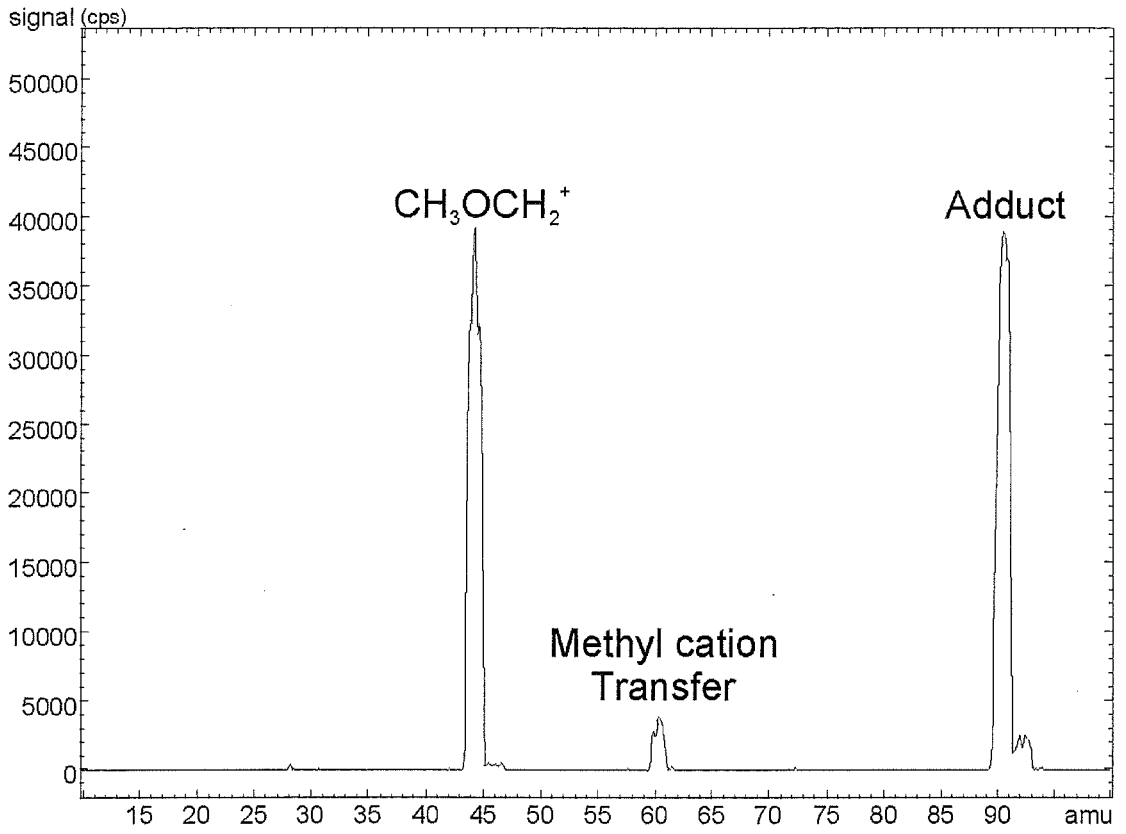

Figure 5.3: The mass spectrum generated when a low flow of dimethylether is reacted with the $CH_3OCH_2^+$ ion.

Reaction with acetaldehyde

Both the adduct and methyl cation transfer products were observed in this reaction system as shown in Reaction 517.

$$CH_3OCH_2^+ + CH_3CHO \Rightarrow CH_3OCH_2^+.CH_3CHO \quad [0.90] \quad (517a)$$

$$\Rightarrow C_3H_7O^+ + CH_2O \quad [0.10] \quad (517b)$$

The rate coefficient was approximately 3.5×10^{-10} cm^3s^{-1} at 0.49 Torr. Small amounts of impurity ions at 45 and 43 amu were observed, presumably due to photoionisation of the neutral but neither these ions, nor a small amount of CH_3^+ (formed by break-up upon injection), will seriously affect the branching ratio.

Section 5.4: Conclusions.

The tabulated value for the proton affinity of cyanogen had been questioned by Petrie [179] after theoretical work suggested it should be ~20 kJ mol^{-1} lower. Thus the

proton affinity of cyanogen has been re-determined via the equilibrium method using the Canterbury SIFT. The value was determined through an investigation of the $C_2H_2/H^+/C_2N_2$ reaction system in both directions. This new experimental measurement agrees well with a value determined using the kinetic data from a previous study of the cyanogen/methyl chloride equilibrium and the new value for the PA of methyl chloride [165]. This study was reported in the previous work of Petrie *et al.* [160] and was investigated by McEwan using the ion cyclotron resonance instrument located at the Jet Propulsion Laboratories in Pasadena, California. The new PA value is 651 ± 2 kJ mol^{-1}, significantly lower than the previous value of 675 kJ mol^{-1} and in good agreement with the theoretical value proposed by Petrie [179]. Further evidence has also been found for the lower PA for SO_2 proposed by Fairley *et al.* in a recent theoretical paper [163].

Further a range of methyl cation transfer experiments have been investigated. It has been shown that methylated cyanogen does not undergo MCT with a wide range of neutral reactants. The methyl cation affinities of these neutral species span quite a range of values and thus the non-observation of methyl cation transfer indicates that C_2N_2 has a barrier to this type of reaction. Cyanogen has also been found to be unreactive with respect to methyl cation transfer with $CH_3OH_2^+$ and $CH_3BrCH_3^+$, both of which should be able to transfer a methyl cation to cyanogen even if it has a relatively low MCA. From these observations it has been surmised that there is a barrier to MCT on most potential energy surfaces involving cyanogen. This agrees with the work of McEwan *et al.* [172]. Several other methyl cation transfer reactions have also been investigated.

In the course of the above investigations it was noted that many of the reactions that were observed for the cyanogen ions involved the formation of an adduct. The reactivity of some of these adducts, primarily $C_2N_2H^+.C_2H_2$, was investigated. These investigations indicate that at least a portion of the adduct ions formed in this manner have covalently bound structures.

Chapter 6:

Selected reactions relevant to the ion-molecule chemistry of the lower ionosphere of Titan.

Section 6.1: A Tour of Titan and its Ion-molecule chemistry.

In Greek mythology all the children of Uranus (heaven) and Gaea (earth) were known as titans. These titans rebelled against their forebears but were defeated when Saturn and his wife Rhea (also a moon of Saturn) banded together with their children (Zeus foremost among them) to combat them. Many of the moons of Saturn are named after these titans and the largest of them bears simply the name Titan, which has also come to mean giant. Titan is indeed a giant being the largest moon in the Saturnian system and the second largest satellite in the solar system, smaller only than Jupiter's Ganymede. Viewed from Earth Titan appears to be larger than Ganymede, due to the ~200km of impenetrable cloud that surrounds it. Its main claim to fame is that it is the only satellite in the solar system with a massive atmosphere, the pressure at its the surface is approximately one and a half times as great as that at the surface of our own Earth. Despite being discovered in 1655 by the Dutch physicist Christiaan Huygens, Titan remains a secretive giant and only recently has information about this satellite begun to leak out from behind the thick veil of haze cloud that surrounds it.

As early as 1908, visual observations had hinted at this thick atmosphere and by 1944 absorption bands of methane had been observed by Gerard Kuiper [180], but it was the Voyager series of spacecraft that began the real study of Titan [181]. When, in 1980, Voyager 1 sent back the first close-up pictures of Titan, all that was visible was a featureless orange haze, totally obscuring the surface underneath. Spectrometers working in the ultraviolet region of the spectra gave more information, detecting emission lines from atomic and molecular nitrogen in the upper atmosphere, characteristic of nitrogen excited by electrons. Infrared measurements have since detected a variety of hydrocarbons and nitrogen-containing compounds. Methane has been found to be one of the major trace species. The composition of Titan's atmosphere as determined by the current best models is shown in Table 6.1. Fuller models, including altitude profiles, can be found in the work of Yung *et al.* [182] and

Keller *et al.* [183], and Yelle *et al.* [184], low altitude profiles can be found in that of Lara and co-workers [185].

Constituent	Stratosphere (40-100 km)	Thermosphere (3900 km)
N_2	< 0.97	> 0.97
CH_4	1-3 x 10^{-2}	8 ± 3 x 10^{-2}
H_2	2 x 10^{-3}	
CO	6 x 10^{-5}	
CO_2	7-30 x 10^{-10}	
H_2O	< 1 x 10^{-9}	
C_2H_6	2 x 10^{-5}	
C_2H_4	4 x 10^{-7}	
C_2H_2	2 x 10^{-6}	~ 1.5 x 10^{-3}
HCN	2 x 10^{-7}	< 5 x 10^{-4}
C_2N_2	1-10 x 10^{-8}	
HCCCN	1-10 x 10^{-8}	

Table 6.1: The detected constituents in Titan's stratosphere and thermosphere. Data obtained from References 182, 184 and 185.

Obviously molecular nitrogen is the predominant species, however the range and amount of molecules containing carbon and nitrogen are great enough to develop complex atmospheric chemistry. The simple hydrocarbons, especially the abundant CH_4, are converted into heavier, more complex species through photochemistry [182] and ion-molecule chemistry. This is an essentially irreversible process. The continued presence of high levels of methane in Titan's atmosphere is one of the continuing mysteries of Titan. The atmospheric temperature near the surface of Titan is approximately 95 K, just five degrees above the triple point of methane (90.7 K) [184]. Consequently methane oceans have been proposed to exist on the surface. Oceans of other liquid hydrocarbons or a mixture of hydrocarbons have also been proposed as the atmospheric models have evolved.

Recently, however, astronomers have begun to observe Titan using longer wavelengths, near the infrared where there are several spectral 'windows' that allow observation of the surface. The major problem with this type of experiment is the presence of strong absorption features in this spectral region from methane. However narrow windows in the methane absorption spectrum around 1.5 to 2μm permit some

surface features to be seen. Ground based observatories and the Hubble Space telescope have been used to make observations of the surface and differentiated bright and dark features have been observed [187].

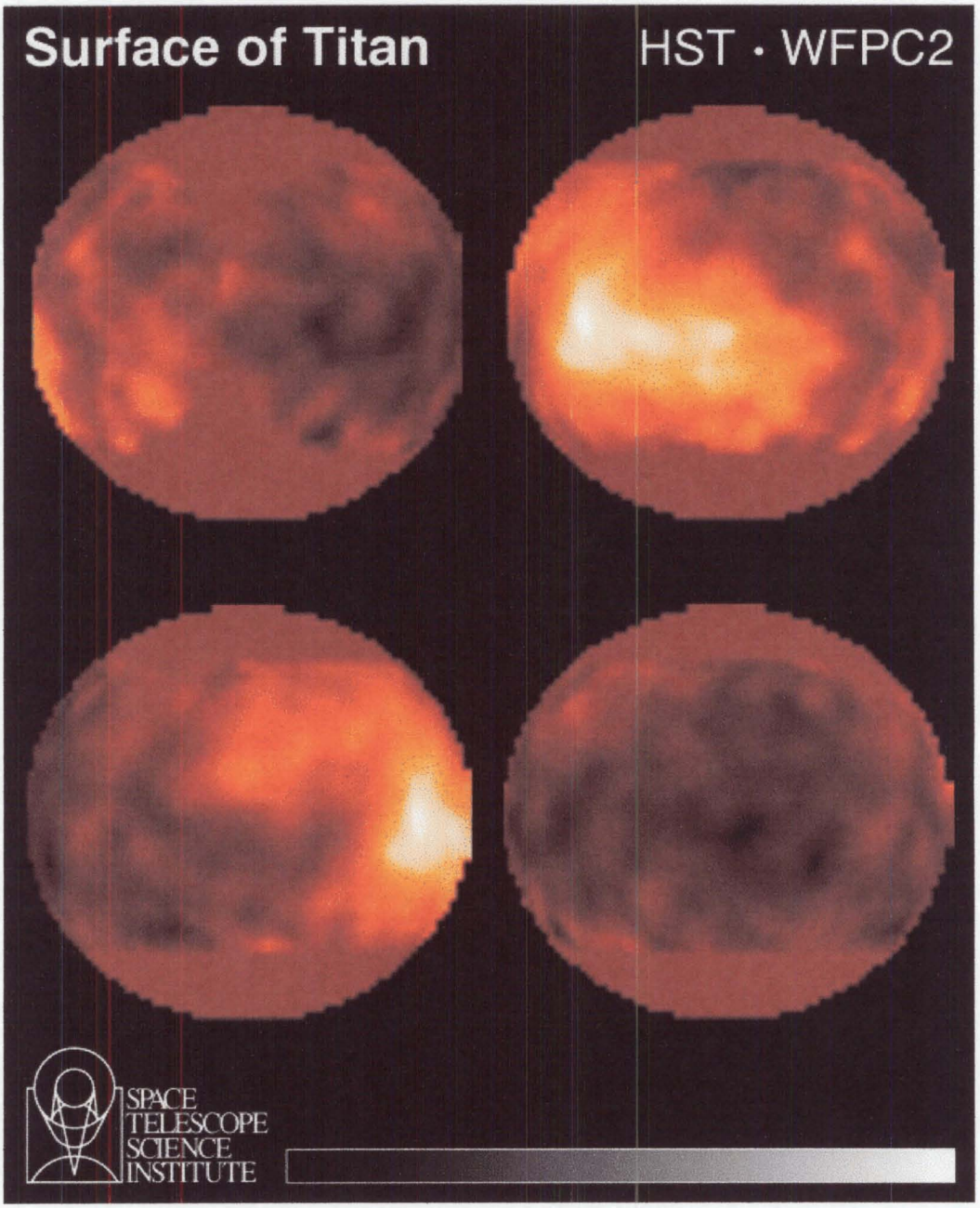

Figure 6.1: The surface of Titan as viewed in the near IR by the Hubble Space Telescope.

These dark features may arise from liquid hydrocarbons that have become concentrated in the low-lying regions. Alternatively they could be the result of the precipitation of dark material from the atmosphere (although the spectrum of the "thiolins" formed in the Miller type experiments [191] do not match the reflectivity of

the surface) which is continuously washed into the lower lying regions of the planet's surface by hydrocarbon 'rain'. Neither of these hypotheses have been confirmed.

In a roundabout fashion this brings us back to the haze clouds. All of the points mentioned in the above paragraph are essentially speculative as direct observation of the lower regions of Titan's atmosphere and the surface are difficult. Cameras operating in the visible region of the spectra can see only a continuous sea of orange cloud tops. The exact nature of these clouds has been a subject of debate also, though they are probably aerosols derived from the accretion of gaseous organic compounds [188]. The main haze layer exists at altitudes ranging from 100-300 km above Titan's surface. The aerosols in this layer are probably formed at higher altitudes by aggregation and begin to 'rain out' towards the surface [189]. These drops fall more slowly on Titan than corresponding rain drops on Earth (approximately six times slower) because of the lower gravitational pull and the droplets may evaporate as they near the surface. The orange colour of the clouds is proposed to arise because of some type of C-H-N polymers present in the aerosol clouds [190]. Simulation experiments, similar as those first performed by Miller, where "Titan-like" atmospheres are subjected to continuous energy deposition have been shown to produce many of the species observed in Titan's atmosphere [191]. A brownish red deposit of the walls on the experimental apparatus is also commonly observed. These deposits, called 'thiolins' by Carl Sagan, are polymeric nitriles and may be similar to the coloured compounds in Titan's clouds. 'Miller-type' experiments simulate the action of atmospheric energy sources such as photons, lightning, or other energetic particle collisions (e.g. cosmic rays and magnetospheric electrons from Saturn) on Titan's atmosphere.

As early as 1973 Titan was envisioned as the target for an entry probe [192] and its extended atmosphere was seen as ideal for study by a fly-by spacecraft. Indeed most of the bodies within the Solar system with an appreciable atmosphere have already been investigated via mass spectrometric means. With the launch on October 15 1997 of the Cassini/Huygens mission [39, 40, 193], Titan will hopefully be added to this list in 2004. The Cassini orbiter carries the Ion and Neutral Mass Spectrometer instrument (INMS) [194] and will pass through the upper atmosphere of Titan (the projected lowest pass is 950 km above the surface [40]) allowing it to sample and characterise the neutral and ionic constituents of Titan's upper atmosphere. Also on

board the orbiter is the 350 kg Huygens probe which will descend through the atmosphere of Titan and land (or splash down) on the surface. The Huygens probe will utilise six scientific instruments on this descent including the gas chromatograph-mass spectrometer, which will sample and identify the neutral species in Titan's atmosphere, from 160 km to the surface [39, 40]. Both of the Cassini mass spectrometers utilise similar quadrupole mass spectrometers and together they should allow characterisation of the ionic and neutral constituents over a wide altitude and pressure range.

An understanding of the ion chemistry that occurs in a Titan-like atmosphere is not only important for modelling the ionospheres of Titan but is also required to help deconvolute the signals that will be returned by Cassini's mass spectrometers as they pass through Titan's atmosphere. Both mass spectrometers (INMS and GC-MS) use electron emission filaments near their entrances to ionise neutral species for study. As a consequence ion chemistry can occur in the throat of the mass spectrometer and may constitute a problem as the probe enters the high pressure region of Titan's atmosphere.

As Titan is surrounded by a large gaseous envelope it is also possible for it to have an ionosphere. Indeed the radio occultations from Voyager 1 established that there is a region in Titan's atmosphere with several thousand electrons per cubic centimetre (though only an upper limit could be determined) [195]. An ionosphere is a region in an atmosphere where there are enough electrons and ions to influence the propagation of radio waves through the atmospheric gas. In the case of the Earth the term usually refers to the region of the atmosphere lying at altitudes between approximately 50 km and one Earth radius (~6400 km). The Earth's ionosphere is divided into several layers based loosely on the electron density, with the ionospheric peak occurring at ~300 km above the planet's surface. At this point there are approximately $1x10^6$ electrons per cm^3 [196]. The main ionisation sources for Earth's ionosphere are solar UV photons.

The method for formation of an ionosphere in Titan's atmosphere cannot be as succinctly summarised. Titan is farther from the Sun so photons from the Sun do not dominate the formation processes quite as much. Also Titan, unlike Earth, has little intrinsic magnetic field so energetic charged particles can enter the atmosphere easily. Thus the ionisation source for Titan's ionosphere is supplied by a range of sources:

photons in the form of solar extreme ultraviolet radiation; *electrons* - both photoelectrons produced by this radiation and electrons trapped in Saturn's magnetosphere [197, 198]; and high energy *cosmic rays* e.g. stellar protons. Titan, much like the Earth's own satellite the Moon, is gravitationally locked so that it always presents the same face to Saturn [197]. This means that the different portions of the atmosphere are subjected to different types of ionisation as Titan completes its 383 hour (~16 day) orbit around Saturn. Figure 6.2 illustrates the different categories of physical condition that can exist for the different sections of Titan's atmosphere.

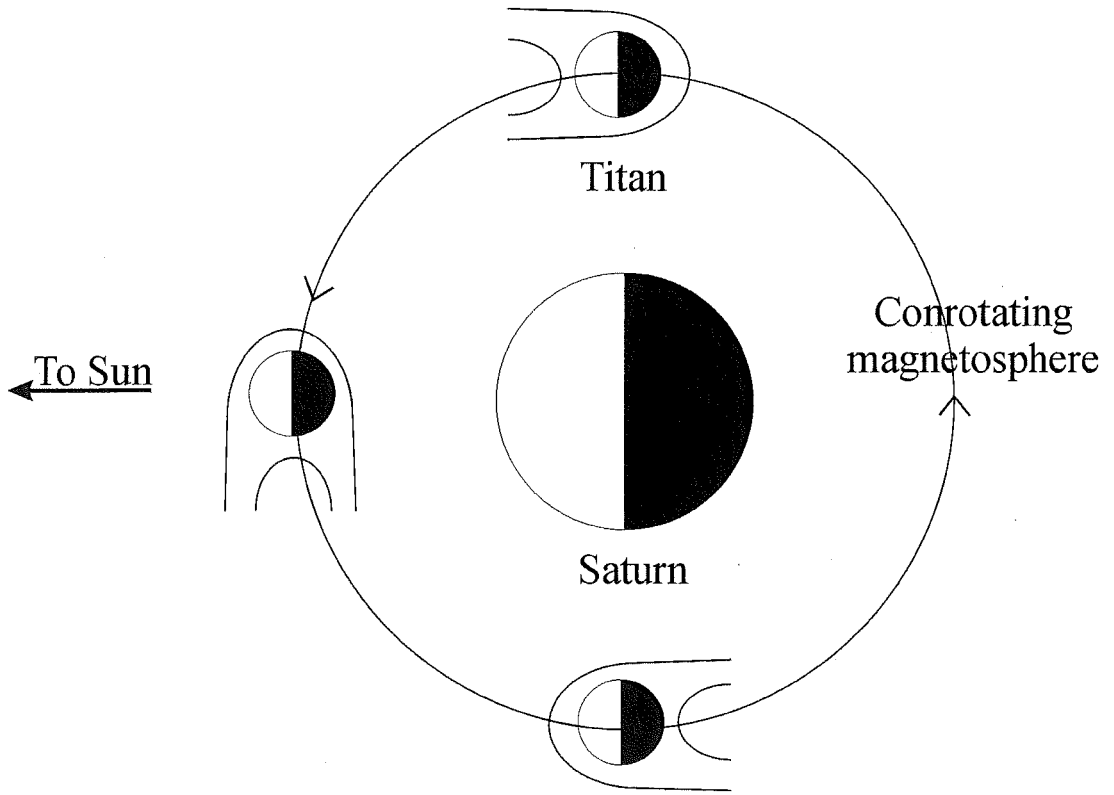

Figure 6.2: A schematic diagram illustrating the different ionisation conditions Titan can experience during its orbit of Saturn. The field lines actually drape at right angles to the paper. Figure after Reference 197.

Keller *et al.* [183, 199] found that the major source of ionisation on the day-side was photoionisation, with photoelectron ionisation next in importance followed by magnetospheric electrons. On the night side magnetospheric electrons are of course the main ionisation source.

A further possible source of ionisation is from cosmic rays [200, 201, 202, 203]. On Earth cosmic ray ionisation produces the base of the lowest level of the ionosphere, the D layer and continue producing ions right down to the ground. Cosmic rays, being

highly energetic, can penetrate deep into any atmosphere and on Titan can ionise and dissociate molecules down to the surface. The cosmic ray spectrum contains a range of species but a large fraction of the energy is carried by highly energetic particles. These particles are mainly protons, though 10-15% are alpha particles and higher nuclei [200]. When these collide with other species, e.g. the neutral species in Titan's atmosphere, they produce electromagnetic and particle cascades that can ionise and dissociate molecules right down into the lower atmosphere of Titan. Thus in one collision a single high-energy cosmic ray distributes its energy among a number of lower energy secondary particles. Capone and co-workers [200] and Molina-Cuberos *et al.* [202] have shown that this produces another source of ionisation on Titan that peaks between 50 and 100 km above the surface, where the pressure is between 10 and 80 Torr. This lower region of the atmosphere is not reached by any of the other sources of ionisation as the haze layer and the column density of nitrogen and other gases above it ensure that all the photons and electrons are absorbed far higher in the atmosphere. Nevertheless, Capone *et al.* have shown that cosmic rays can produce a significant ionosphere at lower levels in Titan's atmosphere. The main primary ions formed by cosmic ray ionisation are N^+ and N_2^+ with the next most likely species to be produced CH_4^+, CH_3^+, and possibly Ar^+. These latter ions are between 10 and 100 times less likely to be produced than molecular and atomic nitrogen ions. Both model studies of the lower ionosphere conclude that Ar^+ is a significant initial ion as they use neutral models [184, 204] that contain up to 11% argon in the atmosphere. The presence of argon in Titan's atmosphere is purely speculatory and has been advanced by several sources to account for the fact that the mean molecular ion weight in Titan's tail was greater than that of nitrogen. The Voyager mission found that the average molecular weight of the ions was between 28.3 and 29.2 *amu*, which suggests the presence of an appreciable fraction of a heavier weight component. The search for noble gases in Titan's atmosphere is one of the major scientific goals of the Titan encounters of the Cassini-Huygens mission [39, 40].

In the course of this present work two categories of reaction which are relevant to the lower, cosmic ray-produced, ionosphere of Titan have been investigated. The first category includes the bimolecular reactions of the ions produced from the termolecular reactions of the primary nitrogenous ion (N^+ and N_2+) with nitrogen (i.e. N_3^+ and N_4^+) with the major trace constituents of Titan's atmosphere. The second

category considers the effect of a nitrogen collision partner on some of the termolecular association reactions that are likely to occur in Titan's lower atmosphere. Specifically, the association chemistry of the terminal ions in Titan's atmosphere, c-$C_3H_3^+$, H_3O^+, and $HCNH^+$, with the major hydrocarbon constituents (CH_4, C_2H_2, and C_2H_4) have been investigated.

Section 6.2: Bimolecular Ion-Molecule Reactions in Titan's lower atmosphere; the reactions of the ions N_3^+ and N_4^+.

§6.2.1: Introduction.

In almost all cases the ion-molecule chemistry in the ionosphere of Titan will be initiated by the ionisation of a nitrogen molecule. This, as shown in reaction 601, will create either a N^+ or a N_2^+ ion.

$$N_2 + (h\nu, \text{e-, or cosmic ray}) \Rightarrow N_2^+ + e^- \quad (601)$$
$$\Rightarrow N^+ + N + e^-$$

These ions then react with other species to build up the more complex ions predicted to be present in Titan's ionosphere. When considering reactive collisions it has usually been assumed in the models that the neutral most likely to be most important is methane. However on a purely statistical basis it is far more likely that any ion formed will encounter a nitrogen molecule many times before a methane molecule is encountered. In the upper regions of the atmosphere the encounter with nitrogen results in an unreactive collision. However, both N^+ and N_2^+ are known to exhibit termolecular association reactions with N_2 [47, 205-216]ref (reactions 602 and 603). Therefore at higher pressures (i.e. lower in the atmosphere), these abundant collisions with nitrogen become *reactive* for both N^+ and N_2^+ to form N_3^+ and N_4^+.

$$N^+ + N_2 + M \Rightarrow N_3^+ + M \quad (602)$$
$$M = He \; k_3 = 2.0 \times 10^{-29} \; cm^6 s^{-2}.$$
$$M = N_2 \; k_3 = 5.0 \times 10^{-29} \; cm^6 s^{-2}.$$

$$N_2^+ + N_2 + M \Rightarrow N_4^+ + M \quad (603)$$

$M = He\ k_3 \geq 2.0 \times 10^{-29}\ cm^6 s^{-2}$.

$M = N_2\ k_3 = 6.0 \times 10^{-29}\ cm^6 s^{-2}$.

The rate coefficients given above for the N_2 bath gas are from the literature [47, 205] while the association rate coefficients with a helium bath gas are those measured using the University of Canterbury SIFT. All of these values are measured at or near room temperature (~300K). The well depths for the N_3^+ and N_4^+ formation reactions, as calculated by previous theoretical investigations [217, 218], are 361 kJ mol^{-1} for N_3^+ and 106 kJ mol^{-1} for N_4^+. Considering that these are relatively strongly-bound species, the measured association rate coefficients are quite slow when they are compared to other association reactions where the products have similarly strong binding energies. The rates of association are, however, probably significantly slowed relative to others by the small number of degrees of freedom available in the association complex in which to distribute the collision energies.

Reactions 602 and 603 are termolecular reactions; that is the rate is dependent on the concentration (or pressure) of not only the reacting species but also on the presence of a third body that carries away some of the energy involved in the initial collision complex. Thus these reactions will become more competitive with bimolecular reactions as one progresses deeper into Titan's atmosphere. Unlike bimolecular reactions, the rate coefficients of association reactions are markedly temperature dependent, becoming faster as the temperature drops due to the reduced energy carried into the initial collision complex by the reactants. The temperature in Titan's ionosphere is considerably lower than 300K (it is approximately 135K at the base of the upper ionosphere, 975 km above the surface) and thus these reactions can reasonably be expected to be faster than the equivalent reactions at room temperature. Deep in Titan's atmosphere, where the pressure is high and the temperature low, a point will be reached where these association reactions will become competitive with bimolecular ion-molecule reactions.

The temperature dependence of Reaction 603 has been previously measured by both Bohringer and Arnold [219] and Rowe *et al.* [47]. They found the temperature-dependent termolecular rate coefficient to have the form $k_3 = 6.5 \times 10^{-29} \times (300/T)^{1.77}\ cm^6\ s^{-1}$ from 20K upwards. This gives a rate coefficient for Reaction 603 of $3 \times 10^{-28}\ cm^6 s^{-1}$ at the temperature of Titan's lower atmosphere or an apparent

bimolecular rate coefficient of $6x10^{-10}$ cm^3s^{-1} at ~100 km above the surface. We have no reason to believe that the temperature dependence for Reaction 602 will be radically different from that for Reaction 603 above. Thus the formation of both N_3^+ and N_4^+ will be efficient at the temperatures and pressures corresponding to Titan's lower ionosphere. Figure 6.3 shows a model constructed by Anicich *et al.*[220] detailing the relative importance of termolecular association versus the major ion loss processes for the nitrogen ions. These loss processes for N^+ and N_2^+ are mainly electron recombination and bimolecular reaction with methane.

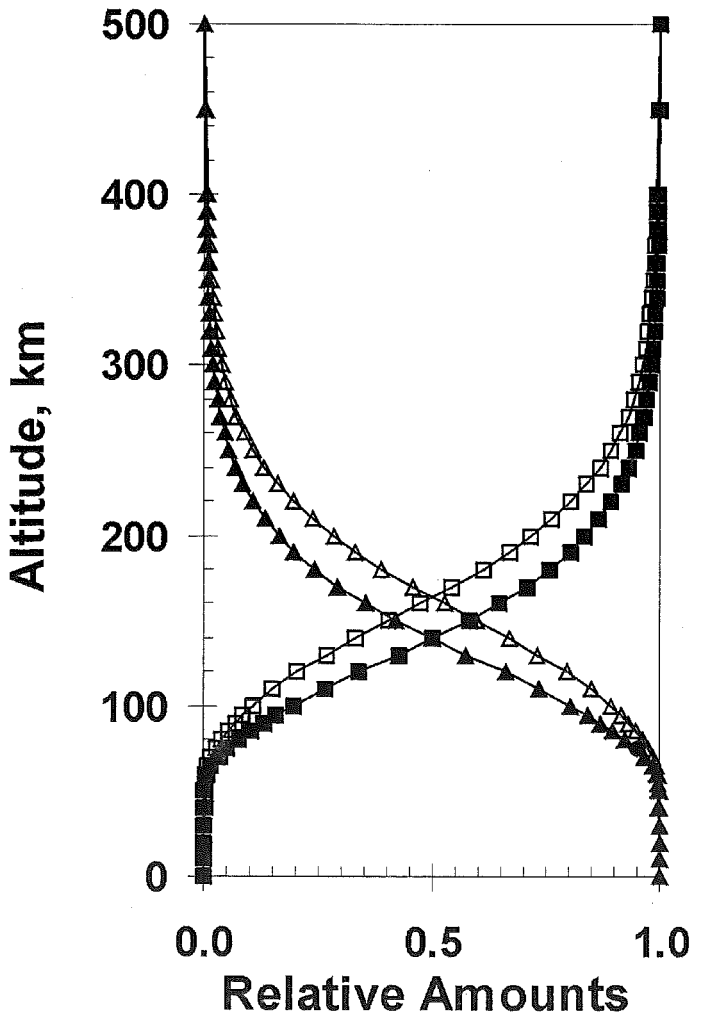

Figure 6.3: The relative importance of N^+ vs. N_3^+ and N_2^+ vs. N_4^+ with altitude in a model Titan atmosphere. The hollow squares represent N_2^+ and the hollow triangles N_4^+. Correspondingly the filled squares are N^+ and the filled triangles are N_3^+.

Another point of interest in the previous low temperature studies is the observation of the ions N_6^+ and N_8^+, i.e. higher cluster ions. The highest temperature total ion profile published by either of these authors is for 65K (from Bohringer and Arnold [219]), at which temperature. At this temperature, the N_6^+ ion may comprise as much as 25% of the total nitrogen ions. Although these higher cluster ions may also play a part in Titan's ion chemistry, they cannot easily be studied in the Canterbury FA-SIFDT. It might be expected that their reactivity should not be drastically different from that of the first cluster ion results that are reported here.

Taking into account all of the factors presented above, the reactions of N_3^+ and N_4^+ can be expected to have an effect on the ion-molecule chemistry occurring in Titan's lower ionosphere. Other formation processes e.g. Reaction 604 may also contribute to the atmospheric concentration of these ions [70].

$$N_2^+ + N + He \quad => \quad N_3^+ + He \qquad (604)$$

§6.2.2: Experimental.

Both the N_3^+ and N_4^+ ions were formed in the flowing afterglow ion source. The ions were generated from an afterglow plasma created by the action of a microwave discharge on a pure nitrogen carrier gas. The discharge forms N^+ and N_2^+ ions directly which then react with the nitrogen bath gas to subsequently form the N_3^+ and N_4^+ ions respectively. The carrier gas in the SIFT reaction tube was, as normal, helium and was usually present at 0.48 Torr. However all the reactions observed proceeded with purely bimolecular kinetics so the nature and pressure of the bath gas should be relatively unimportant. Throughout this section the reactions were performed at ambient temperature (295±5K). As all of the observed reactions are exothermic bimolecular reactions, the effects of temperature should be minimal. Bimolecular rate coefficients are usually temperature insensitive. However some reaction channels may be disfavoured at elevated temperatures [221] where large amounts of rearrangement are required to form the ionic products.

§6.2.3: N_3^+ Results and Discussion.

The reactions of both N_3^+ and N_4^+ were investigated with the significant minor hydrocarbon constituents of Titan's atmosphere, namely CH_4, C_2H_2 and C_2H_4 and also with HCN and 2-butene (C_4H_8). The results for N_3^+ are given in Table 6.2 along with the equivalent reactions of N^+ for comparison.

Neutral	Products			Reaction Rates		N^+ equivalent	
		B R [a]	$-\Delta H°$ [b]	k_{exp} [c]	K_{col} [d]	Products [e]	k_{lit} [f]
Methane	$HCNH^+ + H_2 + N_2$	0.95	481	0.058	1.1	$CH_3^+ + NH$ (0.50)	1.2
	$CH_2NH_2^+ + N_2$	0.05	682			$CH_4^+ + N$ (0.05)	
						$HCN^+ + H_2 + H$ (0.10)	
						$HCNH^+ + H_2$ (0.35)	
Acetylene	$CH_2CN^+ + N_2$	0.90	517	1.2	1.1	$C_2H_2^+ + N$ (0.70)	1.5
	$CNC^+ + H_2 + N_2$	0.05	121			$C_2N^+ + H_2$ (0.15)	
	$HCNH^+ + C + N_2$	0.05	68			$C_2NH^+ + H$ (0.15)	
Ethylene	$C_2H_4^+ + N + N_2$	1.00	15	1.1	1.2	$C_2H_2^+ + NH_2$ (0.10)	1.4
						$C_2H_3^+ + NH$ (0.25)	
						$C_2H_4^+ + N$ (0.35)	
						$HCN^+ + CH_3$ (0.10)	
						$HCNH^+ + CH_2$ (0.15)	
						$C_2HN^+ + H_2 + H$ (0.05)	
2-Butene	$C_4H_8^+ + N + N_2$	1.00	151	1.3	1.4	?[g]	1.8
Hydrogen Cyanide	$HCN_2^+ + N_2$	1.00	-	0.67	3.4	$CH^+ + N_2$ (0.35)	3.7
						$HCN^+ + N$ (0.65)	

Table 6.2 : The reactions of N_3^+ measured in the current study along with the corresponding N^+ reactions, where available, for comparison.

a) B R indicates the branching ratio of the reaction expressed as a fraction of the total ionic products when the neutral flow is extrapolated to zero.

b) The enthalpy of reaction in kJ mol^{-1}. The $\Delta H_f(N_3^+)$ is assumed to be 1502 kJ mol^{-1} [ref].

c) Experimental bimolecular rate coefficients expressed in units of 10^{-9} cm^3 s^{-1}.

d) Collision rate coefficients calculated by the method of Su and Chesnavich [114] for neutrals with a permanent dipole or Langevin collision theory. The units are identical to those used in c)

e) The products of the reaction between the neutral and N^+. Branching ratios are given in brackets. References primarily 1, 222 and 223.

f) Literature rate coefficients. The units are identical to those used in c). References as per e).

g) No literature data exists for this reaction and the products were not determined in the course of the current experiments.

Methane

In their laboratory study of the Earth's ionosphere Smith, Adams, and Miller have previously performed both the N^+ and N_3^+ reactions with methane [224]. In the Canterbury SIFT we have observed two products in Reaction 605.

$$N_3^+ + CH_4 \Rightarrow H_2CN^+ + N_2 + H_2 + 481 \text{ kJ mol}^{-1} \quad [0.95] \quad (605a)$$

$$\Rightarrow CH_2NH_2^+ + N_2 + 682 \text{ kJ mol}^{-1} \quad [0.05] \quad (605b)$$

$$k = 5.8 \times 10^{-11} \text{ cm}^3\text{s}^{-1}$$

This is in excellent agreement with Smith *et al.*, who saw the same two products with an identical branching ratio. Their rate coefficient of 4.8×10^{-11} cm^3s^{-1} is in acceptable agreement with our value. The exothermicities shown assume that the product ions have the $HCNH^+$ (605a) and $CH_2NH_2^+$ (605b) structures and further assume that ΔH_f for N_3^+ is 1502 kJ mol^{-1}. This value has been determined by Maclagan [225] at the G2 level of theory and is similar to the value for $\Delta H_f(N_3^+)$ of 1511 kJ mol^{-1} determined by Haynes et al. from the bond dissociation energy [217]. We assign the $m/z = 28$ product in Reaction 605a as $HCNH^+$ and not N_2^+ (formed by dissociation of the N_3^+ ion), as a reaction channel forming N_2^+ is endothermic.

Despite the fact that each individual channel is significantly exoergic the observed rate coefficient is much less than the Langevin collision rate of 1.1×10^{-9} cm^3s^{-1}. A smaller rate coefficient may be indicative of a barrier somewhere on the potential surface. This barrier may either be in the entrance channel, preventing the collision complex from forming effectively, or in the exit channel to products, making the back dissociation channel relatively more efficient.

By way of comparison, the reaction of N^+ with CH_4 produces four ionic products at a rate that is very close to the Langevin rate ($k_L = 1.4 \times 10^{-9}$ cm^3s^{-1}) as shown in Reaction 606 [1, 224, 226].

$$N^+ + CH_4 \Rightarrow CH_3^+ + NH + 330 \text{ kJ mol}^{-1} \quad [0.50] \quad (606a)$$

$$\Rightarrow HCNH^+ + H_2 + 854 \text{ kJ mol}^{-1} \quad [0.35] \quad (606b)$$

$$\Rightarrow HCN^+ + H_2 + H + 134 \text{ kJ mol}^{-1} \quad [0.10] \quad (606c)$$

$$\Rightarrow CH_4^+ + N + 197 \text{ kJ mol}^{-1} \quad [0.05] \quad (606d)$$

$$k = 1.15 \times 10^{-9} \text{ cm}^3\text{s}^{-1}$$

The extra 365 kJ mol^{-1} available from the N^+ reactant ion, as compared to the N_3^+, appears to change the chemistry radically here. Evidently the slower rate for the N_3^+

reaction is a result of a steric hindrance to reaction from the presence of the N_2 moiety, or, because channels that are exothermic for the N^+ case are no longer available in the N_3^+ encounter. Any barriers to specific channels may be greater in the N_3^+ case than the energy available from the reactants. The major channel observed in the N^+ reaction (hydrogen atom transfer, Reaction 606a) is endothermic for the N_3^+ reactant by 179 kJ mol^{-1} and charge transfer (reaction 606d) is also endothermic (by 42 kJ mol^{-1}). These changes are solely as a result of the lower ΔH_f for N_3^+ compared to ΔH_f for N^+ and this apparently leaves Reaction 605 with significantly fewer energetically available channels. There is some indirect evidence for an exit channel barrier to the formation of $HCNH^+$. Reaction 606b represents only approximately one third of the collision rate ($k_{606b} = 4 \times 10^{-10}$ cm^3s^{-1}) despite being the most exothermic channel. The equivalent channel in the N_3^+ case is approximately seven times slower ($k_{605a} = 5.5 \times 10^{-11}$ cm^3s^{-1}) indicating that the slow rate is not primarily due to excess energy but, more probably, a lack of it in Reaction 605.

Ethylene

Here a single product is observed for the N_3^+ reaction, non-dissociative charge transfer occuring at a rate that is close to the Langevin rate ($k = 1.1 \times 10^{-9}$ cm^3s^{-1}). The nature of the product was confirmed by the use of deuterated ethylene as the $m/z = 28$ product could again conceivably be N_2^+ formed by dissociation of the N_3^+ ion.

In the corresponding N^+ reaction six products are formed as shown in Reaction 607 [222, 227].

$N^+ + C_2H_4$ => $C_2H_3^+ + NH + 437$ kJ mol^{-1} [0.30] (607a)

=> $C_2H_4^+ + N + 388$ kJ mol^{-1} [0.25] (607b)

=> $HCN^+ + CH_3 + 333$ kJ mol^{-1} [0.15] (607c)

=> $C_2H_2^+ + NH_2 + 412$ kJ mol^{-1} [0.10] (607d)

=> $HCNH^+ + CH_2 + 592$ kJ mol^{-1} [0.10] (607e)

=> $CH_2CN^+ + H_2 + 839$ kJ mol^{-1} [0.10] (607f)

Again it appears that the extra energy available from the N^+ ion opens several new channels although only channel 607c is actually endothermic for N_3^+. In this case, unlike the methane reaction above, the lesser energy, or greater steric hindrance, available for N_3^+ does not appear to reduce the rate coefficient to any extent.

Acetylene

The primary channel in this reaction (CH_2CN^+ formation) introduces a nitrogen atom into the product ion, a process that occurs in several of the N_3^+ reactions. The minor ionic products of reaction, C_2N^+ and $HCNH^+$, have also had a nitrogen atom introduced.

The reaction exothermicities in Table 6.3 assume that the C_2N^+ product has the more stable CNC^+ structure, which is equivalent to insertion of a nitrogen atom into the triple bond. The $CC{\equiv}N^+$ ion is also energetically possible but is exothermic by only 15 kJ mol^{-1}. This product ion would result from end-on attack on the acetylene and for it to be the observed structure, there would need to be a barrier preventing rearrangement to the more stable CNC^+ structure. However, as the reaction channel is only slightly exothermic this barrier would not need to be very large.

The reaction of N^+ with acetylene [222] gives only one of the same products as N_3^+ (see Reaction 608). The primary product for Reaction 608 is charge transfer. This charge transfer product channel is 71 kJ mol^{-1} endothermic from N_3^+.

$$N^+ + C_2H_2 \Rightarrow C_2H_2^+ + N + 302 \text{ kJ mol}^{-1} \quad [0.70] \quad (608a)$$

$$\Rightarrow CHCN^+ + H + 354 \text{ kJ mol}^{-1} \quad [0.15] \quad (608b)$$

$$\Rightarrow CNC^+ + H_2 + 484 \text{ kJ mol}^{-1} \quad [0.15] \quad (608c)$$

The CH_2CN^+ product formed in the N_3^+ reaction is apparently stabilised by the molecular nitrogen fragment emitted by the N_3^+ ion. This neutral species can carry off some of the reaction exothermicity as translational energy and thus prevent the product from dissociating further. In a sense clusters (which N_3^+ can loosely be classed as) carry their own third body for association. When, as in the N^+ reaction, the nitrogen molecule is not available, a hydrogen atom is split off the complex in order to carry the excess energy away (Reaction 608b).

Hydrogen Cyanide

The reaction of N_3^+ with hydrogen cyanide yields a somewhat unusual product, HCN_2^+, that has not previously been reported in the literature.

$$N_3^+ + HCN \Rightarrow HCN_2^+ + N_2 \quad (609)$$

The corresponding reaction with N^+ very efficiently forms HCN^+, a process that is not energetically possible for an N_3^+ reactant ion (approximately 275 kJ mol^{-1} endothermic). Recent investigations of the N^+ and HCN reaction have also found a

CH^+ product, representing approximately 35% of the product ions [222]. This product was not observed in the N_3^+ reaction despite being 12 kJ mol^{-1} exothermic.

The structure of the *m/z* 41 product formed in Reaction 609 is unknown but it could conceivably be of an azide-type structure. This raises the possibility that novel trace molecules could be formed in the lower regions of Titan's ionosphere. It is perhaps unsurprising that such a product is not observed in the N^+ case as this reaction course would be equivalent to association. This association, though it is certainly energetically possible from N^+, will be disfavoured when other facile, bimolecular, channels are available unless the HCN_2^+ ion is very stable.

An upper limit can be placed on the value of ΔH_f for HCN_2^+ from the occurrence of Reaction 609. It must be less than 1642 kJ mol^{-1} as the HCN_2^+ product is apparently stable and formed efficiently.

2-Butene (C_4H_8)

This is a very simple reaction, the only product observed, charge transfer, is formed at the collision rate. The reaction with atomic nitrogen ions has not been previously examined for this neutral so an attempt was made to measure it. The rate coefficient was determined to be 1.8×10^{-9} $cm^3 s^{-1}$ but large amounts of impurity ions formed in the reaction flow tube (NO^+, H_2O^+, H_3O^+) prevented an accurate determination of the products or their branching ratio. Charge transfer is still apparently a product though it appears that the main product is at *m/z* = 41. This is likely to be $C_3H_5^+$, which corresponds to the loss of a methyl radical. There may also be a channel at *m/z* = 55 which can represent the formation of $C_2H_5CN^+$ (see the section on the N_4^+/2-butene reaction for further discussion on this ion product).

§6.2.4: N_4^+ Results and Discussion.

Results are given in Table 6.3 for the reactions of N_4^+ with the possible neutral species in Titan's atmosphere investigated during this section of work. Also included for comparison are the same reactions where the N_4^+ ions are replaced by the N_2^+ species.

Neutral	Products			Reaction Rates		N_2^+ equivalent[e]	
		B R [a]	-ΔH° [b]	k_{exp} [c]	k_L [d]	Products[f]	k_{lit} [g]
Methane	$CH_4^+ + 2N_2$	1.0		1.1	1.1	$CH_2^+ + H_2 + N_2$ (0.05) $CH_3^+ + H + N_2$ (0.80) $N_2H^+ + CH_3$ (0.15)	1.1
Acetylene	$C_2H_2^+ + 2N_2$	1.0		0.92	1.1	$C_2H_2^+ + N_2$ (0.35) $HCN^+ + CH$ (0.05) $N_2H^+ + C_2H$ (0.60)	0.4
Ethylene	$C_2H_4^+ + 2N_2$	1.00		~1.1	1.1	$C_2H_2^+ + H_2 + N_2$ (0.20) $C_2H_3^+ + H + N_2$ (0.50) $HCN^+ + HCN + H_2$(0.10) $HCNH^+ + HCN+H$(0.10) $N_2H^+ + C_2H_3$ (0.10)	1.3
2-Butene	$C_4H_8^+ + 2N_2$ $C_3H_5^+ + CH_3 + 2N_2$	? ?		~1.1	1.3	$C_3H_3^+ + CH_3 + H_2 + N_2$ (0.55) $C_3H_5^+ + CH_3 + N_2$ (0.35) $C_3H_5N^+ + CH_2NH_2$ (0.10)	1.3
Hydrogen Cyanide	$HCN^+ + 2N_2$	1.00		2.6	3.2	$HCN^+ + N_2$ (1.0)	0.4

Table 6.3: The reactions of N_4^+ measured in the current study along with a comparison to the equivalent N_2^+ reactions where available.

a) B R indicates the branching ratio of the reaction expressed as a fraction of the total ionic products when the neutral flow is extrapolated to zero.

b) The enthalpy of reaction in kJ mol^{-1}. The $\Delta H_f(N_4^+)$ is assumed to be 1243 kJ mol^{-1} [ref].

c) Experimental bimolecular rate coefficients expressed in units of $1x10^{-9}$ cm^3 s^{-1}.

d) Collision rates calculated by the method of Su and Chesnavich [114]. The units are identical to those used in c) (See footnote in previous table about Langevin rates. This should be the same)

e) Rate coefficients, products, and branching ratios taken from the literature, primarily 1, 222 and 223.

f) The products of the reaction between the neutral and N_2^+. Branching ratios are given in brackets. References as per e).

g) Literature rate coefficients. The units are identical to those used in c). References as per e).

The reaction enthalpies presented in Table 6.3 are subject to question as there is debate in the literature as to structure of N_4^+. Two different structures have been

postulated: a linear structure; and a slightly non-planar Z-shaped structure. Both of these structures are shown in Figure 6.4.

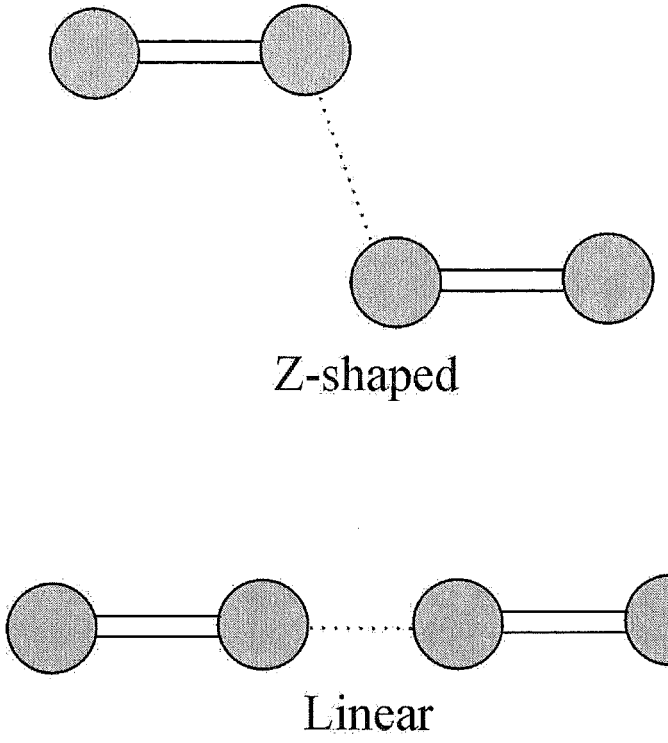

Figure 6.4: The two possible structures of the N_4^+ ion.

The difference between the enthalpies of formation for N_2^+ and N_4^+ is 260 kJ mol^{-1} for Z-shaped N_4^+ and 114 kJ mol^{-1} for the linear isomer, with N_4^+ always being the lower energy ion. At Hartree-Fock (HF) level the most stable N_4^+ structure is the linear form [228, 229], but when Moller-Plesset 4 (MP4) level calculations are performed the Z-shaped structure becomes the minimum [228]. Experimental results are inconclusive but do not strongly support a Z-shaped minimum. Experimental determinations of the binding energy produce values ranging from 48 to 103 kJ mol^{-1} [228], however it appears likely that a value between 100 and 120 kJ mol^{-1} is reasonable [230]. The HF optimised linear structure has a binding energy of approximately 120 kJ mol^{-1} [229] while the calculation by Maclagan [225] gives a dissociation energy of 111 kJ mol^{-1} at G2 level. In comparison the Z-shaped structure has a dissociation energy of 258 kJ mol^{-1}, also at the G2 level of theory. This suggests that the linear structure approximates the experimental results more closely despite the Z-shaped structure being the minimum. Low temperature electron spin resonance (ESR) investigations [231] of the structure of the ions formed in an ionised flow of nitrogen gas also suggest that the linear structure

is correct. The N_4^+ ions studied were trapped in an argon matrix on a copper target at 4K and should have retained their original structure. Further experimental work is needed to resolve this disagreement however as the possibility of a Z-shaped structure was not considered in any of the experimental investigations.

Methane

The product of the reaction between N_4^+ and methane is simple charge transfer, this reaction occurs at close to the collision rate (k_{coll} = 1.07x10^{-9} cm^{3}s^{-1}). The corresponding reaction of molecular nitrogen ions proceeds at a very similar rate but the products are quite different (Reaction 610) [222, 226].

$N_2^+ + CH_4$ => $CH_3^+ + H + N_2 + 117$ kJ mol^{-1} [0.80] (610a)

=> $N_2H^+ + CH_3 + 246$ kJ mol^{-1} [0.15] (610b)

=> $CH_2^+ + H_2 + N_2 + 43$ kJ mol^{-1} [0.10] (610c)

None of these dissociative channels are available to the N_4^+ ion if it is the Z-shaped isomer. For the linear structure the equivalent of channel 610a is 3 kJmol^{-1} exothermic and channel b is also exothermic, by 132 kJmol^{-1}. Channel 610c is still endothermic (by 71 kJmol^{-1}).

Ethylene

As with the methane reaction, the product from the reaction of N_4^+ with ethylene is solely the ionised hydrocarbon, formed at a rate approximating the collision rate. The rate shown in Table 6.3 is only approximate as there is a peak overlap between the reactant ion (N_4^+ *m/z* = 56) and a secondary product ion ($C_4H_7^+$ *m/z* = 55). However the reaction with deuterated ethylene, which alleviates this problem, has a very similar rate coefficient (1.1x10^{-9} cm^{3}s^{-1}) indicating that the rate coefficient for the non-deuterated case is acceptably accurate. The deuterated reaction also confirms the nature of the product, as a *m/z* = 32 ion is observed which can only be $C_2D_4^+$. The product observed in the non-deuterated reaction occurs at *m/z* = 28 which could also possibly be the protonated hydrogen cyanide ion which could be formed by Reaction 611. $HCNH^+$ formation is endothermic if one assumes the Z-shaped N_4^+ structure but only just. For a linear N_4^+ reactant the channel is 146 kJ mol^{-1} exothermic.

$N_4^+ + C_2H_4$ => $HCNH^+ + HCN + H + N_2 - 4$ kJ mol^{-1} (611)

The lack of a $HCNH^+$ product gives some support for a Z-shaped structure, but this is far from a conclusive result.

Again the N_2^+ reaction proceeds at a similar rate but in a more dissociative manner producing 5 products [223], $C_2H_3^+ + N_2 + H$ [0.50], $C_2H_2^+ + N_2 + H_2$ [0.20], $HNC^+ + HCN + H_2$ [0.10], $HCNH^+ + HCN + H$ [0.10], $N_2H^+ + C_2H_3$ [0.10]. The $HCNH^+$ product could also be $C_2H_4^+$ as these products are isobaric and both energetically allowed.

Acetylene

The acetylene reaction is yet another case of an efficient charge transfer reaction from N_4^+. The N_2^+ reaction [222] is again more complex with hydrogen atom transfer being the predominant product as shown in Reaction 612.

$$N_2^+ + C_2H_2 \Rightarrow N_2H^+ + C_2H + 210 \text{ kJ mol}^{-1} \quad [0.60] \quad (612a)$$

$$\Rightarrow C_2H_2^+ + N_2 + 403 \text{ kJ mol}^{-1} \quad [0.37] \quad (612b)$$

$$\Rightarrow HCN^+ + HCN + 147 \text{ kJ mol}^{-1} \quad [0.03] \quad (612c)$$

Hydrogen Cyanide

The only difference observed between the reactions of N_2^+ and N_4^+ with hydrogen cyanide is an enhancement in the rate of the formation of the HCN product for the reaction of N_4^+ ($k=2.6\times10^{-9}$ cm^3s^{-1}) as compared to that of N_2^+ ($k= 3.9\times10^{-10}$ cm^3s^{-1}). The product, in each case, is simply charge transfer. The observed rise in rate coefficient is contrary to the change in the collision rate, which is lowered for the N_4^+ ion due to its increased mass.

2-Butene (C_4H_8)

The reaction of N_4^+ with 2-butene is the only N_4^+ reaction for which we observed a product other than charge transfer. Here dissociative charge transfer causes the loss of a methyl radical giving $C_3H_5^+$ as an ionic product. The exact rate coefficient and product branching ratios for this reaction could not be determined due to a mass coincidence between $C_4H_8^+$ and N_4^+, the rate coefficient however is approximately 1.1×10^{-9} cm^3s^{-1}, which is close to the Langevin rate.

As there have been no previous investigations of the reaction of N_2^+ with 2-butene and so it has been examined in the course of this work. The rate coefficient

was found to be $1.3x10^{-9}$ cm^3s^{-1}, marginally greater that that determined for the reaction of N_4^+ with the same neutral, entirely consistent with theory. The products of the reaction are shown below (Reaction 613).

$N_2^+ + C_4H_8$	=>	$C_3H_3^+ + CH_3 + H_2 + N_2$	[0.50]	(613a)
		$C_3H_5^+ + CH_3 + N_2$	[0.35]	(613b)
		$C_3H_3N^+ + CH_3NH_2$	[0.10]	(613c)
		$C_3H_5N^+ + CH_2NH$	[0.05]	(613d)

These products are partially consistent with expectations, channel 613b was observed with N_4^+ and 613a is essentially a more dissociative form of this same channel. Apparently all charge transfer is now dissociative to give one of these products (613a and b), unlike the N_4^+ reaction where non-dissociative charge transfer is observed. Channels 613c and 613d are quite different to any channel observed with N_4^+. The $C_4H_8^+$ ion product was identified from curvature in the N_4^+ decay, but no evidence for a $m/z = 53$ or 55 product is seen in any of the mass spectra taken during the investigation of the N_4^+ reaction. The product of Reaction 613d may be ethyl cyanide ($C_4H_7^+$ is another possibility) and that of 613c may be acrylonitrile. However a large H_3O^+ impurity was observed when this reaction was being studied so these ions may be the result of protonation (i.e. $C_4H_5^+$ and $C_4H_7^+$ for channels c and d respectively).

Section 6.3: Some implications of the formation of N_3^+ and N_4^+ for the ion-molecule chemistry occurring in Titan's lower ionosphere.

The relevance of the reactions of N_3^+ and N_4^+ in Titan's lower ionosphere is dependent on two factors: the relative densities of N_3^+ and N_4^+ (and higher nitrogen cluster ions) as compared to the non-clustered ions, and the differences in reactivity between the clustered and non-clustered ions. The latter has been highlighted in the previous sections but the implications for the major ion-molecule reaction channels occurring in the ionosphere of Titan will be discussed in this section.

As was discussed in §6.2, the formation of the clustered ions is highly altitude dependent. The deeper into the atmosphere one moves, the more efficient the termolecular formation reactions become and hence the greater influence the clustered ions will have. These ions will exert no great influence on the upper, photon-induced, ionosphere as the pressure at the altitude of this ionosphere (~1050 km) is too low for their formation to be competitive. Figure 6.3 shows the altitude profile of the relative amounts of atomic and molecular nitrogen ions and their respective first clusters with nitrogen (i.e. N_3^+ and N_4^+). This model can be compared with the ion production models of Molina-Cuberos *et al.* [202] and Capone *et al.* [200] to show that at the peak of the ion and electron densities for the lower, cosmic-ray induced, ionosphere (around 100 km) the N_3^+ and N_4^+ ions will predominate over N^+ and N_2^+. Below this altitude one can expect higher clusters to become even more important as the pressure steadily increases and the temperature drops rapidly. The temperature falls from ~140K at 100 km to ~70K at the second thermopause (around 45 km above Titan's surface). This is the minimum temperature experienced in the whole of Titan's atmosphere. Hence the relative amounts of N_3^+ and N_4^+ are enough for them to influence the ion chemistry in the lower ionosphere, but are differences in their ion chemistry sufficient to alter the types of ions that will be present in Titan's lower atmosphere?

The most obvious differences in the ion chemistry are that both of the clustered ion species, N_3^+ and N_4^+, react in a less dissociative manner than do their non-clustered counterparts, N^+ and N_2^+. The N_3^+ ion is also more effective at inserting a nitrogen atom into the ionic products than is N^+. The two families of nitrogen ions will now be dealt with separately. A model incorporating some of this type of ion-molecule chemistry may be found in the work of Molina-Cuberos *et al.* [202]. However this model includes only the reactions of N_3^+ and N_4^+ with methane and not any of the more minor hydrocarbon components of Titan's atmosphere which are included in the experimental section of this study. Unlike these previous mathematical models the following discussion is purely qualitative.

The major ion chemistry of these N_n^+ ions is going to be influenced by what neutral species are present that the ion reacts rapidly with. In the upper atmosphere of Titan, the reaction of N^+ with methane is one of the more important reactions. Two major channels are available forming either CH_3^+ or a cyanide-containing cation (either $HCNH^+$ or HCN^+) in approximately equal fractions. These ions in turn lead (by

a series of further ion-molecule reactions) to the formation primarily of $C_3H_5^+$ ions and the formation of protonated cyanopolyynes. The reaction of N_3^+ with CH_4 however almost exclusively leads to $HCNH^+$ which, at the higher pressures associated with N_3^+ formation, can associate efficiently with C_2H_2 or C_2H_4 (see section 6.4 for further details). Alternatively the $HCNH^+$ ion can protonate certain molecules (those with higher PA than HCN). Chief among these molecules are water and the nitriles (e.g. CH_3CN or HC_3N). The subsequent reactions of these protonated species will, at low altitudes, be characterised by association reactions mainly with acetylene and ethylene. These association reactions can rapidly build up larger, more complex, molecules.

The reactions of N_3^+ with C_2H_2 and C_2H_4, while less important due to the lower mixing ratio of these neutral species, will also be important. The reactions of N_3^+ with acetylene will contribute further to the increase in nitrogen-containing species, producing nitrile ions. This is in contrast to the $N^+ + C_2H_2$ reaction (Reaction 608) which occurs at higher altitudes and produces ions that will result in higher hydrocarbon species. The reaction of N_3^+ with C_2H_4 produces $C_2H_4^+$, which can either undergo termolecular reactions (associating effectively with C_2H_4 [2] and less effectively with CH_4 [201, 222]) or bimolecular reactions (with certain species like cyanoacetylene (Reaction 614)).

$$C_2H_4^+ + HC_3N \Rightarrow H_2C_3N^+ + C_2H_3 \quad [0.85] \quad (614a)$$

$$\Rightarrow H_4C_5N^+ + H \quad [0.15] \quad (614b)$$

At higher altitudes, the reaction of N^+ with C_2H_4 (Reaction 607) not only produces $C_2H_4^+$ but also produces $C_2H_3^+$ (which is converted to higher hydrocarbons) and nitriles (whose chemistry is explained above). Thus it can be seen that N_3^+ has the effect of enhancing nitrile chemistry and producing products that are amenable to association reactions.

The reactions of N_4^+ lead almost exclusively to charge transfer, which reduces somewhat the amount of nitrogen-containing ions when compared to the reaction chemistry at higher altitudes. Instead, most of the reactions of N_4^+ investigated here will ultimately produce the $C_3H_5^+$ ion, which will then associate with acetylene molecules in a stepwise manner to form $C_5H_5^+$, $C_7H_7^+$ and higher hydrocarbons [222]. As an example, when N_4^+ reacts with methane CH_4^+ is first formed. CH_4^+ then reacts with a further CH_4 molecule to give CH_5^+, which can protonate many of the species with

lower number densities which will finally lead mainly to $C_3H_5^+$. A diverse range of other, minor, hydrocarbon ions will also be formed. In this respect the change from N_2^+ to N_4^+ does not affect the initial products much. However due to the increased amounts of association that will occur in the regions where N_4^+ is formed, larger hydrocarbon species will be created.

The CH_5^+ intermediate in the processes outlined above can also be lost by forming a cluster with CH_4 or N_2, albeit very slowly. This cluster will form predominantly in the region from 60 km down where the temperature is low and the pressure high. In this region the amounts of most neutral species are much reduced as they begin to 'freeze out' and this will further enhance cluster formation as there is less CH_5^+ loss [185]. The reactions of the $CH_5^+.CH_4$ species have not been modelled in the current literature models. As this cluster is very weakly bound (the termolecular formation rate coefficient at 300K is approximately 8×10^{-30} cm^6s^{-1} [221]) the presence of another neutral methane molecule on the ion may not affect the reactivity of the cluster significantly. By way of comparison note that in all cases where a reaction occurred with N^+ or N_2^+, a reaction was also observed for N_3^+ or N_4^+ respectively (albeit giving different products). Thus Reaction 615 should occur as its counterpart Reaction 616 is observed to proceed at almost collision rate. The fraction of CO is 500 times less than that of CH_4 but HCO^+ is a terminal ion at these altitudes whereas $CH_5^+.CH_4$ is not.

$$CH_5^+.CH_4 + CO \Rightarrow HCO^+ + 2CH_4 \quad (615)$$

$$CH_5^+ + CO \Rightarrow HCO^+ + CH_4 \quad (616)$$

$k = 9.9 \times 10^{-10}$ cm^3s^{-1}.

The fraction of CO in the atmosphere will be less drastically affected by the temperature change in Titan's lower atmosphere as it is still gaseous at the minimum temperature experienced in Titan's atmosphere.

Section 6.4: Termolecular Associations in Nitrogen; Relevance to Titan's Atmosphere.

§6.4.1: Models of Titan's Ionosphere.

Most of the models of Titan's ionosphere deal with the region around 1050 km above the surface. It is at this point that the electron density and ion density are greatest in Titan's atmosphere, as was shown by the Voyager 1 observations. The overall pressure in this region is well below 1 milliTorr (number density ~$1x10^8$ cm^{-3}) and thus bimolecular kinetics will dominate. However, in the region much lower in the atmosphere (below around 350 km above Titan's surface) there is a significant amount of cosmic ray ionisation. In this lower region the influence of termolecular reactions will become much greater and may even compete with bimolecular reactions. When the reactant ion does not undergo any significant bimolecular reaction (the so-called "terminal" ions in the ionosphere) then termolecular reaction loss of these ions needs to be considered. It was with this in mind that an investigation of the termolecular kinetics for the association reactions of $HCNH^+$, H_3O^+, and cyclic-$C_3H_3^+$ with the principal neutrals N_2, C_2H_2, C_2H_4 and CH_4 was carried out in the Canterbury FA-SIFDT.

The majority of these reactions have previously been studied by Herbst and co-workers [232], however these reactions were performed in a helium bath gas. In most previous SIFT investigations of termolecular reactions, the nature of the bath gas has not been considered overly important due to the fact that these investigations were using the rates of termolecular association to model radiative association. In these cases only an indication of the lifetime of the initial collision complex is important. However, it is well known in the ICR community that the nature of the bath gas has a significant effect on the termolecular rate coefficient and relative stabilisation efficiencies, β_{rel}, are routinely measured. A survey of the literature [2] shows that termolecular rate coefficients measured in a nitrogen bath gas are between 1.5 and 5 times greater than the same coefficients measured in a helium bath gas. It was thus deemed prudent to perform a SIFT investigation of these rate coefficients in a nitrogen carrier.

§6.4.2: Experimental

The association reactions reported in the following sections were performed using the University of Canterbury FA-SIFDT instrument. The carrier gas in the SIFT reaction tube was either helium or nitrogen depending on the desired third body for the reaction under study. Instrument grade helium was used as usual, and the nitrogen gas used was New Zealand Industrial Gases zero grade, purified by passage through a dry ice/acetone cryo-trap.

All measurements were made at 295±5K and the pressure range was approximately 0.2 to 0.7 Torr for the rate coefficients measured in helium and 0.1 to 0.6 Torr for those measured in nitrogen. For both helium and nitrogen bath gasses the upper pressures in the range were obtained by 'throttling' the JVE blower pump by partially closing the 6" gate valve that isolates this pump from the reaction tube. In effect this is conductance limiting the speed of this blower pump and enables a higher pressure to be achieved without increasing the flow of carrier gas through the system.

The reactant ions were generated in the flowing afterglow by using either the moveable ioniser or an off-axis microwave discharge which included a Wood's Horn between the discharge proper and the FA flow tube (see §2.2.3). This was found to be necessary as any photons that entered the main flow tube when a nitrogen carrier was in use, created N_2^+ ions which interfered with the analysis of the system under study. $HCNH^+$ and H_3O^+ were made by admitting the non-protonated precursor into a plasma containing H_3^+ ions.

§6.4.3: Associations with Nitrogen.

To ascertain if any of the "terminal" ions associated with nitrogen at 300K and at pressures of approximately 0.5 Torr, these ions were simply injected into a nitrogen carrier gas and the association product searched for. This method should detect reactions that are much slower than is usually possible for the SIFT technique, down to an effective bimolecular rate coefficient of $1x10^{-15}$ cm^3s^{-1} or lower at carrier gas pressures of ~0.5 Torr. No association reactions for any of the ions H_3O^+, $HCNH^+$, or c-$C_3H_3^+$ were observed with N_2 at room temperature in our flow tube.

However, at least one of these reactions would appear to be likely to proceed under the conditions present in the lower region of Titan's atmosphere. The group of Speller and Fitaire have produced several papers over the years detailing the products of α-particle irradiation or DC discharge on nitrogen/methane mixtures. These experiments have been performed at low temperatures (140-290K) and high pressures (20-80 Torr) and a range of $HCNH^+.nN_2$ clusters (where n =1-6) [233, 234] have been observed. Experiments have also been performed observing the clustering rates of several "impurities" added to simulate the atmosphere of Titan more closely (namely acetylene, and methane [233, 234, 235]). In these experiments switching reactions as well as clustering reactions have been observed. Only the equilibrium constants for the various reactions have been determined. The equilibrium coefficient for Reaction 617 was approximately K_1=0.005 $Torr^{-1}$ at ambient temperature [234].

$$HCNH^+ + 2N_2 \quad => \quad HCNH^+.N_2 + N_2 \qquad (617)$$

Where $$K_1 = \frac{I(HCNH^+.N_2)}{I(HCNH^+).P(N_2)} \qquad (6.1).$$

As the pressures in the current study are less than 1 Torr (~0.5 Torr) one could reasonably expect the ratio $HCNH^+.N_2$: $HCNH^+$ to be well less than 0.0025:1 giving at most ~20 cps at the signal levels used. Speller, Fitaire, and Pointu also found the hydrogen cyanide nitrogen cluster to be very weakly bound (31.8 kJ mol^{-1} [234]), and noted that there may be dissociation upon sampling. This will further decrease the likelihood of observing this cluster ion with nitrogen in the present experiments.

The observations of Speller and Fitaire do not suggest that we should have seen a clustering reaction between $HCNH^+$ and nitrogen and if anything back up our non-observation of this reaction at ambient temperature. However they do suggest that the chemistry in the lower atmosphere of Titan will be strongly influenced by clustering reactions with nitrogen. These may provide a mechanism for effectively building up larger mass ions but, due to the weakly bound nature of these clusters, they are unlikely to provide a method for building up large neutral molecules. Instead they are likely to continue to undergo clustering and switching reactions to produce higher clusters, much like the $H_3O^+.nH_2O$ clusters in the Earth's ionosphere [11, 205, 236]. However it is known that "switching" reactions, where one weakly bound solvating ligand is replaced by another more strongly bound one are efficient. In this manner the

formation of cluster ions may provide a mechanism for rapidly forming strongly bound (possibly even covalent) adducts in Titan's lower atmosphere.

§6.4.4 : Associations with small hydrocarbons.

The association reactions of c-$C_3H_3^+$, H_3O^+, and $HCNH^+$ with CH_4, C_2H_2 and C_2H_4 were investigated using both nitrogen and helium as the buffer gas. No reaction of any kind was observed for the c-$C_3H_3^+$ ion with all three of the listed neutrals or for the other two ions when methane was the neutral reactant. c-$C_3H_3^+$ is thus still a true "terminal" ion, as no reaction, even with minor constituents of Titan's atmosphere, has yet been found. The experimental results for this section are shown below in Table 6.4.

Neutral Reactant	Carrier Gas	H_3O^+	$HCNH^+$	c-$C_3H_3^+$
CH_4	He	NR	NR	NR
	N_2	NR	NR	NR
C_2H_2	He	$7x10^{-28}$	$6x10^{-29}$	NR
	N_2	$\sim 9x10^{-27}$	$4x10^{-28}$	NR
C_2H_4	He	$2x10^{-27}$	$5x10^{-27}$	NR
	N_2	$2x10^{-26}$	$1x10^{-26}$	NR

Table 6.4: The experimentally determined termolecular rate coefficients in both helium and nitrogen carrier gases.

a) The rate coefficients reported here are termolecular rate coefficients for the enhancement of a given process by the presence of a third stabilising body. Units are cm^6s^{-1}.

b) NR means no reaction and implies that no product was seen. This places an upper limit of appromimately $3x10^{-29}$ cm^6s^{-1} on the process.

The termolecular rate coefficients in a nitrogen carrier are between 3 and 13 times faster than for the corresponding reactions in a helium carrier. By comparison with the termolecular rate coefficients previously investigated in both a helium and nitrogen carrier, these current results show a greater increase in efficiency in N_2 when compared with helium. Previous values (predominantly measured for atmospheric reactions such as $NO^+ + H_2O$, $NO^+ + CO_2$, $O_2^+ + O_2$, and $N^+ + N_2$) [2] show and

enhancement in N_2 over He of between 1.5 and 5. It should be noted however that the complexity of the previous systems (i.e. the number of atoms) was usually less. There is not enough literature data to allow a valid comparison to be made between the current data and an average effect for the transition from a helium to a nitrogen bath gas.

H_3O^+ and C_2H_2, C_2H_4..

The amounts of water vapour present in Titan's atmosphere are not accurately known but they are lower than a part per billion in the stratosphere [180]. The model of Yung *et al.* predicts that it should be a minor constituent [182]. If this is the case then a certain amount of H_3O^+ should be found in the ionosphere of Titan. However H_3O^+ does not have any rapid bimolecular reactions with the major neutral constituents of Titan's atmosphere. As a result its association reactions could be influential to the overall ion-molecule chemistry. In both this case and for the $HCNH^+$ reactions, Herbst *et al.* [232] have previously obtained temperature-dependent association rate coefficients for the termolecular reactions with ethylene and acetylene. Fairley and co-workers have also studied the reactions of H_3O^+ with acetylene [237] and ethylene [238] and have performed reaction studies to determine the nature of the products. Matthews *et al.* [239] have also investigated the H_3O^+/C_2H_4 reaction and the $C_2H_7O^+$ isomers generally.

In the reaction of H_3O^+ with acetylene (Reaction 618) Herbst *et al.* [232] found an association rate coefficient (with helium) of 8×10^{-28} cm^6s^{-1} at 300K with a temperature dependence of the form $(300/T)^{3.2}$. This is in excellent agreement with the rate coefficient determined in the current study of 7×10^{-28} cm^6s^{-1} at 300K in a helium carrier.

$$H_3O^+ + C_2H_2 + M \quad => \quad H_3O^+.C_2H_2 + M \qquad (618)$$

The rate in a nitrogen carrier is more than an order of magnitude faster at $\sim 9 \times 10^{-27}$ cm^6s^{-1}. However this rate coefficient is only an approximate as problems were encountered in getting an accurate rate coefficient at lower pressures (<0.45 Torr). The semi-logarithmic plots of H_3O^+ count against C_2H_2 flow at these lower pressures were consistently curved. The rate coefficients obtained at the higher pressures suggested that the initial rates obtained from these curved plots (i.e. the rate of decay at very low flow of acetylene) were the more correct and it is these that have been

used in the determination of the termolecular rate coefficient. The reason for this curvature has not been conclusively determined but it appears that it is present because the H_3O^+ signal is being regenerated at higher flows. There is no possibility of isomerisation at $m/z = 19$, so the only other possibilities are that an excited H_3O^+ reactant ion, most probably vibrationally excited, is present or alternatively that the $H_3O^+.C_2H_2$ product is very weakly bound and breaks up upon sampling. Several factors count against the hypothesis that the reactant ion is excited. Firstly, the problem does not occur in a helium carrier. One could reasonably expect N_2 to be more effective at quenching vibrational excitation (due to the greater mass and the fact that it can itself carry vibrational energy). Second, when the H_3O^+ ion was generated using low energy proton transfer to water (from HCO^+ and HCS_2^+) the problem was still present. Further, the voltages on the downstream lenses were reduced to almost zero, with no decrease in the amount of curvature being observed. This suggests that the product ion is not being dissociated upon sampling. In addition an unknown ion at 57 amu was always observed which appeared to react, at least partly, with the increasing flows of acetylene. This ion could possibly be $N_2H^+.N_2$ which would transfer a proton at the collision rate to any water in the carrier or the reactant gas. As the rate coefficients for these association processes are very low a small water impurity in the reactant gas could affect the outcome markedly. It seems likely that some of the energy received by the H_3O^+ ion upon injection is being used to drive the endothermic proton transfer from H_3O^+ to N_2 (endothermic by 210 kJ mol^{-1}). The product of this then associates with a nitrogen molecule to give the observed 57 amu ion. Essentially the vibrational excitation in the H_3O^+ ion, which is being quenched in a helium carrier, is being trapped in a chemical bond in the nitrogen carrier gas (as N_2H^+) and is being transmitted to the reaction region in this form.

In previous investigations of this reaction in our laboratory Fairley and co-workers looked at the nature of the products from Reaction 618 [237]. They found that 2 isomers were present. One that represented up to 75% of the total product signal was found to react rapidly with ethyl bromide, benzene and 4-fluorotoluene. The other 25% isomer showed a much slower reaction with these neutrals. The identity of these two isomers is not completely certain, however it seems likely that the faster reacting component in the product signal (the "$H_3O^+.C_2H_2$" ion) is in fact protonated vinyl

alcohol ($CH_2CHOH_2^+$), while the slower reacting portion is then identified as the electrostatic complex. An alternative interpretation of the experiment is that the larger fraction of the product (the faster reacting isomer) is the electrostatic complex in which case the smaller component is likely to be protonated acetaldehyde (or protonated oxirane, though this latter interpretation is less likely). This second hypothesis is not supported by the results of ab initio calculations which did not find an interconversion route between the initial collision complex (in effect the electrostatic complex) and either of the possible products. A conclusive determination of the nature of these products was hampered by an inability to create the protonated vinyl alcohol ion in the flow tube in order to perform comparative reaction studies.

Nevertheless, Reaction 618 represents an efficient pathway leading to the rapid build-up of more complex molecules in Titan's lower atmosphere where the stabilising influence of the low temperature and relatively high nitrogen pressures will combine to give a relatively high overall rate. At an altitude of 100 km with the temperature at 140 K and the pressure at ~10 Torr the apparent bimolecular rate coefficient should be approximately collision rate.

The association between H_3O^+ and ethylene occurs in concert with the slightly endothermic proton transfer which gives $C_2H_5^+$. Both ab initio and experimental studies by Fairley *et al.* [238] have shown that the association product in this case is $C_2H_5OH_2^+$, protonated ethanol.

$HCNH^+ + C_2H_2$, C_2H_4.

$HCNH^+$ was observed to associate slowly with both ethylene and acetylene. Herbst and co-workers [232] have previously performed a study of the temperature dependent termolecular rate for both of these reaction using helium as the bath gas in a SIFT. For the *acetylene* case (Reaction 619) they report an ambient temperature association rate of 5×10^{-29} cm^6s^{-1} when M = He. Their temperature dependence takes the form of $k_3 = 5 \times 10^{-29} (300/T)^3$ cm^6s^{-1}.

$$HCNH^+ + C_2H_2 + M \Rightarrow HCNH^+.C_2H_2 + M \qquad (619)$$

The structure of this association product is unknown, however Herbst *et al.* argue that it is unlikely to be protonated acrylonitrile, CH_2CHCNH^+, on the grounds that Reaction 619 proceeds much more slowly than the association rate they calculate

for a protonated acrylonitrile product. By comparing the experimental H_3O^+ and $HCNH^+$ association rates and product identification from the work of both Herbst *et al.* and Fairley with the theoretical rates of Herbst *et al.*, one can begin to draw some conclusions about the likely nature of the adduct products in these systems. In the case of H_3O^+ and ethylene the product is entirely covalent in nature the experimental rate is almost 3 times *greater* than the theoretical rate. For the $H_3O^+ + C_2H_2$ reaction there is almost certainly some covalent association occurring in the reaction, although the amount of this and its structure is still uncertain. In this case the experimental rate coefficient is a factor of 125 *less* than the calculated one. For reaction 619 the experimental rate, as measured both by Herbst and our latest results is approximately 4000 times slower than theory predicts based on the premise that the association product formed is CH_2CHCNH^+. This discrepancy is strongly indicative of an electrostatic or other very weakly bound product ion being formed in this association.

Some preliminary attempts were made to confirm the nature of these association products experimentally. In these experiments $HCNH^+$ was formed in the FA (from HCN in a hydrogen carrier) and then injected into the SIFT reaction flow tube. At the first neutral inlet a high flow of acetylene was introduced, converting approximately half of the $HCNH^+$ to the adduct ($C_3H_4N^+$) having the unknown structural form. Another neutral reagent gas was then introduced into the flow tube at the downstream neutral inlet in order to react with the cluster ion formed upstream and, hopefully, to monitor the nature of this unidentified cluster ion.

The first monitor gas used was HCN which is known to cluster effectively with $HCNH^+$ [240]. If the *m/z*=54 ion is a loosely bound electrostatic cluster, a "switching" reaction where the more weakly bound C_2H_2 ligand will be replaced with the stronger HCN ligand, should take place. The product of the $HCNH^+.C_2H_2 + HCN$ reaction should then produce an ion at 55 amu. If however the $HCNH^+.C_2H_2$ product is a covalent species, a possible structure could be CH_2CHCN^+, protonated acrylonitrile. The reaction between protonated acrylonitrile and HCN has been previously investigated by Petrie *et al.* [243] in the SIFT and they found the product to be the adduct. When hydrogen cyanide was introduced a reaction was indeed evident. The cluster ion signal reduced and two products were observed, one corresponding to $HCNH^+.HCN$ (*m/z*=55) and the other being the adduct of the product $C_3H_4N^+$ species with HCN. Another peak at 59 amu was also observed which apparently was the

result of an acetone impurity in the HCN supply. It is possible that the $HCNH^+.HCN$ ion could be formed directly from the $HCNH^+$ still unreacted in the flow tube (after adding C_2H_2). This process was found to be slow at the pressures used in this experiment (0.5 Torr) with a rate coefficient around 6×10^{-12} cm^3s^{-1}, and so should not make a significant contribution however the acetone impurity prevented an accurate determination of this rate coefficient. Even if this is the formation mechanism for all the $HCNH^+.HCN$ observed this does not alter the fact that a reaction consistent with a more strongly bound ion than an electrostatic complex was observed.

The next monitor gas tried was methyl acetylene (propyne, $CH_3C{\equiv}CH$) which has a proton affinity (PA ($CH_3C{\equiv}CH$) = 748 kJ mol^{-1}) intermediate between those of HCN (PA = 712 kJ mol^{-1}) and acrylonitrile (PA = 785 kJ mol^{-1}). For an electrostatic cluster as the product of Reaction 618 the expectation was that it would either undergo proton transfer or a ligand switch. The reaction between CH_2CHCNH^+ and methyl acetylene has not been studied but $C_3H_4N^+$ reacts with acetylene (which also has a lower PA than CH_2CHCNH^+) very slowly in what is probably an association reaction [241]. The results here were inconclusive, the $C_3H_4N^+$ ions formed in the flow tube did not appear to be completely removed at high methyl acetylene flows but only products consistent with proton transfer (most probably from $HCNH^+$) and ligand switching ($HCNH^+.CH_3C{\equiv}CH$) were observed.

The final neutral monitor chosen was benzene which like propyne, has a PA intermediate between those of HCN and acrylonitrile ($PA(C_6H_6)$ = 750 kJ mol^{-1}). This neutral provided the most conclusive evidence for the presence of two isomers in the $C_3H_4N^+$ ion. At very high benzene flows it was observed that the 54 amu ion had completely reacted away (as had the $HCNH^+$) and that 2 products were visible. These were a major product at m/z = 79 ($C_6H_7^+$) (also formed by proton transfer from unreacted $HCNH^+$) and a more minor one at m/z = 132 ($C_3H_4N^+.C_6H_6$). A mass spectrum recorded under these conditions is shown below.

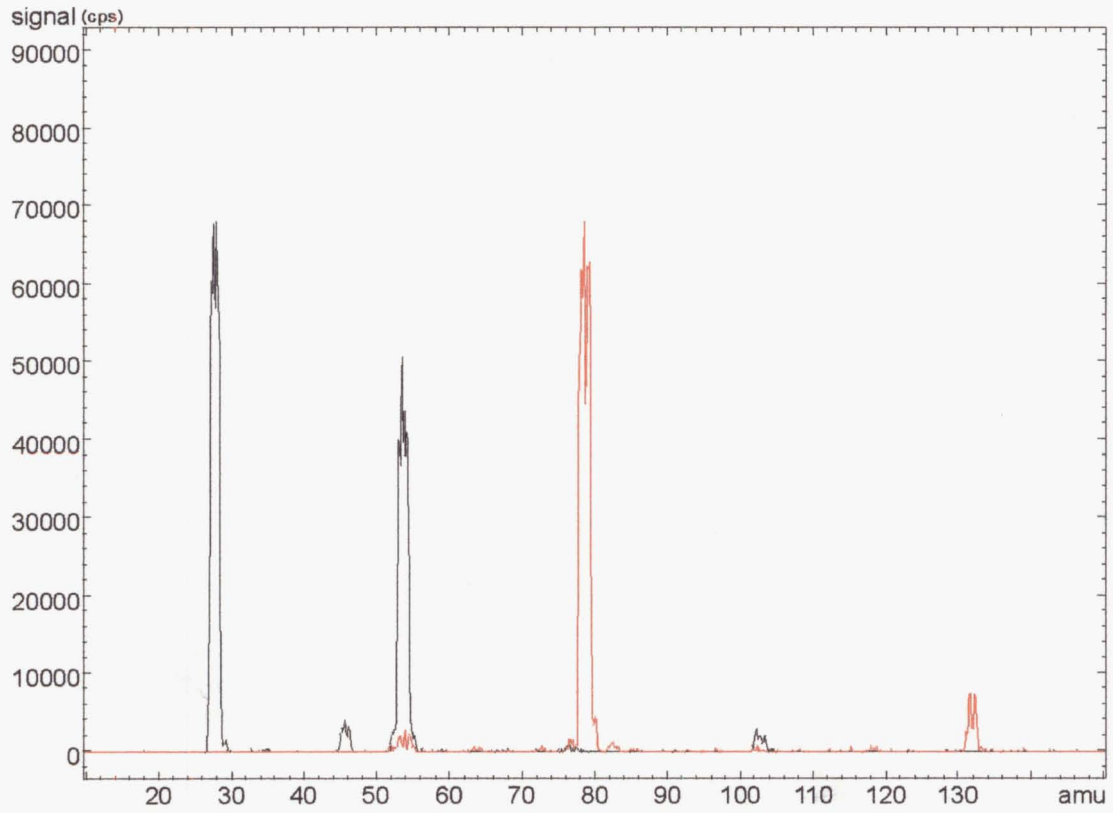

Figure 6.5: A comparison of two mass spectra recorded with (red trace) and without (black trace) benzene flowing.

The kinetics of this process were also investigated, though only in a semi-quantative manner. There is an initial rapid loss of $C_3H_4N^+$ followed by a slower decay that represents up to one third of the initial ions. Thus it appears likely that there is a fraction of the $C_3H_4N^+$ ion formed from the association reaction of $HCNH^+$ and C_2H_2 that is more strongly bound than the remainder (this being the slower reacting fraction which associates). In addition there is a weakly bound ion (e.g. an electrostatic complex) which is unlikely to undergo a further association reaction.

When the effect of varying the different carrier gas species was investigated for Reaction 618, the nitrogen rate coefficient was, as expected, found to be greater. The values determined were: $k_3 = 6 \times 10^{-29}$ cm^6s^{-1} for a helium bath gas; and $k_3 = 4 \times 10^{-28}$ cm^6s^{-1} when M is nitrogen. Our helium rate is in good agreement with that of Herbst while the rate in nitrogen is much accelerated (~7 times faster).

In the reaction between *ethylene* and $HCNH^+$ ions, the rate coefficient in a helium carrier gas, $k_3 = 5 \times 10^{-27}$ cm^6s^{-1} was again in excellent agreement with the Herbst *et al.* result ($k_3 = 7 \times 10^{-27} (300/T)^{2.6}$ cm^6s^{-1} between 210 and 300K). This rate is approximately 50 times lower than the corresponding theoretical rate, which places

it between the ratios obtained for the H_3O^+/C_2H_2 and H_3O^+/C_2H_4 systems. This suggests that a covalently-bound product channel should be expected. The reaction between $HCNH^+$ and C_2H_4 may be an efficient method of forming the protonated ethyl cyanide ion in the lower atmosphere of Titan if indeed this isomer is formed in the reaction. Of course, other isomers are also possible. At approximately the same altitude as the lower ionosphere peak electron density (altitude of 100 km, T=140K, number density $\approx 2.5 \times 10^{18}$ cm^{-3}) the apparent bimolecular rate coefficient for the $HCNH^+/C_2H_4$ reaction will be approximately collision rate.

When the $C_3H_6N^+$ association product formed from the reaction between $HCNH^+$ and C_2H_4 was investigated with benzene (using identical techniques to those outlined above) the behaviour of the product ion indicated that it is largely covalent in nature. The PA of the possible covalent product, ethyl cyanide, is 794 kJ mol^{-1} and is greater than the PA of benzene. Thus protonated ethyl cyanide will not proton transfer to benzene. The proton transfer observed when benzene was added to the flow tube downstream of the formation of the $C_3H_6N^+$ adduct can arise from two sources, remaining unreacted $HCNH^+$ and a $C_3H_6N^+$ isomer with a PA less than benzene (most probably an electrostatic ion). At high benzene flows the number of counts of $C_6H_7^+$ only exceeded the initial number of $HCNH^+$ counts by ~5000 (cf. approximately 55,000 cps of $C_3H_6N^+$). Serious mass discrimination was observed to occur at 135, $C_3H_6N^+.C_6H_6$, amu (it also featured at 79, $C_7H_9^+$) amu but was not so serious) and this hinders an accurate determination of the fraction of weakly bound complex. However even assuming a mass discrimination factor of 2:1 between masses 28 and 79 (an unlikely value - the true value will be considerably less) there is less than 20% of the smaller fraction present. These observations indicate that at least 80% of the $C_3H_6N^+$ ion formed from the reaction of $HCNH^+$ and C_2H_4 is in a covalently bound form.

Section 6.5: Conclusions.

The main differences between the reactions occurring at high and low altitudes in Titan can be best seen by comparing the graphs of ion species for the high and low altitude models e.g. that of Molina-Cuberos [202] with that of Keller *et al.* [183]. The primary low altitude species are more complex. For example $HCNH^+$ abounds around

1100 km but there is almost none present below 400 km as clustering reactions take effect. These clustering reactions can induce changes in the bimolecular chemistry (N_3+, N_4^+) as well as building up more complex species rapidly. It has been shown that these association reactions are more efficient when nitrogen is the third body in the termolecular process (by a factor of 3 to 13). Also, the association reactions of several of the terminal ions in Titan's ionosphere are capable of producing covalently bound products.

Chapter 7:

Ion-molecule association in acrylonitrile.

Section 7.1: Introduction.

§7.1.1: Notes on acrylonitrile.

Acrylonitrile (propenenitrile or vinyl cyanide) is one of more than 100 molecules that have been detected in interstellar clouds by radioastronomical techniques. Matthews and Sears [242] have identified it in the cold molecular cloud TMC 1 from its emission spectrum. Acrylonitrile (and other nitriles) are more easily detected in the interstellar medium (ISM) than are many other species due to the large dipole moments conferred upon them by the presence of the -CN group. Although this and other experimental considerations mean that astronomers are getting a somewhat biased view of the molecules present in these clouds, the ion-molecule chemistry of acrylonitrile is still important to the overall modelling of interstellar processes. The presence of acrylonitrile and other similar nitriles has also been postulated in the atmosphere of Titan [157]. These facts have motivated the investigation of several aspects of the ion-molecule chemistry of acrylonitrile. Petrie *et al.* [241] have studied the reaction chemistry of $C_3H_2N^+$, CH_2CHCN^+, and CH_2CHCNH^+ with a range of simple neutrals using a SIFT and have discussed the implications of these reactions to chemical processes in the ISM [243]. Sun *et al.* [244] have performed reactions of multi-ringed C_n^+ (n = 10 to 18 and 20) ions with neutral acrylonitrile in a FT-ICR. Javahery *et al.* [245] have also studied reactions of fullerene ions with neutral acrylonitrile, reacting it with the mono-, di-, and tri-cations in a SIFT and McEwan *et al.* have examined the association of CH_3^+ with neutral acrylonitrile over a pressure range 10^{-7} Torr to 0.5 Torr [246].

Included in the work of Petrie *et al.* [241] was an investigation of the association chemistry of acrylonitrile ions with neutral acrylonitrile. This work was subsequently continued by Wilson during his PhD. [69], however the SIFT experiments in these investigations were performed using an earlier version of the Canterbury SIFT apparatus. In these earlier experiments the lower injection resolution of the ion selection region (quadrupole mass spectrometer and lens arrays) in the older SIFT

prevented injection of an ion of specified mass without some contamination from adjacent masses. This was subsequently found to have caused a misassignment of the products. These reactions were thus revisited using the greater resolution of the current FA/SIFDT system.

§7.1.2: Association Reactions.

Association reactions are a unique type of ion-molecule reaction. Because the product includes all the atoms from both the ion and the neutral, any excess energy in the collision complex cannot be removed from the complex by loss of fragments as none are produced. Therefore other means of removing the excess energy from the initial collision complex are required or it will back-dissociate or undergo a bimolecular reaction process. There is always some excess energy in any collision complex formed as a result of an ion molecule interaction, be it from reaction exothermicity if a stable product is formed, or translational or vibrational energy in either collision partner. If association is to become an effective process the removal of this excess energy must become efficient. In most ion-molecule association systems that are amenable to experimental observation, this excess energy is removed through collisions with surrounding neutral molecules. Each neutral that interacts with the complex carries away a small portion of energy. Thus the association reaction becomes termolecular i.e. dependent not only on the concentration of the reactant ion and neutral but also on the concentration of some third body, M, which is affecting the de-excitation of the initial, excited, collision complex.

It has been proposed that in the extremely cold, diffuse environment of space, where collision with a stabilising body would be extremely unlikely, a second mechanism of de-excitation could be important namely, the emission of photons [45, 284]. This method of stabilisation is often termed *radiative association* and it relies on the fact that ion lifetimes become much greater at the lower temperatures encountered in interstellar space. A generalised scheme for an association reaction is shown below [174, 175, 247, 248].

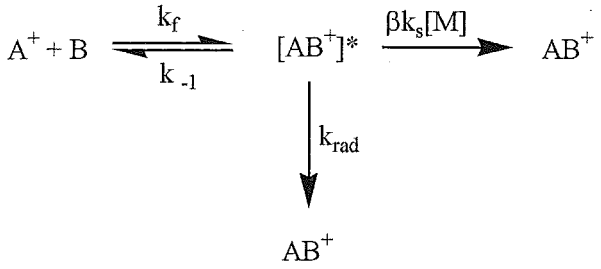

(7.1)

Here $[AB^+]^*$ represents the excited collision complex, k_f is the formation rate coefficient (usually approximated by the collision rate), k_{-1} represents the rate coefficient for unimolecular decomposition back to reactants, k_{rad} is the rate coefficient for radiative association, and $\beta k_s[M]$ represents the rate of stabilisation by a third body (M). A major factor influencing the effectiveness of an association reaction is the lifetime of the excited complex, τ $(AB^+)^*$. Consequently the rate coefficient for stabilisation by collision; i.e. the termolecular association rate coefficient can be used as an experimental indicator of the efficiency of radiative associations, as both are favoured by longer-lived collision complexes.

The association reactions of ions derived from acrylonitrile that will be discussed in this chapter represent a sub-class of association processes as they belong to a group of reactions that occur in competition with an available bimolecular process. Under flow tube conditions, any contributions from radiative stabilisation can be neglected and the model for stabilisation can be formulated as follows:

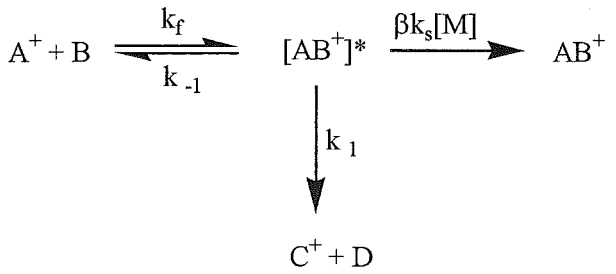

(7.2)

Here βk_s represents the effectiveness of collisional deactivation (k_s is the collision rate coefficient for the de-excitation process and β represents the fraction of collisions that are effective in producing stabilisation. From this equation a model for the competition between the termolecular and bimolecular reaction can be derived. First

$$d[A^+]/dt = -k_f [A^+] [B] + k_{-1} [(AB^+)^*] \quad (7.3)$$

and

$$d[(AB^+)^*]/dt = k_f [A^+] [B] - ((k_{-1} + k_1 + \beta k_s[M])[(AB^+)^*]) \quad (7.4)$$

If one then makes the steady state approximation, that is as $(AB^+)^*$ is an intermediate it quickly reaches a steady concentration where formation and loss processes balance and

$$d[(AB^+)^*]/dt = 0 \qquad (7.5).$$

This means that the concentration, $[(AB^+)^*]$ can be expressed as;

$$[(AB^+)^*] = k_f [A^+] [B] / (k_{-1} + k_1 + \beta k_s[M]) \qquad (7.6).$$

Equation 7.6 can then be substituted into Equation 7.3 to give a solution. However when one observes an association system, the rate coefficient measured does not represent either pure a bimolecular or termolecular reaction process but is instead a pseudo-bimolecular rate coefficient which represents the sum of the two processes at a specific [M] (or bath gas pressure), k_2^{obsd}. Thus

$$d[A^+]/dt = -k_2^{obsd} [A^+] [B] \qquad (7.7)$$

Combining Equation 7.7 with the solution from Equation 7.6 and equating this with Equation 7.3 gives:

$$k_2^{obsd} = k_f ((k_1 + \beta k_s[M]) / (k_{-1} + k_1 + \beta k_s[M])) \qquad (7.8).$$

In the limiting case where [M] = 0, i.e. where no stabilising third body is present, this reduces to:

$$k_2^{obsd} = k_f ((k_1) / (k_{-1} + k_1)) \qquad (7.9)$$

The observed termolecular rate coefficient (k_3^{obsd}) can also be calculated and is defined as $d(k_2^{obsd})/d[M]$. The derivative of equation 7.8 with respect to [M] gives:

$$k_3^{obsd} = (k_{-1} k_f \beta k_s) / (k_{-1} + k_1 + \beta k_s[M])^2 \qquad (7.10)$$

This is known as a "single-well" model and it predicts that the bimolecular process will dominate at low pressures (to the exclusion of the termolecular reaction at low enough pressures) and that as the pressure rises the termolecular process will become increasingly more important. When the pressure is sufficiently high the reaction will enter the "saturation" region in which every complex formed is stabilised by collision . In this situation, only association will be observed and the rate coefficient, k_2^{obsd} will equal k_f.

Section 7.2: Experimental.

§7.2.1: The Ion Cyclotron Resonance Mass Spectrometer (ICR).

During this section of experimental work the second apparatus available for studying ion-molecule chemistry at The University of Canterbury, the Ion Cyclotron Resonance mass spectrometer (ICR), was used. This apparatus gives the Ion-Molecule Reactions group at Canterbury an almost unique ability to follow the dynamics of association reactions across a wide pressure range. The ICR at Canterbury has been described previously by Wilson in his PhD. thesis [69] and several comprehensive descriptions of the range of the technique and its theory have also been published [164]. In the interests of completeness however, a short description of the experimental set-up and the theory of the ICR technique, as it relates to this section of work, will be given.

The ICR technique operates in a much lower pressure regime than does the SIFT, operating in the range approximately 5×10^{-8} to 1×10^{-3} Torr. Thus it allows us to study the behaviour of association systems outside the pressure saturated region that is most commonly encountered in the SIFT. An investigation of association in the pressure range encompassed by both techniques gives a unique insight into the association process.

Ion cyclotron resonance spectrometry relies, as the name implies, on the cyclic movement of the ions within the ICR reaction cell. This cell, shown in Figure 7.1, is constructed of two pairs of stainless steel plates arranged around the inside of a rectangular tube. The cell is fixed within a strong magnetic field which is supplied by an external electromagnet.

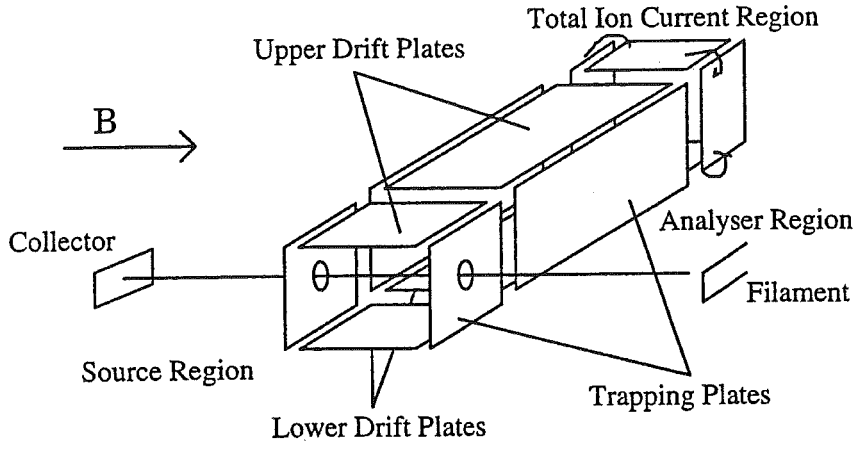

Figure 7.1: A schematic diagram of the ICR cell at the University of Canterbury.

The upper and lower plates are known as the drift plates and they supply an electric field that is perpendicular to the vector of the magnetic field. It is these crossed electric and magnetic fields that form the heart of the technique. When the forces on the ion provided by these two fields are combined they impart to the ions a velocity in a direction that is perpendicular to both of their vectors i.e. along the axis of the cell into the page in Figure 7.1. This combination of vectors is shown in Figure 7.2. The side plates (or trapping plates) have a small repulsive voltage on them to prevent ions from 'leaking' out of the sides of the ICR cell.

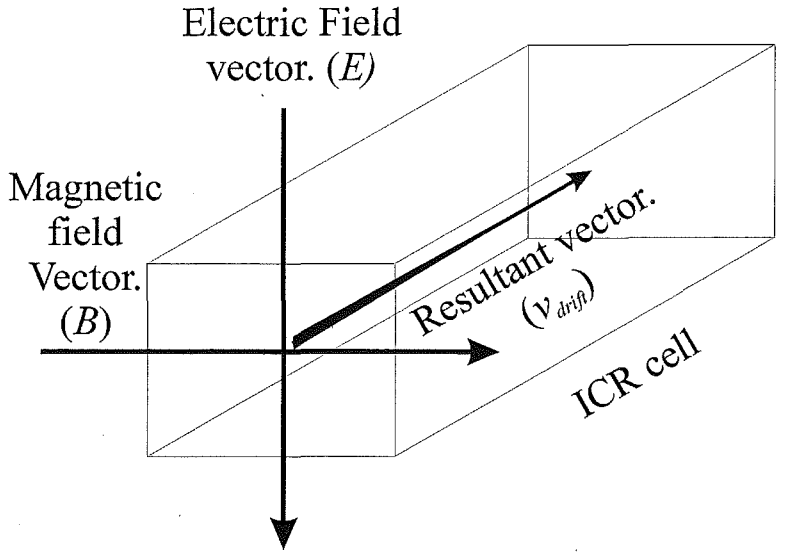

Figure 7.2: The vector combinations that lead to drift motion within an ICR cell. B represents the magnetic vector, ε the electric vector, and v_{drift} the resultant ion drift motion.

In the presence of a large magnetic field an ion with a velocity perpendicular (v) to the magnetic field vector (**B**) undergoes an interesting phenomenon. A force perpendicular to both v and **B** will be generated that, when the magnetic field is large, will cause circular motion. For this circular motion the acceleration, a, is v^2/r, where v is the drift velocity and r the radius of the ion path. Thus the force on the ion can be written as shown in Equation 7.11.

$$F = ma = mv^2/r \qquad (7.11)$$

This force is also equal to the product of the magnetic field (B), the velocity (v) and the charge on the ion (e), so that 7.11 can be rewritten as 7.12.

$$ma = mv^2/r = evB \qquad (7.12)$$

If ω_c is the angular frequency in radians per second this equation may then be converted to:

$$mv/r = m\omega_c = eB \qquad (7.13).$$

From 7.13 the basic cyclotron equation can be evaluated, that is:

$$\omega_c = eB/m \qquad (7.14)$$

This shows that the angular frequency is independent of the ion drift velocity. A result that is especially useful when one notes that the frequency of the circular motion ($\nu_c = \omega_c/2\pi$) is directly related to the angular velocity. This means that at a particular magnetic field, an ion of a specific mass will have a unique frequency of rotation known as the "cyclotron frequency". When a radio frequency (RF) signal of an identical frequency is applied to the drift plates the rotating ions will absorb energy from the RF generator and thus increase the radius of their orbits. This is the essence of ion detection in the ICR as the magnitude of the absorption at a particular RF frequency is directly proportional to the number of ions with that cyclotron frequency i.e. the number of ions with a specific mass. By scanning the RF generator across a range of frequencies a mass spectrum of all the ions formed in the ICR cell can be generated from the energy absorbed.

The University of Canterbury ICR uses a cell of the three-section type (see Figure 7.1). These three sections are the ion source region, the reaction region and the total ion current (TIC) region. Ions are formed by electron impact, usually using a modulated electron beam. The subsequent modulation of the ion beam ensures that only ions formed from this electron beam (and their products) are detected, as a lock-in amplifier is used to select only those ions with this chosen frequency of modulation. After their formation, the ions are drifted into the reaction region where ion chemistry can be monitored. Radio frequency power is provided to the reaction region using either a Hewlett Packard model 3314A function generator or a Stanford research Systems model DS340 function generator and any power absorption is monitored using a capacitance balanced bridge [287]. The final (TIC) region is connected to a sensitive picoammeter (a Keithley 602 solid state electrometer) which provides a monitor for the total number of ions present in the ICR cell.

The ICR has two main modes of operation, trap mode and drift mode. The mode that is most relevant to this work is drift mode as it allows the ICR to be

operated at higher pressures than are possible with trap mode. Drift mode ICR essentially uses the ICR cell as a small flow tube, with ions being conducted through the reaction region at a constant velocity (v_{drift}). Thus, though the drift velocity is unimportant in determining the cyclotron frequency, it is important when ion-molecule kinetics are being considered as it determines the length of time that the ions spend inside the source and reaction regions of the ICR cell. These "drift times" are determined experimentally by operating the ICR in a pulsed mode of operation and applying a quenching pulse to the reaction region (which is an attractive pulse applied to the side trapping plates that removes all the ions from the reaction region) at a range of times after the ion creation pulse. By monitoring the ion current profile with respect to time, the time required for ions to exit the source and the time required to traverse into the TIC region can be determined

In a drift mode experiment, the peak heights for all ionic reactants and products are recorded (at a specific pressure) and then iteratively fitted to a model. At Canterbury this process is performed using a series of FORTRAN programs written by Anicich [249]. These programs calculate the apparent bimolecular rate coefficient for the process at a single pressure using the power absorption equations of Comisarow [288] and the two measured drift times. By obtaining these rate coefficients at several pressures one can ascertain the behaviour of the reaction over the range of pressures accessible to the ICR technique.

§7.2.2: The Drift Tube.

In the course of this investigation the drift tube (DT) installed in the reaction flow tube of the FA/SIFDT was used. This piece of equipment and the theory behind its application are well described in Sections 1.2-6 and 2.3 of the PhD. thesis of Fairley [71]. In brief, the drift tube consists of a set of 50 stainless steel rings that are connected to an electronic circuit which places a potential gradient onto each of the rings. This gradient is arranged such that it increases as one passes down the flow tube from the upstream to downstream end of the DT. Consequently ions entering the DT are accelerated by the potential gradient. The acceleration generated by the voltage gradient is offset by deceleration from collisions with the carrier gas inside the flow tube. This means that a steady state velocity is reached by the ions in the tube, that is

known as the drift velocity, (v_{drift}). The drift velocity is higher than the ion velocity in the absence of a field gradient. The increased velocity affects each ion-reactant collision as there is more energy in each collision, as a result of the increased translational energy. This additional energy can be used to drive reaction channels that are endothermic (or disfavoured) at thermal energies i.e. it is roughly equivalent to increasing the temperature at which the reaction occurs. It is usually not, however, strictly correct to make this comparison as the ions do not rapidly vibrationally equilibrate to a higher temperature. Using a carrier gas with a higher molecular mass will usually get the internal energy state of the ions to equilibrate closer to the ion-carrier gas centre-of-mass energy (the theoretically correct measure of the energy of interaction between the ion and the neutral gases in the SIFDT).

Section 7.3: Results.

§7.3.1: The reaction $CH_2CHCN^+ + CH_2CHCN$.

The reaction between the molecular acrylonitrile ion and neutral acrylonitrile (Reaction 701) has been studied previously in the SIFT by Petrie *et al.* [241] and in the ICR by Wilson [69].

$$CH_2CHCN^+ + CH_2CHCN \Rightarrow CH_2CHCNH^+ + C_3H_2N \quad (701a)$$

$$+ M \Rightarrow (CH_2CHCN)_2^+ + M \quad (701b)$$

In the ICR experiments, in both drift mode and trap mode, the rate coefficient was 2.5×10^{-9} cm^3s^{-1} and self-protonation, Reaction 701a, was essentially the only product observed. In the models below both recently measured results and older results by Wilson on the Canterbury ICR and McEwan and Anicich [250] on the JPL ICR are used.

In the previous SIFT study the only product reported was channel 701b with an apparent bimolecular rate coefficient of 2.0×10^{-9} cm^3s^{-1}. This result was obtained with a pressure of 0.30 Torr of helium in the flow tube and it suggests that the reaction is approaching saturation as the bimolecular channel has essentially been removed and the rate coefficient is similar to the collision rate. The protonated acrylonitrile ion (i.e. the ionic product of channel 701a) was observed in the earlier study, but was discounted as a reaction product as it was believed to be the result of significant amount of leakage of $m/z = 54$ ion from the ion source. Because the CH_2CHCNH^+ ion also rapidly reacts with acrylonitrile (see §7.3.2), the deconvolution

of its formation and loss processes from observed data proved to be impossible. In the new FA/SIFT however it was possible to inject only a single ion mass and thus the analysis of results was simpler. Figure 7.3 shows the profile of the precursor and product ions obtained for the reaction of CH_2CHCN^+ with a mixture of helium and acrylonitrile.

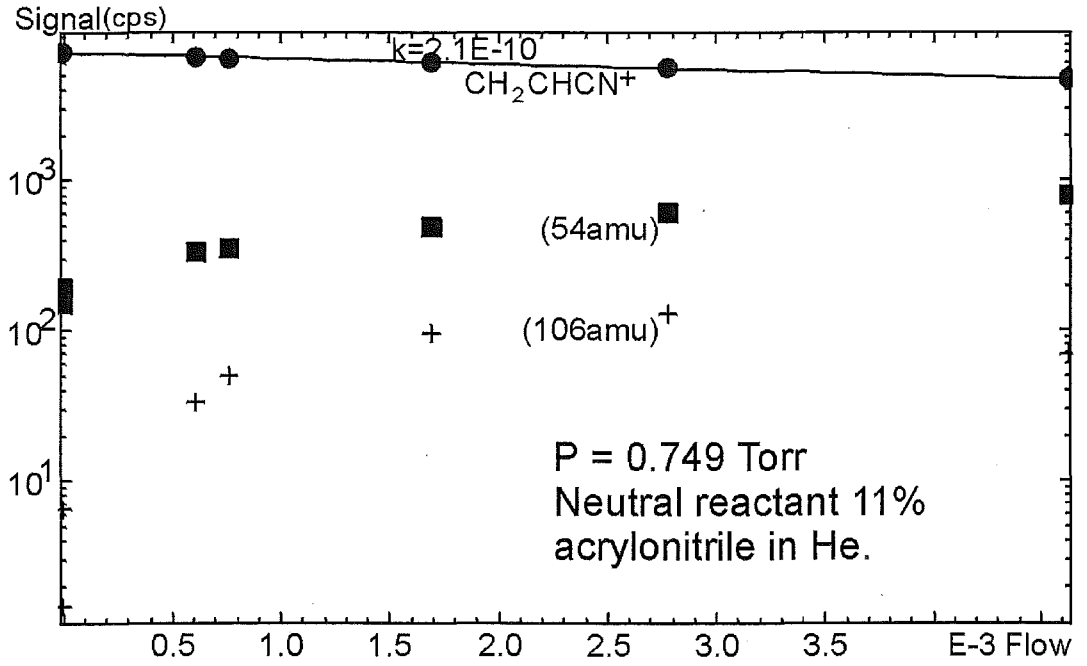

Figure 7.3: A semi-logarithmic plot of the primary and product ions for the CH_2CHCN^+/CH_2CHCN reaction system against the flow of a ~12% He/CH_2CHCN mixture. The 53^+ ion is CH_2CHCN^+, 54^+ CH_2CHCNH^+ and 106^+ is the dimer ion $(CH_2CHCN)_2^+$.

Reaction 701 was studied using both pure acrylonitrile vapour as well as an approximately 12% mixture of acrylonitrile vapour in helium. This latter mixture was prepared as acrylonitrile is known to be a 'sticky' gas that is, it adsorbs readily on to the walls of the glass volumes used for gas handling and flow measurement. This adsorption can result in inaccurate flow measurements and from this, error in the measurement of the rate coefficients. It is also possible that the pure acrylonitrile vapour may form neutral dimers and this will also prevent accurate flow measurements. The mixture was calibrated by comparing the rate coefficient obtained for Reaction 702 with the mixture with the rate for a pure acrylonitrile reactant. Reaction 702 was assumed to proceed at the collision rate ($k_{coll} = 5.1 \times 10^{-9}$ cm^3s-1) rather than measured due to the fact that similar problems would also hamper the accurate determination of this rate coefficient.

$$H_3O^+ + CH_2CHCN \Rightarrow CH_2CHCNH^+ + H_2O \quad (702)$$

The rate coefficients obtained when pure acrylonitrile vapour was the reagent were consistently approximately one third less than those obtained using the helium-diluted mixtures. This bears out the need for such a mixture. However, both data sets showed the same behaviour i.e. the rate coefficient had levelled out to a rate coefficient less than the collision rate for the process (k_{coll} = 3.7 x 10^{-9} cm^3s-1, k_{expt} = 3.0 x 10^{-9} cm^3s^{-1} using a 12% mixture). The rate coefficients obtained were essentially invariant throughout the pressure range investigated (0.25-0.75 Torr helium). In order to obtain this highest pressure (0.75 Torr) the reaction tube Roots blower pump had to be 'throttled' in order to reduce its pumping speed. At the highest pressure the observed rates were approximately 10% lower than elsewhere. This was traced to the slight "break-up" of the CH_2CHCN^+ ion upon injection into the tube. This "break-up", which may be caused by increased turbulence in the region of the venturi injector, gave CN^+. The CN^+ ion will then react with acrylonitrile to generate a 53 amu ion (Reaction 703) [241] causing an apparent reduction in the observed rate coefficient.

$$CN^+ + CH_2CHCN \Rightarrow CH_2CHCN^+ + CN \quad \text{or}$$

$$C_2N_2H^+ + C_2H_2 \quad [0.75] \quad (703a)$$

$$\Rightarrow c\text{-}C_3H_3^+ + N_2 + C \quad [0.16] \quad (703b)$$

$$\Rightarrow CH_2CHCN^+.CN \quad [0.09] \quad (703c)$$

Channel 703c represents association and should become more rapid at the higher pressures involved. The product of this channel was observed concurrently with the observation of CN^+, confirming the assignment of the interfering reaction. Reducing the FA nose cone injection voltage raised the observed rate coefficient but did not entirely eliminate the interference.

Product distributions were obtained using only the acrylonitrile/helium mixture due to the need to accurately measure low flows during a product distribution determination. The observed branching ratio was 70% CH_2CHCNH^+ (701a) and 30% adduct (701b) at a flow tube pressures between 0.25 and 0.75 Torr of helium.

To further probe the nature of the collision complex formed in this reaction, the product distribution was also examined using the DT capability of the FA/SIFDT. The reaction was studied at five different E/N values, each increasing the kinetic energy involved in the interaction between the reactant ion and neutral. The mobility of CH_2CHCN^+ at each of these E/N values was experimentally determined by pulsing

the rings within the DT as described by Fairley [71]. The E/N values were varied by altering the DT voltage while maintaining the tube pressure at 0.35 Torr. The mean centre-of-mass energy involved in the ion/reactant neutral encounter, E_r, is given by the formula

$$E_r = 3/2\ k_BT + [m_r/(m_i + m_r)](KE_{ion} - 3/2\ k_BT) \quad (7.15).$$

where m_i and m_r are the masses of the ion and reactant neutral respectively, k_B is the Boltzman constant, T is the carrier gas temperature and KE_{ion} is the ion kinetic energy from the Wannier formula (see Equation 3.1). As E_r rises, the raw rate coefficient falls, due to the decrease in the lifetime of the excited collision complexes. The amount of association drops concurrently until, at approximately ~0.1 eV, no association at all is visible. The decrease in the efficiency of association is due to the population of higher energy levels in the collision complexes which means that more collisions (i.e. more time) are required to stabilise them below the dissociation and reaction barriers decreasing the likelihood of stabilisation. Further, the lifetime of the association complexes decreases markedly with increasing energy. The behaviour with increasing E_r is shown in Figure 7.4.

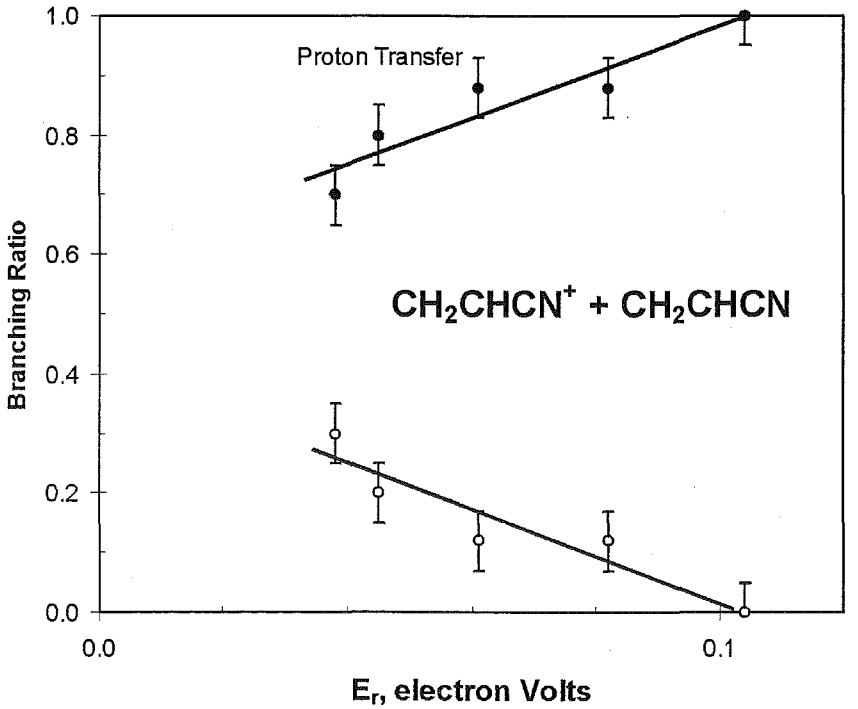

Figure 7.4: The variation in the branching ratio with increasing E_r for the CH_2CHCN^+/CH_2CHCN system.

§7.3.2: The reaction $CH_2CHCNH^+ + CH_2CHCN$.

In the current study Reaction 704 was studied both in the SIFT and in the ICR using the drift mode technique.

$$CH_2CHCNH^+ + CH_2CHCN + M \Rightarrow (CH_2CHCN)_2H^+ + M \quad (704)$$

In the SIFT studies the third body (M) is helium while in the ICR study the parent gas, acrylonitrile, was used. The reaction has previously been investigated in the Canterbury ICR by Wilson using an acrylonitrile bath gas [69] and by Anicich and McEwan [250] in the Jet Propulsion Laboratories ICR [251, 252] using both helium and acrylonitrile bath gases. A previous SIFT investigation [263] has also been performed using the older version of the SIFT at Canterbury.

The current ICR results are shown in Figure 7.5 along with a linear fit. From this fit the three-body rate can be calculated. The value obtained ($k_3 = 1.2x10^{-23}$ cm^6s^{-1}) is in excellent agreement with the previous determinations of $k_3 = 1.2$ and $1.25x10^{-23}$ cm^6s^{-1} reported by Wilson [69] and Anicich and McEwan [250] respectively.

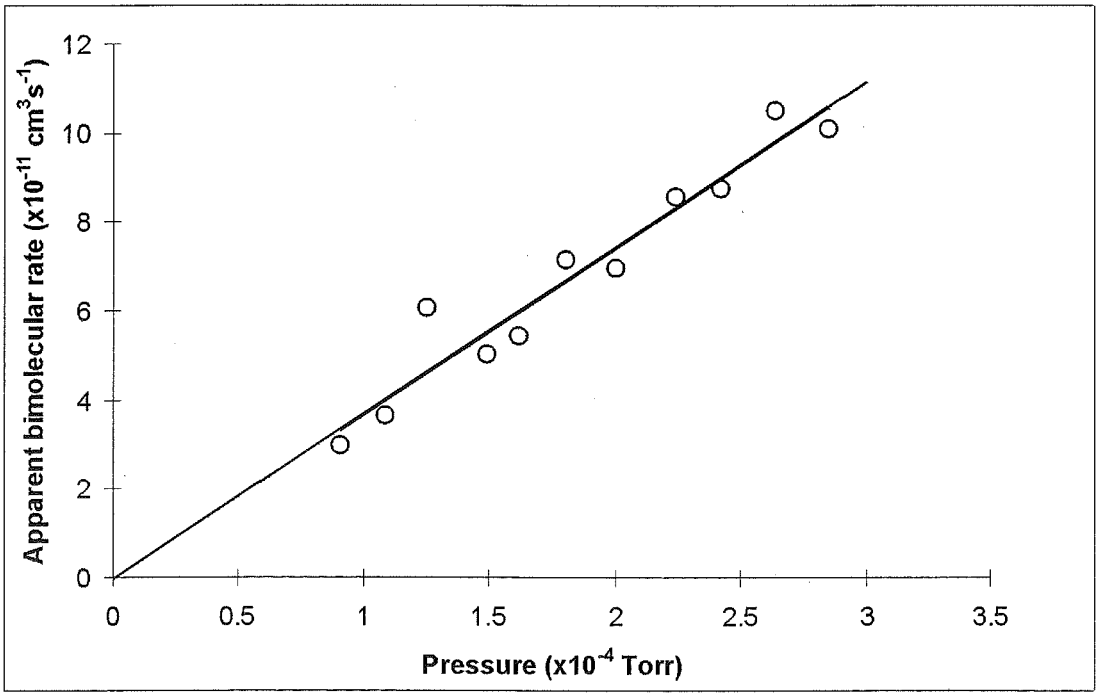

Figure 7.5: The termolecular association of CH_2CHCNH^+ with acrylonitrile measured in the ICR.

As was the case in §7.3.1, the reaction of the protonated acrylonitrile ion (CH_2CHCNH^+) with acrylonitrile (Reaction 704) was investigated in the SIFT using

both pure acrylonitrile as well as a mixture of acrylonitrile diluted in helium as the neutral reactant. The CH_2CHCNH^+ ion was generated in the FA using a dilute mixture of acrylonitrile in helium and using both electron impact and microwave discharges as the ionisation method. A comparison of the rate coefficients obtained using both pure acrylonitrile and an acrylonitrile/helium mixture is shown in Table 7.1.

Pure acrylonitrile		~12 % acrylonitrile mixture in helium	
Pressure[a]	Rate coefficient[b]	Pressure[a]	Rate coefficient[b]
0.34	1.4[c]	0.25	1.7[e]
0.61	1.4[c]	0.48	2.0[e]
0.25	1.3[c]	0.75	2.0[e]
0.44	1.3[d]	0.25	1.4[f]
0.65	1.4[d]	0.49	1.6[f]
		0.75	1.7[f]

Table 7.1: Selected average rate coefficients for Reaction 704 in the SIFT using both pure acrylonitrile and an acrylonitrile/helium mixture as the neutral reactant.

a) Pressure in the reaction flow tube in units of Torr. Pressures of above ~0.5 Torr were achieved by conductance-limiting the Roots blower pump by partially closing the manual gate valve normally used to isolate the 6" pump line from the reaction tube.

b) Experimental rate coefficients. Units are 10^{-9} cm^3 s^{-1}.

c) and d) These values were experimental runs obtained on different days.

e) and f) Two separate experimental runs each using a ~12% CH_2CHCN/He mixture recorded on different days.

From Table 7.1 it can be seen that generally the rate coefficients measured for Reaction 704 using a pure acrylonitrile mixture are lower than those measured using a mixture. This would suggest that the flows of acrylonitrile are being over-estimated in the case of the pure vapour, probably as a result of the occurrence of adsorption. However, the trends are similar in both cases, i.e. the rate coefficient appears to slowly increase with increasing pressure. The magnitude of the rate coefficient is similar to that previously measured by Petrie *et al.* [241], who observed a pseudo-bimolecular rate coefficient for Reaction 704 of 1.30×10^{-9} cm^3s^{-1} in 0.300 Torr of helium. Note that the rate coefficients obtained in both studies are significantly less than the collision rate coefficient ($k_{coll} = 3.6 \times 10^{-9}$ cm^3s^{-1}).

Section 7.4: Analysis.

§7.4.1: The competition between bimolecular and termolecular channels in the reaction of CH_2CHCN^+ with acrylonitrile.

Inspection of the 'standard' model for competition between bimolecular and termolecular channels (§7.1.2) shows that, at saturation, the termolecular channel should dominate. This happens because the collision complex is rapidly stabilised before any back dissociation can occur over the barrier leading to bimolecular reaction. This barrier is represented by E_B in the graphical representation of the standard single-well model which is shown in Figure 7.6. Ions whose energy content drop below this level will remain trapped in the potential well as the association product.

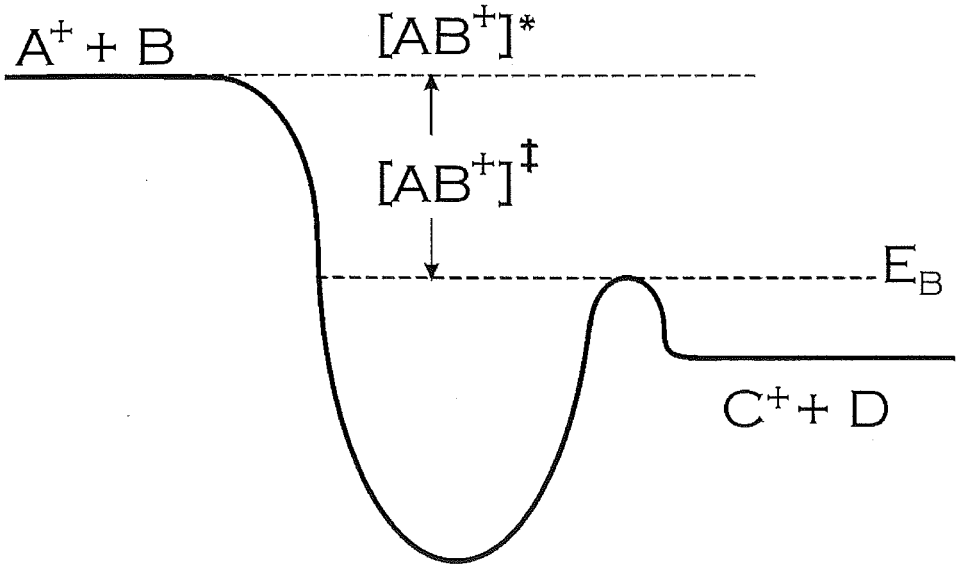

Figure 7.6: A schematic diagram of the potential energy surface most commonly used to represent a single-well association model. Ions stabilised below $[AB^+]^*$ will not dissociate back to reactants. Ions stabilised below the level of $[AB^+]^‡$ i.e. below E_B, the barrier to bimolecular reaction, will be trapped as the association product ion.

It can easily be seen that this model does not correctly describe the CH_2CHCN^+/CH_2CHCN system, as it cannot model 'saturation' at a level where the bimolecular reaction still dominates. To model this system a different description is required, the simplest of which is the double-well potential energy surface shown in Figure 7.7.

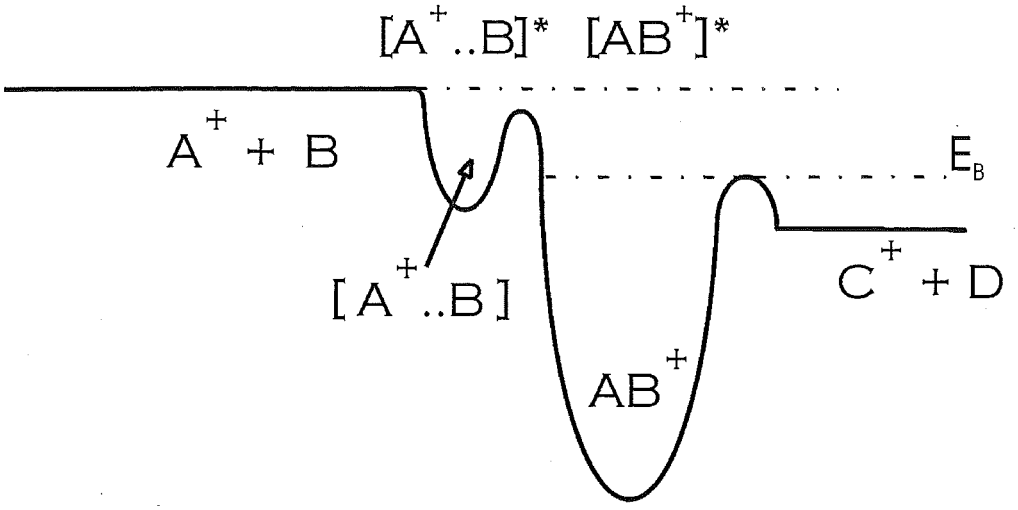

Figure 7.7: A schematic representation of the double-well potential energy surface used in this work to model the competition between bimolecular and termolecular kinetics in the CH_2CHCN^+/CH_2CHCN system. [A...B$^+$] represents a loosely bound collision complex and AB$^+$ a more strongly bound one. Bimolecular reaction can occur from either complex.

This model is similar to that proposed by Mautner [253] for certain reactions of carbonium ions with amines. It is however subtly different from the traditional double-well model proposed by Brauman and co-workers [285, 286]. Brauman's model only allows reaction from the second well, and has no provision for the stabilisation of either of the ion-molecule complexes involved. In the model postulated for this system two complexes are formed, a loosely bound one, (A...B$^+$)*, that is in equilibrium with reactants and a second more tightly bound complex, (AB$^+$)*. Both of these complexes have exit channels available to the bimolecular product. The relevant reactions are shown below.

$$A+ + B \underset{k_{-1}}{\overset{k_f}{\rightleftharpoons}} [A+...B]^* \xrightarrow{k_p} C^+ + D \qquad (7.16)$$

$$[A+...B]^* \underset{k'_{-1}}{\overset{k_t}{\rightleftharpoons}} [AB^+]^* \xrightarrow{k_p'} C^+ + D \qquad (7.17)$$

$$[AB^+]^* \xrightarrow{\beta k_s[M]} AB^+ \qquad (7.18)$$

The model described in equations 7.16 to 7.18 has two outcomes that are different from the previous single well model (§7.1.2). Firstly, the model allows a limiting rate coefficient that is less than the collision rate when the reaction is "pressure-saturated". Secondly, it allows there to be multiple channels present in this saturation region. Essentially the two complexes have very different regions of influence. The *tight complex* is similar to a standard model and will become "saturated" (i.e. all the ions entering the *tight complex* will be stabilised before any unimolecular decay can occur) in the pressure region of the SIFT measurement, 0.25-0.75 Torr. The second, *loose complex* does not live long enough to be stabilised at any of the pressures available in the SIFT and will thus provide a continual source of bimolecular products throughout the pressure range investigated. If the Equations 7.15 through 7.17 are solved in a manner similar to that discussed in §7.1.2, expressions for the behaviour of the two channels with pressure can be derived.

$$k_{obs}^{C+} = \frac{k_f (k_p Z + k'_p k_t)}{(YZ - k'_{-1} k_t)} \tag{7.19}$$

$$k_{obs}^{AB+} = \frac{k_f k_t \beta k_s [M]}{(YZ - k'_{-1} k_t)} \tag{7.20}$$

Here $Y = (k_{-1} + k_p + k_t)$ and $Z = (k'_{-1} + k'_p + \beta k_s[M])$ and the formation and stabilisation rates were assumed to be their respective collision rates i.e. $k_f = 3.6 \times 10^{-9}$ $cm^3 s^{-1}$ and $k_s = 5.5 \times 10^{-10}$ $cm^3 s^{-1}$. A fit of this model to the experimental points is shown in Figure 7.8. This plot was obtained by an iterative fit of the model to the experimental points where k_{-1}, k'_{-1}, k_p, k'_p, and k_t were allowed to vary. More correctly the model would also allow β to vary also, however reducing k_s in this manner does not affect the fit radically in the areas where experimental points have been able to be gathered and so this has not been included in the model. A value of β in the range 0.05-0.15 gives a good visual fit to the beginning of the rise of the termolecular channel, as would be expected.

Because of the number of variables in the fit, the solution obtained for the individual unimolecular rate coefficients (these being the parameters which were

varied in order to fit the model) will not be unique. Consequently the values for the lifetimes of the tight and loose complexes (usually obtained by summing the inverse of all unimolecular rate coefficients exiting the complex) will not be accurate.

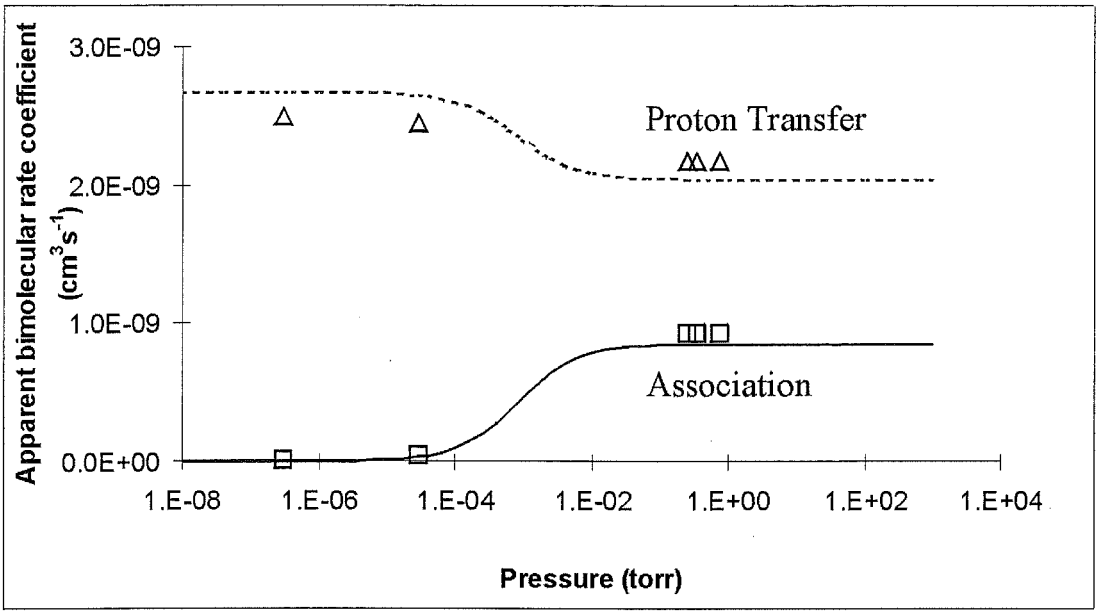

Figure 7.8: The fit of the double-well potential model to the experimental data for the CH_2CHCN^+/CH_2CHCN system.

The **relative** values of these unimolecular rate coefficients will however give an indication of the relative importance of each channel after making the assumption that all collisions enter the reaction system through the loose complex. For the *loose complex* approximately 20% of the complexes formed dissociate to reactants, 25% of them undergo a transition to the *tight complex* and the remaining 55% form CH_2CHCNH^+. The *tight complex* leads almost exclusively to association where possible, otherwise it will back-dissociate to the *loose complex*. A slightly altered model proposed by Anicich *et al.* [251] removes the $k'_{-1}\,k_t$ term in the denominator of both expressions to mathematically simplify the expressions. This achieves a slightly better fit and indicates that ~40% of the tight complex react to give CH_2CHCNH^+.

§7.4.2: The termolecular association of protonated acrylonitrile with acrylonitrile.

In the CH_2CHCNH^+/CH_2CHCN system, termolecular association to give the proton bound dimer ($(CH_2CHCN)_2H^+$) was the only reaction outcome observed in either instrument. This greatly simplifies the analysis of the data and a simple single-well model can be used to account for the observed trends. This model is essentially the same as that discussed in §7.1.2, but it is further simplified as there is no bimolecular channel involved. Equation 7.3 can thus be reduced to:

$$k_2^{obsd} = k_f \beta k_s[M] / (k_{-1} + \beta k_s[M]) \quad (7.21)$$

Equation 7.20 provides the basis for iteratively fitting the experimental data to this model using k_{-1} and β as the adjustable parameters. In this discussion β is a strictly relative value as there is not enough data to obtain an absolute β value for this reaction with an acrylonitrile bath gas. Thus we assign $\beta = 1$ to the case where acrylonitrile is the third body and determine a relative β value for the M = He case. The other unimolecular rate coefficients in the model, k_f and k_s, are set to their respective reaction capture rate coefficients. Figure 7.9 shows this model applied to the system for both the helium and acrylonitrile bath gases while Table 7.2 lists the important parameters of the model.

Parameter	Units	Value
k_f [a]	$cm^3\ s^{-1}$	3.6×10^{-9}
k_s [a]	$cm^3\ s^{-1}$	1.7×10^{-9}
k_{-1}/β	s-1	1.11×10^{6}
β_{rel} (M = helium)	-	0.15
k_3 (M = CH_2CHCN)	$cm^6\ s^{-1}$	1.2×10^{-23}
k_3 (M = He) [b]	$cm^6\ s^{-1}$	8.1×10^{-25}

Table 7.2: The evaluation of the rate coefficients in the CH_2CHCNH^+/CH_2CHCN system using the model shown in equation 7.21.

a) Calculated using the method of Su and Chesnavich [114].

b) From the unpublished work of Anicich and McEwan [250].

The model also allows us to place a limit on the lifetime (τ) of the excited complex $(CH_2CHCN)_2H^+$*. The actual value calculated is $\beta\tau$, where β in this case represents

the **absolute** value of β, and will lie between 0 and 1. Thus $\tau \geq 0.90$ μs. The **relative** β (M =He) shown above (0.15 for this system) is only a measure of the relative effectiveness of helium at stabilising $(CH_2CHCN)_2H^+$* as compared to acrylonitrile.

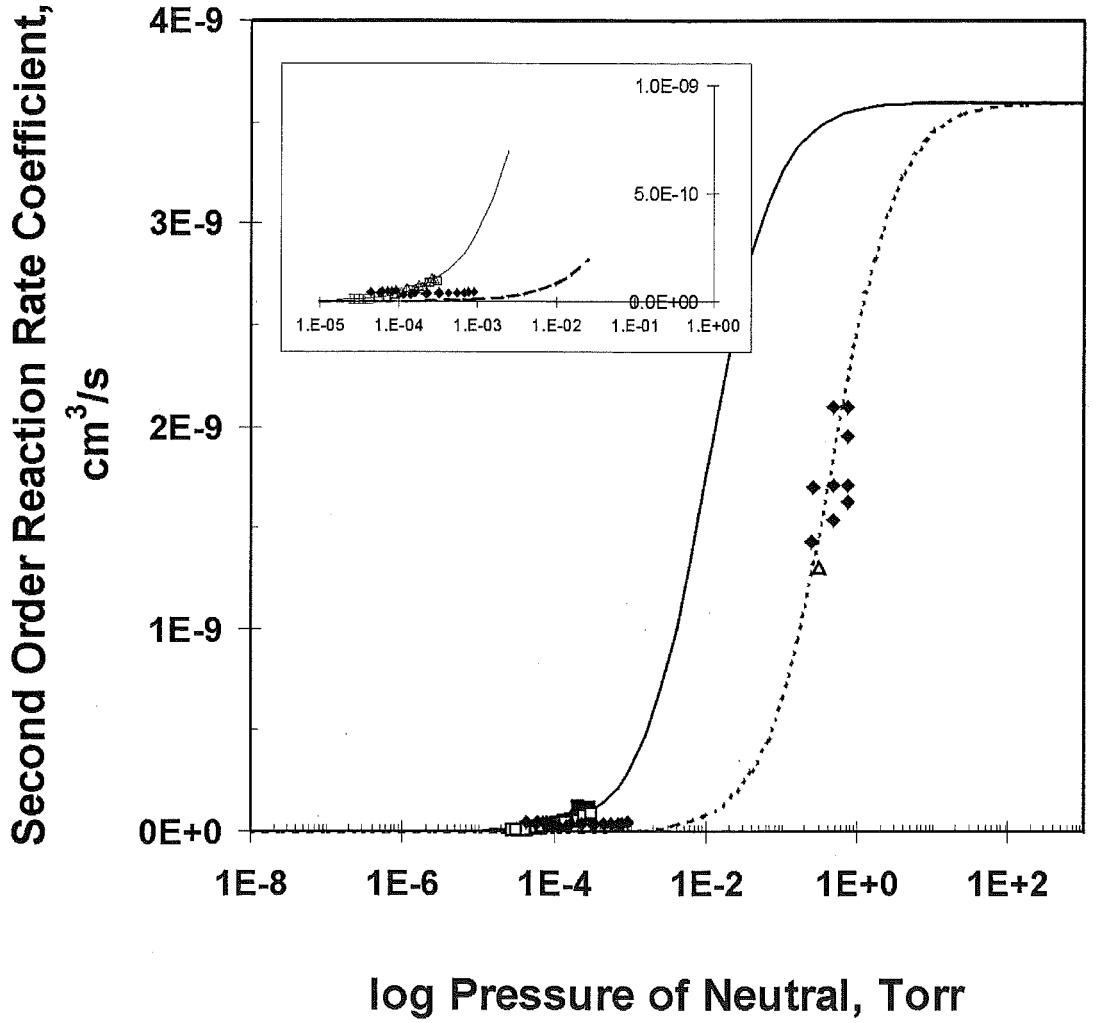

Figure 7.9: The variation in the apparent bimolecular rate coefficient for the CH_2CHCNH^+/CH_2CHCN system shown as a function of logarithm of P, the pressure of the bath gas. The solid line represents the model for M = acrylonitrile, while the dotted one is for M = helium. The inset shows the same variation over the pressure range covered by the ICR data only. The hollow triangle represents the rate coefficient reported by Petrie et al. [241] in a previous SIFT experiment. The inset shows an expanded fit to the low pressure data. The solid diamonds are the helium data obtained by McEwan and Anicich [250], the hollow squares the data by the same workers from a acrylonitrile bath gas and the hollow triangles a new determination from the Canterbury ICR.

The **absolute** β values can be calculated only in special circumstances. In similar systems, values of β of approximately 0.1 for the parent gas have been found previously [174]. The lifetime of the initial collision complex with respect to unimolecular dissociation could thus be as high as 9μs.

It should be noted however that the model is heavily dependent on the assignment of the SIFT points as a slowly increasing with increasing pressure. The values plotted are those from a single experiment using an acrylonitrile/helium mixture as the neutral reactant. Because the pressure range available in the SIFT is limited, the difference expected in the observed bimolecular rate coefficients is not large. Experimental scatter means that one cannot totally rule out the possibility that the reaction has indeed saturated at the lower value seen in the SIFT.

Section 7.5: Conclusions.

The reactions of two ions generated from acrylonitrile (CH_2CHCN^+ and CH_2CHCNH^+) with neutral acrylonitrile have been studied over a range of pressures (using both a SIFT and an ICR) to determine the behaviour of the termolecular channel in each system.

The reaction involving the non-protonated ion, CH_2CHCN^+ was found to be a complex with the rate coefficient 'saturating' below the collision rate and with a significant amount of bimolecular channel still present. These observations require one to invoke a model different from the standard single-well model usually used to describe association reactions. A two-well potential model was found to give a good fit to the experimental results. This model contains two excited complexes, a loose complex that does not saturate at the pressures available in the SIFT and a more standard, tight, complex which saturates at the upper pressures available in the SIFT.

On the other hand a simple single-well model can effectively model the CH_2CHCNH^+/CH_2CHCN system. Only a single product is observed in either the ICR or the SIFT, *viz* the proton bound dimer $(CH_2CHCN)_2H^+$. A lifetime of ≥ 0.90μs was determined for the excited $[(CH_2CHCN)_2H^+]^*$ complex.

Chapter 8

Ion-molecule processes involving carbon atoms as the neutral reactant.

Section 8.1: Introduction.

§8.1.1: The importance of ion-neutral carbon atom chemistry.

In the currently models of the ion chemistry occurring in both dense and diffuse interstellar clouds (ISC) the reactions of atomic species have a significant effect on the chemistry. Indeed in the diffuse ISC hydrogen (the most abundant element in interstellar space) exists as both the atomic and molecular forms in roughly equal amounts. The amounts of the other atomic elements present in ISC are much less, however their chemistry is still important.

The reactions of H, N, and O atoms with a range of ionic species relevant to molecular synthesis in the interstellar medium (ISM) have previously been studied [70, 254-260]. This is not the case with carbon atoms. Finding a convenient, quantifiable source of carbon atoms for a flow system has proved to be a considerable experimental challenge. Carbon atoms are quite reactive with many neutral species and have a tendency to rapidly recombine, forming C_2 and other higher clusters and eventually soot. Carbon atom-neutral chemistry has been studied, but never in a fast flow system such as that which it is necessary to operate with the SIFT. Photochemical dissociation of carbon suboxide (C_3O_2), dissociation of CO by metastable argon atoms, and laser ablation of graphite rods are the most common methods that have been used in the past for these studies of carbon atom-neutral reactions.

The amounts of atomic carbon in the ISM are relatively small, and neutral carbon is relatively easily photoionised to give C^+ ions [260]. As an example, on the path to ζOphiuci (a diffuse ISC) the relative column abundance (relative that is to H atom concentration) of carbon atoms (in both the neutral and ionic form) is ~$4x10^{-4}$. This can be compared to ~$7x10^{-4}$ for neutral atomic oxygen and ~$1x10^{-4}$ for N atoms [42]. The relative abundance of these atoms gets even lower as one moves into the more

dense regions of the ISM where the majority of molecular synthesis takes place. In the dense ISC the fractional abundance of atomic carbon is ~$4x10^{-8}$ at 10K (relative to molecular hydrogen = 1) [42]. The diffuse clouds are probably more representative of the early ISM where the abundances of atomic species is greater, as many of the atoms have not yet been 'locked up' in molecular species. However it has been shown that many "metal-rich" stars apparently act as effusive sources for carbon, enriching the relative carbon atoms concentrations around themselves [261]. (Note metal is being used here in an astronomical sense and refers to any element above helium and thus carbon is a metal in the interstellar sense). These "metal-rich" stars are common in the Milky Way and thus are assumed to be plentiful elsewhere in the Universe.

Most of the species observed in the interstellar medium contain one or more carbon atoms however and they must be generated in some manner. The reactions of ionised carbon atoms have been extensively studied and found to be quite rapid with many species. However the bimolecular reaction between C^+ and H_2 is exceedingly slow [1, 262] slowing at lower temperatures.

$$C^+ + H_2 \Rightarrow CH^+ + H \quad (801a)$$

$$C^+ + H_2 + M \Rightarrow \text{products} \quad (801b)$$

$k_{801a} = 1.2x10^{-16}$ cm^3s^{-1} @ 300K.

The termolecular channel presumably leads to the adduct, CH_2^+. It is important to note that neither of these channels are efficient at beginning the hydrocarbon ion-molecule chemistry that is observed in the ISM. As a consequence Reaction 802 is a very important reaction to study, and this is discussed more fully in the next section. Neutral atomic carbon may also participate in reactions with hydrocarbon ions to build up into larger hydrocarbon ions.

§8.1.2: The Reaction $H_3^+ + C$.

Of all the reactions involving neutral carbon atoms, the reaction between H_3^+ and C (Reaction 802) is without a doubt the most important.

$$H_3^+ + C \Rightarrow CH^+ + H_2 \quad (802a)$$

$$\Rightarrow CH_2^+ + H \quad (802b)$$

The gas phase synthesis of polyatomic molecules in interstellar clouds begins with the ionisation of hydrogen or helium. Because of the preponderance of hydrogen in most of the molecular formation regions this process usually results in the formation of the H_3^+ ion. This ion is able to proton transfer to almost all species encountered in the interstellar medium and is responsible for initiating most of the ion-molecule chemistry in the ISM.

In order to generate hydrocarbons in the ISM from clouds containing mainly hydrogen with trace amounts of other species, carbon-containing ions must first be generated from components of the early galaxy which are very simple. In young regions of the interstellar medium most of the carbon present will be in simple forms such as atomic carbon, CH radicals and CO molecules. Chemi-ionisation of these species by helium may initiate hydrocarbon chemistry e.g. Reaction 803 generates C^+ which can subsequently insert into more complex hydrocarbons and so build larger hydrocarbon ions.

$$He^+ + CO \quad => \quad C^+ + O + He \qquad (803)$$

However in most molecular formation regions atomic and molecular hydrogen have a much greater column density than any other species. Therefore Reaction 802 will be a relatively more important reaction with respect to the generation of ionic hydrocarbon species than those initiated from ionic carbon atoms (e.g. Reaction 801). Furthermore Reaction 801 is exceedingly slow and would provide a serious "bottle-neck" to the formation of more complex hydrocarbon species if it was the only gas phase method for building small hydrocarbon ions. The products of Reaction 802, CH^+ and CH_2^+, can react further with hydrogen, via known reactions, to produce CH_3^+ and CH_5^+ which can then build up larger hydrocarbon species.

Due to the difficulties met in producing quantifiable amounts of neutral carbon atoms in an ionic reactor this fundamental reaction (Reaction 802) has not yet been studied experimentally. Theoretical chemistry leads experimental chemistry in this regard with two high-level ab initio studies of Reaction 802 being performed in the last ten years. It could be argued that these theoretical determinations are largely unnecessary, as the reaction is known to be exothermic and when proton transfer is exothermic reaction usually proceeds at or close to the collision rate (see Chapter 4). For Reaction 802 however, the spin states of the reactants add complications to this simple analysis. For channel 802a the ground state reactants approach on a triplet

potential energy surface (PES) (C is ^3P and H_3^+ is $^1A_1'$) while the products are on a singlet PES (CH^+ and H_2 are both $^1\Sigma$). The lowest potential energy surface which correlates the products with the reactants is an excited $CH^+(a^3\Pi) + H_2$ surface. If this excited triplet surface is not attractive a curve crossing event will be required for reaction to take place. This possible requirement of crossing from a triplet to a singlet surface may create a barrier to the otherwise exothermic reaction and thus slow the rate. The similar reaction of H_3^+ + N atoms (Reaction 804) has been investigated by both experimental and theoretical means and has been found not to proceed for a similar reason [263].

$$H_3^+ + N \quad => \quad NH^+ + H_2 \qquad (804)$$

The first theoretical investigation of the reaction of H_3^+ and carbon atoms, by Talbi and DeFrees [264, 265] in 1991, showed that Reaction 802a can proceed without a barrier at the MP2/6-31G** level of theory. However, these authors found no intermediates that could lead to a CH_2^+ product and concluded that the only possible product was CH^+. Higher level calculations by the same authors confirmed the presence of a stable intermediate leading to CH^+. This T-shaped $CH^+.H_2$ intermediate could be accessed from both reactions and products (in the upper $^3\Pi$ state) even at the energy levels encountered at conditions typical of dark interstellar clouds (T~10K). The CH^+ ($^3\Pi$) product formed will phosphoresce down to the ground $X\,^1\Sigma$ state which is lower in energy than the stable $^3\Pi$ state by 1.1 eV. This reduction in exothermicity has no discernible effect in the H_3^+ + C case, but should prevent another possibly important reaction in protonating carbon atoms, that of HCO^+ + C, from occurring at all. Carbon monoxide is a relatively abundant ion in the ISM and is easily protonated by H_3^+, and as a result HCO^+ is another of the more important ionic species in the ISM having been detected by radioastronomy techniques and is the most abundant ion. Further calculations by the same authors give a rate of 2.3×10^{-9} cm^3s^{-1} at 300K for the reaction between H_3^+ and C atoms when the carbon fine structures (i.e. the angular momentum quantum number) are in thermal equilibrium. If the C atoms are all in the $^3P_0$ state then the rate becomes somewhat higher.

Subsequently an investigation performed by Bettens and Collins [266] using a new automated PES growing system and applying the MCSCF (multiconfiguration self consistent field) method with a 6-31 G** basis set, has confirmed most of the

conclusions of Talbi and DeFrees. The only major difference between the findings of the two studies is that on the PES constructed by Bettens and Collins, CH_2^+ is a product. They found that, at one important $CH^+.H_2$ configuration, the ground and first excited states are almost degenerate. For this reason the authors used a "state-averaging" procedure with the lowest two states on their PES. From the upper of these two states the results were similar to those of Talbi and DeFrees - the only product being CH^+ ($a\ ^3\Pi$). However on the ground state surface a CH_2^+ ($^2A_1$) product was observed. The trajectories that lead to this product were observed to have spent a considerable amount of time in the vicinity of two new CH_3^+ intermediates where the carbon atom is essentially inserted into the middle of the H_3^+ triangle. It was found that although these complexes initially lead to CH^+ in some cases the CH^+ and H_2 fragments did not initially separate. Partial rotation of the nearby H_2 fragment causes this entity to come closer to the carbon side of the CH^+ moiety which then captures a hydrogen atom. The total rate coefficient for these processes, assuming that the carbon atom fine states are in thermal equilibrium, was found to be 1.4×10^{-9} cm^3s^{-1} at 300K and the CH_2^+ channel (channel 802b) was found to represent approximately 1% of the total products.

§8.1.3: Previous attempts at ion-molecule chemistry involving neutral carbon atoms.

The work presented in this chapter is a continuation of work begun by Scott in his PhD. Thesis [70]. The generation and monitoring of neutral carbon atoms in a flow reactor is not a trivial problem and is one that neither the work of Scott nor the current endeavours have been able to provide an adequate solution for.

Scott attempted two experimental techniques, both based around the previously successful method (used to generate N, O, and H atoms) of using a microwave discharge. The first method was to directly discharge a dilute mixture of CO in either helium or argon. A N_2O^+ monitor ion was used, which is postulated to have a reaction with carbon atoms with CN^+ being the product (Reaction 805). The known reaction of N_2O^+ with CO does not interfere (i.e. it does not give an ionic

product with the same *m/z* ratio) with this CN^+ formation reaction or the possible secondary charge transfer reaction from CN^+ to CO to give CO^+.

$$N_2O^+ + C \quad => \quad CN^+ + NO + 1.6eV \qquad (805)$$

In these experiment the atom probe became liberally coated with soot for some distance downstream of the discharge but no CN^+ or CO^+ ions were observed.

The second method used an atom probe into which a section of thin, capillary-like, glass tube had been inserted. The microwave discharge was established on this region of the probe with argon flowing past. This process generates a high flux of $Ar^*(^3P_{2,0})$ metastables which can react with CO to produce C-atoms either by a direct or an indirect process (as outlined in Reactions 806-808).

$$Ar^*(^3P_{2,0}) + CO \quad => \quad C + O + Ar + <0.5eV \qquad (806)$$

$$Ar^*(^3P_{2,0}) + CO \quad => \quad CO^*(A\ ^1\Pi \text{ and } b\ ^3\Sigma^+) + Ar + <1.1eV \qquad (807)$$

$$CO^*(a\ ^3\Pi) + CO \quad => \quad C(^3P) + CO_2 + 0.4eV \qquad (808)$$

The $CO^*(a\ ^3\Pi)$ state is a metastable state that results from the decay of the $b\ ^3\Sigma^+$ state. Using this system Scott observed that significant concentrations of metastable argon atoms were generated and could transit the length of the probe and then enter the flow tube. This was determined by admitting a flow of neutral ethylene into the flow tube and observing that it was significantly ionised by the action of these metastable atoms (Ar ($^3P_2$) = 11.55 eV, Ar ($^3P_0$) = 11.72 eV, IP (C_2H_4) = 10.51 eV). Further, significant amounts of soot were observed on the inside of the probe and small signals of CO_2^+ were observed when ions capable of ionising neutral carbon dioxide were used as the monitor ion. However at no time was any direct evidence for the formation of carbon atoms observed, over a wide range of monitor ions. The levels of carbon atoms generated by either of these techniques are probably very low by the time they enter the flow tube. Whether this is due to atom-atom recombination, atom-neutral reaction, or atom-wall reactions is unknown however.

Section 8.2: Experimental techniques attempted in this work and results.

§8.2.1: Carbon atom techniques involving carbon suboxide.

Carbon suboxide synthesis.

Carbon suboxide (C_3O_2) is a gas at standard temperature and pressure, however it begins to thermally decompose around 15°C to give a brownish polymer [267]. For this reason it is essential to have an efficient synthesis for carbon suboxide if it is to be used as a precursor for carbon atoms. Samples may be stored under liquid nitrogen but even then will have a limited lifetime. Due to experimental difficulties that were encountered in the following literature preparations, a reasonably detailed synthesis will be presented here.

The basic method follows that of Miller and Fately [89] which is in turn similar to the method of Long *et al.* [268]. Both involve the dehydration of malonic acid ($C_3H_4O_4$) with phosphorus pentoxide. It was found necessary to use large excesses of the phosphorus pentoxide (~100g for 8g malonic acid) and 50g of furnace-dried sand was added to distribute the heating. In all the preparations performed in this work a magnetic stirrer was used. The magnetic flea inside the reaction vessel invariably became jammed as the reaction mixture thickened so it is recommended that a vacuum sealed mechanical stirrer run by a slow drive motor be used in future in place of this magnetic stirrer. Dehydration is performed under vacuum at approximately 125°C. Note that malonic acid can decarboxylate to give acetic acid and CO_2. This process occurs at approximately 140°C and provides significant impurities. The gaseous products are first passed through a dry ice/acetone trap to remove any acetic acid and then into a liquid nitrogen trap. The addition of the dry ice/acetone trap was suggested by Strauss *et al.* [269] and replaces the lime tower (Ca + CaO) used by Long *et al.* [268]. The 'product' trapped by liquid nitrogen cooling was then allowed to warm to dry ice/acetone temperatures and successive portions of carbon dioxide removed. Final purification was achieved through the use of an ethanol slush bath.

Carbon atom generation via the flash photolysis of C_3O_2.

Husain and his group have been studying the atom-neutral reactions of various atomic carbon states with a range of neutral molecules for quite some time. They [270, 271. 272] and other workers [273, 274] have had considerable success generating carbon atoms using an ultraviolet (UV) flash apparatus with C_3O_2. The primary processes are shown below however Braun *et al.* suggest that Reaction 809b is not significant when the correct wavelengths are used [273].

$$C_3O_2 + h\nu \quad => \quad C(^3P) + 2CO \qquad (809a)$$

$$=> \quad C_2O + CO \qquad (809b)$$

Husain and co-workers use a slow-flow system where the decay of the carbon atoms generated by each pulse is monitored in absorption by a vacuum monochromator operating at 166nm (C [$3s(^3P_0) \leftarrow 2p^2(^3P)$]). Though the rate reported for Reaction 810 is quite fast, the system should provide sufficient carbon atoms for kinetic evaluation of ion-carbon atom reactions to be achieved.

$$C(^3P) + C_3O_2 \quad => \quad \text{products} \qquad (810)$$

$$k = 1.8 \times 10^{-10}\ cm^3s^{-1}.$$

It should be possible to get a rough calibration of the amount of carbon atoms generated by monitoring the amount of carbon monoxide concurrently generated and halving it.

In our experiment flash photolysis was effected using apparatus constructed by Prof. Leon Phillips in this Department. A schematic diagram of the equipment designed to test the concept is shown below.

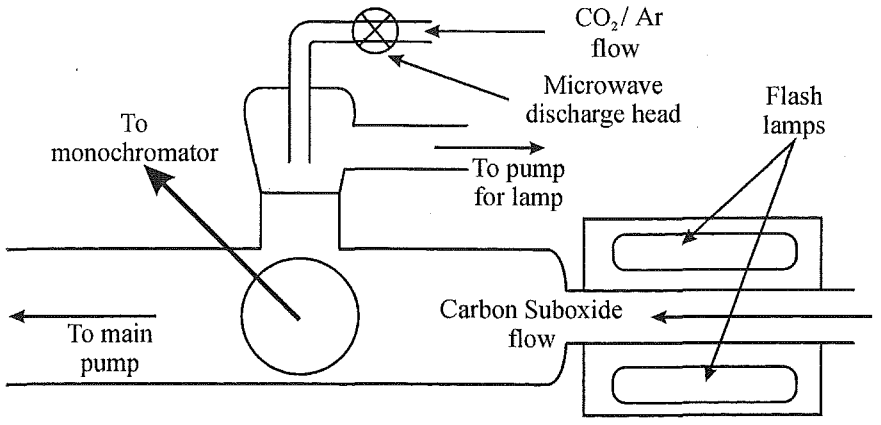

Figure 8.1: The general layout of the flash photolysis equipment designed to generate and monitor a flow of neutral carbon atoms.

A dilute mixture of carbon suboxide and helium flows past the flash lamps in a pyrex tube. These broad-spectrum lamps are pulsed at a high repetition rate (~15 Hz) in an effort to provide as continual as possible ultra violet irradiation to the flowing helium/C_3O_2 mixture. It was hoped that this UV irradiation would dissociate the flowing suboxide effectively. In order to detect the carbon atoms a monochromator was set to observe the 166 nm line of excited carbon atoms. A carbon lamp provided the reference signal for this line. This lamp consisted of a flow of a dilute argon/carbon dioxide mixture which was subject to a microwave discharge and gave a bright blue discharge.

A small background of 166 nm emission was seen from this carbon lamp, however the signal did not significantly increase when the flash apparatus was used to irradiate the carbon suboxide. Several attempts with different samples of carbon suboxide were investigated, but without success.

It was later realised that there was a flaw in the experimental methodology presented above; namely that carbon suboxide has essentially no absorptions in the region that was being irradiated [275]. The main absorption band is situated in the range 145-180 nm which is well into the vacuum ultraviolet region of the spectrum. The presence of an air gap and normal glass walls in the reactor will effectively block off any light below 200 nm. Thus the carbon suboxide flow was absorbing only very small amounts of energy from the flash lamps and undergoing very little dissociation. The dissociation dynamics of carbon suboxide at 193, 248, and 266 nm have been investigated by McFarlane *et al.* [276] using either a neodinium:YAG laser or an excimer laser. Reaction 809a was found to become important at wavelengths shorter than 207 nm where single photon processes are capable of producing carbon atoms. At 193 nm the branching ratio between C_2O + CO and C + 2CO was found to be 94%:6%. This may be compared to the branching ratio of Braun *et al.* [273] who found that in the range 140-170 nm somewhere >75% of the dissociations gave carbon atoms. Clearly the poor absorbance of energy above ~185 nm is affecting this product ratio. Carbon atoms formed at the other wavelengths used in the McFarlane *et al.* study (248 and 266 nm) were found to be generated by two-photon processes and were at very low levels.

C_3O_2 discharge-based systems.

After it was found impractical to proceed with the flash lamp approach several other different methods using a microwave discharge and carbon suboxide were attempted. This methodology was similar to the second method attempted by Scott [70] presented above. In these cases the hope was to replicate the photolysis process (Reaction 809) without the need for vacuum UV light.

Several attempts were made using a system designed to allow helium (2^3S) metastables to react with the suboxide. The first experiments were performed using a hydrogen carrier in the SIFT reaction tube. Kr^+ ions were injected from the FA (see Chapter 4 for details) and a high signal of H_3^+ was generated. In place of the usual ring inlet (used for kinetic studies) an atom-type probe [70, 277] with a large mixing volume included was used at the most downstream inlet. The atom probe used was identical to that used by Scott for his NO titration work except the glass coil had been removed. A flow of helium was passed through a microwave discharge and then the carbon suboxide was added further down the probe (i.e. closer to the inlet to the SIFT flow tube).

No direct evidence of C atom formation was observed. However there was indirect evidence for CO formation from the reaction of He (2^3S) with C_3O_2 as the signal at $m/z = 29$ (either N_2H^+ or HCO^+) was seen to drop when the microwave discharge was turned off. This was taken to be indicative of neutral CO formation in the discharge region. The isobaric N_2H^+ ion was discounted as the formation of N_2 in the discharge was deemed unlikely.

This CO could either result from carbon suboxide, indicating concurrent carbon atom formation, or from CO_2, which would give an oxygen atom. No evidence for the fast $H_3^+ + O$ reaction [70, 278] (in the form of OH^+ or H_2O^+) was observed which would be expected if CO_2 was the source of CO. In the presence of excess hydrogen, both OH^+ and H_2O^+ would be converted to H_3O^+ ion making an absolute determination difficult as H_3O^+ is always present as an impurity ion. There was also no evidence for CH_3^+ formation (the product of secondary reactions with the hydrogen carrier from both CH^+ and CH_2^+).

It was surmised that the reaction distance was too great and that any carbon atoms formed were undergoing neutral reactions - either with C_3O_2 [270], another neutral, polymerising, or undergoing wall reactions. Thus the large reaction volume

was removed from the probe, and the "showerhead" inlet through which the C_3O_2 was being added was reversed in order to eject the gas in the same direction as the neutral flow. These modifications proved unsuccessful as high signals of H_3^+ were also generated from the microwave discharge. It is possible that an OH^+ and H_2O^+ signal were observed here, indicating oxygen atom formation. The complexity of the system was judged to be too great however and other alternatives were pursued.

A further discharge approach was attempted using argon metastables, which were generated upstream in the neutral inlet system. The metastable energies of argon (Ar ($^3P_2$) = 11.55 eV, Ar ($^3P_0$) = 11.72 eV,) are significantly lower than that of the helium metastables. They are also lower than the appearance energies for any ionic fragments formed from carbon suboxide, the lowest of which is C_2O^+ at approximately 14.5eV [92]. In these experiments a helium carrier rather than a hydrogen one was used as the last experiments using helium metastable generated large amounts of H_3^+ from reactions of helium ions with the hydrogen carrier or by discharge of hydrogen gas that had diffused back up the atom probe.

The first attempt used a relatively standard atom probe, but the levels of metastable atoms (using ethylene as a monitor (IP (C_2H_4)=10.51 eV) were found to be quite low. The probe was then modified to include an approximately 40 mm section of thin (4 mm o.d.) glass tube. This has been shown to increase the density of the metastables produced by the discharge [70]. In this case the test, again using a flow of ethylene as a monitor for the metastable atoms, showed in excess of 10 pA (i.e. ~40,000 cps) of ion signal at the molybdenum disk, indicating that there were plenty of metastable atoms being produced.

The probe was then set up with a signal of H_3^+ ions in the reaction flow tube. It was not possible to introduce a sufficient signal of H_3^+ at as low an energy as is desirable and thus HeH^+ and ArH^+ signals were also observed. With the discharge on, but *without* the carbon suboxide flowing, a small signal at *m/z* = 14 was observed, probably N^+ from nitrogen impurities in the helium and/or argon supply. When the carbon suboxide was added, new peaks were seen that correspond to $HC_3O_2^+$, $C_3O_2^+$ (small), HCO_2^+ and an unidentified signal at 43 amu. When the discharge was switched back on after being switched off (in order to determine if the 43 amu ion was a result of the discharge) the ion signal at 43 amu was observed to be much greater than any of the primary ions could generate. Thus it seems that this ion is being

generated in the discharge rather than being the reaction of the H_3^+ ion (or any of its products) with a neutral reactant. The nature of this ion is however unknown. No evidence for the occurrence of Reaction 809 was observed either in the form of carbon atoms or new CO molecules. It appears that argon metastables are ineffective at forming carbon atoms from carbon suboxide.

§8.2.2: Other attempts at carbon atom generation.

Active nitrogen and cyanogen.

Another method for the generation of carbon atoms in a flow tube involves the reaction of "active nitrogen" with carbon-containing compounds. Kley *et al.* [279, 280] and others [281] have used this method to produce carbon atoms for reaction studies that have been monitored with a monochromator. Essentially the method involves adding very small amounts of cyanogen to a flow of pure nitrogen gas which has passed through a microwave discharge. Other carbonaceous compounds have been used as a "fuel" gas as well as C_2N_2 (HCN, C_2H_2, CH_4, C_2H_6, C_2H_4, C_3H_4) but all give exclusively C (^3P). Of all of these reactants, C_2N_2 was found to be the most effective. The reaction in the C_2N_2 case is believed to begin by the –C-C- bond breaking of cyanogen to give one (Reaction 811) or two (Reaction 812) CN radicals.

$$N + C_2N_2 \Rightarrow CN + CN_2 \quad (811)$$

$$N_2^* + C_2N_2 \Rightarrow 2CN + N_2 \quad (812)$$

Both N atoms and nitrogen metastables (N_2^*) can be found in the "active nitrogen" formed after discharging a flow of pure nitrogen. Whichever of these reactions (or possibly both) initiates the chain it is believed that the next reaction is:

$$CN + N \Rightarrow N_2 + C \quad (813).$$

Kley *et al.* report a nearly stoichiometric yield of carbon atoms when very small amounts of cyanogen are used. In these experiments [279, 280] the total concentrations used were in the range 5-25 Torr of Ar and N_2 and between 10^{-2} and 5×10^{-4} Torr of C_2N_2. Although it was reported that the nitrogen atom density was higher than the carbon atom density [280] it was hoped that there would still be enough carbon atoms to observe.

Several different variants of the C_2N_2 titration reaction were investigated in the present study. The first experiment was performed using pure nitrogen, pure cyanogen and an atom probe [70] that had ~160 mm reaction distance between the introduction of the cyanogen gas and entry into the SIFT flow tube. The microwave discharge was placed at two different distances from the point of introduction of cyanogen in different experiments. Cyanogen was introduced to the probe via a showerhead type glass inlet that added gas in the same direction as the flow i.e. away from the discharge. The two different distances were used to test whether back-streaming of cyanogen would allow it to be directly subjected to the microwave discharge, thus causing sooting in a similar fashion to that observed by Scott. With the microwave discharge approximately 200 mm upstream from the inlet where cyanogen was introduced, no clear indication of carbon atom formation was seen with an H_3^+ monitor ion. Note that this monitor ion was not exceptionally pure with small (~1/4 of the primary ion count) impurities of He^+ and HeH^+. An initially encouraging $m/z = 38$ ion signal was observed (presumably C_2N^+) but this was found to also be present without the active nitrogen flowing. Thus it is likely to be a result of the reaction between helium ions and cyanogen (Reaction 814).

$$He^+ + C_2N_2 \Rightarrow C_2N^+ + N + He + 491 \text{ kJ mol}^{-1} \quad (814)$$

This reaction has not been previously observed but C_2N^+ is one of the major products in the similar reaction between He^+ and HC_3N. A small amount of N^+ was observed, indicating that there was atomic nitrogen present. No direct test for nitrogen atoms was attempted however (e.g. injecting the $C_2H_2^+$ ion and observing a decay with the N_2/N mixture, noting that only *atomic* nitrogen reacts with $C_2H_2^+$). One potential problem is that any product of the H_3^+ + C reaction (presumably mainly CH^+) could react further with one of the other neutrals present in the mixture. An association of CH^+ with molecular nitrogen has been reported (Reaction 815), but no evidence of a 41 amu ion that was correlated with the discharge was observed in the present study.

$$CH^+ + N_2 + M \Rightarrow CHN_2^+ + M \quad (815)$$

$$k = 5\text{x}10^{-29} \text{ cm}^6\text{s}^{-1} \text{ (M = He)}$$

$$k = 8\text{x}10^{-13} \text{ cm}^3\text{s}^{-1} \text{ @ 0.5 Torr He.}$$

It seems likely that a reaction of CH^+ with cyanogen would give $HC_2N_2^+$ (at least partly) as cyanogen has a PA similar to that of water, for which proton transfer is the major channel observed when it is reacted with CH^+.

With the microwave discharge moved closer to the cyanogen inlet by 60 mm no major differences were observed as compared to the case presented above. During the course of this investigation, the nitrogen was accidentally switched off with the microwave discharge still running. Within a few seconds the area surrounding the discharge became heavily sooted as cyanogen diffused up into this region. A bright blue discharge glow was observed concurrently with this event. The "soot" appeared to be partly a cyanogen polymer as an argon discharge on this region (without cyanogen flowing) gave neutral C_2N_2 (detected as $C_2N_2H^+$ in the SIFT) and ionic and neutral CN_2 (detected as C_2N^+ and HC_2N^+ respectively). It seems likely that an amorphous C-N polymer was formed.

The probe was then cleaned and reinstalled and further experiments conducted. The first used a nitrogen/argon mixture as the source gas for the "active nitrogen". It was deemed possible that there was insufficient break-up of the cyanogen to CN radicals when only nitrogen was used and it was hoped that the presence of argon metastables would help this situation. Little difference was found here compared with the previous experiments, except that there was no mass 38 ion signal observed. This is probably because there were much less He^+ impurity ions present at this time. This system was also less ideal as the product of Reaction 815 (CHN_2^+) was no longer observable because of a mass co-incidence with ArH^+. In all cases however the m/z = 41 ion was observed to drop with increasing cyanogen flow which suggests that the ion was ArH^+. This ArH^+ is the result of the reaction of HeH^+ + Ar(formed from H_3^+ excited during the injection process) and H_3^+ (v>1) + Ar. There were always small but significant amounts of each present due to the necessity to use slightly higher FA nose cone voltages than is usual in an effort to boost the H_3^+ signal. Other tests using more dilute "fuel gas" mixtures were also tried (approximately 10% and 1% mixtures of C_2N_2 in helium) but with little noticeable effect.

In the literature it appears that in all cases where the formation of carbon atoms was observed, the formation of these C atoms was accompanied by the observation of a blue chemiluminesce or 'flame'. Excited CN radicals are usually proposed to be the source of this glow and these are probably necessary for the formation of the carbon atoms. This glow was never observed in the current experiments. The exact reason for the non-observance of this phenomenon is unknown. Possible explanations include the gas mixture composition used (e.g. too

much or not enough cyanogen), the overall pressure, the distances between the discharge, cyanogen introduction and the inlet to the tube (i.e. probe design), or power in the microwave discharge. If this work is to be pursued further, a test rig resembling that constructed for the flash photolysis work should be constructed and the individual variables optimised in a situation where the carbon atoms can be directly observed.

Microwave discharge on dilute carbon dioxide mixtures.

In an approach similar to that used by Scott, a microwave discharge was applied directly to a flowing stream of carbon dioxide. A very dilute mixture (~5%) of carbon dioxide in helium had been reported to produce carbon atoms without significant sooting [282]. No evidence of either sooting or carbon atom generation was seen in the current investigation. H_3^+ was again used as the ionic probe. Subsequently it has been reported that the probe needs to be maintained at elevated temperatures to get reasonable carbon atom yields using this technique.

Section 8.3 Conclusions.

Unfortunately the main result of this section of work has been to add more data to the list of unsuccessful methods that have been tried in order to produce carbon atoms in a fast flow reactor such as the SIFT. However it is encouraging that the method that was seen as the most likely candidate for solving this problem, the flash photolysis of carbon suboxide, has not failed out of hand. The wavelengths used for the photolysis in the current study are now believed to be too long to be effective in dissociating the carbon suboxide. A new reactor, incorporating a co-axial flash system, no air gap between the flash lamp and the carbon suboxide cell, with Suprasil quartz walls in the reactor will need to be constructed in order to effectively assess the merits of this technique. This will allow vacuum ultraviolet radiation to reach the carbon suboxide efficiently and will hopefully allow this to be dissociated via Reaction 809. The synthesis of relatively pure carbon suboxide has been optimised and should no longer present a problem for this method.

Other methods reported in the literature have also been tried and have not been successful. The active nitrogen method of Kley *et al.* appears the next most

probable method to succeed and construction of a test rig with a monochromator to detect the carbon atoms may help in perfecting this method if further development is deemed necessary.

Chapter 9

Final comments and suggested further work.

Section 9.1: A summary.

One of the most important goals of this work was to upgrade the previous SIFDT at the University of Canterbury to a flowing afterglow sourced FA-SIFDT. The previous SIFDT suffered somewhat from the ion sources (both low and high pressure electron impact type sources) that were available for use in it. These ion sources limited the range and counts of ions that could be created and were labour intensive, requiring frequent cleaning. Also problematical in the ion source region of the old SIFDT was the resolution on the upstream quadrupole and the energy of injection. This meant that it was not uncommon to not be able to inject a single mass without contamination from ions at adjacent masses. The new FA-SIFDT has solved many of these problems and much of the work presented in this thesis would simply not have been possible on the previous SIFDT. A detailed discussion of the design, construction and testing of the FA-SIFDT is presented in Chapter 2 of this work.

Also presented is a comparison of the two major types of venturi injector, the hole injector, first constructed at Birmingham, and the annulus injector, designed at NOAA. The performance of two different inner venturis each with the same cross-sectional area for gas injection has been investigated with respect to a range of performance indicators. The annulus injector was found to have superior performance when the pumping efficiencies and ability to inject cluster ions was compared. Little difference was discernible between the two injectors when the transmission efficiency of each was investigated and neither inlet was capable of injecting the 2-propenyl cation without it isomerising to the more stable allyl form. The annulus injector was also found to be more capable of operating without a companion, non-critical inlet, through which to direct part of the carrier gas flow. Thus it would seem that the annulus injector is slightly more efficient at forming the necessary barrel shock and that injection through the annulus injector is marginally less energetic. One however must balance against this the increased mechanical complexity of the annulus injector

and this alone may make potential SIFT users choose the apparently somewhat inferior, but certainly simpler, hole-type venturi injector.

In concert with the creation of the new FA-SIFDT the Canterbury ion-molecule group has begun studies of the trace components in air samples using the SIFT as a chemi-ionisation mass spectrometer. This technique is known as SIFT-MS. Using the SIFT in this manner it is possible to identify and measure the amounts of many trace species present in air in real time. Because of the nature of the chemi-ionisation agents used (O_2^+, H_3O^+, and NO^+) this can be done without the need for trapping or preconcentration of the gases, as none of the chemi-ionisation agents have significant reactions with the major species present in air.

In the course of this work several preliminary studies have been conducted using the SIFT-MS. The analysis of breath has been a major focus and two projects of this type have been invetsigated. The first is observing the changes in the major trace species present on breath (ammonia, acetone, and isoprene) as the subjects undergo exercise. The levels of acetone have been shown to rise, presumably as a result of the rise in importance of fatty acid metabolism and thus an increase in the production of ketone bodies (including acetone) in the subject's body. The levels of isoprene drop off rapidly after exercise is begun and stay at a constant low level throughout the exercise. This is believed to be a result of the increased gas expiration rate flushing the body of isoprene, i.e. loss processes exceeding formation processes. The low level remains low for some time after exercise was terminated. The results for ammonia are still inconclusive but it appears that the amount of ammonia on the breath is not radically effected by exercise. The second breath study deals with the identification and monitoring of solvent levels on the breath of subjects exposed to polluted air. The SIFT-MS enables rapid quantification of the amounts of solvent on a subject's breath and can be easily used to monitor the fall-off of solvent concentration in the breath of a person exposed to even low levels of solvent. Tests using a mixture of xylene and mesitylene have shown the applicability of the SIFT technique to this type of analysis and its ability to measure multiple solvent concentrations simultaneously.

The other trace gas analysis system that has been investigated is the analysis of the gases emitted by a soil block after an artificial urine solution is added. This has been performed using head-space analysis. The soil block is sealed in a container for a short amount of time and then the gas collected during this time is analysed. The SIFT

technique has a great advantage over the gas chromatographic techniques that are conventionally used in that it can measure concentrations rapidly with a minimum amount of sample manipulation. Ammonia and nitric oxide have been detected in the headspace above the soil and their time profiles monitored.

The reactions of H_3^+, N_2H^+, and H_3O^+ with a range of small and medium hydrocarbons have been investigated. H_3^+ is ubiquitous in the interstellar medium and may play an important role as an ionic agent for partially reversing molecular synthesis. It has a very low proton affinity and thus its proton transfer reactions are usually very exothermic. This leads to the dissociation of the neutral reactant into a number of smaller ionic and neutral fragments. As well as this interstellar interest there is also a desire to understand how the energy involved in a proton transfer reaction is partitioned among the products. In the current study it has been observed that when many exothermic reaction channels exists those reaction channels that are greater than 100 kJ mol^{-1} are most commonly observed. Also when the exothermicity of the reaction exceeds approximately 200 kJ mol^{-1} other, dissociative, reactions become much more likely.

Chapter 5 contains a re-evaluation of the proton affinity of cyanogen. Petrie remarked that, with a lowering of the PA of methyl chloride the literature was left with a contradiction. A new value of 651±2 kJ mol^{-1} has been determined using the equilibrium method. This value has been determined by reference to the C_2H_2/C_2N_2 proton transfer system which has been observed in both directions. The previously measured CH_3Cl/C_2N_2 system has also been re-evaluated using the new, lower, value for the PA of methyl chloride and this value agrees well with the value determined by the newly measured cycle. The reactions of several of the alkyl ion-cycanogen adducts have also been investigated, in particular the methyl cation affinity of cyanogen. In all the cases investigated these alkyl cation-cyanogen adducts behaved in a manner that in consistent with a strongly bound, covalent-type, structure. Several other methyl cation transfer reactions, of the methylated formaldehyde and dimethyl ether ions, have also been investigated.

Chapter 6 contains ion-molecule reactions relevant to the atmosphere of Titan. These reactions can be divided into two broad classes, bimolecular reactions of N_3^+ and N_4^+ with a range of hydrocarbons, and the termolecular associations of several of the terminal ions in Titan's atmosphere (H_3O^+, $HCNH^+$, c-$C_3H_3^+$) with

methane, ethylene, and acetylene in both helium and nitrogen carriers. The reactions of the N_3^+ and N_4^+ ions were shown to be generally less dissociative than their counterpart N^+ and N_2^+ reactions.

No association reactions between c-$C_3H_3^+$ and any neutral were observed, nor were any association reactions of methane observed with any of the three ions investigated. The remaining association reactions were seen to be between 3 and 13 times more efficient in a nitrogen carrier than a helium one. The magnitude of this effect is greater than that indicated by the previously available literature results which (for more simple systems) suggested that the associations would be between 1.5 and 5 time more rapid. Finally the structures of the adducts formed from the reactions of $HCNH^+$ and C_2H_2 and C_2H_4 were investigated using a range of neutral reagents. The reaction of the $C_3H_4N^+$ adduct with benzene indicates that approximately one third of the ions formed from the reaction of $HCNH^+$ and acetylene are of a relative strongly bound form (and are able to associate with benzene). This ions are probably covalently bound. In the second reaction system the $C_3H_6N^+$ adduct was shown to be primarily strongly bound and was able to associate with benzene.

The association reactions of CH_2CHCN^+ and CH_2CHCNH^+ with acrylonitrile were also investigated. These reaction have been studied before at Canterbury but the resolution of the previous SIFT was not great enough to inject only a single ion. The CH_2CHCN^+/CH_2CHCN system was found to have two products, one with bimolecular kinetics and one with termolecular kinetics. Contrary to expectations the bimolecular channel is still the dominant channel at SIFT tube pressures and the reaction appears to be pressure saturated. In order to account for this observation a two-well model has been proposed such that there is one complex (the loosely bound one) that is not saturated at SIFT pressures and another (the tightly bound one) that is. The complexes have very different lifetimes and the loose complex will only be saturated at much higher pressures and it thus provides a continual source of bimolecular channel. The CH_2CHCNH^+ system is much simpler showing only termolecular reaction that has yet to saturate at SIFT pressures.

Finally work has continued on the attempts to generate a measurable flow of neutral carbon atoms to use as a neutral reactant for ion-atom reaction studies. Flash photolysis of carbon suboxide was attempted without success. This is due to the use of the incorrect wavelength irradiation and a new vacuum UV flash cell will be needed

to continue this work. An active nitrogen-cyanogen system was also tried, again without any obvious success.

Section 9.2: Suggestions for further work.

One major advantage of the new FA-SIFDT was the increased ion counts available. Now that it has been realised how much this increased ion count simplifies the work, especially when the SIFT is being used as a SIFT-MS instrument for trace gas analysis, there is a desire to further increase this available ion current. The limiting factor now appears to be the ion source and some attempt has been made to construct a new glow (or hollow cathode) type ion source. This initial work has been promising but unsuccessful. More work needs to be done on this type of ion source and perhaps one where the FA is not used (like that used for Lindinger's PTR-MS instrument) would be helpful. A Wood's horn should also be installed on the previously constructed hollow cathode source as the current problem may be photons emitted by the He^+ ions [24].

The previously unserviceable liquid nitrogen cold trap above the 6" diffusion pump has recently been replaced, though it is too soon to tell if it will keep the upstream quadrupole cleaner.

The efficiacy and usefulness of trace gas analysis with the Canterbury SIFT has been shown in this work, and it appears that this field of study will become an important one for the Canterbury ion-molecule group. An independent validation of trace gas analysis at Canterbury should be performed, perhaps using a commercial gas mixture. Such work has been done by Smith and Spanel on their instruments in Britain [51], but has not been performed at Canterbury.

The analysis of the changes in breath VOC concentration should be further pursued, probably to more extreme conditions. It would be interesting to see if the onset of ammonia production that occurs with the beginning of muscle metabolism can be observed using this technique. More investigations of the sampling procedure also need to be performed as it is often difficult to get good samples from subjects who are approaching exhaustion. The analysis of solvent levels on breath is currently continuing and appears to be very promising, the levels of solvents of subjects blood

has also been measured. A combined study of breath, blood and urinalysis would be the most effective method of monitoring and characterising the uptake and destruction of organic solvents in the human body. This is also an ideal opportunity for the SIFT to be applied to real world, industrial applications, and the monitoring of solvents levels in the breath and blood of subjects who are regularly exposed to solvents would also be a worth while project.

A further investigation of the differences observed between soil samples made in different manners (i.e. watered before or concurrent with the addition of the artificial urine) would be beneficial to a more thorough understanding of this system. Investigation of the soil response to different concentrations and amounts of this "urine" should also be undertaken.

There are several further experiments that could add greater understanding to the energetic proton transfer systems discussed within Chapter 4. Some lower pressure studies of some of the reaction would be useful to ensure that the carrier gas is not having an effect on the product distribution. This work would be best done in a two section ICR instrument where the ions could be thermalised before they are transported into the reaction cell. The reactions of HeH^+ and He_2H^+ should be further persued in an effort to extend the energy range of this study and also to characterise the reactions of the novel, He_2H^+ species. Further the reactions of a species with a proton affinity between water and nitrogen would also help to complete the picture begun by the data presented here. Possible candidates for this task could be HNO_2^+, or HSO_2^+. Finally a theoretical investigation of the barriers to formation of the individual channels for some of these reactions would begin to help in an understanding of just how much energy is actually deposited in the collision complex when proton transfer occurs.

It would also be useful to remeasure some of the faster H_3^+ reactions using a dilute mixture of the neutral gas in helium as the neutral reactant. This would enable one to determine if the rate coefficients of these faster reactions are less than the collision rate due to a systematic instrument effect, or real chemical effect.

The initial results of the methyl cation transfer reactions from $CH_3OCH_2^+$ and $(CH_3)_3O^+$ suggest that this type of investigation would be relatively easy in the FA-SIFDT. A fuller investigation of the reactions presented here, and a range of other similar is desirable in order to gain a better understanding of methyl cation transfer

processes. Due to the high counts of $CH_3OCH_2^+$ available and the fact that it has been observed to transfer a methyl cation it would seem an ideal reactant for such an investigation. The reaction of $CH_3OCH_2^+$ with cyanogen would also be interesting to see if the trend of not observing methyl cation transfer to cyanogen is continued with this reactant.

Further reactions of N_3^+ and N_4^+ with acetylenic species are also suggested. It has been observed that N_3^+ gives the novel $C_2H_2N^+$ product when reacted with acetylene and it could be posited that this is the result of reaction with the C≡C moiety. Further reactions with neutrals such as methylacetylene, diacetylene, and cyanoacetylene could yield interesting results. Further investigation of the H_3O^+/C_2H_2 reaction system is also needed in order to ascertain the reason for the curved decays that were observed for this system. Low temperature reactions of the CH5+.CH4 ion should also be performed. It seems likely that this ion will be important in the lower reaches of Titan's lower ionosphere and the exact nature of the bonding that occurs between the CH_5^+ and methane moiety will determine whether this ion provides an efficient method of protonating species at low altitudes or provides a nucleation centre for further association.

Finally, the work begun on the reaction of H_3^+ with carbon atoms needs to be continued. The next step is probably the construction of a co-axial flash stsyem with Suprasil quartz walls in order to attempt the vacuum UV photolysis of carbon suboxide. This is the simplest system that has been attempted over the course of the investigations of method of forming carbon atoms and I believe it should be pursued until it has been conclusively shown whether it is suitable for a fast flow reactor.

References.

1 V.G. Anicich, J. Phys. Chem. Ref. Data, 22, 1469, (1993).

2 Y. Ikezoe, S. Matsuoka, M. Takebe, A. Viggiano, *Gas phase ion-molecule reaction rate coefficients through 1986*, Ion reaction research group of the mass spectrometry society of Japan, Tokyo, (1987).

3 M.J. McEwan, L.F. Phillips, *The chemistry of the atmosphere*, Edward Arnold, London, Chapter 6, (1975).

4 W. Deiminger, R. Leitinger, K. Davies, in *The upper atmosphere: Data analysis and interpretation*, W. Dieminger, G.K. Hartmann, R. Leitinger Eds. Springer-Verlag, Berlin, p644-705, (1996).

5 J.W. Chamberlain, D.M. Hunten, *Theory of planetary atmospheres. An introduction to their physics and chemistry. Second edition*, Academic Press, Orlando, Chapter 5, (1987).

6 B.W. Reinisch, in *The upper atmosphere: Data analysis and interpretation*, W. Dieminger, G.K. Hartmann, R. Leitinger Eds., Springer-Verlag, Berlin, p370, (1996).

7 G.C. Reid, in *Physics and Chemistry of Upper Atmospheres*, B.M. McCormac Ed., D. Reidel Publishing Company, Dordrecht and Boston, p99, (1973).

8 A.A. Viggiano, D.E. Hunten, *J. Mass Spectrom.*, **34**, 1107, (1999).

9 P.H. Dawson Ed., *Quadrupole mass spectrometry*, Elsevier Scientific, Amsterdam, (1976).

10 W.M. Brubaker, *Advances in Mass Spectrometry*, **4**, 293, (1967).

11 D. Smith, P. Spanel, *Mass Spectrom. Revs.*, **14**, 255, (1995).

12 F.C. Fehsenfeld, *Int. J. Mass Spectrom. Ion Phys.*, **16**, 151, (1975).

13 F. C. Feshenfeld, A. L. Schmeltekopf, P. D. Goldan, H. I. Schiff, E. E. Ferguson, *J. Chem. Phys.*, **44**, 4087, (1966).

14 F. C. Feshenfeld, A. L. Schmeltekopf, P. D. Goldan, H. I. Schiff, E. E. Ferguson, *J. Chem. Phys.*, **44,** 4095, (1966).

15 N. Twiddy, *Contemp. Phys.*, **15**, 427,(1974).

16 E.E. Ferguson, *Adv, in Electron. Electron Phys.*, **24**, 1, (1968).

17 E.E. Ferguson, *Revs. Geophys. Space Phys.*, **9**, 997, (1971).

18 A. Good, D.A. Durden, P. Kebarle, *J. Chem. Phys.*, **52,** 222, (1970).

19 N.G. Adams, D. Smith, *Int. J. Mass Spect. Ion Phys.*, **21**, 349, (1976).

20 N.G. Adams, D. Smith, *Int. J. Phys. B*, **9**, 1439, (1976).

21 D. Smith, N. G. Adams, *Advances in Atomic and Molecular Physics,* **24,** 1, (1988).

22 N.G. Adams, D. Smith, in *Techniques for the Study of Ion Molecule Reactions, Techniques in Chemistry Volume XX,* J.M. Farrar, W.H. Saunders Eds., **John** Wiley and Sons, New York, 165, (1988).

23 D. Smith, P. Spanel, *Experimental Methods in the Physical Sciences,* **29,** 273, (1995).

24 S.T. Graul, R.R. Squires, *Mass Spectrom. Revs.,* **7,** 263, (1988).

25 A.J. Kliore, in *Venus and Mars: Atmospheres, Ionospheres, and Solar Wind Interactions. Geophysical Monograph 66*, J.G. Luhman, M. Tatrallyay, R.O. Peppin Eds., American Geophysical Union, 265, (1992).

26 S.K. Atreya., *Atmospheres and Ionospheres of the Outer Planets and their Satellites*, Springer Verlag, Berlin, 28, (1986).

27 R.W. Schunk, A.F. Nagy, *Rev. Geophys. Space Phys.*, **18**, 813, (1980).

28 L. Colin, *J. Geophys. Res.*, **85**, 7575, (1980).

29 C.T. Russell, in *Venus and Mars: Atmospheres, Ionospheres, and Solar Wind Interactions. Geophysical Monograph 66*, J.G. Luhman, M. Tatrallyay, R.O. Peppin Eds., American Geophysical Union, 225, (1992).

30 W.C. Knudsen, in *Venus and Mars: Atmospheres, Ionospheres, and Solar Wind Interactions. Geophysical Monograph 66*, J.G. Luhman, M. Tatrallyay, R.O. Peppin Eds., American Geophysical Union, 237, (1992).

31 D.M. Hunten, in *Encyclopedia of the Solar System*, P.W. Weissman, L.A. McFadden, T.V. Johnson Eds., Academic Press, San Diego, p147, (1999).

32 A.F. Nagy, T.E. Cravens, S.G. Smith, H.A. Taylor Jnr., H.C. Brinton, *J. Geophys. Res.*, **85**, 7795, (1980).

33 H.B. Niemann, W.T. Kasprzak, A.E. Hedin, D.M. Hunten, N.W. Spencer, *J. Geophys. Res.*, **85**, 7817, (1980).

34 H.A. Taylor Jnr., H.C. Brinton, S.J. Bauer, R.E. Hartle, P.A. Cloutier, R.E. Daniell Jnr., *J. Geophys. Res.*, **85**, 7765, (1980).

35 S.K. Atreya, *Atmospheres and Ionospheres of the Outer Planets and their Satellites*, Springer Verlag, Berlin, (1986).

36 D. Smith, P. Spanel, *Int. J. Mass Spectrom. Ion Proc.*, **129,** 163, (1993).

37 D. Smith, *Chem. Rev.*, **92,** 1473, (1992).

38 T. Gougousi, R. Johnsen, M.F. Golde, *Int. J. Mass Spec. Ion Proc.*, **149,** 131, (1995).

39 *Passage to a ringed world. The Cassini-Huygens mission to Saturn and Titan. NASA SP-533*, L.J. Spilker Ed., National Aeronautics and Space Administration, Washington, (1997).

40 *Cassini mission plan. 699-100, Revision F*, J.C. Frautnik Custodian, Jet Propulsion Laboratory, Pasadena, (1995).

41 E. Herbst, *Annual Review of Physical Chemistry,* **46,** 27, (1995).

42 W.W. Duley, D.A. Williams, *Interstellar Chemistry*, Academic Press, London, (1984).

43 E.F. van Dishoek, J.H. Black, *Astrophys. J. Suppl.*, **62**, 109, (1986).

44 R. Federman, *Astrophys. J.*, **257**, 125, (1982).

45 D. Smith, *Int. J. Mass Spec. Ion Proc.*, **129,** 1, (1993).

46 B.R. Rowe, D.C. Parent, *Planetary and Space Science,* **43,** 105, (1995).

47 B.R. Rowe, G. Dupreyat, J.B. Marquette, P. Gaucheral, *J. Chem. Phys.*, **80,** 4915, (1984).

48 P. Spanel, D. Smith, *Medical and Biomedical Engineering and Computing,* **34,** 409, (1996).

49 D. Smith, P. Spanel, *Int. Rev. Phys. Chem.*, **15,** 231, (1996).

50 D. Smith, P. Spanel, J. Thompson, B. Rajan, J. Cocker, P. Rolfe, *Appl. Occup. Environ. Hyg.*, **13,** 817, (1998).

51 P. Spanel, J. Cocker, B. Rajan, D. Smith, *Ann. Occup. Hyg.*, **41,** 373, (1997).

52 W. Lindinger, A. Hansel, A. Jordan, *Int. J. Mass Spectrom. Ion Proc.*, **173,** 191, (1998).

53 W. Lindinger, A. Hansel, A. Jordan, *Chem. Soc. Revs.*, **27,** 347, (1998).

54 A. Hansel, A. Jordan, R. Holzinger, P. Prazeller, W. Vogel, W. Lindinger, *Int. J. Mass Spectrom. Ion Proc.*, **149,** 609, (1995).

55 W. Lindinger, J. Hirber, H. Paretzke, *Int. J. Mass Spectrom. Ion Proc.*, **129,** 79, (1993).

56 L. Colin, *J. Geophys. Res.*, **85**, 7575, (1980).

57 D. Smith, P. Spanel, T. Holland, W. Singari, J. Elder, *Rapid Comm. Mass Spec,* **13,** 724, (1999).

58 P. Spanel, D. Smith, T.A. Holland, W.A. Singary, J.B. Elder, *Rapid Commun. Mass Spec.,* **13,** 1354, (1999).

59 D. Smith, P. Spanel, S. Davies, *J. Appl. Physiol.,* **87,** 1584, (1999).

60 A. Jordan, A. Hansel, R. Holzinger, W. Lindinger, *Int J. Mass Spectrom. Ion Proc.,* **148,** 1, (1995).

61 P. Prazeller, T. Karl, A. Jordan, R. Holzinger, A. Hansel, W. Lindinger, *Int. J. Mass Spec.,* **198,** L1, (1998).

62 P. Spanel, S. Davies, D. Smith, *Rapid Communications in Mass Spec.,* **12,** 763, (1998).

63 P. Spanel, D. Smith, *Rapid Comm. in Mass Spec.,* **13,** 585, (1999).

64 R. Fall, T. Karl, A. Hansel, A. Jordan, W. Lindinger, *J. Geohys Res. (Atmos),* **104,** 15963, (1999).

65 D.B. Milligan, D.A. Fairley, C.G. Freeman, M.J. McEwan, *Int. J. Mass Spec.*, submitted, (1999).

66 J.S. Knight, *Ph.D. Thesis*, University of Canterbury, (1986).

67 J.S. Knight, C.G. Freeman, M.J. McEwan, N.G. Adams, D. Smith, *Int. J. Mass Spec. Ion Proc.*, **67**, 317, (1985).

68 S. Petrie, *Ph.D. Thesis*, University of Canterbury, (1991).

69 P.Wilson, *Ph.D. Thesis*, University of Canterbury, (1994).

70 G. Scott, *Ph.D. Thesis*, University of Canterbury, (1997).

71 D.Fairley, *Ph.D. Thesis*, University of Canterbury, (1998).

72 D. Smith, N. G. Adams, *J. Phys. D: Appl. Phys.,* **13,** 1267, (1980).

73 G. I. Mackay, G. D. Vlachos, D. K. Bohme, H. I. Schiff, *Int. J. Mass Spec. Ion Phys.,* **36,** 259, (1980).

74 J. M. Van Doren, S. E. Barlow, C. H. Depuy, V. M. Bierbaum, *Int. J. Mass Spec. Ion Proc.,* **81,** 85, (1987).

75 J.M. van Doren, *Ph.D. Thesis*, University of Colorado, Boulder CO. Chapter 1, (1987).

76 P. Spanel, D. Smith, *Advances in Atomic, Molecular, and Optical Physics,* **32,** 307, (1994).

77 F.C. Feshenfeld, K.M. Evenson, H.P. Broida, *Rev. Sci. Instrum.*, **36,** 294, (1965).

78 B.L. Bentz, C.G. Bruhn, W.W. Harrison, *Int. J. Mass Spectrom. Ion Phys.*, **28,** 409, (1978).

79 P. Baltayan, J.C. Pebay-Peyroula, N. Sadeghi, *J. Chem. Phys.*, **78,** 2942, (1983).

80 B.L. Upschulte, R.J. Shul, R. Passarella, R.G. Keesee, A.W. Castleman Jnr., *Int. J. Mass Spectrom. Ion Proc.*, **75,** 27, (1987).

81 F. Howorka, F.C. Feshenfeld, D.L. Albritton, *J. Phy. B*, **12**, 4189, (1979).

82 G. Dupeyrat, B.R. Rowe, D.W. Fahey, D.L. Albritton, *Int. J. Mass Spectrom. Ion Phys.*, **44,** 1, (1982).

83 L. Holland, W. Steckelmacher, J. Yarwood, *Vacuum manual*, E. & F.N. Spon, London, p15-42, (1974).

84 S. Dushman, D.G. Worden, in *Scientific foundations of Vacuum technique. Second edition*, J.M. Lafferty Ed., John Wiley and Sons, New York, Chapter 2, (1962).

85 V.N. Fishman, J.J. Grabowski, *Int. J. Mass Spectrom.*, **177,** 175, (1998).

86 N.G. Smith, D. Smith, *Int. J. Mass Spec. Ion Phys.*, 21, 349, (1976).

87 G.O. Brink, *Rev. Sci. Instrum.*, 37, 857, (1966).

88 D.A. Fairley, D.B. Milligan, L.M. Wheadon, C.G. Freeman, R.G.A.R. Maclagan, M.J. McEwan, *Int. J. Mass Spec.*, **185,** 253, (1999).

89 F.A. Miller, W.G. Fately, *Spectrochimica Acta,* **20,** 253, (1964).

90 *Handbook of Chemistry and Physics 80th Edition*, D.R. Lide Ed., Chemical Rubber Company Press, Boca Raton, (1999).

91 S.G. Lias, J.E. Bartmess, J.F. Liebman, J.L. Holmes, R.D. Levin, W.G. Mallard, *J. Phys. Chem. Ref. Data*, **17**, Supplement #1, (1988).

92 http://webbook.nist.gov/chemistry/

93 A.G. Harrison, *Chemical ionization mass spectrometry*, CRC Press, Boca Raton, (1983).

94 R.G. Ewing, G.A. Eiceman, J.A. Stone, *Int. J. Mass Spec.*, **193,** 57, (1999).

95 J. Sunner, M.G. Ikonomou, P. Kebarle, *Anal. Chem.*, **60**, 1308, (1988).

96 J. Sunner, G. Nicol, P. Kebarle, *Anal. Chem.*, **60**, 1300, (1988).

97 E.A. Mason, E.W. McDaniel, *Transport properties of ions in gases*, John Wiley and Sons, New York, (1988).

98 D. Smith, N. G. Adams, *Rate Coefficients in Astrochemistry*, 153, 1988

99 P. Spanel, S. Davies, D. Smith, *Rapid Commun. Mass Spec.*, **13,** 1733, (1999).

100 P. Spanel, D. Smith, *Int. J. Mass Spec. Ion Proc.*, **167,** 375, (1997).

101 P. Spanel, Y. Ji, D. Smith., *Int. J. Mass Spectrom. Ion Proc.*, **166,** 25, (1997).

102 P. Spanel, D. Smith, *Int. J. Mass Spectrom.*, **176,** 203, (1998).

103 P. Spanel, D. Smith, *Int. J. Mass Spec.*, **185,** 139, (1999).

104 P. Spanel, D. Smith, *Int. J. Mass Spec.*, **181,** 1, (1998).

105 P. Spanel, D. Smith, *Int. J. Mass Spec.*, **189,** 213, (1999).

106 P. Spanel, D. Smith, *Int. J. Mass Spec.*, **184,** 175, (1999).

107 P. Spanel, D. Smith, *Int. J. Mass Spectrom. Ion Proc.*, **172,** 137, (1998).

108 P. Spanel, D. Smith, *Int. J. Mass Spectrom. Ion Proc.*, **172,** 239, (1998).

109 P. Spanel, D. Smith, *Int. J. Mass Spectrom.*, **176,** 167, (1998).

110 T.L Williams, N.G. Adams, L.M. Babcock, *Int. J. Mass Spectrom. Ion Proc.*, **172,** 149, (1998).

111 E.P.L. Hunter, S.G. Lias, *J. Phys. Chem. Ref. Data*, **27**, 413, (1998).

112 D.K. Bohme, in *Interaction between ions and molecules*, P. Ausloos Ed., Plenum, New York, 489, (1975).

113 G. Bouchoux, J. Y. Salpin, D. Leblanc, *Int. J. Mass Spec. Ion Proc.*, **153,** 37, (1996).

114 T. Su, W.J. Chesnavich, *J. Chem. Phys.*, **76,** 5183, (1982).

115 D.A. Fairley, D.B. Milligan, C.G. Freeman, M.J. McEwan, P. Spanel, D. Smith, *Int. J. Mass Spec.*, **193,** 35, (1999).

116 M. Phillips, *Scientific American,* **7,** 52, (1992).

117 T.H. Risby, S.S. Sehnert, *Free Radical Biol. and Med.*, **27,** 1182, (1999).

118 R.H. Garrett, C.M. Grisham, *Biochemistry*, Saunders College Publishing, Fort Worth, (1999).

119 W. Ament, J. R. Huizenga, E. Kort, T. W. van der Mark, R. G. Grevink, G. J. Verkerke, *Int. J. Sports Med.*, **20,** 71, (1999).

120 J. Stegemann, *Exercise physiology. Physiologic bases of work and sport*, Georg Theimr Verlag, Stuttgart, 79, (1981).

121 J. Jarnberg, G. Johansen, *Toxicology Applied Pharmacology*, **155**, 203, (1999).

122 I. Eide, K. Zahlsen, *Archives of Toxicology*, **70**, 397, (1996).

123 R.J. Haynes, R.R. Sherlock, in *Mineral nitrogen in the plant-soil system*, R.J. Haynes Ed., Academic Press, Orlando FL, 242, (1986).

124 T.J. Clough, *Ph.D. Thesis*, Lincoln University, Christchurch, New Zealand, Chapter 2, (1994).

125 M.J. McEwan, L.F. Phillips, *The chemistry of the atmosphere*, Edward Arnold, London, 275, (1975).

126 T.R. Geballe, T. Oka, *Nature,* **384,** 334, (1996).

127 Royal Astronomical Society news release, May 12, (1999).

128 E. Graham IV, D.R. James, W.C. Keever, I.R. Gatland, D.L. Albritton, E.W. McDaniel, *J. Chem. Phys.*, **59**, 4648, (1973).

129 R. Johnsen, C. Huang, M.A. Biondi, *J. Chem. Phys.*, **65**, 1539, (1976).

130 J. Kim, L. Theard, W. Huntress Jnr., *Int. J. Mass Spec. Ion Phys.,* **15,** 223, (1974).

131 C.R. Blakley, M.L. Vestal, J.H. Futrell, *J. Chem. Phys.,* **66,** 2392, (1977).

132 J.J. Leventhal, L. Friedman, *J. Chem. Phys.,* **50,** 2928, (1969).

133 G.B.I. Scott, D.A. Fairley, C.G. Freeman, M.J. McEwan, *Chem. Phys. Lett.,* **269,** 88, (1997).

134 M.J. McEwan, C.L. McConnell, C.G. Freeman, V.G. Anicich, *J. Phys. Chem.,* **98,** 5068, (1994).

135 V. Aquilanti, G.G. Volpi, *J. Chem. Phys.,* **44,** 3574, (1966).

136 V. Aquilanti, G.G Volpi, *J. Chem. Phys.,* **44,** 2306, (1966).

137 G.I. Mackay, K. Tanaka, D.K. Bohme, *Int. J. Mass Spec. Ion Phys.*, **24**, 125, (1977).

138 J. Kim, L. Theard, W. Huntress Jnr., *Int. J. Mass Spec. Ion Phys.,* **15,** 223, (1974).

139 A.S. Fiaux, D.L. Smith, J.H. Futrell, *J. Am. Chem. Soc.,* **98,** 5773, (1976).

140 A.B. Rakshit, *Int. J. Mass Spec. Ion Phys.,* **41,** 185, (1982).

141 K.J. Miller, *J. Am. Chem. Soc.*, **112**, 8533, (1990).

142 P. Spanel, D. Smith, M. Henchman, *Int. J. Mass Spectrom. Ion Proc.,* **141,** 117, (1995).

143 P. Ausloos, S.G. Lias, T.J. Buckley, E.E. Rogers, *Int. J. Mass Spec. Ion Proc.,* **92**, 65, 1989.

144 K. Giles, N.G. Adams, D. Smith, *Int. J. Mass Spec. Ion Proc.*, **89**, 303, (1989).

145 R.D. Smith, J.H. Futrell, *Int. J. Mass Spec. Ion Phys.*, **20,** 71, (1976).

146 N.G. Adams, D.K. Bohme, E.E. Ferguson, *J. Chem. Phys.*, **52,** 5101, (1970).

147 D.K. Bohme, G.I. Mackay, H.I. Schiff, *J. Chem. Phys.*, **73**, 4976, (1980).

148 J. Glosik, N.D. Twiddy, G. Javahery, E.E. Ferguson, *Int. J. Mass Spec. Ion Proc.*, **109,** 75, (1991).

149 D.K. Bohme, N.G. Adams, M. Moseman, D.B. Dunkin, E.E. Ferguson, *J. Chem. Phys.*, **52,** 5094, (1970).

150 M.B. Milleur, R.L. Matcha, E.F. Hayes, *J. Chem. Phys.*, **60,** 674, (1974).

151 I. Baccarelli, A. Gianturco, F. Schneider, *Int. J. Quant. Chem.*, **74,** 193, (1999).

152 R.D. Poshusta, W.F. Siems, *J. Chem. Phys.*, **55,** 1995, (1971).

153 M.F. Falcetta, P.E. Siska, *Mol. Phys.*, **88,** 647, (1996).

154 T. Amano, F. Scappini, *J. Chem. Phys.*, **95,** 2280, (1991).

155 G. Cazzoli, C. Degli Esposti, F. Scappini, *J. Chem. Phys.*, **97,** 6187, (1992).

156 W.W. Duley, D.A. Williams, *Interstellar Chemistry*, Academic press, London, Chapter 4, 66, (1984).

157 V.G. Kunde, A.C. Aikin, R.A. Hanel, D.E. Jennings, W.C. Maguire, R.E. Samuelson, *Nature,* **292,** 686, (1981).

158 D. B. Milligan, D. A. Fairley, M. Mautner, M. J. McEwan, *Int. J. Mass Spec.*, **179,** 285, (1998).

159 A.B. Raksit, D.K. Bohme, *Int. J. Mass Spec. Ion Phys.*, **57,** 211, (1984).

160 S.A.H. Petrie, C.G. Freeman, M.J. McEwan, M. Mautner (Meot-Ner), *Int. J. Mass Spec. Ion Proc.*, **90,** 241, (1989).

161 C.A. Deakyne, M. Mauntner (Meot-Ner), T.J. Buckley, R. Metz, *J. Chem. Phys.*, **86,** 2334, (1987).

162 P. Botschwina, P. Sebald, *Chem. Phys.*, **141,** 311, (1990).

163 D. A. Fairley, G. B. I. Scott, D.B. Milligan, R. G. A. R. Maclagan, M. J. McEwan, *Int. J. Mass Spec. Ion Proc.*, **178,** 79, (1998).

164 T.A. Lehman, M.M. Bursey, *Ion cyclotron resonance spectrometry*, John Wiley and Sons, New York, (1976).

165 M.N. Glukhovtsev, J.E. Szulejko, T.B. McMahon, J.W. Gauld, A.P. Scott, B.J. Smith, A. Pross, L. Radom, *J. Phys. Chem.*, **98,** 13099, (1994).

166 P.J.A. Ruttink, P.C. Burgers, J.K. Terlouw, *Chem. Phys. Letts.*, **229,** 495, (1994).

167 G.A. McGibbon, P.C. Burgers, J.K. Terlouw, *Chem. Phys. Letts.*, **218,** 499, (1994).

168 G. Bouchoux, J.Y. Salpin, *J. Am. Chem. Soc.*, **118,** 6516, (1996).

169 F. Turecek, D.E. Drinkwater, F.W. McLafferty, *J. Am. Chem. Soc.*, **111,** 7696, (1989).

170 J.I. Brauman, C.-C. Han, *J. Am. Chem. Soc.*, **110,** 5611, (1988).

171 C.A. Deakyne, M. Mauntenr (Meot-Ner), *J. Phys. Chem.*, **94,** 232, (1990).

172 M.J. McEwan, D.A. Fairley, G.B.I. Scott, V.G. Anicich, *J. Phys. Chem.*, **100,** 4032, (1996).

173 Z. Karpas, M. Mautner (Meot-Ner), *J. Phys. Chem.*, **93,** 1859, (1989).

174 S.C. Smith, P.F. Wilson, P. Sudkeaw, R.G.A.R. Maclagan, M.J. McEwan, V.G. Anicich, W.T. Huntress, *J. Chem. Phys,* **98,** 1944, (1993).

175 M.J. McEwan, A.B. Denison, W.T. Huntress Jnr, V.G. Anicich, J. Snodgrass, M.T. Bowers, *J. Phys. Chem.*, **93,** 4064, (1989).

176 V.G. Anicich, A.D. Sen, M.J. McEwan, S.C. Smith, *J. Chem. Phys.*, **100,** 5696, (1994).

177 M.J. McEwan, V.G. Anicich, W.T. Huntress, P.R. Kemper, M.T. Bowers, *Chem. Phys. Lett.*, **75**, 278, (1980).

178 V.G. Anicich, A.D. Sen, W.T. Huntress Jnr., M.J. McEwan, *J. Chem. Phys.*, **102**, 3256, (1995).

179 S. Petrie, *J. Phys. Chem. A,* **102,** 7835, (1998).

180 A. Coustenis, F. Taylor, *Titan: The Earth-like moon. Series on atmospheric, oceanic, and planetary physics - Volume 1*, World Scientific, Singapore, (1999).

181 See articles in *Science*, **212**, 159-243, (1981). and *Nature*, **292**, 675-755, (1981).

182 Y.L. Yung, M. Allen, J.P. Pinto, *Apstrophys. J. (Suppl),* **55,** 465, (1984).

183 C.N. Keller, V.G. Anicich, T.E. Cravens, *Planet. Space Sci.*, **46,** 1157, (1998).

184 R.V. Yelle, D.F. Strobell, E. Lellouch, and D. Gautier, *European Space Agency Special Publication. SP 1177*, 243, (1997).

185 L.M. Lara, E. Lellouch, J.J. Lopez-Moreno, R. Rodrigo, *J. Geophys. Res. (Planets)*, **101**, 23261, (1996).

186 W. Reid Thompson, T. J. Henry, J. M. Schwartz, B. N. Khare, C. Sagan, *Icarus,* **90,** 57, (1991).

187 S.G. Gibbard, B. Macintosh, D. Gavel, C.E. Max, *Icarus,* **139,** 189, (1999).

188 E. Chassefiere, M. Cabane, *Planet. Space Sci.,* **43,** 91, (1995).

189 R. Lorenz, *New Scientist,* 12 April, 34, (1997).

190 M. Cabane. E. Chassefiere, *Planetary and Space Science,* **43,** 47, (1995).

191 W. Reid Thompson, T. J. Henry, J. M. Schwartz, B. N. Khare, C. Sagan, *Icarus,* **90,** 57, (1991).

192 *The Atmosphere of Titan.* D.M. Hunten Ed., *NASA SP-340*, (1974).

193 R. Lorenz, *New Scientist,* 14 December, 34, 1996

194 W. Kasprzak, H. Niemann, D. Harpold, J. Richards, H. Manning, E. Patrick, P. Mahaffy, *SPIE Proceedings,* **2803,** 129, (1996).

195 G.F. Lindal, G.E. Wood, H.B. Hotz, D.N. Sweetnam, V.R. Eshelman, G.L. Tyler, *Icarus*, **53**, 348, (1983).

196 *The Upper Atmosphere: Data analysis and interpretation*, W. Diemenger, G.K. Hartmann, R. Leitinger Eds., Springer-Verlag, 644-789, (1996).

197 A.F. Nagy, T.E. Cravens, *Planet. Space Sci.,* **46,** 1149, (1998).

198 W. H. Ip, *Astrophys. J.,* **362,** 354, (1990).

199 C.N. Keller, T.E. Cravens, L. Gan, *J. Geophys. Res. (Space Physics),* **97,** 12117, (1992).

200 L.A. Capone, J. Dubach, S.S. Prasad, R.C. Whitten, *Icarus,* **55,** 73, (1983).

201 L.A. Capone, R.C. Whitten, J. Dubach, S.S. Prasad, W.T. Huntress Jnr., *Icarus,* **28,** 367, (1976).

202 G.J. Molina-Cuberos, J.J. Lopez-Moreno, R. Rodrigo, L.M. Lara, *J. Geophys. Res. (Planets),* **104,** 21997, (1999).

203 L. A. Capone, J. Dubach, R. C. Whitten, K. Santhanam, *Icarus,* **44,** 72, (1980).

204 R.E. Samuelson, R.A. Hanel, V.G. Kunde, W.C. Maguire, *Nature*, **292**, 688, (1981).

205 A. Good, D.A. Durden, P. Kebarle, *J. Chem. Phys.,* **52,** 212, (1970).

206 K. Hiroaka, S. Fujimaki. M. Nasu, A. Minamitsu, S. Yamabe, H. Kouno, *J. Chem. Phys.,* **107,** 2551, (1997).

207 N.R. Daly, R.E. Powell, *Int. J. Mass Spectrom. Ion Phys.*, **16,** 443, (1975).

208 W. Freysinger, F.A. Khan, P.B. Armentrout, P. Tosi, O. Dmitriev, D. Bassi, *J. Chem. Phys.*, **101,** 3688, (1994).

209 D.R. Bates, *Chem. Phys. Lett.*, **123,** 187, (1986).

210 H. Bohringer, F. Arnold, *J. Chem. Phys.*, **77,** 5534, (1982).

211 P. A. M. Van Koppen, P. R. Kemper, A. J. Illies, M. T. Bowers, *Int. J. Mass Spec. Ion Proc.*, **54,** 263, (1983).

212 A. B. Rakshit, *Int. J. Mass Spec. Ion Phys.*, **36,** 31, (1980).

213 W. B. Maier II, *J. Chem. Phys.*, **61,** 3459, (1974).

214 M. Meot-Nor (Mautner), F. H. Field, *J. Chem. Phys.*, **61,** 3743, (1974).

215 P. A. M. van Koppen, M. F. Jarrold, M. T. Bowers, L. W. Bass, K. R. Jennings, *J. Chem. Phys.*, **81,** 288, (1984).

216 L.G. McKnight, K.B. McAfee, D.P. Sipler, *Physical Review,* **164,** 62, (1967).

217 C.L. Haynes, W. Freysinger, P.B. Armentrout, *Int. J. Mass Spec. Ion Proc.*, **149/150,** 267, (1995).

218 Haynes, C.L., W. Freysinger and P.B. Armentrout, *Int. J. Mass Spectrom. Ion Proc.* **150** 267, (1995).

219 H. Bohringer, F. Arnold, Int. J. Mass Spec. Ion Phys., 61, 3742, 1974 (125).

220 V.G. Anicich, D.B. Milligan, D.A. Fairley, M.J. McEwan, *Icarus*, submitted, (1999).

221 S. Dheandhanoo, R. Johnsen, M.A. Biondi, *Planet. Space Sci.*, **32,** 1301, (1984).

222 V. G. Anicich, M. J. McEwan., *Planet. Space Sci.*, **45,** 897, (1997).

223 M. J. McEwan, G.B.I. Scott, V.G. Anicich, *Int. J. Mass Spec. Ion Proc.*, **172,** 209, (1998).

224 D. Smith, N.G. Adams, T.M. Miller, *J. Chem. Phys.*, **69,** 308, (1978).

225 R.G.A.R. Maclagan, private communication.

226 B.R. Rowe, J.B. Marquette, G. Dupeyrat, E.E. Ferguson, *Chem. Phys. Letts.*, **113**, 403, (1985).

227 Smith and Adams Chem Phys Letts, 76, 418, (1980).

228 V. Frecer, D.C. Jain, A-M. Sapse, *J.Phys. Chem.*, **95,** 9263, (1991).

229 S. de Castro, H. Schaefer III, *J. Chem. Phys,* **74,** 551, (1981).

230 H.H. Teng, D.C. Conway, *J. Chem. Phys.*, **59**, 2316, (1973).

231 L. Knight, K. Johannessen, D. Cobranchi, E. Earl, D. Feller, E. Davidson, *J. Chem. Phys.*, **87,** 885, (1987).

232 Herbst E., Smith D., Adams N.G., McIntosh B.J., *J. Chem. Soc. Faraday Trans. 2,* **85,** 1655, (1989).

233 A. Ricard, G. Cernogora, M. Fitaire, L. Hochard, N. Kouassi, C. Speller, J.R. Vacher, *Planet. Space Sci.,* **43,** 41, (1995).

234 C.V. Speller, M. Fitaire, A.M. Pointu, *Nature,* **300,** 507, (1982).

235 J. R. Vacher, E. Le Duc, M. Fitaire, *Planet. Space Sci.,* **45,** 1407, (1997).

236 .L. McCrumb, P. Warneck, *J. Chem. Phys.,* **67,** 5006, (1977).

237 D.A. Fairley, G.B.I. Scott, C.G. Freeman, R.G.A.R. Maclagan, M.J. McEwan, *J. Chem. Soc. Faraday Trans.*, **92**, 1305, (1996).

238 D.A. Fairley, G.B.I. Scott, C.G. Freeman C.G., R.G.A.R. Maclagan, M.J. McEwan, *J. Phys. Chem A,* **101,** 2848, (1997).

239 K.K. Matthews, N.G. Adams, N.D. Fisher, *J. Phys. Chem. A,* **101,** 2841, (1997).

240 M. Meot-Ner (Mautner), *J. Am. Chem. Soc.,* **100,** 4694, (1978).

241 S. Petrie, T.J. Chirnside, C.G. Freeman, M.J. McEwan, *Int. J. Mass Spec. Ion Proc.,* **107,** 319, (1991).

242 H.E. Matthews, T.J. Sears, *Astrophys. J.*, **272**, 149, (1983).

243 S. Petrie, C.G. Freeman, M.J. McEwan, *Mon. Not. R. Astr. Soc.,* **257,** 438, (1992).

244 J. Sun, H-F. Grutzmacher, C. Lifshitz, *J. Am. Chem. Soc.,* **115,** 8382, (1993).

245 G. Javahery, S. Petrie, J. Wang, H. Wincel, D.K. Bohme, *J. Am. Chem. Soc.*, **115**, 9701, (1993).

246 M.J. McEwan, D.A. Fairley, G.B.I. Scott, V.G. Anicich, *J. Phys. Chem.*, **100**, 4032 (1996).

247 M.T. Bowers, R.D. Cates, *J. Am. Chem. Soc.,* **102,** 3994, (1980).

248 D.B. Milligan, P.F. Wilson, M.J. McEwan, V.G. Anicich, *Int. J. Mass Spec.*, **185**, 663, (1999).

249 V.G. Anicich, Private communication.

250 M.J. McEwan, V.G. Anicich, Unpublished work.

251 M.J. McEwan, A.B. Denison, V.G. Anicich, W.T. Huntress Jr., *Int. J. Mass Spec. Ion Proc.*, **81**, 247, (1987).

252 V. G. Anicich, W. T. Huntress Jnr., M. J. McEwan, *J. Phys. Chem.,* **90,** 2446, (1986).

253 M. Meot-Nor (Mautner), *J. Am. Chem. Soc.,* **101,** 2389, (1979).

254 G.B.I. Scott, D.B. Milligan, D.A. Fairley, C.G. Freeman, M.J. McEwan, *J. Chem.Phys.,* **112,** 4959, (2000).

255 G.B.I. Scott, D.B. Milligan, D.A. Fairley, C.G. Freeman, M.J. McEwan, *J. Phys. Chem.,* **103,** 7470, (1999).

256 M.J. McEwan, G.B.I. Scott, N.G. Adams, L.M. Babcock, R. Terzieva, E. Herbst, *Astrophys. J.*, **513**, 289, (1999).

257 G.B.I. Scott, D.A. Fairley, C.G. Freeman, M.J. McEwan, V.G. Anicich, *J. Phys. Chem.*, **103**, 1073, (1999).

258 V. Le Page, Y Keheyan, T. Snow, V. Bierbaum, *Int. J. Mass Spec.,* **185,** 949, (1999).

259 F.C. Feshenfeld, *Astrophys. J.,* **209,** 628, (1976).

260 M. Sablier, C. Rolando, *Mass Spec. Revs.,* **12,** 285, (1993).

261 E. Herbst, *Angew, Chem. Int. Ed. Engl.*, **29**, 595, (1990).

262 D. Gerlich, R. Disch, S. Scherbarth, *J. Chem. Phys.,* **87,** 350, (1987).

263 D.B. Milligan, D.A. Fairley, C.G. Freeman, M.J. McEwan, *Int. J. Mass Spec.*, submitted, (1999).

264 D. Talbi, D.J. DeFrees, *Chem. Phys. Letts.,* **179,** 165, (1991).

265 D. Talbi, D.J. DeFrees, E. Herbst, *Ap. J,* **374,** 390, (1991).

266 R.P.A. Bettens, M.A. Collins, *J. Chem. Phys.,* **108,** 2424, (1998).

267 L.H. Reyerson, K. Kobe, *Chem. Revs.*, 7, 479, (1930).

268 D.A. Long, F.S. Murfin, R.L. Williams, *Proc. Roy. Soc. A,* **223,** 251, (1954).

269 C.E.M. Strauss, S.H. Kable, G.K. Chawla, P.L. Houston, I.R. Burak, *J. Chem. Phys.,* **94,** 1837, (1991).

270 N. Haider, D. Husain, *J. Chem. Soc. Faraday Trans.,* **89,** 7, (1993).

271 D. Husain, L.J. Kirsch, *J. Photochem.,* **2,** 297, (1973).

272 D. Husain, A.X. Ioannou, *J. Chem. Soc. Faraday Trans.,* **93,** 3625, (1997).

273 W. Braun, A.M. Bass, D.D. Davis, J.D. Simmons, *Proc. Roy. Soc A,* **312,** 417, (1969).

274 D. Chastaing, P.L. James, I.R. Sims, I.W.M. Smith, *Phys. Chem. Chem. Phys.,* **1,** 2247, (1999).

275 H. Kim, J. Roebber, *J. Chem. Phys.*, **44,** 1709, (1966).

276 J. McFarlane, J.C. Polanyi, J.G. Shapter, J.M. Williamson, *J. Photochem. Photobiol. A,* **46,** 139, (1989).

277 G.B.I. Scott, D.A. Fairley, C.G. Freeman, M.J. McEwan, V.G. Anicich, *J. Chem. Phys.*, **109,** 9010, (1998).

278 D.B. Milligan, M.J. McEwan, *Chem. Phys. Letts.*, submitted, (1999).

279 D. Kley, N. Washida, K.H. Becker, W. Groth, *Chem. Phys. Letts.*, **15,** 45, (1972).

280 N. Washida, D. Kley, K.H. Becker, W. Groth, *J. Chem. Phys.*, **63,** 4231, (1975).

281 E.A. Ogryzlo, J.P. Reilly, B.A. Thrush, *Chem. Phys. Letts.*, **23,** 37, (1973).

282 L.F. Phillips, Private communication.

283 D.R. Bates, *Mon. Not. R. Astron. Soc.*, **111**, 303, (1951).

284 D.R. Bates, E. Herbst, in *Rate Coefficients in Astrochemistry*, T.J. Millar, D.A. Williams Eds., Kluwer Academic Publishers, Dordrecht and Boston, 17, (1988).

285 W.N. Olmstead, M. Lev-On, D.M. Golden, J.I. Brauman, *J. Am. Chem. Soc.*, **99**, 992, (1977).

286 J.I. Brauman, *J. Mass Spec.*, **30**, 1649, (1995).

287 J. Wronka, D.P. Ridge, *Rev. Sci. Instrum.*, **53**, 491, (1982).

288 M.B. Comisarow, *J. Chem. Phys.*, **55**, 205, (1971).

289 J. Baynes, M.H. Dominiczak, *Medical Biochemistry*, Mosby, London, 173, (1999),

290 D.L. Smith, J.H. Futrell, *J. Phys. B.*, **8**, 803, (1975).

291 R.D. Smith, J.H. Futrell, *Int. J. Mass Spec. Ion Phys.*, **20**, 347, (1976).

292 R.D. Smith, J.H. Futrell, *Int. J. Mass Spec. Ion Phys.*, **19,** 201, (1976).